CONCRETE CYLINDRICAL SHELL ROOFS PRESTRESSED WITHIN THE SHELL SURFACE

by A.G. Park

Supervised by J.C. Scrivener

Thesis presented by A.G. Park for the degree of Doctor of Philosophy

CIVIL ENGINEERING REPORT No. 74-6

JUNE 1974

Department of Civil Engineering
University of Canterbury
Christchurch
New Zealand

ERRATA

p.6 Fig. 2.1(c): replace "m_1" with "m_{12}" and "m_{12}" with "m_1"

p.9 Fig. 2.2: replace "$n_1 - 8.3\%$" with "$n_{12} - 8.3\%$"

p.10 Line 9: replace "$\sin(n\pi/z)$" with "$\sin(n\pi/2)$"

p.48 Line 19: replace ".35d" with "$.35d/C_1$"

p.92 Line 14: replace "E_D" with "E_s"

p.92 Line 16: replace "E_s" with "E_D"

p.102 Table of Cable Data:

replace Cable Force 1 "410 lb" with "2160 lb"
and
replace Cable Force 3 "2160 lb" with "410 lb"

p.103 Table of Cable Data:

replace Anchorage Force 3 "2160 lb" with "0 lb"

p.123 Fig. 5.17: replace "+ outwards" with "- outwards"
and
replace "- inwards" with "+ inwards"

p.124 Line 19: The crack referred to is not shown on Fig. 5.14(b). Referring to Fig. 5.14(b) the crack extends one sixth of the arc distance into the shell from the bottom left hand corner of the extrados (as drawn) and from the top left hand corner of the intrados.

p.127 Line 23: replace "3rd" with "1st"

p.129 Line 3: min A_s, replace ".45" with ".045"

p.145 Line 6: replace "this" with "the range of applicability of beam theory"

ABSTRACT

Cylindrical shells, constructed of precast concrete elements prestressed together by means of cables within the curved surface, are shown to have satisfactory and predictable behaviour under static load. By careful choice of prestressing layout, cracking can be delayed until a considerable surface load has been applied. An existing elastic analysis method for effects of prestress, based on the D.K.J. equation, is adapted to improve its accuracy and efficiency. A method is given for calculating the effect of the stiffness of the traverse on the distribution of anchorage force to the shell. This can be particularly important when the anchorage is placed close to the shell edge.

Circular cylindrical shell roof models without edge beams and prestressed within the curved surface with both straight and draped cables were tested to failure. Four of the five shells were constructed from precast elements. Strain and deflection measurements were obtained for all shells and confirmed the reliability of the analysis method.

A flexural beam type ultimate load analysis is devised which accurately predicts the ultimate loads of a range of shells including the model shells tested. This analysis is developed into a design technique.

Some approximate methods are developed for the working load analysis of cylindrical shells prestressed within the shell surface.

ACKNOWLEDGEMENTS

I wish to make grateful acknowledgement for help received during the course of this project and extend my thanks to the following people.

Professor H.J. Hopkins, Head of the Civil Engineering Department, under whose overall guidance this study was made;

Dr. J.C. Scrivener, supervisor for the study, for his encouragement and constructive guidance throughout this project, and for his many helpful suggestions during the preparation of this thesis;

The Technical Staff of the Civil Engineering Department for their assistance in the experimental programme, in particular Messrs. J.S. Sheard and J.G.C. Van Dyk.

I wish to gratefully acknowledge financial aid from the New Zealand Portland Cement Association in the form of the 1970 N.Z.P.C.A. Scholarship; and to the University Grants Committee for experimental equipment and materials under Research Grant 68/271.

Finally, I wish to thank my wife, Diane, for her constant encouragement and help.

TABLE OF CONTENTS

LIST OF FIGURES

Page

LIST OF TABLES

NOTATION

Each notation is defined where it first appears in the text. For convenience of reference the more important are listed below:

a	constant defining parabola
a	depth of compression block
a'	depth to centroid of compression block
a_n	nth Fourier coefficient in the x direction
a_{ni}	nth Fourier coefficient for the ith strip
a_m	mth Fourier coefficient in the y direction
A,B,C,D	constants of integration for beam on elastic foundation theory
A_c	area of concrete in compression
A_s	prestressed steel area
A'_s	non prestressed steel area
A_t	concrete area in compression required to balance tendon force T_t
b	breadth of edge beam
b	effective width of traverse
c	distance of a point force from the end of a semi-infinite beam
c	parameter describing parabolic cable
c'	coefficient for rectangular stress block depth
C	concrete compressive force
d	anchorage eccentricity as an arc distance from the crown
d	depth to centroid of prestressing steel from the top of the crown
d	thickness of traverse
d'	vertical lever arm
d_e	slanted lever arm
e	anchorage eccentricity + cable drape, as an arc distance from the crown

e_{cy} concrete yield strain

e_{sL} steel strain due to surface loading at ultimate moment

e_{sp} steel strain due to prestressing

e_{su} steel strain at ultimate moment

e_{sy} nominal steel yield strain

E Young's modulus

f drape of prestressing cable as an arc length

f_c allowable average concrete compressive stress

f'_c concrete cylinder strength

f'_s ultimate prestress steel stress

f_{su} steel stress at ultimate moment

f_{sy} nominal steel yield stress

f_t concrete tensile strength

F_x, F_y, F_z line loads/unit length in curvilinear coordinates

F_x, F'_y, F'_z line loads/unit length in Cartesian coordinates

g parameter describing parabolic cable

$g_i(x)$ equation of ith strip

h parameter describing parabolic cable

I moment of inertia of shell cross-section

I_z moment of inertia of traverse

k reaction/unit length, for unit deflection in beam on elastic foundation theory

k positive integer

kd neutral axis depth from top of the crown

L shell span

m positive integer

M general expression for a moment

m_1 longitudinal moment/unit length

m_{12} twisting moment/unit length

m_2 transverse moment/unit length

M_o corrective moment, which with point force Q_o is applied to the end of a semi-infinite beam to remove redundant forces which occur when it is "cut" from an infinite beam

M'_o redundant moment on the end of a semi-infinite beam, when it is "cut" from an infinite beam

M''_o moment due to corrective actions M_o and Q_o

M_{uL} ultimate moment

n positive integer

N principal normal

n_1 longitudinal normal force/unit length

n_{12} shear force/unit length

n_2 transverse force/unit length

P prestressing force

P_a prestressing anchorage force

Q dimensionless constant used by Holand

Q_o point force of equal magnitude to redundant shear force V'_o

r positive constant

r_1, r_2 shell reactions/unit length

R radius of shell middle surface

R_i radius of shell intrados

R_o radius of shell extrados

t shell thickness

t parameter describing parabola

T unit tangent

T_t tendon force

u displacement in x direction

v displacement in y direction

V general expression for shear force

V'_o redundant shear force

V''_o shear force due to corrective actions M_o and Q_o

w radial displacement

W reaction/unit length in beam on elastic foundation theory

x,y,z	shell axes - Cartesian coordinates
x,y',z'	shell axes - curvilinear coordinates
X,Y,Z	surface loads/unit length in x,y,z directions
α,β,γ	positive constants
ε	strain
θ,ξ,ϕ,Ψ	variables in beam on elastic foundation theory
κ	curvature
μ	coefficient of friction
ν	Poission's ratio
σ_k,σ_n	coefficients used in modifying Fourier coefficients
ϕ_k	half included angle

CHAPTER ONE

INTRODUCTION AND OBJECTIVES

1.1 INTRODUCTION

Prestressing offers two main advantages to the designer of cylindrical shells.

First, the large edge beams traditionally used on cylindrical shells may be reduced in size, or, if the shell is prestressed within the curved shell section itself, eliminated completely. This removes the main architectural objection to cylindrical shells. However, by reducing or eliminating the edge beams the inherent stiffness of the shell is reduced. This may lead to excessive cracking, although with careful choice of prestress cable layout, flexural cracking can be avoided until a reasonable load has been applied. For many cases it is possible to retard crack appearance until after design working load, thus effectively waterproofing the shell and eliminating the need for any external membrane. A further advantage is that while the section is uncracked, the whole cross-section is effective in resisting deflections.

Secondly, shells can be made of precast elements and joined by means of the prestressing cables. With high labour costs, as in New Zealand, precasting offers considerable advantages that make the use of cylindrical shells a viable economic proposition. Precast elements could be made in a repeatable mould in a factory, thus reducing the problems associated with the placing and curing of a thin layer of in situ concrete on a relatively

large slope. By the use of top moulds, shells with larger included angles could be constructed more easily than with in situ pouring of shells. Precasting should ensure faster erection on site, thus making construction progress less dependent on weather conditions. Also a reduced amount of skilled site labour would be required.

1.2 HISTORICAL BACKGROUND

The elastic analysis of circular cylindrical shells, prestressed within the shell surface, has been solved. de Litter[1] in 1963 and Berndt[2] in 1966 described a method for the analysis of circular cylindrical shells with straight prestressing cables and in 1969 Bryant and Scrivener[3] gave a different method which can be used for both straight and draped cables. Both these techniques use a Fourier type analysis and require the summing of approximately 10 Fourier terms to obtain reliable results. The accuracy of results from these techniques was confirmed by the authors with tests on elastic models.

The series of tests carried out by Bryant[6,52] on an aluminium shell (L = 39.12 in., R = 19.94 in., t = .1309 in., ϕ_k = .526 rad., no edge beams) appear to be the most comprehensive tests that have been done on an elastic prestressed cylindrical shell model. On his shell he tested five straight cable positions with anchorage eccentricity/half arc length of 0.048, 0.337, 0.667, 0.833, 0.972. Three draped parabolic cable layouts were also tested, with anchorage eccentricity/ half arc length of 0.500, 0.667, 0.833. At midspan for these three tests the cable was at a distance around the arc of 0.972 times the half arc length. All eight cable layouts

were symmetrical. Bryant obtained accurate and repeatable experimental results for his series of tests. He found that his theory accurately predicted the longitudinal stresses away from the traverse and also the frequent changes in sign of the transverse moments. Transverse stresses away from and shear stresses close to the traverse were predicted to within 10%. At the crown, vertical deflections were given to within 3% of experimental results, but near the edges the agreement was between 5% and 25%.

Up to the present time, very few tests have been carried out on concrete cylindrical shells, prestressed within the shell surface. In 1961 Bouma et al[4] reported a series of tests on eleven intermediate length cylindrical shells, one of which was prestressed both in the edge beams and in the shell surface. They found that while prestressing can improve working load behaviour, consideration of the effect of overloads must be made, particularly with regard to the shell membrane reinforcement, or premature failure may occur. Scrivener and Megget[5] in 1967 carried out what appears to be the only reported test on a single cylindrical shell, prestressed within the curved surface and not having edge beams. This shell ($^{L}/R = 2$, $\phi_k = 30^{o}$) had ungrouted straight cables, which were designed to balance the tensile midspan edge stresses due to dead load. Scrivener and Megget found that despite the lack of edge beams, the shell had acceptable deflection and strain levels at normal working loads. The shell was found to recover to near its original state on removal of overloads of up to twice the working load.

1.3 OBJECTS OF THIS RESEARCH

The object of the experimental part of this research

was to carry out a systematic series of model tests to obtain reliable data on the behaviour of concrete cylindrical shell roofs, without edge beams, prestressed within the shell surface. Results from these tests were to be used:

i) To determine whether shells can be designed by an elastic analysis to behave satisfactorily up to design working load.

ii) To ascertain the effect which cracking of the concrete and elongation of the steel has on the behaviour of the shells.

iii) To study the ultimate load behaviour and failure mechanism, and how these are altered with changes in shell parameters.

The second part of the research was to develop an existing computer program written by Bryant[6], so that circular cylindrical shells, with or without edge beams, could be analysed elastically for surface loading and for prestress loading - prestress loading to be either from straight or draped cables in either the edge beam or shell surface.

The final object of the research was to develop a simple method for the analysis of cylindrical shells, prestressed within the shell surface, such as could be used in a design office for preliminary analysis. For satisfactory design, the behaviour of the shell at design working load must be able to be determined, and also it must be known that satisfactory ultimate load behaviour will occur.

CHAPTER TWO

ELASTIC ANALYSIS

The elastic shell equation used throughout this thesis is the commonly used Donnel-Karman-Jenkins[7] equation:

$$\frac{Et^3}{12(1-\nu^2)} \nabla_1^8 w + \frac{Et}{R^2}\frac{\partial^4 w}{\partial x^4} = \nabla_1^4 Z + \frac{1}{R}\left[\frac{\partial^2}{\partial y^2} - \nu\frac{\partial^2}{\partial x^2}\right]\frac{\partial X}{\partial x} - \frac{1}{R}\left[\frac{\partial^2}{\partial y^2} + (2+\nu)\frac{\partial^2}{\partial x^2}\right]\frac{\partial Y}{\partial y}$$

where $\nabla_1^8 = \nabla_1^4 \nabla_1^4$, $\nabla_1^4 = \nabla_1^2 \nabla_1^2$, $\nabla_1^2 = \left(\frac{\partial^2}{\partial x^2} + \frac{\partial^2}{\partial y^2}\right)$

and E = Young's modulus

R = shell radius

t = shell thickness

ν = Poisson's ratio

x,y,z = Coordinate directions, defined in Figure 2.1(a)

X,Y,Z = Surface loads in x,y,z directions

u,v,w = Displacements in x,y,z directions

Shell forces and moments are also defined in Figure 2.1 for future reference.

The D.K.J. equation is derived using Navier's hypothesis, small deflection theory and assuming linear - elastic thin shell action. In addition the effects of radial shear forces on the shell deflection are ignored.

If the curved ends are assumed to be supported on knife edge supports, with complete rigidity in their own plane, $v = w = 0$, and complete flexibility in planes perpendicular to their middle surface, $m_1 = n_1 = 0$, the equation can be solved by means of a Levy type solution. The formulation and method of solution of the equation can be found in many

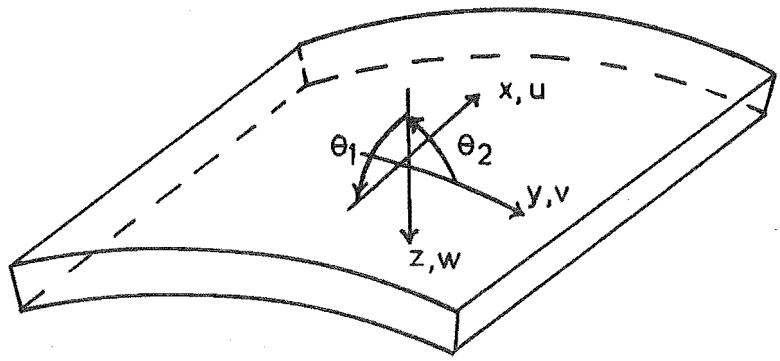

(a) Shell coordinate axes and displacements

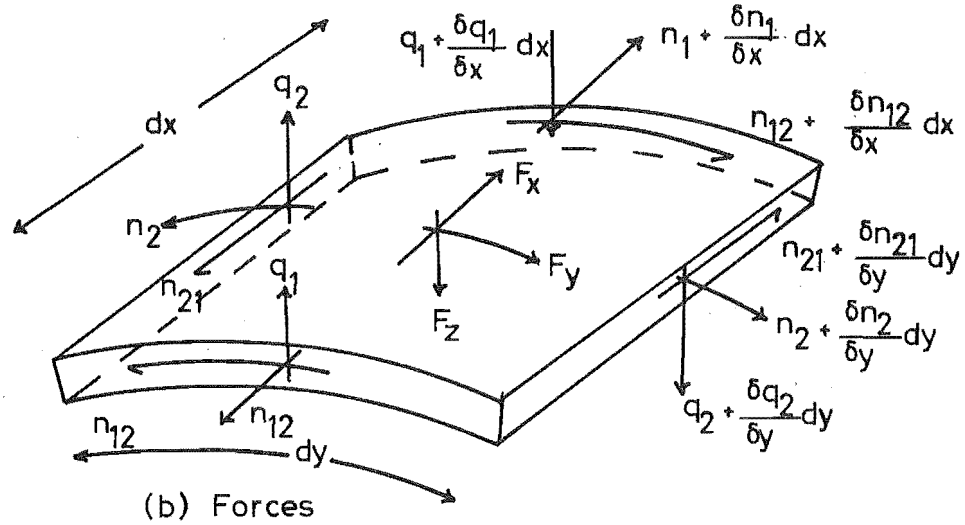

(b) Forces

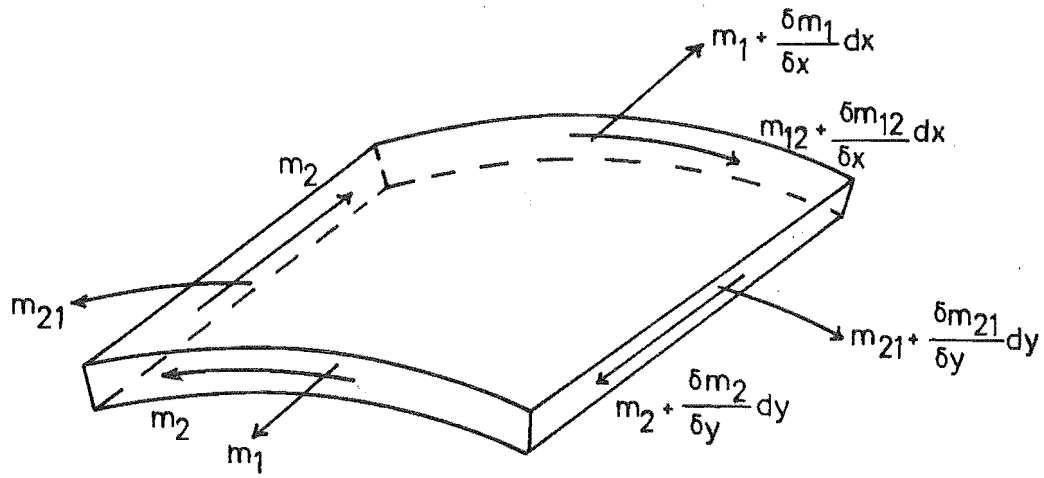

(c) Moments

FIG. 2.1 POSITIVE SHELL AXES, DISPLACEMENTS, ACTIONS AND SURFACE LOADS.

standard texts[8,9,10,11]. McNamee[8] gives a particularly clear presentation as does Billington[9] who shows the derivation of the D.K.J. equation from general shell theory.

Elastic theoretical results used in this thesis were obtained by use of a computer program "D.K.J." described in Appendix A, which is based on the D.K.J. equation. An indication that the accuracy of the D.K.J. computer program is good is given in Figures A.1 and A.2 where results from the "D.K.J." computer program are compared with results given by Billington[9] and Gibson[22]. A brief description of the loading formulations used is given in Sections 2.2, 2.3.2, 2.3.4, and 2.4.

2.1 RANGE OF APPLICABILITY OF D.K.J. EQUATION

Due to the dropping of terms during the formulation of the D.K.J. equation, the range of applicability of the equation is limited. There is, however, some confusion between different texts as to this limit. Billington[9] suggests that it is reasonable to use the D.K.J. equation for short ($L/R < \frac{1}{2}$) and intermediate ($\frac{1}{2} < L/R < 2\frac{1}{2}$) shells, but that the more rigorous methods of Holand[12] or A.S.C.E[13]. should be used for larger shells. Ramaswamy[11] recommends that the D.K.J. equation be used for short ($L/R \leq 1.6$) shells and that for intermediate ($1.6 \leq L/R \leq \pi$) length shells an "exact" theory (Holand, Flügge, Dischinger) should be used.

Holand[12], and most other authorities, consider the Flügge theory to be the most accurate yet tractable shell theory. He carried out an extensive study of a number of shell equations and presents a graph (ref.12, pp54) of the percentage differences in results from D.K.J. theory as

compared with Flügge theory. Differences from the Flügge theory are given for the first Fourier term (the second coefficient showing similar trends) and are plotted against a dimensionless constant Q ,

where $Q = R\sqrt[8]{\beta^4\alpha^4}$ $\qquad \beta = \sqrt[4]{\dfrac{3(1-\nu^2)}{R^2t^2}}$

$$\alpha = \frac{n\pi}{L}$$

$$n = 1,2,3...$$

and hence Q is proportional to $\sqrt[8]{\dfrac{R^6}{t^2L^4}}$.

As Q is reduced the percentage differences from the Flügge theory increase as does the rate of increase in differences. The minimum value of Q for which differences are given by Holand is 2.5. These differences are given on Figure 2.2. Figure 2.2 also shows the range of L/R and R/t for which Q is greater than 2.5. In this range the differences between results using D.K.J. theory and Flügge theory are less than the differences given on Figure 2.2 for $Q = 2.5$, and should be acceptable for design purposes.

2.2 SURFACE LOADING

In order that the governing differential equation may be solved, loading must be expressed in the form:

$$\left.\begin{aligned} X &= \Sigma X_o \cos \gamma y \sin \alpha x \\ Y &= \Sigma Y_o \sin \gamma y \cos \alpha x \\ Z &= \Sigma Z_o \cos \gamma y \cos \alpha x \end{aligned}\right\} \quad \ldots \quad (2.1)$$

$$\alpha = \frac{n\pi}{L} \text{ , } \gamma = \text{a constant}$$

Two particular loading cases are considered below.

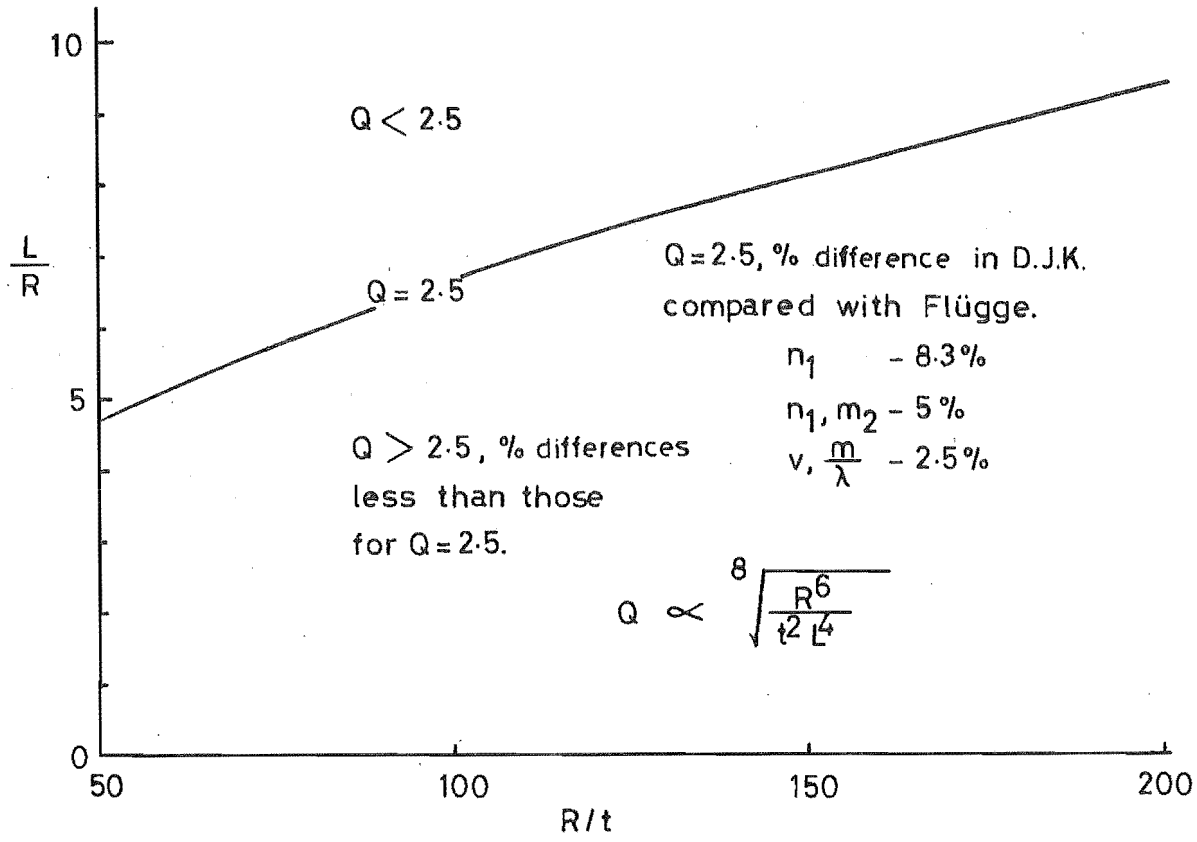

FIG. 2.2 ACCURACY OF D.K.J. EQUATION.

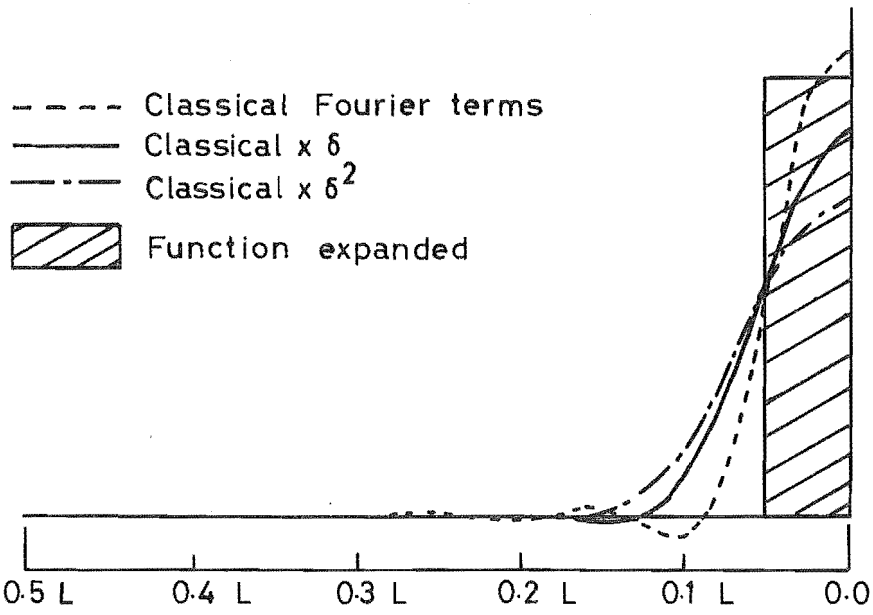

FIG. 2.3 EFFECT OF REPEATED APPLICATION OF SIGMA FACTOR.

2.2.1 Dead Load

At any position on the shell cross-section, distance y around the arc from the crown, the dead load force P per unit area can be resolved into two components Y and Z where:

$$Y = P \sin\phi, \quad Z = P \cos\phi \quad \text{and} \quad \phi = {}^{y}/_{R}$$

This is the same form as equations (2.1) if $\phi = {}^{y}/_{R} = \gamma y$. In order that uniform dead load is obtained along the shell Y, Z must be expressed in the form $(4P/\pi n) \sin(n\pi/z)$. Hence for dead load:

$$X = 0.0$$

$$Y = \frac{4P}{\pi} \Sigma \frac{1}{n} \sin\frac{n\pi}{2} \sin\frac{y}{R} \cos\frac{n\pi x}{L}$$

$$Z = \frac{4P}{\pi} \Sigma \frac{1}{n} \sin\frac{n\pi}{2} \cos\frac{y}{R} \cos\frac{n\pi x}{L}$$

2.2.2 Radial Load

At all points on the shell for a uniform radial pressure P, $X = Y = 0$ and $Z = P$. In a similar manner to dead load:

$$Z = \frac{4P}{\pi} \Sigma \frac{1}{n} \sin\frac{n\pi}{2} \cos\frac{n\pi x}{L} ; \quad \cos\gamma y \equiv 1$$

2.3 PRESTRESSING IN SHELL SURFACE

A number of methods, some approximate, have been proposed for the analysis of cylindrical shells prestressed within the shell surface. Approximate methods where the line loads (forces from friction and cable drape) have been replaced by equivalent loads along the shell edge have been used by Bouma et al[4], Haas[14], Dehousse[15] and Bieger[16]. While these approximate methods may give satisfactory results under

favourable circumstances, their overall accuracy is doubtful and the use of a more accurate method is preferable. For the more accurate methods, described in the following sections, there are two fundamentally different techniques for representing both the anchorage force and the line loads.

2.3.1 Anchorage Force - 1st Method

Berndt[2] and de Sitter[1] solve the problem of the anchorage force on the end of the shell in two steps.

In the first stage the shell is considered as being simply supported along the straight edges and the anchorage force is expanded along the curved end as a Fourier series P(y) :

$$P(y) = \frac{2P}{R\phi_K} \cos \alpha_n d \cos \alpha_n y$$

where $\alpha_n = (\frac{2n+1}{2R\phi_K})\pi$; $n = 0,1,2...$

d = anchorage eccentricity

The boundary conditions are:

i) Curved ends

$w = v = m_1 = 0$, $n_1 = P(y)$

ii) Straight edges

$m_2 = n_2 = 0$; $n_{12} \neq 0$, $r_2 \neq 0$

The second stage consists of removing the unwanted actions, n_{12} and r_2 , along the straight edges by a complementary function solution with the shell simply supported on the curved ends.

2.3.2 Anchorage Force - 2nd Method

The second technique, developed by Bryant and Scrivener[3], assumes that the structure is simply supported

at the curved ends and that the anchorage force is introduced to the shell as a shear force over a short longitudinal length of the shell adjacent to the traverse. The analysis technique is a particular case of that used for draped cables described in Section 2.3.4.

2.3.3 Line Loads - 1st Method

The method used by Berndt[2] and also investigated by Bryant[6] is to substitute the line loads by statically equivalent surface loads which are then developed as a double Fourier series:

$$F = \sum_n a_n \begin{matrix} \sin \alpha x \\ \cos \alpha x \end{matrix} \sum_m a_m \begin{matrix} \sin m\gamma y \\ \cos m\gamma y \end{matrix}$$

n,m are odd integers

Berndt reports that he found good agreement between model test results and results using his method of analysis. However, Bryant found that the above method did not give satisfactory convergence for some shell actions and so he developed the following method.

2.3.4 Line Loads - 2nd Method

The method described in this section is largely a summary of a paper by Bryant and Scrivener[3].

First the shell is divided up into a number of transverse strips of width $L/2m$, m being an integer, throughout which the line load intensities are considered constant. A number of equally spaced shell generators are then considered along the cable profile and the line loads divided between them. For each transverse strip the line load is divided between the two closest generators in the inverse ratio of the distances the cable is from the two generators. Along the

generators the line load components F_x, F_y, F_z are replaced by the actions n_{12}, n_2, r_2. The anchorage load is considered to be a shear load (n_{12}) spread into the shell along two generators adjacent to the anchorage and treated similarly to the line loads.

These actions, n_{12}, n_2, r_2, are then expanded as a Fourier series along each generator in order that a Levy type solution may be applied. If $g_i(x)$ is the equation along a generator for a line load component (value $f(x_i)$) of the ith transverse strip.

$$g_i(x) = f(x_i) \frac{8}{\pi} \sum_n a_{ni} \begin{matrix}\sin \\ \cos\end{matrix} \frac{n\pi x}{L}$$

where $a_{ni} = \frac{1}{n} \sin \frac{n\pi}{4m} \cos \frac{n\pi x_i}{L}$, $n = 1, 3, 5...$

and x_i = distance of strip i from the centreline.

Then from the sum of all strips

$$f(x) = \sum_{i=1}^{m} g_i(x) = \frac{8}{\pi} \sum_n a_n \begin{matrix}\cos \\ \sin\end{matrix} \frac{n\pi x}{L}$$

where $a_n = \sum_{i=1}^{m} a_{ni} f(x_i)$, $n = 1,3,5 ..$

For each Fourier term the analysis is carried out as follows:

i) The shell is considered as a complete tube and solved for each pair of symmetrical (one from each side of the centreline) generators. This is done by assuming that the loaded generators divide the tube into two shells and hence the generator loads can be considered as edge loads at the junctions of the shells. By a complementary function solution and considering the carry over from one shell to the other, the actions and displacements can be found at

required points anywhere on the tube.

ii) All the complete tube solutions are then added together and the required shell "cut" from the tube, unwanted edge sections being removed by an ordinary complementary function solution.

Bryant and Scrivener[3] have compared results obtained by the above generator line-load method with experimental results obtained for a number of cable layouts on a prestressed aluminium model shell. Good correlation was obtained.

2.3.5 Convergence of Generator Line Load Technique

From the results of trial runs, Bryant and Scrivener found that if 10 Fourier terms (n=1,3...19) were summed for an anchorage load spread 0.05L into the shell along two closely spaced generators, a reasonable approximation of the anchorage load was obtained. For draped cables they found that a generator spacing of $R\phi_k/6$, $m = 20$ transverse strips and 6 Fourier terms were required to give the same order of accuracy as that obtained for the anchorage load.

An attempt, as described below, was made by the present author to improve the convergence of the solution by using different methods for modifying the classical Fourier coefficients. However it was found that little improvement in the convergence could be obtained from that using the parameters and method suggested by Bryant and Scrivener. The greatest variation between methods occurred in the vicinity of the cable near the traverse. Away from this area there was negligible difference between many of the methods. For the anchorage force a triangular shear pulse was considered in addition to the rectangular shear pulse used by Bryant

and Scrivener. Expressions for the rectangular and triangular pulses are:

Rectangular pulse

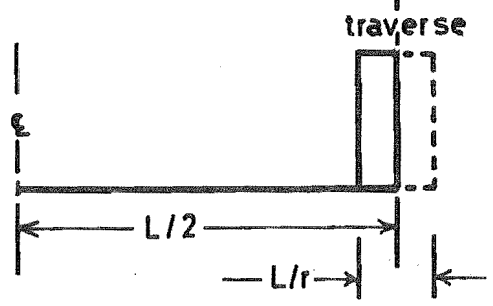

$$f(x) = \frac{8\, f(x_i)}{n} \sin \frac{n\pi}{2r} \cos \frac{n\pi}{2}$$

$n = 1, 3 \ldots$

and for anchorage force

$$f(x_i) = \frac{P}{L/R}$$

Triangular pulse

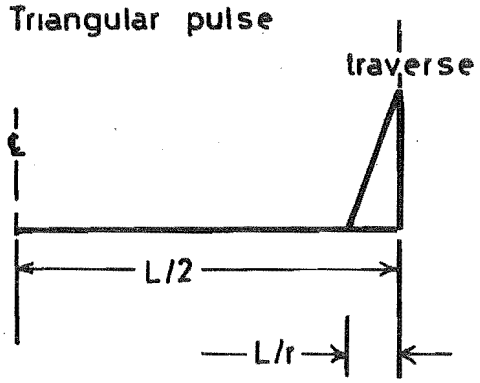

$$f(x) = \frac{8\, r\, f(x_i)}{(n\pi)^2} \cos \frac{n\pi}{2} \left(1 - \frac{1}{r}\right) \sin \frac{n\pi}{2r}$$

$n = 1, 3 \ldots$

Three methods of modifying the Fourier coefficients were tried. All of these methods distort the original function and hence a balance must be reached between this distortion and the reduction in Gibbs oscillations. The methods used were:

Sigma Factor This method is described by Lanczos[17] and involves multiplying the Fourier coefficients by a factor σ_k.

$$\sigma_k = \frac{\sin k\pi/n}{k\pi/n}$$

where n = the number of Fourier terms to be considered

$k = k^{th}$ Fourier term.

The effect of multiplying by the sigma factors is essentially to replace a function $f(x)$ by $f(\bar{x})$ where

$$f(\bar{x}) = \frac{n}{2\pi} \int_{-\frac{\pi}{n}}^{\frac{\pi}{n}} f(x + t)\, dt$$

This new function smooths the original function by taking at each point the arithmetic mean between the limits $\pm\pi/n$. Multiplication by the sigma factors can be repeated on the new function, i.e. if the sigma factors were to be applied twice, the classical Fourier coefficients would be multiplied by σ_k^2. At each step the convergence becomes stronger, but the operation of local smoothing distorts the function and stronger convergence is obtained, not to the original function but to a modified function. The reduction in Gibbs oscillations and distortion of the function is shown in Figure 2.3 for a rectangular anchorage block, where it can be seen that for σ_k^2 the slope of the graph is less than σ_k. As a steep slope is required in order that the line load is applied as near the end of the shell as possible, any use of the sigma factor beyond σ_k is not advisable.

Fejér Arithmetic Mean Again described by Lanczos[17], this method involves taking the arithmetic mean of the partial sums of the Fourier coefficients up to the nth term.

If $S_o = f_o$, $S_1 = f_o + f_1$, $S_2 = f_o + f_1 + f_2$ etc.

$$\sigma_n = \frac{S_o + S_1 + S_2 + \cdots S_{n-1}}{n}$$

$$\text{Lim. } \sigma_n = f(x)$$

This is equivalent to multiplying each Fourier term by $P_k(n)$

where $P_k(n) = (1 - \frac{k}{n})$

The summation converges to $f(x)$ from below as shown in Figure 2.4, for a rectangular anchorage pulse. Figure 2.4 also shows that the Gibbs oscillations can sometimes be completely eliminated, but that the slope at the discontinuity is less than that for the σ_k factor (Figure 2.3).

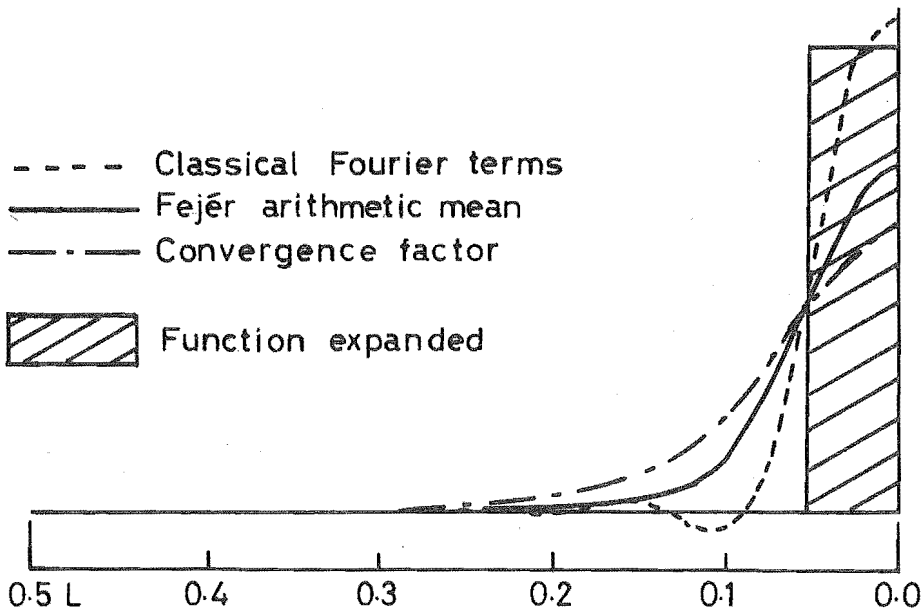

FIG. 2.4 EFFECT OF FEJÉR ARITHMETIC MEAN AND CONVERGENCE FACTOR.

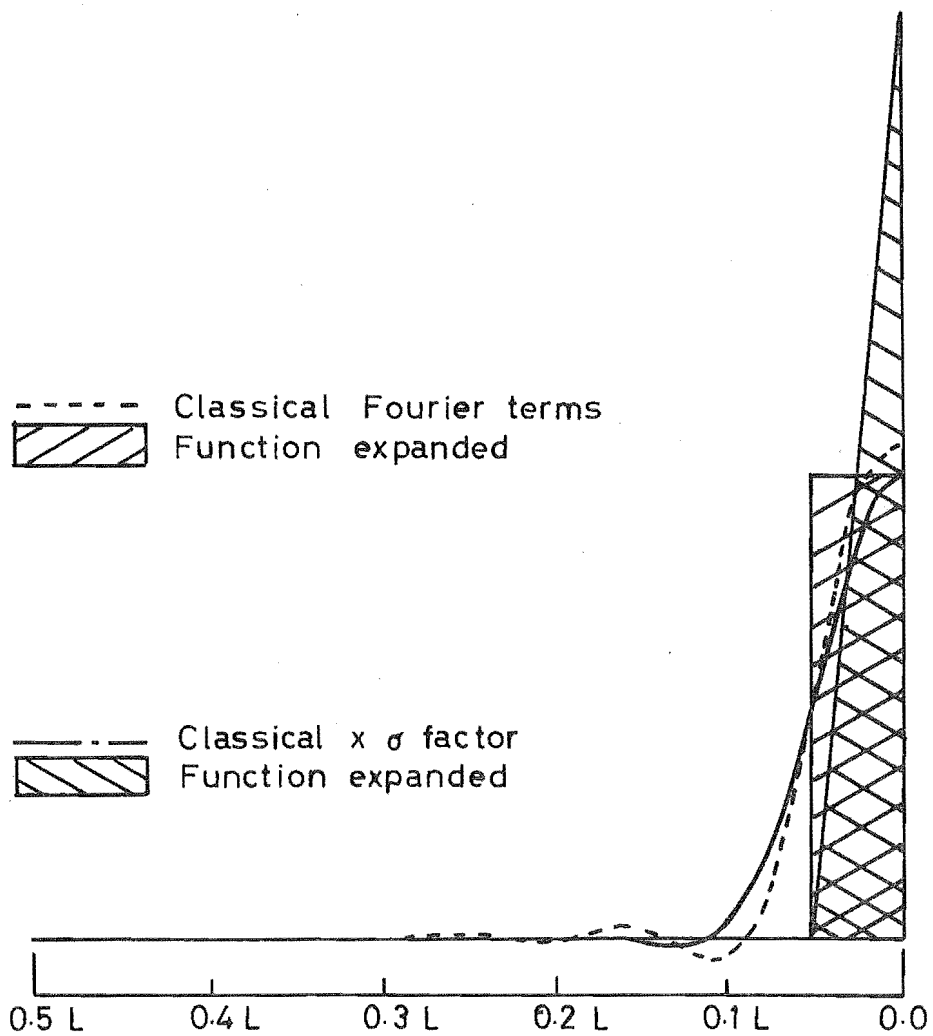

FIG. 2.5 COMPARISON OF TRIANGULAR AND RECTANGULAR PULSE EXPANSIONS.

Convergence Factor This method is presented by Bary[18]. Each Fourier term is multiplied by $1/\log_e k$ except when $k = 0$ or 1. Figure 2.4 shows that although the convergence factors eliminate the Gibbs oscillations, the slope at the discontinuity is less than that given by the other methods.

2.3.6 Convergence of Anchorage Loads

As the distance over which the anchorage pulse is assumed to act is decreased, the rate of convergence of the Fourier series decreases.

The best method of applying the anchorage force using a rectangular pulse is to use the classical Fourier coefficients and a pulse spread 0.05L into the shell. This is the same as suggested by Bryant and Scrivener. For a triangular pulse the best method is to use the σ_k x classical Fourier coefficients, spreading the pulse again 0.05L into the shell. These two expansions are compared in Figure 2.5. There is little difference between the two expansions although σ_k x classical Fourier coefficients would appear to be better as with this expansion the total anchorage force is applied to the shell closer to the traverse. Computer results from the D.K.J. program show negligible difference between the two expansions, except near the anchorage line close to the traverse.

The above discussion is for 10 Fourier terms; however, similar behaviour occurs for different numbers of terms. If less than 10 terms are used the Gibbs oscillations will be greater and the slope at the discontinuity less. The choice of method would depend on whether the force is to be applied near the end of the shell or whether the oscillations are to be dampened.

Rish[19], in connection with the prestressing of edge beams, has suggested a method for reducing the number of Fourier terms required. The prestressing force is applied as a triangular shear pulse spread 0.25 L into the shell, which gives an almost perfect parabolic distribution after 4 Fourier terms as shown in Figure 2.6.

Using a simplified form of the characteristic equation an edge correction is then made to return the prestress force to the corners of the shell by applying corrective shear forces to both the edge beam and shell edge. The corrective shear forces increase linearly to the traverses, from zero at the quarter points, and their effect on the prestress force distribution in the shell is shown in Figure 2.6.

It would appear that this technique could also be used for prestressing in the shell surface if the generator line load method is used. However, the technique was not tried out as it was felt it would give no more accuracy than the present D.K.J. computer program and that a reduction in the number of Fourier terms summed would make only a slight difference in computation time required.

2.3.7 Convergence of Line Loads

Similar trends between different Fourier expansions occur for line loads as for the anchorage loads. The best methods are the classical Fourier coefficients used by Bryant and Scrivener or σ_k x classical Fourier coefficients. These are compared in Figure 2.7 for a line load at L/4 , similar trends occurring for line loads at other positions along the shell length.

From Figure 2.7 it can be seen that the choice of method depends on whether a better peak is required (classical

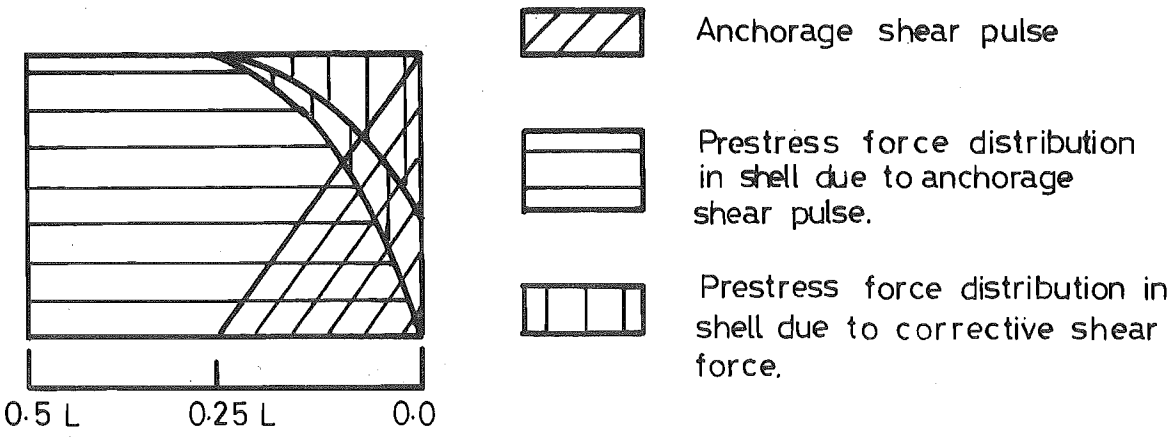

FIG. 2·6 PRESTRESS FORCE DISTRIBUTION USING RISH'S METHOD.

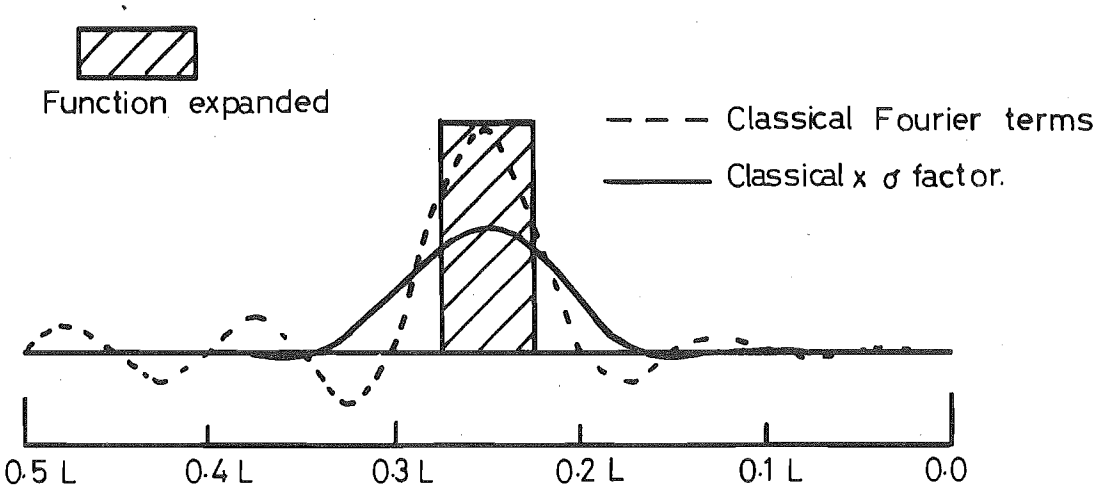

FIG. 2·7 COMPARISON OF LINE LOAD EXPANSIONS.

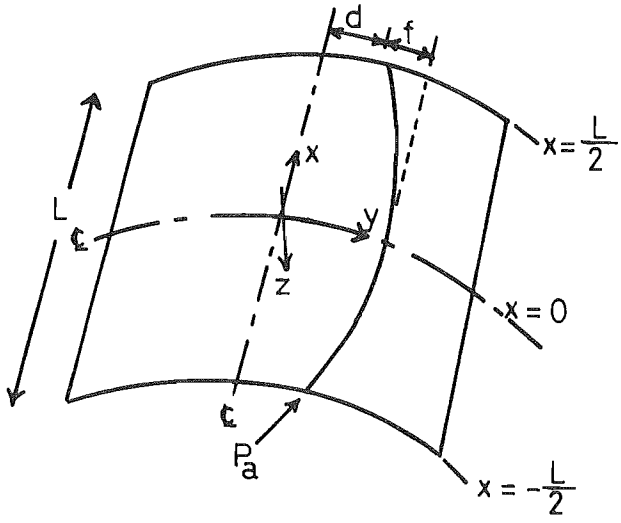

FIG. 2·8 CURVILINEAR SHELL COORDINATE SYSTEM

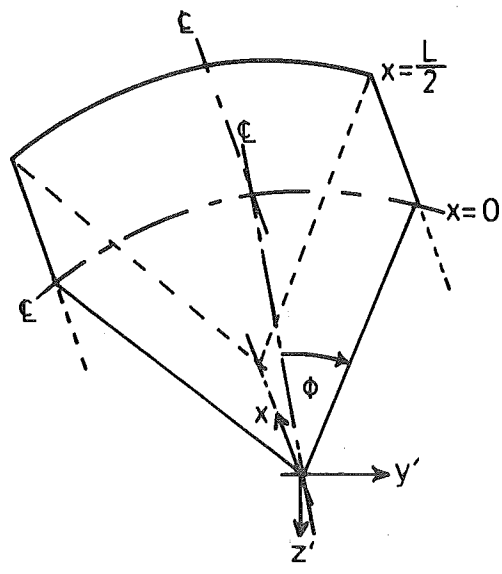

FIG. 2·9 CARTESIAN SHELL COORDINATE SYSTEM

coefficients) or whether a better convergence of the line load, but spread over a greater length of shell, is desired. However, as the effect of line loads is of a secondary order compared with the anchorage load, the difference between the effects from the two expansions will be small, except close to the line load.

2.3.8 Line Loads Due to a Parabolic Cable In A Circular Curve

The line loads derived in this section occur when a cylindrical shell of constant radius is prestressed with a cable which is parabolic in the developed shell surface.

Using the curvilinear coordinate system of Figure 2.8 the parametric equations of the parabola in the developed shell surface can be written:

$$x = \frac{t}{2a}$$

$$y = e - ax^2 \qquad \text{where} \quad e = d + f$$

$$= e - \frac{t^2}{4a} \qquad\qquad a = \frac{4f}{L^2} .$$

Bryant and Scrivener have used curvilinear coordinates to calculate the line loads due to a parabolic cable in a circular curve, however it is simpler to use the Cartesian coordinates of Figure 2.9 and thus the parametric equations become:

$$x = \frac{t}{2a}$$

$$y' = R \sin \phi \qquad \text{where} \quad \phi = \frac{y}{R}$$

$$z' = -R \cos \phi \qquad\qquad = \frac{4ae - t^2}{4aR}$$

A point on the cable can be defined by a position vector

$$r(t) = \left(\frac{t}{2a} , R \sin \phi , - R \cos \phi\right),$$

therefore

$$\frac{dr}{dt} = \frac{1}{2a} (1, - t \cos \phi, - t \sin \phi)$$

and $\frac{d^2r}{dt^2} = \frac{1}{2a}(0, -\cos\phi + c\sin\phi, -\sin\phi - \cos\phi)$, $c = -\frac{t^2}{2aR}$

Unit Tangent - T Kreyszig[20] (pp271) defines the unit tangent, T , as

$$T = \frac{\frac{dr}{dt}}{\left|\frac{dr}{dt}\right|}$$

$$= \frac{\frac{1}{2a}(1, -t\cos\phi, -t\sin\phi)}{\frac{1}{2a}\sqrt{1+t^2}}$$

$$= \frac{1}{\sqrt{1+t^2}}(1, -t\cos\phi, -t\sin\phi).$$

Curvature - κ

$\kappa N = \frac{dT}{ds} = \frac{dT}{dt} \cdot \frac{dt}{ds}$ N = Principal Normal

κ = Curvature

therefore

$$\kappa N = \frac{2a}{(1+t^2)^2}\{t, -[(1+t^2)(\cos\phi - c\sin\phi) - t^2\cos\phi], - [(1+t^2)(\sin\phi + c\cos\phi) - t^2\sin\phi]\}.$$

Now $\kappa = \left|\frac{dT}{ds}\right|$

$$= \frac{2a}{(1+t^2)}\sqrt{t^2 + (1+t^2)(\cos^2\phi + \sin^2\phi)\left(c^2 + \left[1 - \frac{t^2}{1+t^2}\right]^2\right)}$$

therefore

$$\kappa = \frac{2a}{(1+t^2)^{3/2}}\sqrt{t^2c^2 + c^2 + 1}$$

Principal Normal - N

$$N = \frac{\frac{dT}{ds}}{\left|\frac{dT}{ds}\right|}$$

$$= \frac{(1+t^2)^{3/2}}{2a\sqrt{t^2c^2+c^2+1)}} \quad \frac{2a}{(1+t^2)^2} \{-t,-[(1+t^2)(\cos\phi - c\sin\phi) - t^2\cos\phi]$$

$$- [(1+t^2)(\sin\phi + c\cos\phi) - t^2\sin\phi]\}$$

$$= \frac{1}{(1+t^2)^{\frac{1}{2}}(t^2c^2+c^2+1)} \{-t,-[\cos\phi - c\sin\phi - t^2c\sin\phi],$$

$$-[\sin\phi + c\cos\phi + t^2c\cos\phi]\}$$

Line Loads in x, y', z' Coordinates Consider a small length of cable δ_s shown in Figure 2.10.

$$\delta\theta = \frac{\delta s}{R} = \delta_s \kappa$$

The resultant force due to the cable curvature is $P\delta\theta$ and it is directed along the principal normal.

$$P\delta\theta = P\delta_s\kappa$$

This can be written as a force/unit length in the x direction

$$= P\kappa \frac{ds}{dx} .$$

Similarly, forces directed along the unit tangent/unit length in the x direction

$$= (\omega + \nu.P\kappa) \frac{ds}{dx} ,$$

where ω = wobble factor

= force/unit length to bodily move the cable.

Now $\frac{ds}{dx} = \frac{ds}{dt} \cdot \frac{dt}{dx}$ and $x = \frac{t}{2a}$

therefore $\frac{dt}{dx} = 2a$.

Also $\frac{ds}{dt} = \sqrt{(\frac{dx}{dt})^2 + (\frac{dy'}{dt})^2 + (\frac{dz'}{dt})^2}$

$$= \frac{1}{2a}\sqrt{1+t^2}$$

therefore $\frac{ds}{dx} = \sqrt{1+t^2}$

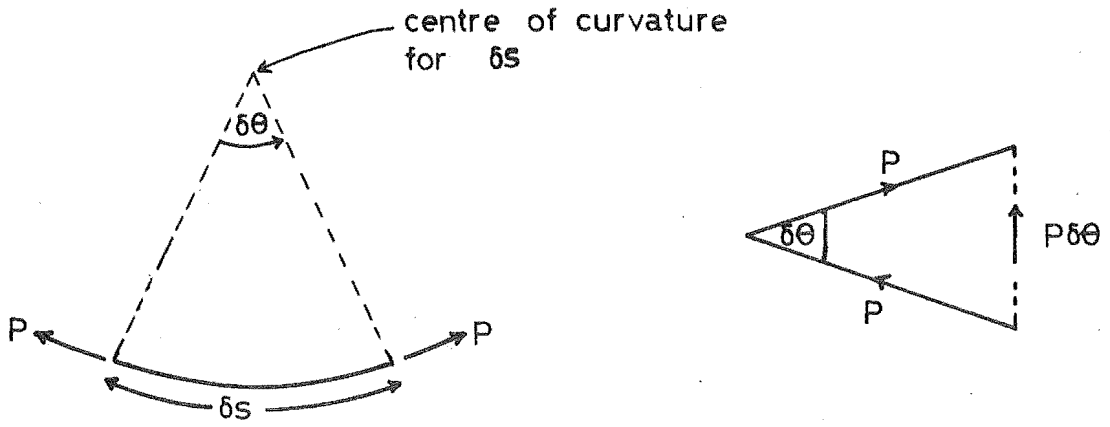

FIG. 2·10 FORCES ACTING ON AN ELEMENTAL LENGTH OF CABLE.

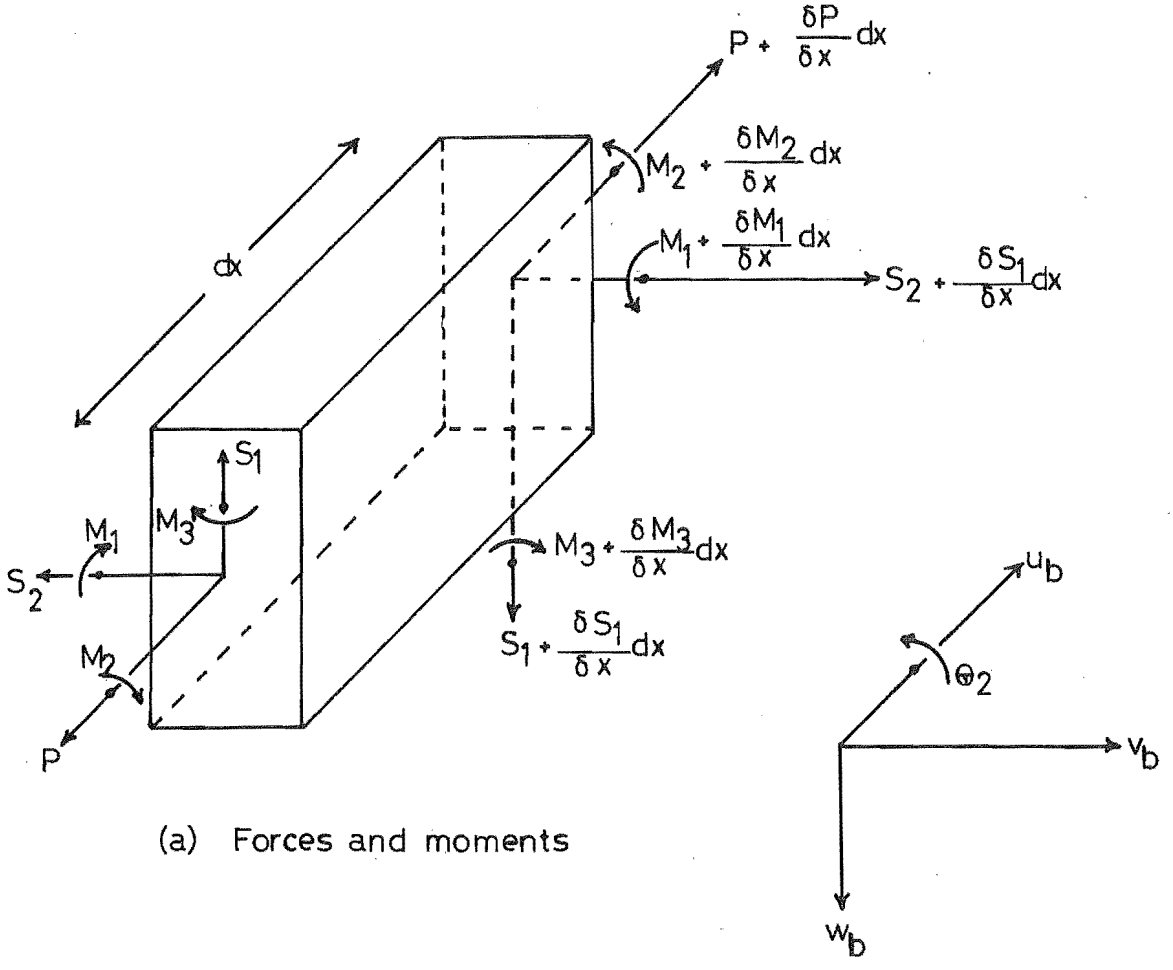

(a) Forces and moments

(b) Displacements

FIG. 2·11 POSITIVE EDGE BEAM ACTIONS AND DISPLACEMENTS.

If $g = \sqrt{t^2c^2 + c^2 + 1}$ and $h = \sqrt{1 + t^2}$

the curvature force

$$P\kappa \frac{ds}{dx} = \frac{2agP}{h^2}$$

and tangential force

$$(\omega + \nu P\kappa)\frac{ds}{dx} = (\omega + \frac{2ag}{h^3}\nu P)h \ .$$

Resolving these forces in the x, y', z' directions

$$F_x = -\frac{2atP}{h^3} + \omega + \frac{2ag}{h^3}\nu P$$

$$F_y' = -\frac{2a}{h^3}P(\cos\phi - c\sin\phi - t^2c^2\sin\phi) - (\omega + \frac{2ag}{h^3}\nu P)t\cos\phi$$

$$F_z' = -\frac{2aP}{h^3}(\sin\phi + c\cos\phi + t^2c^2\cos\phi) - (\omega + \frac{2ag}{h^3}\nu P)t\sin\phi$$

Line Loads in x, y, z Coordinates The forces F_x, F_y', F_z' can now be resolved into components along the curvilinear coordinate directions.

$$F_x = F_x = -\frac{2atP}{h^3}P + (\omega + \frac{2ag}{h^3}\nu P)$$

$$F_y = F_y'\cos\phi + F_z'\sin\phi = \frac{2a}{h^3}P - (\omega + \frac{2ag}{h^3}\nu P)t$$

$$F_z = F_z'\cos\phi - F_y'\sin\phi = \frac{-2acP}{h}$$

These are the same forces obtained by Bryant and Scrivener except that in their paper they have mistakenly multiplied the forces by h .

At the traverse, the anchorage force component in the x direction is

$$P_{ax} = P_a(\frac{dx}{ds})_{x=\frac{L}{2}} \qquad P_a = \text{Anchorage force}$$

$$= \frac{P_a}{\sqrt{1 + a^2L^2}} \ .$$

2.4 EDGE BEAMS

The effect of edge beams on a cylindrical shell can be considered by means of a complementary function solution[9,10].

In order to obtain compatibility with the shell edge, all loading on the edge beam must also be expanded as Fourier series. For a prestress cable draped parabolically in the edge beam, the loading on the edge beam can be expressed in the form,

$$P_B = \frac{4 P_A}{\pi} \sum_n \frac{1}{n} \cos \frac{n\pi x}{L}$$

$$M_B = \frac{4 P_A}{\pi} \sum_n \frac{1}{n} \cos \frac{n\pi x}{L}$$

$$V_B = \frac{32 P_A f}{L^2 \pi} \sum_n \frac{1}{n} \cos \frac{n\pi x}{L}$$

where P_A = prestress anchorage force acting on edge beam

P_B = normal force along edge beam due to prestressing

M_B = moment along edge beam due to prestressing

e = anchorage eccentricity at end

V_B = shear force along edge beam due to prestressing

f = cable drape.

Positive actions and displacements at the centroid of the edge beam are shown in Figure 2.11. The solution requires that compatibility of displacements and actions along the shell-edge beam junction be maintained. In order to do this, a translation matrix is used to obtain the actions and displacements of the edge beam at the junction. A rotation matrix is then applied to obtain the actions and displacements in the same coordinate system as that of the shell, at the shell edge.

2.5 EFFECT OF TRAVERSE ON THE DISTRIBUTION OF ANCHORAGE FORCES

The distribution of prestress anchorage force along the end of the shell will depend on the properties of the traverse. For instance if a traverse is made stiffer, the forces will be spread into the shell over a greater arc length. Hence rather than assuming that the anchorage force is spread equally down two generators at some arbitrary distance close to the anchorage, an analysis technique is presented below which takesinto account the effect of the traverse stiffness on the distribution of anchorage forces to the shell. The effect of the traverse is particularly important when the cable is near the edge of the shell as the transverse moment and radial deflection may be significantly affected.

The following analysis technique, based on the theory of beams on elastic foundations, is a means of calculating the distribution of anchorage prestress force, including the effect of the traverse (beam) on the end of the shell (elastic foundation). In Section 2.5.7 the method is shown to give good correlation with experimental results.

2.5.1 Assumptions

The basic assumptions made are that both in-plane shear force between the traverse and the shell, and curvature of the shell are neglected. The first approximation is not serious as the in-plane shear force between shell and traverse due to prestressing is generally small, and the second approximation is reasonable if the anchorage force distribution is spread over a relatively short arc length, as would occur in a majority of shells.

2.5.2 Theory

The theory for beams on elastic foundations has been taken from Timoshenko[21].

For a beam on an elastic foundation, the reaction from the foundation/unit length = - ky = W

where y = deflection of beam and foundation

k = reaction/unit length when y = 1 .

Now for a beam $W = EI_Z \frac{d^4y}{dx^4}$

$= -ky$

therefore $EI_Z \frac{d^4y}{dx^4} = -ky$.

The general solution is $y = e^{\beta x}(A \cos \beta x + B \sin \beta x) + e^{-\beta x}(C \cos \beta x + D \sin \beta x)$

where $\beta = \sqrt[4]{\frac{k}{4EI_Z}}$

Considering the case of an infinite beam with a single point load, P , the boundary conditions are:

i) At points infinite from the load, y = 0.0 ,

therefore $A = B = 0$ and $y = e^{-\beta x}(C \cos \beta x + D \sin \beta x)$

ii) At point where the load is applied, i.e. $x = 0$, $\frac{dy}{dx} = 0$,

therefore $C = D$ and $y = C e^{-\beta x}(\cos \beta x + \sin \beta x)$

Now for $x = 0$, $\frac{d^3y}{dx^3} = 4\beta^3 C e^{-\beta x} \cos \beta x$

and shear force, $V_{x=0} = -EI_Z(\frac{d^3y}{dx^3}) = -\frac{P}{2}$.

Therefore $C = \frac{P}{8\beta^3 EI_Z}$

$Y = \frac{P\beta}{2k} e^{-\beta x}(\cos \beta x + \sin \beta x)$

and the moment $M = -EI \frac{d^2y}{dx^2}$

$= -\frac{P}{4\beta} e^{-\beta x}(\sin \beta x - \cos \beta x)$.

Using the notation $\phi = e^{-\beta x}(\cos \beta x + \sin \beta x)$

$\Psi = -e^{-\beta x}(\sin \beta x - \cos \beta x)$

$$\theta = e^{-\beta x}\cos \beta x$$

$$\xi = e^{-\beta x}\sin \beta x$$

$$\left.\begin{aligned} y &= \frac{P\beta}{2k}\,\phi(\beta x) \\ M &= \frac{P}{4\beta}\,\Psi(\beta x) \\ V &= \frac{P}{2}\,\theta(\beta x) \end{aligned}\right\} \quad \ldots\ (2.2)$$

Considering the case of a moment, M_o, being applied at the end of a semi-infinite beam it can be shown that:

$$\left.\begin{aligned} y &= \frac{M_o}{2\beta^2 EI_z}\,\xi(\beta x) \\ M &= M_o\,\theta(\beta x) \\ V &= -\beta M_o\,\phi(\beta x) \end{aligned}\right\} \quad \ldots\ (2.3)$$

Using the above two cases, the distribution of y, M, V can be found for a point load on a beam of semi-infinite length, as shown diagrammatically in Figure 2.12. Referring to Figure 2.12, the redundant forces M_o' and V_o' at the end of a semi-infinite beam when it is "cut" from an infinite beam, can be found from equation (2.2).

i.e. $M_o' = \frac{P}{4\beta}\left[\Psi(\beta c)\right]$ and $V_o' = \frac{P}{2}\left[\theta(\beta c)\right]$.

From equations (2.2) and (2.3), the actions V_o'' and M_o'', due to corrective forces Q_o and M_o applied at the end of the semi-infinite beam can be found.

i.e. $M_o'' = \frac{Q_o}{4\beta} + \frac{M_o}{2}$ and $V_o'' = -\frac{Q_o}{2} - \frac{M_o\beta}{2}$.

Hence by equating $M_o' + M_o'' = 0$ and $V_o' + V_o'' = 0$ it can be shown that

$$\left.\begin{aligned} Q_o &= P\,(2\left[\theta(\beta c)\right] + \Psi(\beta c)) \\ M_o &= -\frac{P}{\beta}\,(\Psi(\beta c) + \theta(\beta c)) \end{aligned}\right\} \quad \ldots\ (2.4)$$

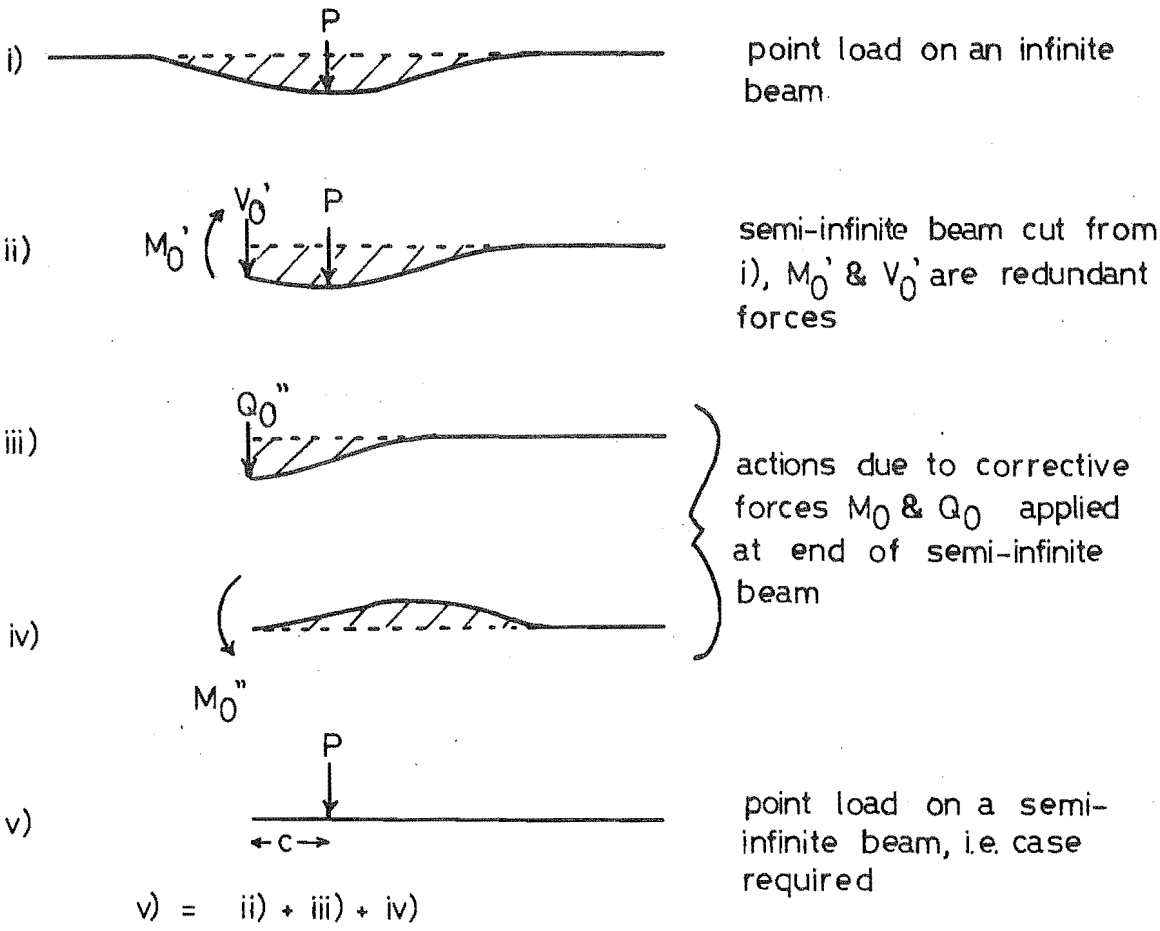

FIG. 2.12 DISTRIBUTION OF ACTIONS FOR A POINT LOAD ON A SEMI-INFINITE BEAM.

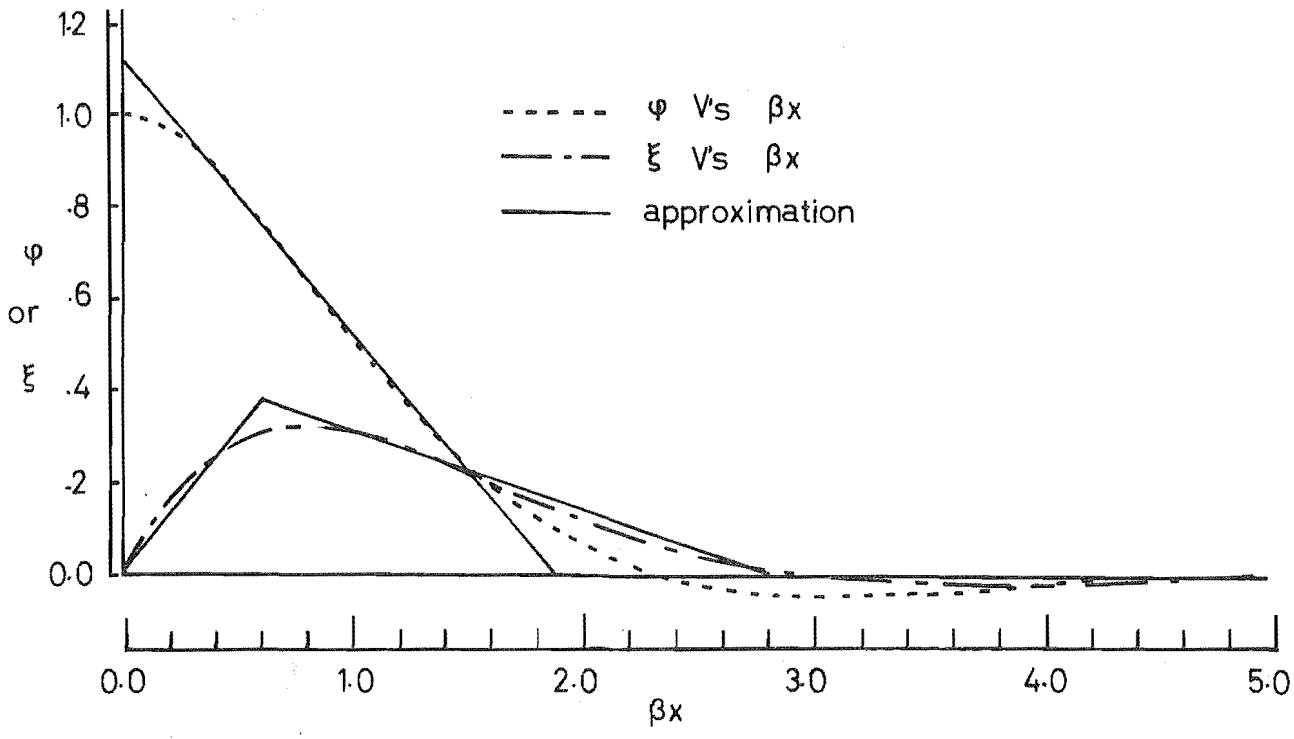

FIG. 2.13 VARIATION OF φ AND ξ WITH βx.

Thus for a point load distance c from the end of a semi-infinite beam,

$$W = -ky = \frac{P\beta}{2}\{\phi[\beta(c-x)]\} + \frac{Q_o\beta}{2}\{\phi[\beta(x)]\}$$

$$+ M_o\beta^2\{\xi[\beta(x)]\} \qquad .....(2.5)$$

i.e. W is a function of ϕ and ξ. These two functions are plotted in Figure 2.13 for variation in βx.

The distance from a point force over which bending occurs is given by Timoshenko as $^5/\beta$, however for practical deformations and forces a value of $^2/\beta$ would seem reasonable. This means that a beam may be considered semi-infinite if part of it lies further than $^2/\beta$ from the point force. If a point force is applied to a beam at a distance greater than $^2/\beta$ from both ends of the beam (i.e. an "infinite" beam) the last two terms of equation (2.5) can be ignored.

To calculate the distribution of prestress anchorage force from the traverse (beam) to the shell (elastic foundation), equation (2.5) is used. Typical force distributions are shown in Figure 2.14, both for an anchorage force close to and away from the edge. When the anchorage is near the edge the maximum force/unit arc length is greater than when the anchorage is away from the edge. Also the maximum force/unit arc length occurs at the edge of the shell and not at the anchorage.

The technique can be used in a generator - line load type computer program by summing the force distribution over discrete arc lengths of the shell. The resultant forces are then applied to the shell as point loads at the centroids of the force blocks.

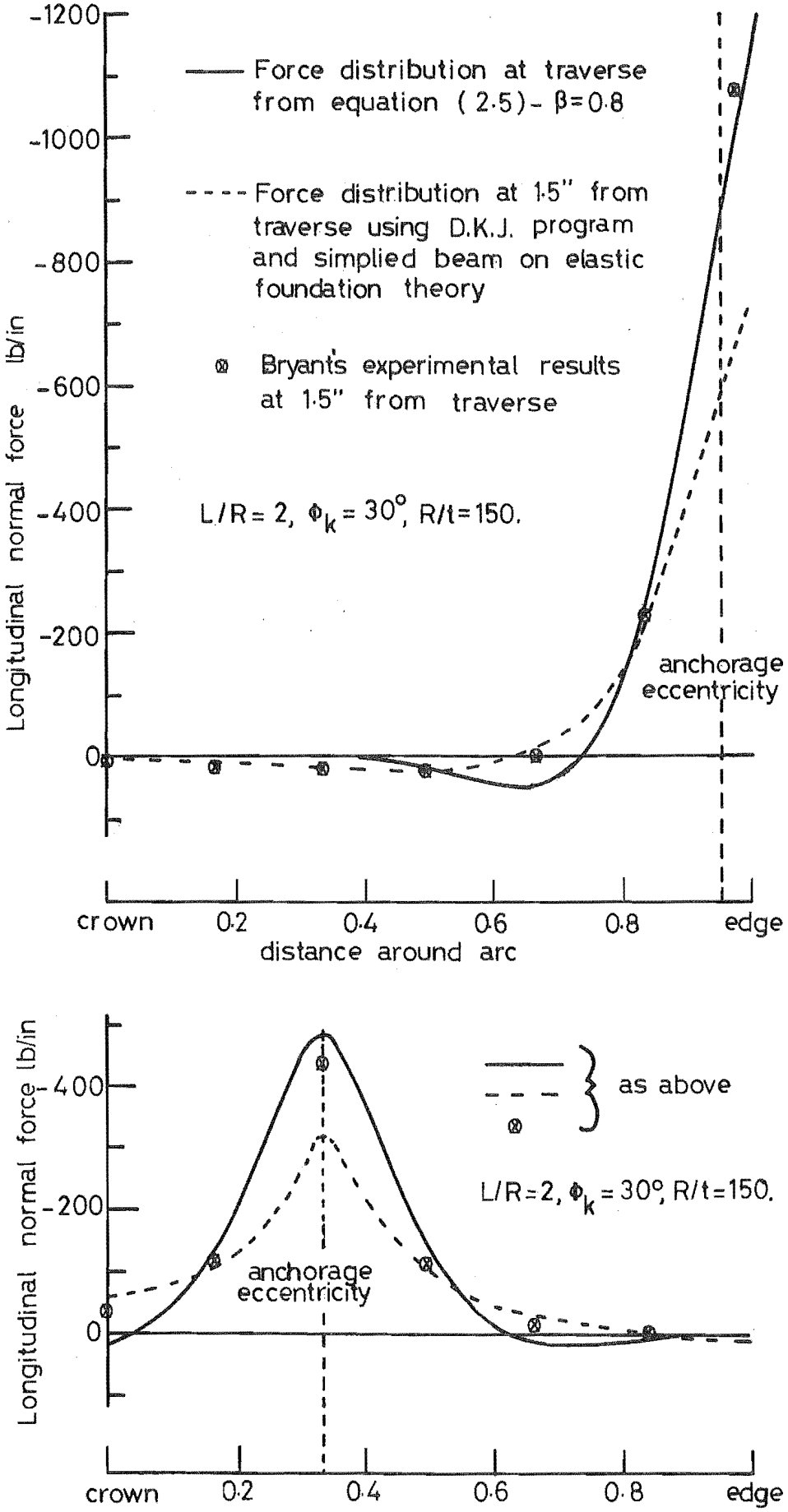

FIG. 2.14 COMPARISON OF EXPERIMENTAL AND THEORETICAL N_1 DISTRIBUTIONS NEAR TRAVERSE

2.5.3 Determination of β

$$\beta = \sqrt[4]{\frac{k}{4E_t I_z}}$$

E_t = Young's modulus of traverse

k = force for unit deflection/unit length

Assuming the shell acts as a column,

$$k = P/\delta = \frac{t E_s}{L}.$$

E_s = Young's modulus of shell

I_z = 2nd moment of area of the traverse

For a solid traverse,

$$I_z = \frac{bd^3}{12}$$ where d = thickness of traverse

b = effective width of traverse.

By considering the A.C.I.[40] recommendations for the effective widths of L-beams, b has been defined by:

$$b \leq 6 \times d$$

$$\leq 1/6 \times \text{anchorage eccentricity}$$

$$\leq 1/2 \times \text{depth of traverse at anchorage}$$

Hence
$$\beta = \sqrt[4]{\frac{12t E_s}{4 L E_t bd^3}}$$

and if $E_t = E_s$

$$\beta = \sqrt[4]{\frac{3t}{L bd^3}} \quad .$$

... (2.6)

2.5.4 Summary of Method

i) Calculate β from equation (2.6)

ii) Calculate M_o and Q_o from equation (2.4)

iii) Using equation (2.5) the distribution of prestress force from the traverse to the shell can be calculated.

N.B. Timoshenko[21] presents tables of ϕ, Ψ, θ and ξ.

2.5.5 Simplification

The above method involves the summing of non-linear relationships in order to find the distribution of prestress force around the arc on the end of the shell. The following procedure, which has been found to give satisfactory results, is suggested in order to simplify calculations.

i) Calculate β from equation (2.6).

ii) Calculate M_o and Q_o from equation (2.4).

iii) Approximate ϕ and ξ curves to the triangular shapes shown in Figure 2.13.

iv) Sum the forces on each side of the anchorage separately, and calculate the centroid of each force block.

v) Use the two forces calculated, acting at their respective centroids, to find the effect of the prestress anchorage force on the shell.

When the anchorage is further than $\frac{1.9}{\beta}$ from the shell edge, the above simplification gives two equal forces, $\frac{P}{2}$, at a distance of $\pm\frac{1.9}{3\beta}$ from the anchorage.

2.5.6 Effect of Change in β

If the relative stiffness of a traverse is increased, β will decrease. Except near the edge, the only effect that a decrease in β will have is to spread the anchorage force over a larger arc length, the distribution curve remaining a similar shape. However, near the edge, as well as spreading over a larger distance, the curve will change shape.

As β is decreased for anchorages near the edge of the

shell, the maximum values of radial deflection and transverse moments also decrease. When the anchorage is away from the edge, there is no significant variation in any actions as β is varied.

2.5.7 Comparison with Experiment

For a shell with an anchorage near the edge, Figure 2.15 shows a comparison of theoretical results with experimental results obtained by Bryant for his shell, test 2, an aluminium model with $L/R = 2$, $R/t = 150$, $\phi_k = 30^o$ and anchorage eccentricity/half arc length = .95. The actions compared are transverse moment along the crown and vertical deflection (due largely to the radial deflection component) along the edge. These are the actions most sensitive to changes in distribution of anchorage force and are being compared at their positions of maximum value. The three sets of theoretical results were obtained using the D.K.J. computer program. Results using Bryant's method were obtained by considering two equal anchorage forces at $\pm R/100$ from the anchorage; and results obtained by considering the effect of the traverse on the distribution of anchorage force on the end of the shell were found by both the simplified method of Section 2.5.5 and the more accurate method summarized in Section 2.5.4. In the latter method the anchorage force distribution was divided into eight point forces. It can be seen from Fig. 2.15 that both the methods where the effect of the traverse is considered give theoretical results which are in good agreement with experimental results. Both for the transverse moment and vertical deflection the simplified method gives slightly lower values than the more accurate method.

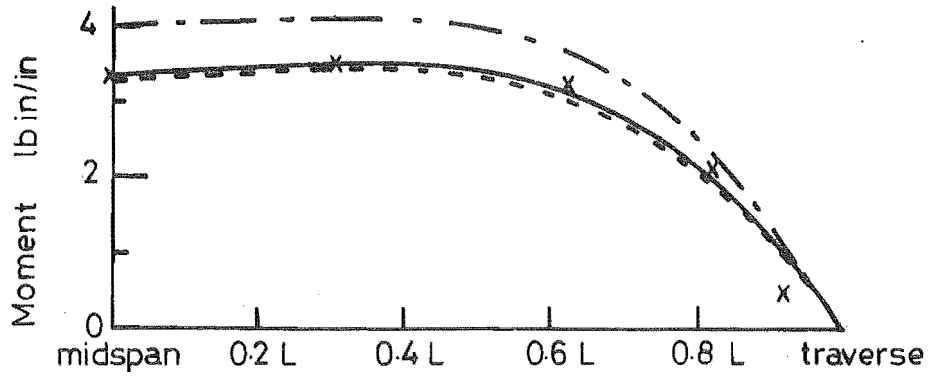

(a) TRANSVERSE MOMENT AT CROWN

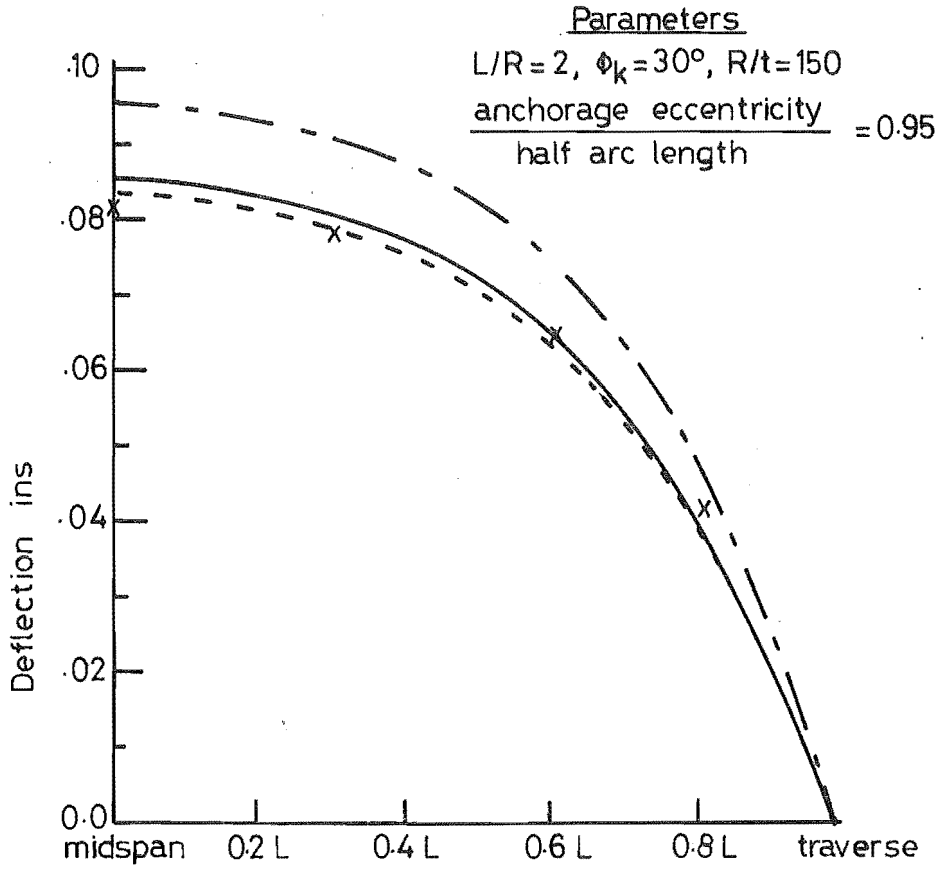

(b) VERTICAL DEFLECTION AT EDGE

x Bryants experimental results.

——— Accurate beam on elastic foundation method - anchorage force considered as 8 point forces. (β = 0·8)

– – – – Simplied beam on elastic foundation method - anchorage force considered as 2 point forces.(β = 0·8)

—·— Bryant & Scrivener method - anchorage force considered as 2 equal point forces.

FIG. 2.15 COMPARISON OF RESULTS FOR ACTIONS MOST AFFECTED BY THE TRAVERSE STIFFNESS

Figure 2.14 shows a comparison of n_1 close to the traverse for two of Bryant's tests, one with the anchorage near the edge and the other with the anchorage away from the edge influence. The experimental results are compared with those obtained from the D.K.J. computer program using the simplified method of considering the effect of the traverse on the distribution of anchorage force, and the actual distribution of prestress anchorage force on the end of the shell given by equation (2.5). The results from the computer program do not predict the peak values accurately and this is to be expected near the traverse, due to the method of applying the anchorage force in the program. However it can be seen that the actual distribution of anchorage force on the end of the shell given by equation (2.5) gives a good indication of the peak values of n_1, for a short distance into the shell.

CHAPTER THREE

ULTIMATE LOAD BEHAVIOUR

From a study of the available literature about experimental tests on cylindrical shells, it is soon evident that there are three basic mechanisms (flexure, buckling, shear) by which a cylindrical shell may fail. Flexural failure may occur either by a beam or a yield line type mechanism. Failure of any particular shell may be a combination of the three mechanisms and of other minor methods of failure, e.g. shell - traverse junction failure.

A method of design for a beam type flexural failure of a prestressed cylindrical shell without edge beams is presented below. For completeness the other failure mechanisms are detailed and discussed with particular reference to prestressed cylindrical shells.

3.1 BEAM TYPE FAILURE

This type of failure is common in long reinforced cylindrical shells and is characterised by transverse flexural cracks emanating from the edge at midspan. The whole shell acts as a beam, simply supported on its traverses. Failure is generally initiated by yielding of the tensile reinforcement, followed by fracture of the tensile reinforcement or by crushing of the concrete at the midspan crown.

Lundgren[34], in conjunction with his stringer theory, first proposed a beam type analysis to obtain the ultimate carrying capacity of a cylindrical shell. In this type of analysis, the longitudinal applied moment on the shell section at ultimate load is assumed to be resisted by a couple formed

between the longitudinal compressive force of the compressive stress block at the crown, and the tensile force carried by the longitudinal reinforcement. Lundgren assumed that the shell acted as two inclined beams with effective lever arm d_e as shown in Figure 3.1. However, for vertical loading, the same results are obtained if the shell is assumed to act as a whole, with effective lever arm d' as shown in Figure 3.1. This is the method Baker[35] proposed for a beam type analysis for long cylindrical shells. In addition, Baker gives a method for calculating the transverse bending moment on a transverse strip of the shell by considering the external load on the strip, and the shear difference across the strip. Baker also considered short shells and proposed a method[36] in which some of the load is carried to the supports by longitudinal slab bending between the supports. Gouda[37] tested a long reinforced shell with edge beams and found that Baker's theory gave good agreement with experiment when the ultimate concrete stress was reduced to take account of buckling. Ernst et al[38] have extended the work of Lundgren and Baker to take into account diagonal tensile stresses, the thrust caused by the horizontal components of the difference in tangential shears, and the inelastic instability of the shell. They carried out a series of three tests to confirm the technique but unfortunately all their shells failed in diagonal tension and hence no comparison of experimental and theoretical flexural beam type failure results was possible.

Sawczuk[39] has applied plastic beam theory to the ultimate load analysis of cylindrical shells in connection with his kinematic limit analysis technique, and has obtained good correlation with some experimental shells tested.

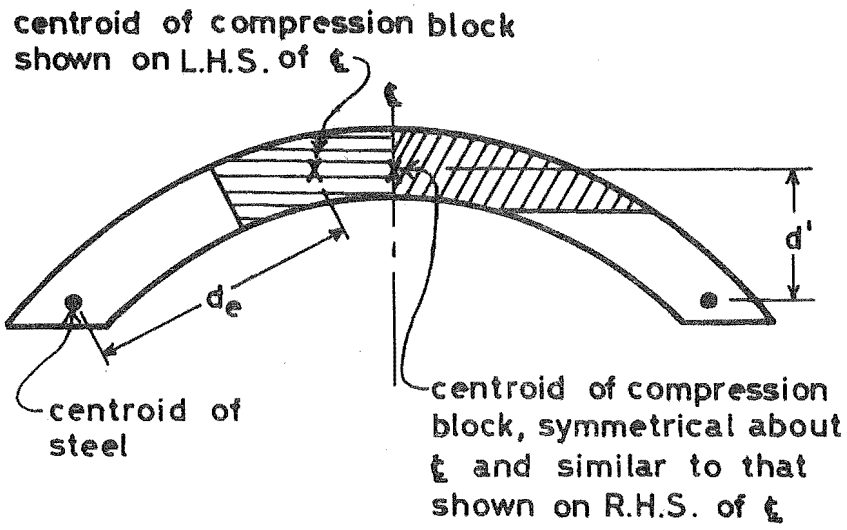

d_e — lever arm assumed by Lundgren

d' — lever arm used in this thesis

FIG. 3.1 LEVER ARMS FOR ULTIMATE LOAD ANALYSIS

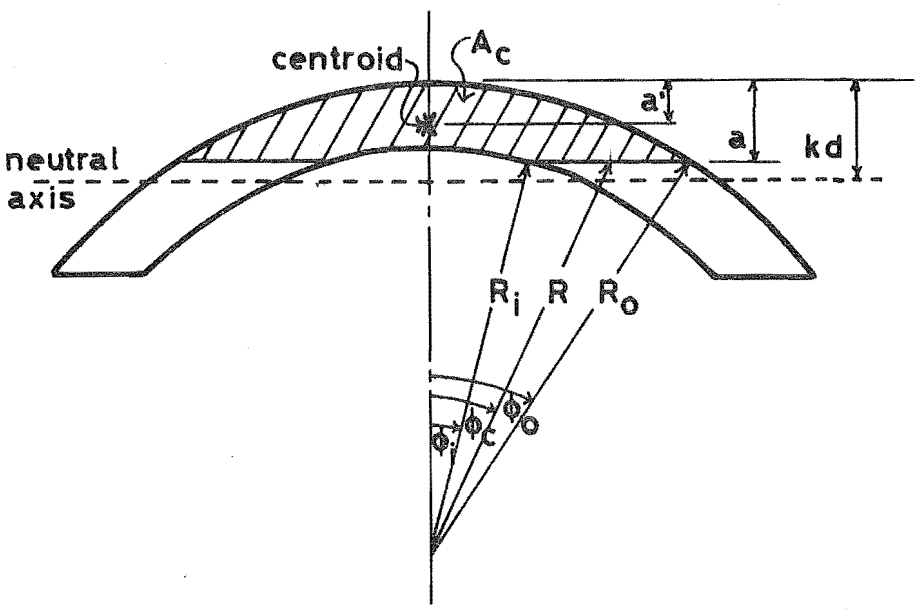

FIG. 3.2 CONCRETE COMPRESSION BLOCK NOTATION

Although short and intermediate length reinforced shells seldom fail in a beam type manner, prestressed shells of these lengths may do so. This is because with prestressed shells, edge beams can be eliminated and hence the lever arm and ultimate moment capacity are substantially reduced.

The following analysis technique is suggested as a means of calculating the ultimate moment capacity of a prestressed cylindrical shell without edge beams. It has been found to give results which agree well with experimental results obtained by the author from a series of five model tests. The method of analysis is similar in principle to previous techniques for cylindrical shells, which are in turn similar to the conventional ultimate load analysis technique of prestressed concrete beams.

3.1.1 Assumptions

(i) Failure is primarily a flexural failure.

(ii) Plane sections before loading remain plane at ultimate load.

(iii) Change in shape of shell cross-section is neglected.

(iv) Tensile strength of concrete is neglected.

(v) Tendons are bonded.

3.1.2 Flexural Failure Modes

Two types of failure are liable to occur:

(i) Excessive elongation of the prestressing steel before failure, causing the neutral axis to rise with eventual failure by fracture of the tendon or crushing of the concrete at the crown - "under-reinforced".

(ii) Little elongation of the tendons occurring before

a brittle fracture of the concrete takes place at the crown - "over-reinforced".

Of these failures, failure by elongation of the prestressing steel followed by crushing of the concrete at the crown is the most desirable. Warning of imminent failure is given and crushing of the concrete will result in a less catastrophic failure than fracture of the tendons. An analysis technique is given in the next section.

3.1.3 Analysis of "Under-Reinforced" Shell

In the following analysis only the effect of the prestressing steel is included. Non-prestress steel can be included as shown in Section 3.1.7.

At ultimate load the external moment is resisted by an internal couple comprising the tensile force in the prestressing steel and a compressive force in the concrete at the crown, the extreme fibre of the concrete being at yield strain. Accepted values for concrete strain at ultimate load vary from 0.003 to 0.004. A value of 0.003 has been used in the calculations for this thesis, which is the value suggested by the A.C.I.[40]. The steel strain at ultimate load, e_{su}, can only be established by a trial and error process. However, in most shells the neutral axis will be high and thus e_{su} will be large. As a first approximation e_{su} is taken to be the nominal yield strain, e_{sy} (.2% set). The steel strain, e_{su}, calculated using the approximation, should be checked to ensure that e_{sy} is in fact reached at ultimate load.

Procedure

i) Calculate the total tendon force, T_t, assuming the tendons are at yield.

$$T_t = f_{sy} A_s$$

where f_{sy} = nominal steel yield stress (.2% set)

A_s = area of prestressing steel.

ii) Calculate the area of concrete, A_t, required to balance T_t assuming maximum concrete strain has been reached, and using the conventional[40] rectangular stress block for concrete in compression at ultimate moment. The maximum average concrete stress,

$$f_c = .85 f'_c$$

where f'_c = concrete cylinder strength,

therefore $A_t = \frac{T_t}{f_c}$

iii) Calculate a', the distance from the top of the crown to the centroid of the concrete compression block A_t. Parameters defining the compressive stress block are given in Figure 3.2.

If the depth of the compression block, a, is less than the shell thickness t then:

$$A_t = R_o^2 (\phi_o - \frac{\sin 2\phi_o}{2})$$

and a' = depth to the centroid of compression block

$$= R_o (1 - \frac{2 \sin \phi_o - \sin 2\phi_o \cos \phi_o}{3(\phi_o - \frac{\sin 2\phi_o}{2})})$$

where $\phi_o = \cos^{-1}(\frac{R_o - a}{R_o})$

$R_o = R + \frac{t}{2}$

R = radius of shell middle surface

t = shell thickness

ϕ_o can be calculated by trial and error from

$A_t = R_o^2(\phi_o - \frac{\sin 2\phi_o}{2})$. However it can be most easily found by rearranging the equation as

$$\frac{2A_t}{R_o^2} = 2\phi_o - \sin 2\phi_o$$

$\frac{2A_t}{R_o^2}$ can be calculated and the value of $2\phi_o$ found directly from Figure 3.3. As a' is small, the ultimate moment will be little affected by small errors in the value of a'. By approximating the compressive stress block to a triangle, a' can be simplified to,

$$a' = \frac{2}{3} R_o(1 - \cos \phi_o)$$

If a is greater than t :

$$A_t = \phi_o R_o^2 - \phi_i R_i^2 - R_o R_i \sin (2[\phi_o - \phi_i])$$

$$a' = R_o - \frac{\frac{2}{3}\{R_o^3 \sin\phi_o - R_i^3 \sin\phi_i - R_o R_i (R_o - a)\sin(2[\phi_o - \phi_i])\}}{\phi_o R_o^2 - \phi_i R_i^2 - R_o R_i \sin(2[\phi_o - \phi_i])}$$

where $\phi_c = \cos^{-1}(\frac{R_o - a}{R})$, $\phi_i = \cos^{-1}(\frac{R_o - a}{R_i})$

$$R_i = R - \frac{t}{2} .$$

These expressions can be simplified with little loss of accuracy by,

$$A_t = 2R\phi_c t$$

$$a' = R(1 - \frac{\sin\phi_c}{\phi_c}) + \frac{t}{2}$$

and $\phi_c = \frac{A_t}{2Rt}$.

To find whether a is greater or less than t, assume $a = t$ and $A_c = 2R\phi_c t$.

Then if $A_t < A_c$, $a < t$

if $A_t > A_c$, $a > t$

iv) The lever arm, d', of the prestressing tendon and

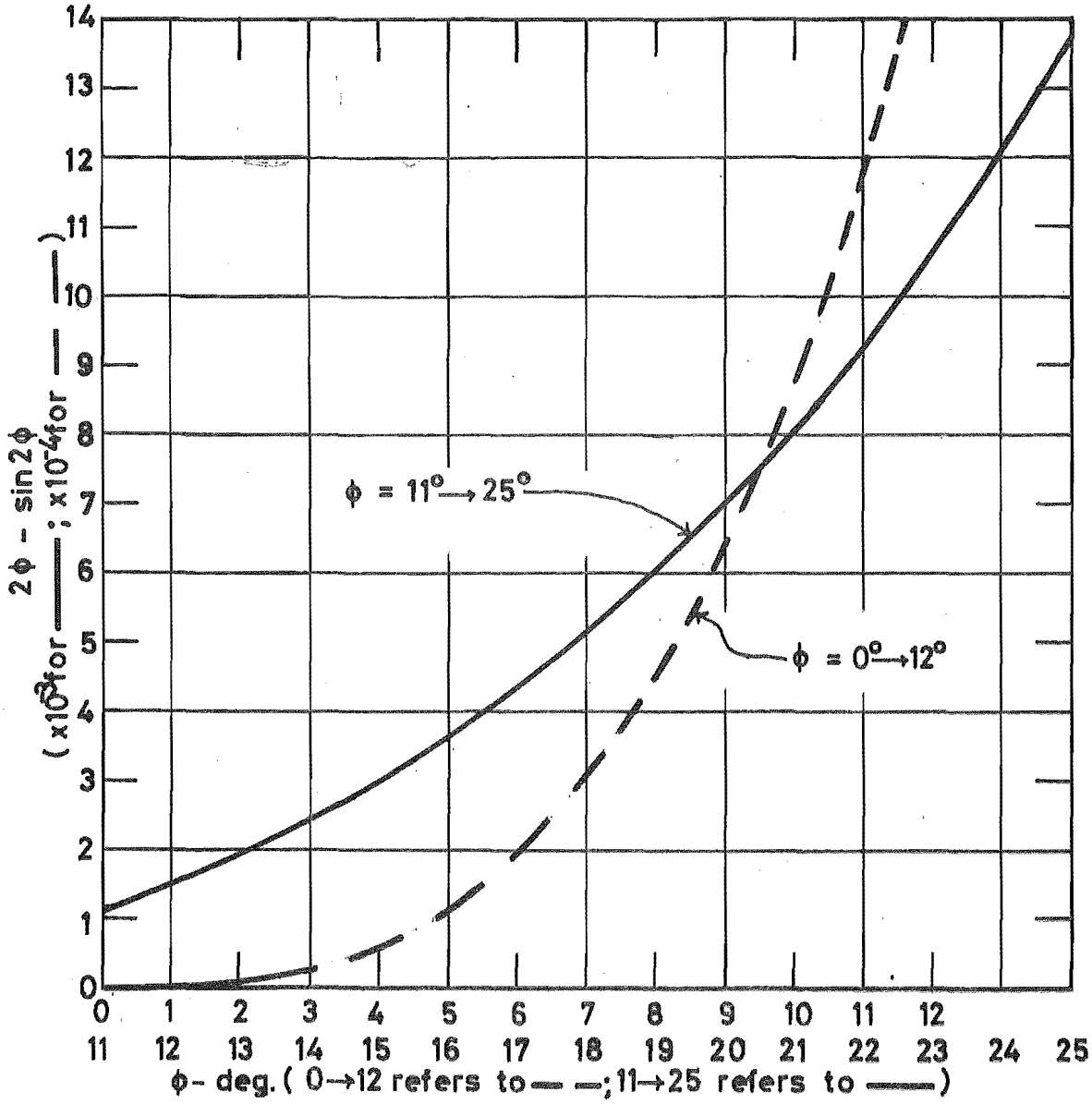

FIG. 3.3 VARIATION OF (2φ - sin 2φ) WITH φ

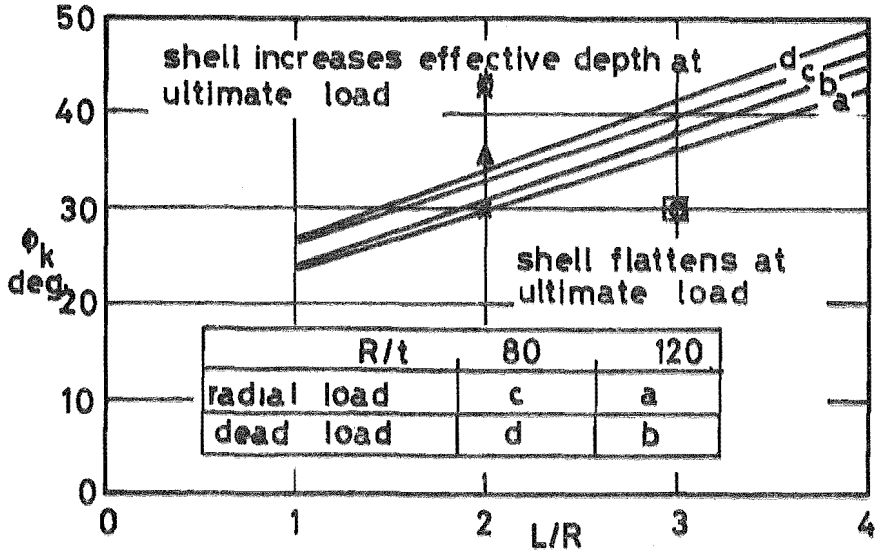

——— from "D.K.J." computer program

x o □ Δ shells 1,2,3,4&5 respectively

FIG. 3.4 VARIATION OF L/R AND ϕ_k FOR ZERO MIDSPAN CROWN DEFLECTION UNDER SURFACE LOAD

concrete compression block can now be calculated.

$$d' = d - a'$$

where d = depth to the centroid of the prestressing steel from the top of the crown.

(v) The ultimate moment, M_{uL}, of the shell cross-section can now be calculated.

$$M_{uL} = d' \times T_t$$

(vi) The actual strain in the steel must now be checked to ensure $e_{su} \geq e_{sy}$. If $e_{su} < e_{sy}$, the correct theoretical ultimate moment will be less than that calculated and the calculations should be redone using a lower value of e_{su}. If $e_{su} > e_{sy}$ the ultimate moment calculated will be slightly less than the correct theoretical value. A more accurate value could be calculated by assuming a higher value of e_{su}, however, the difference in final moment will be small.

The steel strain e_{su} can be calculated from

$$e_{su} = e_{sL} + e_{sp}$$

where e_{sp} = steel strain due to prestressing

e_{sL} = steel strain due to surface loading at ultimate moment

$$= \frac{d - kd}{kd} e_{cy}$$

kd = the depth of the neutral axis from the top of the crown

$$= \frac{a}{c_1}$$

$$a = R_o(1 - \cos\phi_o)$$

C_1 = .85 - .05/1000 psi over 4000 psi.

From the stress strain diagram for the prestressing

steel, f_{su} can be calculated. By a trial and error process an accurate value of f_{su} may be found, as shown below.

3.1.4 Accurate Determination of f_{su}

i) Assume maximum strain in the concrete is reached at the extreme fibre (o.003).

ii) Assume a steel strain, e_{su}, at ultimate load.

iii) Calculate the depth to the neutral axis from

$$kd = \frac{e_{cy}}{e_{cy} + e_{sL}} d \quad \text{where} \quad e_{sL} = e_{su} - e_{sp} .$$

iv) The depth of the compression block and hence the area of concrete in compression can now be calculated.

v) Calculate the concrete compression force from

$$C_c = f_c A_c .$$

vi) The required steel stress can now be calculated from

$$f_{su} = \frac{A_s}{C_c}$$

and hence the steel strain, e_{su}, can be found from the stress strain diagram.

vii) Estimate a new value of e_{su} and repeat from (ii) until the steel strain assumed equals the steel strain calculated.

3.1.5 Limitation of Maximum Steel Content to Prevent Brittle Fracture

If the neutral axis is low at ultimate load, the steel will not elongate sufficiently to give warning of failure - a brittle failure occurs. Although there will be no sharp demarcation between under and over reinforced sections, an approximate limit for the neutral axis depth

to prevent brittle fracture can be obtained. This is done by calculating the depth of the neutral axis when the extreme fibres of the concrete reach the maximum useable strain, .003, and the prestressing steel yields - a "balanced" failure. For prestressing steel there is no flat yield plateau, however the .2% set strain is commonly assumed as the strain where yielding begins.

For a "balanced" failure,

$$kd = \frac{e_{cy}}{e_{cy} + e_{sL}} d \quad , \quad e_{sL} = e_{sy} - e_{sp} .$$

Using the stress strain curves given by Lin[42] for prestressing steels and assuming the tendons are stressed to 0.7x ultimate stress[40] (e_{sp} = .0035 to .006), maximum kd lies between .35d and .43d . The actual value depends on the steel used. If the neutral axis depth exceeds the depth for balanced failure, yielding of the prestressing wire cannot occur and a brittle failure will result. Using the Dutch Concrete Code, Lundgren[34] suggests limiting the neutral axis depth to .4d and for rectangular beams the A.C.I.[40] effectively limits the neutral axis to .35d. Thus limiting the neutral axis depth to less than .35d would seem reasonable.

To ensure that the neutral axis is limited to .35d, the maximum allowable steel area must be limited to that which is just sufficient to balance the concrete compressive force, $C_{.35d}$, when the neutral axis is at .35d.

$$C_{.35d} = 2 R \phi_{.35d} \; t \; f_c \quad \text{where} \quad \phi_{.35d} = \cos^{-1}\left(\frac{R_o - a_{.35d}}{R}\right)$$

$$T = A_s \; f_{sy}$$

$$\text{therefore} \quad A_s \leq 2 R \phi_{.35d} \; t \frac{f_c}{f_{sy}} .$$

If the effects of the non-prestress steel are significant,

the following must be satisfied:

$$A'_s f_y + A_s f_{sy} \leq 2 R \phi_{.35d} \, t \, f_c$$

If required, the maximum allowable moment on the section can be calculated from

$$M_{uL} \leq C_{.35d} \, (d - a'_{.35d})$$

$$\leq 2 R \phi_{.35d} \, t \, f_c \left(d - \left[R\left(1 - \frac{\sin \phi_{.35d}}{\phi_{.35d}}\right) + \frac{t}{2} \right]\right)$$

3.1.6 Limitation of Minimum Steel Content to Prevent Steel Fracture

Prestressing steels have a relatively low ultimate strain (compared to mild steels) and if the neutral axis rises sufficiently, failure of the tendons may occur before crushing on the concrete. Although the effect is not necessarily undesirable, the steel strain at ultimate load should be checked to ensure that the steel can take the required strain.

The maximum neutral axis depth, above which this effect may occur can be easily calculated. Assuming an ultimate prestress strain of 4.0%, the minimum allowable as specified in A.S.T.M. - A - 421,

$$kd = \frac{e_{cy}}{e_{cy} + e_{sL}} \quad , \quad e_{sL} = 0.04 - e_{sp}$$

From Section 3.1.5 $e_{sp} = 0.0035 \rightarrow 0.006$ and therefore

$$kd(\text{maximum}) = 0.081d$$

If the neutral axis depth is less than .081d , the ultimate steel strain must be checked to ensure fracture of the steel does not occur. A minimum steel area can be calculated so that this mode of failure does not occur.

If $a < t$, $C_{.081d} = f_c R_o^2 (\phi_{.081d} - \frac{\sin 2\phi_{.081d}}{2})$

$$A_s \geq \frac{f_c}{f'_s} R_o^2 (\phi_{.081d} - \frac{\sin 2\phi}{2} .081d)$$

where $\phi_{.081d} = \cos^{-1}(\frac{R_o - a_{.081d}}{R_o})$

$a_{.081d} = .081 C_1 d$

If $a > t$ $A_s \geq \frac{f_c}{f'_s} 2 R\phi t$

where $\phi = \cos^{-1}(\frac{R_o - a_{.081d}}{R})$.

If the ultimate strain of the prestressing steel is greater than 4.0%, the critical minimum steel area will be smaller.

3.1.7 Effect of Non-Prestress Steel

The non-prestress steel will generally contribute only a small amount to the ultimate moment of the section. The actual contribution can be calculated as follows:

i) Assume the neutral axis is at same position as calculated when only prestressing steel is considered.

ii) Calculate strain and hence forces in reinforcement assuming linear strain distribution.

iii) Sum the total tensile force, calculate the area of concrete required to balance it and hence neutral axis depth. This and the original neutral axis position give limits between which the true neutral axis will lie.

iv) This new neutral axis position will normally be little different from that obtained by considering the prestressing steel only, and hence the reinforcement forces calculated in (ii) can be used to find the

contribution of the reinforcement to the ultimate moment.

v) If the new neutral axis position is significantly different from that obtained by considering only the prestressing steel, a new estimate of neutral axis depth must be taken between the limits found, and the calculations repeated from (ii).

3.1.8 Discussion

Assumptions. The assumptions made are all commonly used in rectangular beam design and would be completely acceptable for use with cylindrical shells, except for assumption (ii) which implies a linear strain distribution, and assumption (iii), that of neglecting the change in shape of the shell cross-section.

For the five model shells tested by the author (see Chapters 4 and 5), assumption (ii) is satisfied for all the models except the 5th shell which had the largest included angle.

Assumption (iii) is definitely not correct. However it is only of real concern when a shell opens, i.e., reduces its curvature, under load, thus causing the effective depth to be reduced. For these shells a reduction in ultimate moment capacity from that calculated must be made. Shells 2 and 3 ($^{L}/R = 3$, $\phi_k = 30^{\circ}$) tested by the author opened under surface loading, resulting in a 7% loss in effective depth at ultimate load.

For shells where assumption (ii) is not strictly correct, i.e. relatively large ϕ_k, the incorrectness of the assumption results in the calculated ultimate moment being

larger than that which would be obtained using the actual strain distribution. However for these shells the cross-section closes, creating a greater lever arm than assumption (iii) would indicate, and this effect, which tends to increase the ultimate moment, more than compensates for the above.

Hence the method presented will give an "accurate' or conservative value for the ultimate moment except when the shell flattens as surface load is applied.

Tendency of Shells to flatten. The tendency of a shell to flatten under surface load is a geometric property depending on L, R, ϕ_k and t . From the author's experimental results, it would appear that whether a shell opens or closes at ultimate load, depends on whether the shell deflects inwards or outwards at the midspan crown in an elastic surface load analysis. In Figure 3.4 the variation of L/R versus ϕ_k for zero deflection at the midspan crown under surface load is shown for $R/t = 80$ and $R/t = 120$. If the above reasoning is correct, then those shells lying in the portion below the curve should flatten at ultimate load. It can be seen that for a given ϕ_k and R the tendency to flatten increases as L is increased, as would be expected.

Applicability of Rectangular Beam Theory. Mattock and Kriz[43] carried out a series of bending tests on triangular shaped beams and L beams, loaded in such a manner as to give triangular compression zones, to see the applicability of ultimate load theories based on those for rectangular sections. They found good experimental and theoretical agreement, except where compression failure occurred or the cylinder strength of the concrete was low. From their

results they concluded that the simplified ultimate load theory, using an equivalent rectangular stress distribution, is satisfactory for design purposes.

For cylindrical shells, provided compression failures and low cylinder strengths are avoided as would normally be desirable, the conclusions of Mattock and Kriz would seem applicable, particularly for the case where the neutral axis is less than the shell thickness. In this case the compression block approaches a triangular block as was tested by Mattock and Kriz. Further, if the concrete compression block assumed is in error, the calculated ultimate moment will be little different from the true ultimate moment. This is because large changes in the area of the compressive block and location of the resultant compressive force cause little variation in the effective depth, and hence in the ultimate moment.

In the case where the neutral axis depth is greater than the shell thickness, the rectangular beam theory gives conservative moments, as the centroid of the compression block is further from the neutral axis than in the corresponding rectangular beam.

3.2 YIELD LINE MECHANISM

This failure mechanism commonly occurs in intermediate lengths shells and has been observed by numerous experimentors[4,44,45,46,47]. It is characterised by two longitudinal yield lines, a hogging yield line at the crown and a sagging yield line approximately midway between the crown and the shell edge. Diagonal tension cracks may complete the failure mechanism. However, particularly in longer narrower shells, the torsional resistance of the

longitudinal shell segments is small and this may allow failure to occur in the absence of shear cracks.

The negative moment at the crown is normally the largest transverse moment and hence longitudinal cracking occurs at the crown first. This cracking has been found by Bouma et al[4] to cause the transverse positive moments to increase both in magnitude and in the arc distance over which they are spread. Positive moment cracking soon follows. The shell can continue to take the load until the yield moments are obtained at the cracks, i.e. linear hinges form leading to failure finally.

The load, P , at which the first longitudinal crack occurs can be quite accurately found by

$$P = \frac{M_s}{M_u}$$

where M_s = moment resistance of uncracked shell section

M_u = maximum moment due to unit surface load (elastic theory)

Due to moment redistribution, the load at which the second longitudinal crack forms is difficult to calculate.

Ultimate load can be calculated by means of the kinematic approach of limit analysis[29,48]. As this is an upper bound approach the equation for the failure load must be minimized, and in practice this is difficult, unless the failure mechanism has been found from experiment. Moore[28] and Mileykowsky[47] have obtained theoretical results which agree well with experiment.

It has been found by experiment[4,45,46,47] that shells designed on the basis of elastic analysis have a satisfactory factor of safety against failure by a yield line mechanism, and furthermore, warning of failure is given. In a recent

paper Darvall and Billington[49] have found that for intermediate length shells which are typically reinforced, the load deflection curves follow nearly the same trilinear approximation to failure, and that the collapse load is approximately $3\frac{1}{3}$ times design load.

Hence it appears that if the shell steel is proportioned on the basis of elastic theory working load analysis, satisfactory ultimate load behaviour in the transverse direction occurs. With prestressing, the transverse moments can be reduced, but if the reinforcing is reduced accordingly, premature failure of the shell in the transverse direction may occur. This was observed by Bouma et al[4] in their prestressed shell where no negative moment reinforcement was provided at the crown. At a load of two times design load a crack occurred at the crown which opened completely and thus the shell was unable to transmit moment across the crack. Although failure did not occur until three times design load when a positive moment crack occurred, a reinforced shell of similar dimensions with both top and bottom reinforcement failed at a higher (11%) load.

3.3 SHEAR FAILURE

In a cylindrical shell, the largest in-plane shear stresses normally occur in the shell membrane near the four corners, resulting in diagonal cracking. Failure may occur through failure of the diagonal tension reinforcement or crushing of the concrete at the corners.

Harris and White[44] have carried out a series of tests on reinforced mortar cylindrical shells of various lengths, with edge beams, and found that although diagonal cracking occurs it does not cause failure except in short shells.

Hedgren[45] who tested a shell of intermediate length ($^{L}/R = 2$, $\phi_k = 30^{o}$) with no edge beams but with thickened edges, and Darvall et al[46] who tested a shell similar to Hedgren's, but twice as long and continuous over an interior support, found that although diagonal tension cracking did not cause failure, the diagonal cracking participated in the final transverse bending failure mechanism. In both these cases, diagonal cracking occurred at a load 1.6 times design load, with failure occurring at 4 times load. Ernst et al[38] have carried out a series of three tests on intermediate ($^{L}/R = 2$, $\phi_k = 46^{o}$) length cylindrical shells with edge beams, all which failed in diagonal tension in the outer thirds of the longitudinal span of the shell, when failure had been expected in flexure at midspan. However their method of line loading at the $^{1}/3$ rd points of the longitudinal span would accentuate a diagonal tension type failure, as maximum shear force and bending moment would occur together at the $^{1}/3$ rd points. For a uniform loading, as is normally assumed by designers, maximum longitudinal bending moment occurs at midspan where there is zero shear force. Maximum shear force occurs at the traverse where there is little bending moment. Newman[27] has carried out an extensive study of the shear failure mechanism in cylindrical shells, by testing 30 long shells ($^{L}/R = 5$, $\phi_k = 45^{o}$), a large number of which failed in shear. However, as Newman was particularly interested in the elastic rather than the non-elastic behaviour, only three of his shells were reinforced. In the unreinforced shells, once diagonal cracking began failure occurred. Newman found that a mesh in the shell surface increased the ultimate load by redistributing the load and reducing the force at the edge beam - traverse junction.

Hence, although diagonal tension cracks occur in cylindrical shells, they are of little consequence if reinforcement is provided, except in short shells where a shear failure may occur. In longer shells, diagonal tension cracks may contribute to the failure mechanism.

Scrivener[23] has tested a reinforced mortar shell without edge beams and of similar dimensions to the 1st prestressed shell tested by the author ($^{L}/R = 2$, $\phi_k = 30^{\circ}$). Whereas Scrivener observed diagonal cracks, at an applied load of 62 lb/ft^2, which increased rapidly in length, the author found no evidence of diagonal cracks occurring in the 1st shell. This shell failed at 175 lb/ft^2. Scrivener and Megget[5] have tested an ungrouted prestressed shell similar in dimensions to the above mentioned shells. The shell failed at 134 lb/ft^2 and again no evidence of diagonal cracking was found. Other prestressed shells tested by the author indicate that where diagonal cracking does occur in prestressed shells, it begins at a higher load than that which would cause diagonal cracking in a similar non-prestressed shell.

Thus a shear failure is less likely to occur in a prestressed shell than in a non-prestressed shell of similar dimensions. By the use of prestressing in the shell surface the magnitude of the diagonal tension force is reduced and diagonal cracking may be delayed considerably. Draped cables would be more efficient in delaying crack formation as long as the anchorage was not so close to the crown that the cable did not pass through the critical shear zone. An unlikely type of failure could occur if the prestress force was sufficiently large so as to cause a compression type failure at the corner.

3.4 BUCKLING

With prestressing, concrete cylindrical shells can be built with longer spans and edge beams can be reduced in size or eliminated completely, thus increasing the possibility of buckling. This is because both the edge beams and traverses offer restraint to an overall buckling of the shell. If the span is lengthened, the restraining influence of the traverses on the centre portion of the shell is reduced.

Most of the formulae which have been presented[50] for the buckling of cylinders have been developed for complete cylinders or shallow curved panels, and the majority of tests carried out have been on metal or plastic models where the material properties are known accurately, and where cracking is not a problem. Based on the above results, buckling formulae[34] have been suggested for concrete shells. However at present little is actually known about the buckling behaviour of concrete cylindrical shell roofs. The present author has not investigated the problem.

CHAPTER FOUR

DESIGN, CONSTRUCTION AND TESTING OF MODEL SHELLS

Five circular cylindrical model shells were constructed from micro-concrete and tested to failure. Each shell was prestressed with grouted prestress cables, and none of the shells had edge beams. The dimension of the shells are given in Table 4.1.

The 1st shell ($^{L}/R = 2$, $\phi_k = 30^o$) was a one piece shell and the primary purpose of this shell was to develop a satisfactory technique for designing, constructing and testing of the model shells. The second aim of the 1st shell test was to obtain results for a single piece shell for comparison with results from the other shells which were all segmented. In addition to finding the effect of increasing the L/R ratio from that used in the 1st shell, shells 2 and 3 ($^{L}/R = 3$, $\phi_k = 30^o$) were tested to obtain results for two identical shells, one with straight cables and the other with draped cables. To see the effect of an increase in subtended angle, with particular emphasis on the failure mechanism and ultimate load, shells 4 ($^{L}/R = 2$, $\phi_k = 35.8^o$) and 5 ($^{L}/R = 2$, $\phi_k = 43^o$) were constructed and tested. The 5th shell parameters were also chosen so that the effect of a large cable drape could be seen.

In the choice of prestressing layout, the design aim was to restrict cracking in the shell, and if possible to have no tension anywhere in the shell, between prestress + dead loads and prestress + dead + live loads. It was also attempted to ensure that the shells would have a failure mechanism that gave warning of oncoming failure and also a

Shell		1	2	3	4	5
R	ins	48	48	48	48	48
L	ins	97.625	144.125	144.125	95.0	95.0
ϕ_k	radians	.5236	.5236	.5236	.625	.75
t	ins	.614	.625	.625	.680	.669
N		1	3	3	3	3
g	ins	-	47.5	47.5	31.0	31.0
T	ins	1.625	1.625	1.625	2.0	2.0
a	ins	2.5	2.25	2.25	2.0	2.0
b	ins	6	6	6	6	6
c	ins	1.0	1.5	1.5	1.5	1.5
P	lbs	1875	2160	2160	1600	2000
P_L	lbs	0	0	0	0	0
d	ins	22.8	22.8	22.8	28.0	34.0
e	ins	22.8	22.8	22.8	28.0	34.0
f	ins	0.0	0.0	0.0	0.0	0.0
P	lbs	1790	2160	2160	1600	2000
P_L	lbs	0	0	160	0	500
d	ins	18.6	20.4	15.9	26.0	20.0
e	ins	18.6	20.4	20.4	26.0	30.0
f	ins	0.0	0.0	4.5	0.0	10.0
P	lbs		2160	2160		
P_L	lbs		0	250		
d	ins		18.0	9.0		
e	ins		18.0	18.0		
f	ins		0.0	9.0		

P_L = prestress loss along cable

N = number of cylindrical segments

Shell Reinforcing - 1st shell, spot welded mesh, see Fig. 4.3
- Other shells, 14 g spot welded mesh at 1½ centres

Dowel Bars (10 g, 4" long) - Between traverse and shell: at 6" centres from crown
- Between shell segments: at crown, and for shells 2 & 3 at ±15" arc distance from crown, shell 4 at ±24" shell 5 at ±28"

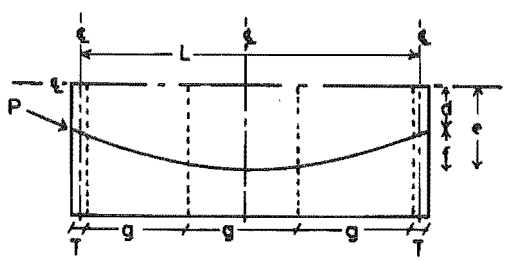

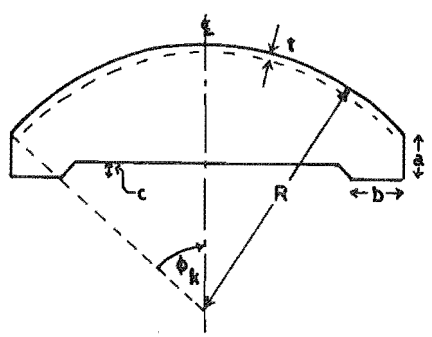

TABLE 4.1 DIMENSIONS OF SHELLS TESTED

reasonable factor of safety against collapse. This latter criterion was difficult to ensure as the ultimate load theory was being formulated during the shell tests.

4.1 CHOICE OF MODEL DIMENSIONS

The shells to be tested were to be thin shells in the intermediate range.

A shell thickness of 0.6" was decided upon as being the thinnest practical size to construct the models, considering two or three layers of reinforcement and grouted prestressing cables were to be fitted into the section.

A steel mould used by Scrivener[23] (R = 48", L = 96", $\phi_k = 30^o$) was available and it was decided to use this to get the basic shape of the shells. This gave a R/t ratio of 80 which was considered satisfactory for thin shell action, and the L/R ratio of two enabled a one piece, intermediate length shell to be constructed.

In order to construct shells with a larger included angle than 30^o a new mould (R = 48', L = 32", $\phi_k = 50^o$) was constructed. The radius was kept at 48" in order to reduce the number of variables between the shells.

A full size shell thickness of 3" was assumed and this gave a model:full scale length ratio of 1:5. Using dimensional analysis with Young's modulus, L and t as relevant physical quantities, complete similitude of the model and the full size shell could be obtained except for the density, which in the model was only 1/5 of that required.

4.2 DESIGN LOADING AND STRESSES

For complete similitude the same load must be applied to the model shell as to the full size shell. Thus the model shells were designed for a dead load of 36 lb/ft^2 and assumed live load of 20 lb/ft^2. As the model density was only $^1/_5$ of that required, the entire working load of 56 lb/ft^2 was assumed to be applied externally to the shell by the airbag.

A concrete cylinder strength of 4000 psi and a design steel reinforcing stress of 20,000 psi were assumed for the models. The reinforcement was porportioned according to the working stress provisions of the A.C.I. (318-71) Concrete Code[40] using a modulus ratio of 7.

The prestressing steel stress was kept below 0.7 x ultimate stress as recommended by the A.C.I.[40]. Except for friction loss along the cables, no allowance for loss of prestress force was necessary.

4.3 CHOICE OF SHELL ELEMENT

The initial decision to be made in the choice of element is whether transverse or longitudinal elements should be used. Transverse elements have the considerable advantage, that prestressing cables required in the shell to resist edge tensile forces, may be able to be used to join the elements. However longitudinal elements may be easier to transport and also have the advantage that areas of potentially high tensile stress are not cut. Longitudinal elements may, however, cut areas of high transverse moment.

Transverse elements have been used in this series of model tests as these seem the most likely elements to be

used in practice. Joints have been kept away from midspan in order to avoid areas of potentially high tensile stresses.

Longitudinal elements are, however, being used. An American Company[24] is marketing prestressed, precast cylindrical shells made of three longitudinal elements. These elements are pre-tensioned longitudinally and have transverse steel projecting from each element, which is welded to the steel of the neighbouring element. These elements come in spans of up to 100 feet and require no formwork for erection.

4.4 FORMWORK

The main requirement in the design of the formwork was that the concrete shell elements could be stripped from the mould without undue strain or cracking. It was also necessary that segments of shells could be successfully cast, and that there be some means of holding the reinforcing steel and prestressing cable ducts in place. The formwork also had to be rigid enough to allow sufficient vibration for the mortar to be compacted.

4.4.1 Shells 1, 2 and 3

The first three shells ($\phi_k = 30^o$) were constructed on the mould initially used by Scrivener[23], which was modified by the author. The curved portion of the mould was formed by rolling a 8'-0" x 4'-2" x 1/4" mild steel plate to an arc of 4'-0", which was then spot welded onto curved stiffener plates at the ends and centre to hold it in shape. Along the straight edges the mould was mounted on two 6" x 3" angle runners which were joined by 4" x 2" channels at their ends and midpoint to form a rigid base. Running along each

longitudinal edge of the curved mould, and bolted to the 6" x 3" angle, was a shaped $\frac{5}{8}$" x $\frac{1}{4}$" mild steel strip to prevent the mortar running off the edge of the mould. Attached to each end of the base was an adjustable end plate, bolted to the channel through a 2" x 2" x 2" packing block. This acted as an edge to screed to and also formed a mould within which the traverses were cast. A 4'-4" x 2" x $\frac{1}{4}$" plate bolted to the packing block formed the bottom of the traverse mould. The assembled formwork is shown in Figure 4.1, prior to the pouring of two elements for shells 2 and 3. In order to allow segments of shells to be cast, curved wooden dividing strips of 4'-0" radius and 0.6" high were cut from a sheet of 7 ply marine plywood. These can be seen in Figure 4.1. To prevent movement during the pouring of the mortar, a groove was cut along the outside of each strip and a piece of No.8 gauge mild steel wire tensioned over each strip. For the 1st shell, a single piece shell, corrugated cardboard packing was used at the ends of the steel mould to allow for shrinkage of the shell.

4.4.2 Shells 4 and 5

The formwork used for shells 4 and 5 was constructed from a 7'-0"x 2'-8" x $\frac{1}{4}$" mild steel plate rolled to a 48" radius. This plate was held in shape at its end by curved stiffener plates. Two 4" x 2" channel sections were used to keep the bases of the stiffener plates the correct distance apart and also to provide a base for the mould. Attached to the stiffener platers were two curved end plates, of slightly larger radius than the stiffeners, to provide an accurate surface for screeding. Shaped sections of $\frac{5}{8}$" x $\frac{1}{4}$" were again used to prevent the mortar running off the curved surface. These were screwed onto the mould

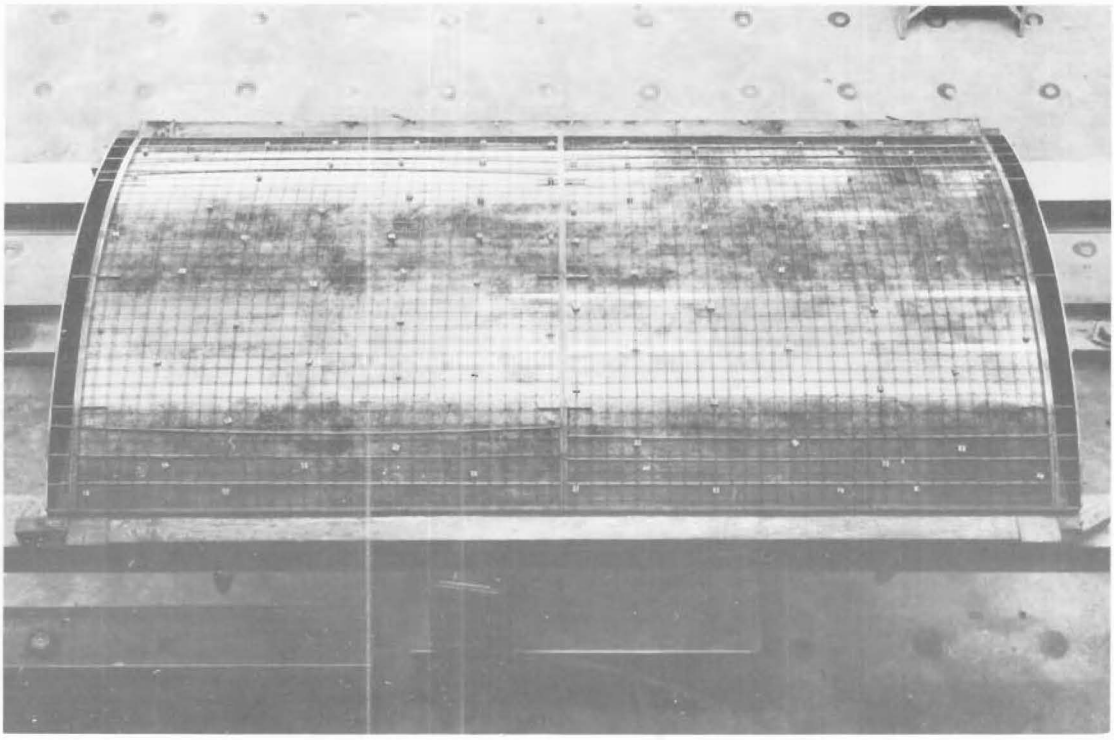

FIG. 4·1 ASSEMBLED SHELL MOULD USED FOR SHELLS 1, 2 & 3.

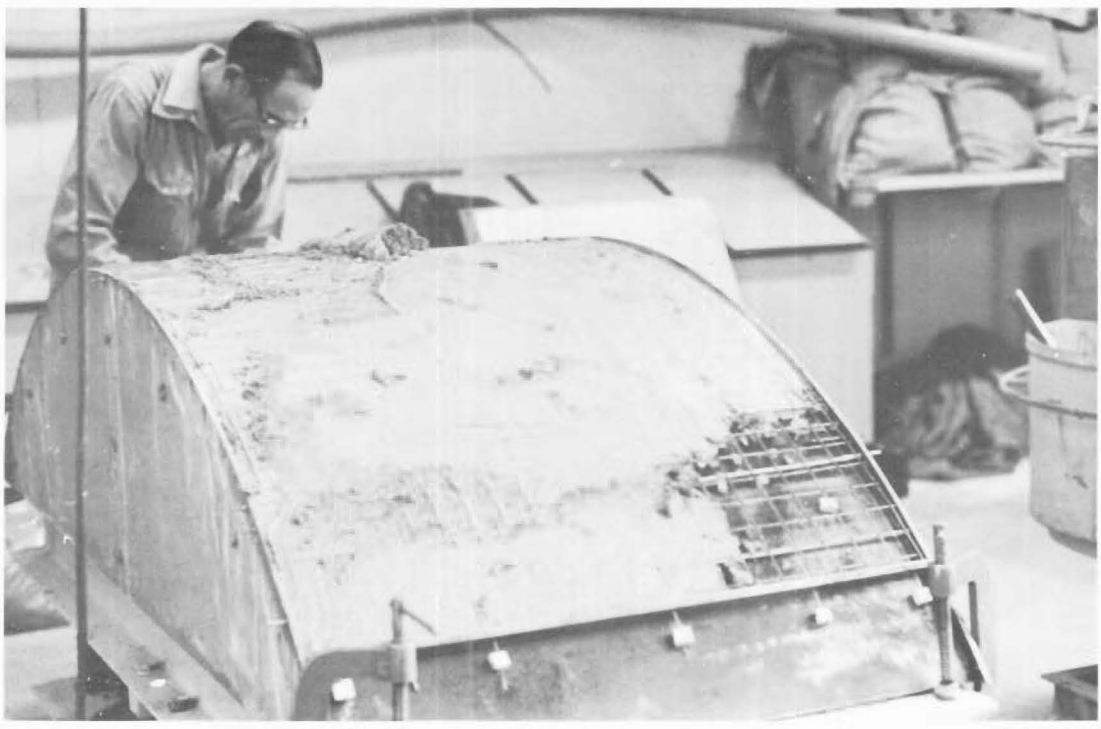

FIG. 4·2 ASSEMBLED SHELL MOULD USED FOR SHELLS 4 & 5.

and could be attached at any required arc distance. The assembled mould is shown in Figure 4.2 during pouring of one of the 5th shell elements. Traverses were constructed by removing the end plates and bolting them onto a channel section at the required distance apart. All connections in the formwork were bolted in order to avoid distortions which can occur during welding.

4.5 REINFORCING STEEL

For ease of construction and placement of the reinforcing, spot welded meshes were used for the curved portions of the shell. These meshes were made by a local firm from straight lengths of cold drawn wire, for which typical stress-strain curves are given in Appendix B.1. However, as the heat of the spot welding weakened the wire in the vicinity of the joint, the effective stress-strain curve was that of a spot welded wire. Typical stress-strain curves for spot welded wires are given in Appendix B.1. Another advantage of the spot welding was that the mesh was given an initial curvature, thus facilitating placement on the mould.

To position the mesh correctly for pouring, mortar packing blocks were placed under the mesh at approximately one foot centres as can be seen in Figure 4.1. The mesh was then held onto the mould by means of 22 g piano wires tensioned over the top of the mesh.

4.5.1 1st Shell Mesh

This mesh was designed and detailed specifically for the 1st shell. High tensile stresses near the midspan edge under prestress load + working loads resulted in a

large percentage of reinforcing steel in these areas. Diagonal steel was tied under the spot welded mesh to resist shear stresses at the corners. The mesh used is shown in Figure 4.3. Due to a misunderstanding with the fabricator, the mesh was made in four parts and bronzed together along the transverse and longitudinal centre lines.

4.5.2 Other Shell Meshes

For simplicity, economy and speed of construction of segmented shells, it is desirable to have a standard mesh for all elements. Thus an identical mesh, 14 g (.080" diameter) at 1½" x 1½" centres, was used in the shell cross-sections for shells 2, 3, 4 and 5. Alternatively, two standard meshes could be used, one for the centre elements where transverse moments and edge tensile forces are high, and the other for the end elements where shear stresses are high.

4.5.3 Traverse Meshes

The meshes for the traverses were made from cold drawn bars with similar properties to those used in the shell mesh. These bars were joined by a bronze-silver alloy commercial preparation, "Easy-Flow". To ensure that the traverse did not fail before the shell, the traverse reinforcement was designed for forces 1½ x those actually calculated at design working load. Basically the traverse reinforcement meshes consisted of 6 g horizontal bars at ½" to 1½" centres with 14 g vertical bars at 1½" centres.

4.6 PRESTRESSING STEEL

The shells were prestressed with 12 g (.104" diameter) or 10 g (.128" diameter) high tensile steel, the stress-

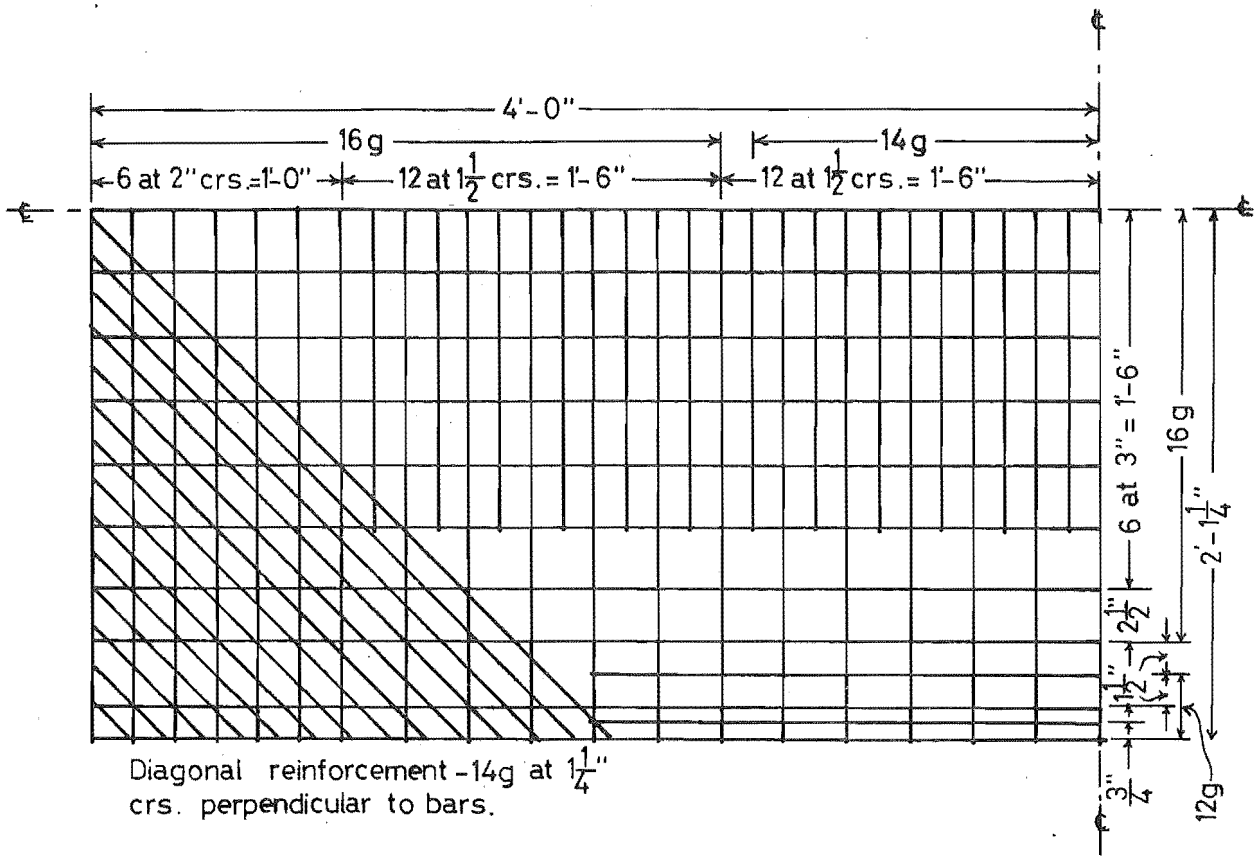

FIG. 4·3 1st SHELL REINFORCING MESH

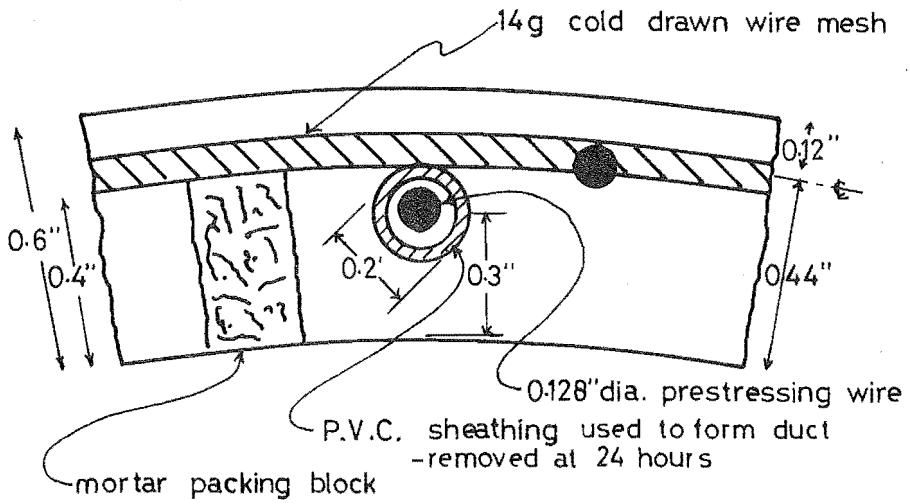

FIG. 4·4 TYPICAL SHELL CROSS-SECTION

strain curves for which are given in Appendix B.1.

The prestressing steel was placed in the centre of the shell section with the reinforcing mesh directly above it as shown in Figure 4.4. Ducts for the prestressing steel were formed by lengths of cold drawn wire, of the same diameter as the prestress steel to be used, covered with a P.V.C. tubing. The P.V.C. covered wires were positioned by passing them through holes drilled in the end plates and the wooden dividing strips. To maintain the wires in the centre of the section, and to maintain the correct curve for curved cables, the wires were also tied to the reinforcing mesh.

4.7 CONCRETE MIX AND CASTING

4.7.1 Concrete Mix

In the design of the micro-concrete mix several conflicting demands had to be met. The mix had to be of sufficient workability so that it could be compacted and finished to a smooth surface, but cohesive enough to stay on the shell mould, without segregating, during compaction. It was also desirable that the cement content be as low as possible in order to minimize shrinkage.

With the mix of Scrivener[23] as a basis, and the maximum aggregate size being determined from cover requirements ($^2/_3$ of minimum cover), several trial mixes were made. The mix given in Table 4.2 was decided upon for the 1st shell. This proved successful and was used for shells 2 and 3 as well. In an attempt to reduce the compressive strengths of 7,300 - 9,300 psi, but maintain the same workability the water/cement and aggregate/cement ratios were altered slightly for shells 4 and 5 resulting in compressive strengths of

Aggregate Proportions for All Shells				
B.S. Sieve	7-14	14-15	25-52	52-100
%	50	20	5	25
By Weight	Aggregate/Cement		Water/Cement	
Shells 1,2,3	2.5		0.4	
Shells 4,5	3.12		0.47	

Cement - Ordinary Portland Cement

Aggregate - River Sand

TABLE 4.2 MICRO-CONCRETE MIX PROPORTIONS

6,200 - 8,000 psi. Fuller details of the micro-concrete properties are given in Appendix B2. Both mixes used fall within the recommendation given by Rowe[25].

4.7.2 Casting

A two cubic foot Cumflow concrete mixer was used to mix the micro-concrete, Two mixes were necessary for each mortar pour for shells 1, 2 and 3. The proportions of all mixes were closely controlled to ensure consistency between mixes.

For shells 1, 2 and 3 compaction was successfully achieved by vibrating the formwork with an air-gun and a "Kanga" hammer. Both these were hand held and had a ram at their ends which oscillated rapidly up and down. As the end traverses required the most vibration these were filled first and compacted by vibrating the end plates. Mortar was then placed on the curved surface and compacted in two layers. Compaction was achieved by holding the air gun to the under-side of the steel mould, trowels being used to keep the

mortar thickness reasonably uniform. Compacting the end traverses and curved surface took about three-quarters of an hour, after which a transverse steel screed, cut to the arc of the shell top surface, was passed over the shell three or four times. This screed sat on the 6" x 3" angle runners forming the base of the mould, and was pushed along by means of the air gun and "Kanga" hammer. Only a small amount of mortar was allowed to build up in front of the screed, the surplus being removed by a trowel. This screeding left the shell with a reasonably uniform thickness. Final screeding was carried out to the accurately machined and positioned end plates with a 3¼" x 1¼ aluminium T section. This left the shells with a smooth surface.

Elements for shells 4 and 5 were cast on the new formwork which was small enough to fit on an available vibrating table. For these elements the mortar was compacted in two layers with the vibrating table operating at 1000 rpm. Only longitudinal screeding was used.

4.7.3 Curing and Stripping

The mortar for the first three shells was moist cured for 7-10 days by covering the top surface of the shells with two layers of scrim which was kept continually damp. Evaporation was lessened by placing a piece of black plastic over the top. The scrim was first placed on the shell 4-5 hours after screeding was finished, to allow the mortar sufficient time to harden, so that crazing of the surface would not occur. Elements of shells 4 and 5 were cured for 7-10 days in a fog room.

At 24 hours the end plates, the timber blocks which shaped the feet of the traverses, and the longitudinal

$^{5}/_{8}$" x $^{1}/_{4}$" side strips were removed. The P.V.C. tubing and wires forming the prestressing cable ducts were also stripped after 24 hours. As P.V.C. does not bond with mortar, both wire and P.V.C. sheathing were easily extracted, leaving a perfectly clean duct.

The 1st shell was stripped from its formwork by jacking up the steel mould and packing the feet of the traverse. The mould was then lowered out from beneath the shell by means of hydraulic jacks, care being taken to lower it evenly to prevent the shell being damaged. Compressed air was forced between the shell and mould to get initial movement. For the remaining shells, the elements were easily slipped off the moulds. In all cases the underside of the shells had a smooth glass like finish. Prior to casting, the moulds were coated with varnish to facilitate stripping.

4.7.4 Variation of Thickness

Due to the method of screeding the variation in thickness of each shell was small. After testing, holes were punched in the surface of the shells and thickness measurements made with a micrometer. Variation in thickness was generally within ±10% of the average thickness. Typical thickness measurements are given in Table 4.3 for the 1st shell.

TABLE 4.3 TYPICAL SHELL THICKNESS MEASUREMENTS

	Equal Spacings Around Shell Arc						
Equal Spacings along shell	.663	.661	.663	.606	.616	.616	.648
	.622	.624	.642	.626	.614	.689	.674
	.595	.615	.630	.640	.609	.628	.620
	.594	.622	.628	.630	.645	.641	.618
	.530	.564	.588	.605	.590	.598	.585
	.625	.586	.569	.561	.561	.560	.616

Average = .614 ins, Standard deviation = .0324

Results for 1st shell

4.7.5 Test Specimens

From each mix, a number of 4" x 2" cylinders and 12" x 6" x ½" reinforced slabs were taken. The slabs were tested in flexure and were reinforced with 14 g 1½" x 1½" spot welded mesh placed at the same depth as the shell reinforcement.

For shells 1, 2 and 3 a number of the test specimens were vibrated by the air gun and cured in a similar manner to the shells. All other test specimens were vibrated at 3000 r.p.m. for three minutes on the vibrating table and cured in the fog room.

Details of the testing techniques, and results obtained are given in Appendix B2.

4.8 PRESTRESSING SYSTEM

Considerable time was spent in developing a suitable prestressing system as it was required to satisfy several demanding requirements. It was necessary that both .104" and .128" diameter prestressing wires could be stressed and maintained accurately at the required load, that each wire could be grouted, and that the system could be reused several times. During surface loading it was desirable that the change of load at the anchorage could be followed accurately. A prototype system was built and tested before the final design, detailed in Figure 4.5 was chosen. All components were made of mild steel. The fully assembled system is shown on the 1st shell in Figure 4.6, and a description of the system is given in the following sections.

4.8.1 Solid Bearing Block

The bearing block was designed to be positioned

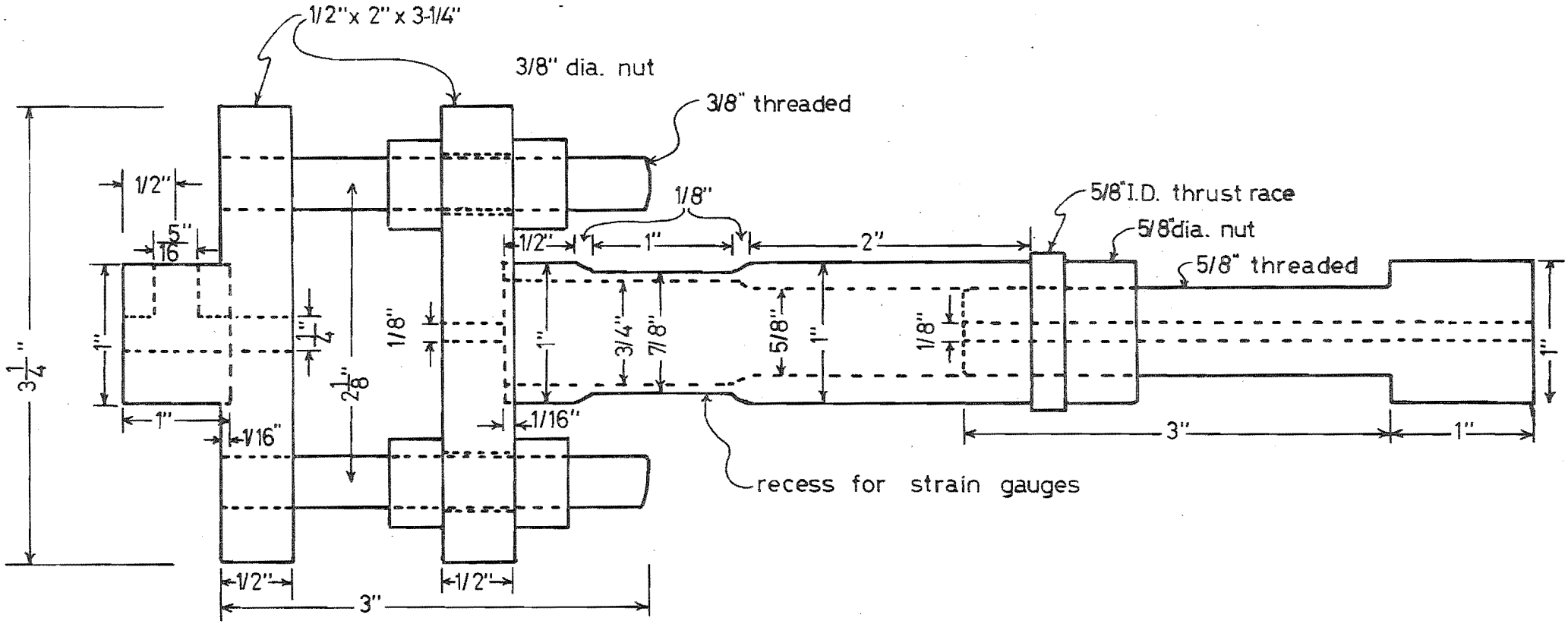

FIG. 4-5 DIMENSIONS OF PRESTRESSING SYSTEM

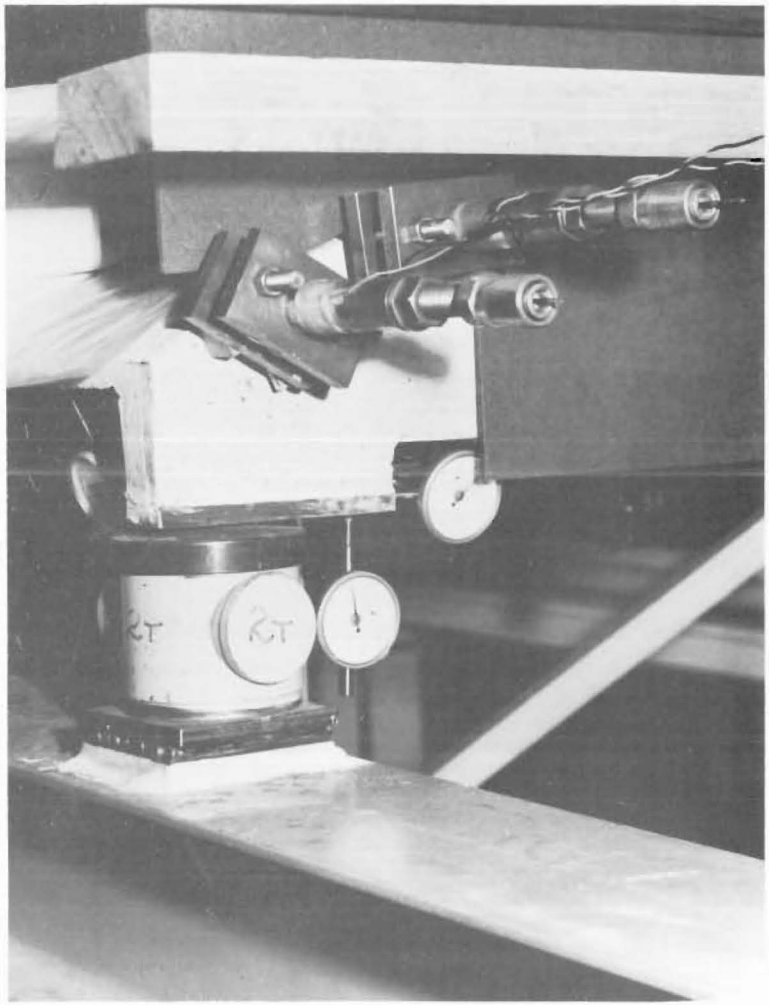

FIG. 4.6 PRESTRESSING SYSTEM, TWO TON LOAD CELL AND ROLLER SUPPORT.

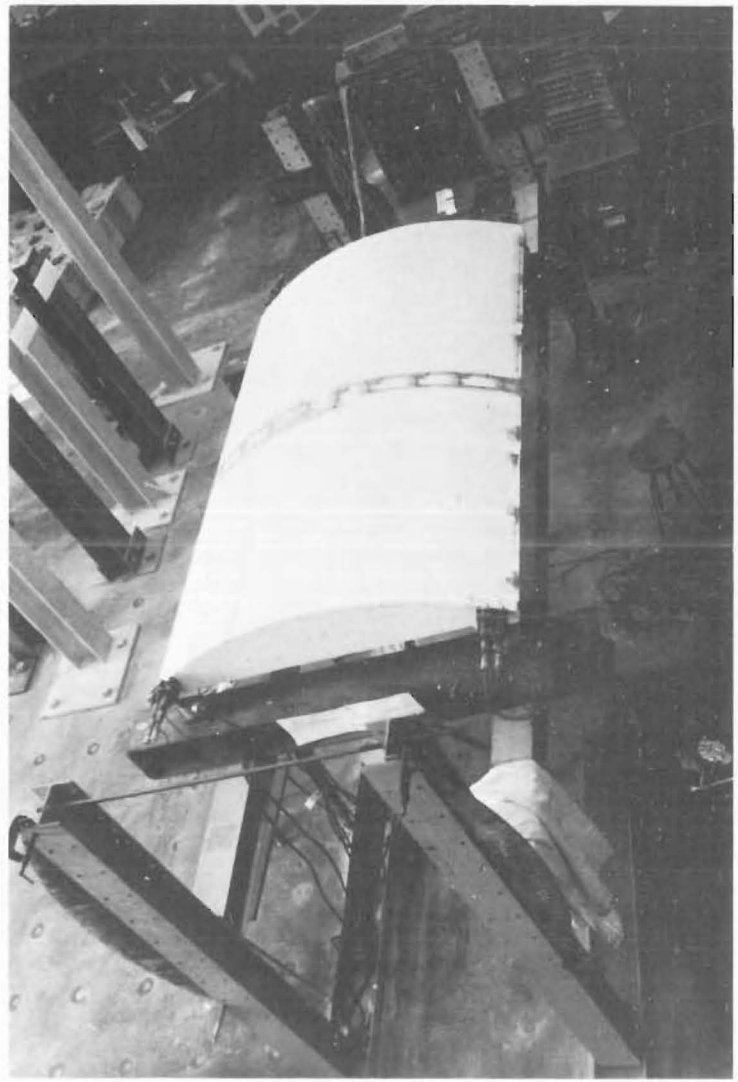

FIG. 4.7 4th SHELL PRIOR TO TESTING SHOWING DATA LOGGER AND STRAIN GAUGE LAYOUT.

in place over the cable duct hole, so that the main axis of the load cell and jack would be parallel to the wire where it came out of the shell. This was particularly important for the shells with curved tendons where tapered washers and mortar were used to pack the bearing blocks to get the correct angle. The mortar also served to seal the bearing block-shell interface to prevent loss of grout during the grouting of the wires. Grout was pumped into the wire duct through a nozzle screwed into the top of the bearing block.

4.8.2 Adjustable Bearing Block

This served to allow any small error in the lining up of the wire and jack axis to be corrected. To prevent grout from spraying out, the wire was sealed with wax or mortar where it came through the plate nearest the shell.

4.8.3 Load Cells

The load cells were incorporated in the prestressing system and remained in place during the complete shell test. Each load cell was designed to take a load of up to 2500 lb and still be within the elastic range of the mild steel.

The load cells each had four active strain gauges mounted symmetrically around the recess in the load cells, with their main axis parallel to the main axis of the load cell. Kyowa 120 ohm temperature compensated strain gauges (KF - 5 -C1-11) were used. Adjacent pairs of gauges were connected in series and then each set of pairs on each load cell were connected in parallel, to give an effective resistance of 120 ohm.

Various strain gauge cements were tried and the two component room setting compound Kyowa EP-18, recommended by the manufacturers of the gauges, was found to be the most satisfactory. Araldite, a commonly used glue for load cells was found to be as good, but this glue has the disadvantage that it requires three days of heat treatment to get the best results. Both these glues were found to be shock resistant and to have negligible creep under load (2400 lbs) during a four day test period.

After wiring up the gauges they were waterproofed with Budd GW-1 waterproofing compound, and then coated with petroleum micro-crystalline wax for mechanical protection. Lead wires to the load cells were twin twisted 7/0076" copper wires, fifteen feet long. All load cells were connected to a Budd P-350 portable strain indicator through a switch box with SPI Croydon rotary stud switches. No switch box changes in resistance could be detected. All connections were soldered except the connection to the Budd bridge, where horseshoe terminals were used.

To check the repeatability of readings, a prototype load cell was cycled 80 times up to 2400 lbs over a period of a week. It was found that the apparent strain as read on the strain bridge gradually increased for a given load for up to 10-15 cycles of load. From there until 80 cycles there was negligible increase - between 20-30 μstrain increase at maximum load. The four day creep test mentioned above was carried out after the 40th cycle. Thus it was decided to cycle all load cells 20 times to full load before use.

For the 1st shell test a two arm circuit was used, with a strain gauge mounted on a spare load cell being used

as a dummy gauge for all the active load cells. However, during the calibration of the load cells for the 2nd shell test, it was noticed that the zero for the load cell altered when the lead wires from the load cells, or dummy, were bundled up. This zero drift did not occur if the wires from the dummy and load cell were twisted together and then bundled up. It was concluded that there must be some inductance effect, and to overcome this, dummy gauges were mounted on each load cell and the four lead wires twisted together. The dummy gauges (KF-5-C1-11) were attached at right angles to the active gauges with Kyowa CC-15 strain gauge cement. These gauges were also protected with waterproofing compound and wax.

Before each test, each load cell to be used was cycled two or three times, and then three calibration runs to full load were taken. For all load cells a straight line calibration curve was obtained, and the accuracy of the load cells was such that cable loads could be set to within 20 lb. ✓ Three calibration runs were made on the load cells after each shell test and these were found to give calibration curves of the same slope as before testing, but sometimes with slightly different zero readings. Calibration was carried out on an Avery 25,000 lb test machine, and because of a lag between actual and indicated load on the test machine during unloading, calibration was only carried out with increasing load.

4.8.4 Jack

The jacks were machined from a 1" diameter mild steel round. A $^{5}/_{8}$" diameter ball race was placed between the load cell and the $^{5}/_{8}$" nut which screwed the jack up and down.

This was to prevent wear on the load cells and to prevent any torsion effects on the load cells, which may have affected the load cell readings. The jacks allowed approximately 2" of play at each end and this was found to be ample to take up any slackness in the system once the cables had been anchored, and to stress the cables to the required load. In addition, 2" movement could be obtained from the adjustable bearing block. It was necessary to use this for the 3rd shell when one of the ball races collapsed and the jack could not be used.

4.8.5 Anchorages

These were standard barrel and two wedge type anchorages which bore directly onto the end of the jack. To prevent damage to the end of the shell, the wedges, instead of being hammered into the barrel, were forced into its core by a demountable mechanical device. The wedges could be loosened by lightly tapping the barrel.

4.9 JOINING, PRESTRESSING AND GROUTING

All these operations were carried out with the shells on the reaction frame, so that strain gauge leads would not have to be disconnected between the sets of readings taken during prestressing of the shell, and surface load testing.

The 1st shell was lifted into position by means of a steel rig which supported it under the traverse at each corner. It was then prestressed and grouted with roller supports under the load cells allowing horizontal movement. For the remaining shells, the segments were lifted into place on a timber rig which supported the elements longitudinally on each side between the crown and edge. The traverses were then fitted

into place, and then the whole shell joined with the shell elements able to slide on the timber rig to take up movement. Prior to final prestressing, the timber frame was dismantled and the shell placed on roller supports.

4.9.1 Joining

All segments were joined by a two component epoxy resin "Boscrete No.10 Epoxy", the main properties of which are: tensile strength 5,000-7,000 psi, compressive strength 18,000-25,000 psi, and flexural strength 10,000-15,000 psi. The preparation is commonly used in construction and maintenance of concrete structures.

If the surfaces to be joined were more than $^{1}/_{16}$" apart at any place when pushed together, a rotary disc grinder was used to grind off the high spots. The surfaces were then prepared by brushing with a wire brush and cleaning with methyl ethyl ketone.

The shell segments were joined by coating each surface of the joints with resin and then pulling the whole shell together with the pair of prestressing wires closest to the crown, to give an average compression of 100-200 psi over the whole shell transverse cross-section. Due to the layout of the prestressing cables it was impossible to get an even compressive stress over the whole cross-section.

To line up the shell segments, 4" long, 10 g dowel bars were inserted in holes in each side of the joint which had been formed in a similar fashion to the cable ducts. The dowel bars were anchored by filling the holes with resin during the joining process, except for the dowel bars between the end segments and traverses for shells 2 and 3. These had been

anchored to the traverse reinforcement and set in the traverse during pouring. As well as helping to line up the segments, the dowel bars were designed to carry all the working load shear force across the joints.

From the experience of the 2nd shell where difficulty was found in grouting the shell, each prestressing duct for shells 3, 4 and 5 was protected at each joint from inflow of resin by a 2" long steel shim sleeve.

4.9.2 Prestressing

After the 24 hours required for the epoxy resin to set, each shell was prestressed to its final level of stress. This was carried out for each symmetrical pair of wires by alternately stressing each wire in small (200 lb) load increments, to prevent undue eccentric forces from acting on the shell. Initially the cables were only loaded at one end so that the prestress loss along the shell could be measured. The loss along any cable was easily obtained by subtracting the loads recorded by the load cells at each end of the cable. No line losses could be measured along the straight cables. When the cables were stressed to approximately one half their final required value, each end of the cable was stressed in alternate load increments. The line losses for the full cable loads for use in the theoretical analysis were obtained by direct proportion from the measured line losses for smaller loads. Some of the measured loss was due to non-alignment of prestressing cable ducts between segments.

Prior to grouting, minor adjustments to the prestressing loads were made.

4.9.3 Grouting

The shells were all grouted with a grout consisting

of three parts of cement to one part of water by weight.

The grout was forcedinto the cable duct at 40-60 psi by means of a converted paint sprayer. Throughout the grouting operation the grout was kept continuously stirred and the flow from the delivery nozzle kept continuous in order to prevent grout from setting in the delivery tube. Prior to grouting all cable ducts in the shell were filled with water, to prevent the duct from absorbing water from the grout, and thus causing the grout to lose its fluidity. It was found that under water pressure, numerous leaks developed on both the intrados and extrados. These were plugged with a dental moulding compound similar to plaster of Paris. All cables appeared to be grouted successfully, except in the 2nd shell, where for some ducts it was not possible to get the grout to flow from one end of the duct to the other.

4.10 STRAIN MEASUREMENT

4.10.1 Strain Gauges

Kyowa 120 ohm polyester backed wire filament strain gauges (KP-20-A1) were used on all shells and test specimens to measure surface strains. The gauge length of 20 mm was eight times the maximum mortar aggregate size used. This was considered adequate as Carmichael[26] suggests a minimum gauge length of 1½ times the maximum aggregate size.

Except for the 1st shell, approximately 60 gauges were mounted on each shell. These were positioned at approximately six inch centres across the transverse centreline, and at one foot centres along one longitudinal edge. At each gauge position, gauges were mounted longitudinally on both the intrados and extrados. Across the transverse centre line,

gauge pairs were also mounted transversely. A typical layout of strain gauges is shown in Figure 4.7 for the 4th shell. For the 1st shell one quarter of the shell was strain gauged with 100 gauges. These were located at approximately six inch centres on four transverse cross-sections at distances of 0", 18", 36" and 45" from the centre line. Gauges were mounted longitudinally along the edge, both longitudinally and transversely along the two centre lines of the shell, while at other gauge locations 45^{o} rosettes (KP-10-B3) were used. At all locations, gauges were placed on both the extrados and intrados.

The surface of the shell where gauges were to be mounted, was prepared with a rotary disc grinder and emery paper. This was to ensure that the top cement layer was removed and that the surface was smooth. The surface was cleaned with a solvent, methyl ethyl ketone. An area of about twice the size of the gauge was then coated with cc-15 cement and the gauge affixed by holding it on to the surface with finger pressure for 30 seconds. Four hours were required for the cement to set completely.

Copper terminal strips were cemented beside each gauge with Eastman 910 contact cement, and the two lead wires from the strain gauge soldered to the strip. These terminal strips protected the gauges from accidental pulling. For shells 1, 2 and 3, three foot lengths of 7/.0040" plastic insulated copper cable were soldered to the terminal strips and then brought to the edge of the shell where twenty foot leads of 7/.0100" twin twisted cables were soldered on. For shells 4 and 5, the heavier cables (7/.0100") were taken right to the gauges as it was found that the insulation cover of the thin wires was being cut on the shell edge during testing.

All gauges were checked to ensure that the resistance was 120 ohm and that there were no air bubbles under the gauge. This was done by connecting the gauge to a strain bridge with a needle indicator and then lightly rubbing the gauge with a finger. If any air bubbles were present the needle would flicker. Gauges were also checked to ensure that the resistance between the gauge and the shell was at least 500 megohms. The resistance was normally found to be between 5,000-10,000 megohms.

All gauges were water proofed with Budd GW-1 water-proofing compound. Extrados gauges were, in addition, covered with a layer of micro-crystalline petroleum wax for mechanical protection.

4.10.2 Strain Recording

A 200 channel strain data logger, manufactured for the Civil Engineering Department at Canterbury University by Edac (New Zealand) Ltd., was used to record strains from the shell, and can be seen in Figure 4.7. The data logger operated on a two arm circuit and required a separate dummy gauge for each active gauge. For the 1st shell, the gauges from Bryant's[6] shell were used as dummies and for the other shell tests the gauges on the 1st shell were used as dummy gauges. A power supply to feed the gauges was built into the logger and all circuits were kept alive continually. Gauges were connected to the logger in modules of twenty and the controls allowed the reading of any one gauge or group of modules. The data logger converted voltage differences to strains, and these could be read out onto a typewriter, tape punch or visual display panel. Reading of the gauges could be carried out at the rate of 1.3 seconds per gauge.

The makers claimed an accuracy of ±10 μ strains for the logger and this was easily obtained when it was operating properly. Except for the 3rd shell, calibration of the logger before and after each test indicated that it was operating to within ±5 μ strains. A check was kept for erroneous readings by connecting a Philips PR9249A/12 standard resistance box across the first channel of each module of twenty gauges. These standard boxes each had two temperature compensated gauges mounted inside them and thus the resistance did not change.

During testing of shells 1 and 3, zero drifts of the strain gauges of up to 50 μ strains occurred. This was corrected by subtracting from each gauge reading the drift of the standard box connected to the same module. By comparing zero readings recorded during these tests, it was found that the majority of gauges drifted to within ±10 μ strains of the drift of the standard box connected to the same module.

4.11 DEFLECTION MEASUREMENT

Deflection dial gauges mounted on a 1" x 1" x ¼" angle iron frame were used to record the displacements of the shell. This frame was bolted to the floor and was completely independent of the main reaction frame. Dial gauges used were of ½", 1" or 2" travel and divided into .01", .001" or .0001" divisions. Brass pads, 1" x 1" x 1/16", were glued to the shells for the dial gauge plungers to bear upon. All gauges were read, and readings recorded, manually.

Approximately 40 deflection gauges were positioned normal to the shell surface on the intrados of each shell during surface load testing. These were positioned at approximately

six inch centres along the transverse centre line and at twelve inch centres along both the longitudinal centre line and one edge. Different additional cross-sections and longitudinal sections were also gauged in each shell test. During prestressing, except for the 1st shell, deflection measurements were taken only across the transverse centre line.

For shells 3, 4 and 5, horizontal deflection measurements were taken at the midspan edge. These deflection gauges bore against a brass strip, glued to the shell intrados, which had been bent down to be in a vertical plane. However, due to rotation and vertical deflection of the shell edge, and consequently of the brass strip also, the deflection gauges did not accurately measure the horizontal movement of the shell edge. They did, however, give an indication of the direction of horizontal edge movement.

At the corners of each shell, three dial gauges were positioned - mutually at right angles - to record the movement of the shell on its supports. From these measurements, the remaining deflection readings obtained were corrected to give the displacement of the shell at each dial gauge location relative to unyielding supports.

4.12 REACTION FRAME

The reaction frame was constructed mainly from 6" x 6" x 15.7 lb universal column. Four 7'-0" columns, placed at the corners of a 13'-6" x 3'-9" rectangle, were joined along each long side by lengths of universal column, upon which the shell was placed during testing. Each column was bolted to the floor and each pair of end columns were tied together with a threaded ½" diameter bar.

For shells 1, 2 and 3 a flat reaction deck made of 2" x 6" x 4'-6" dressed rimu planks, bolted to lengths of universal column, was used. The deck was lined with 1/8" ivory board to prevent the air bag being pinched by the planks. Figure 4.8 shows the fully assembled reaction frame prior to the second shell test.

Shells 4 and 5, with larger included angles, were tested with the curved reaction deck shown in Figure 4.9. The reaction surface was formed from a sheet of 1/16" mild steel, shaped and strengthened with ½" plywood formers attached to the existing reaction deck. The steel sheet was secured to the formers.

4.13 LOADING TECHNIQUE

The shells were loaded by an air bag being inflated between the shell extrados and the reaction deck. A new airbag was constructed for each different size shell. In order to allow for movement between the airbag and shell surface, two layers of plastic, coated in French chalk, were placed between the airbag and shell.

For shells with 30° half included angle a flat reaction deck and 12" deep rectangular airbags were used. For testing, an initial gap of 4" was left between the crown of the shell and the reaction deck. This allowed for a 2" deflection of the shell edge before the airbag lost contact with the shell. However, at the very edge, the airbag tended to lift off the shell due to the large curvature of the unrestrained side of the airbag. This effect was minimized by timber side supports (see Figure 4.8) made from 3/8" hardboard backed by two lengths of 6" x 2" timber. The 6" x 2" timber was bolted to the

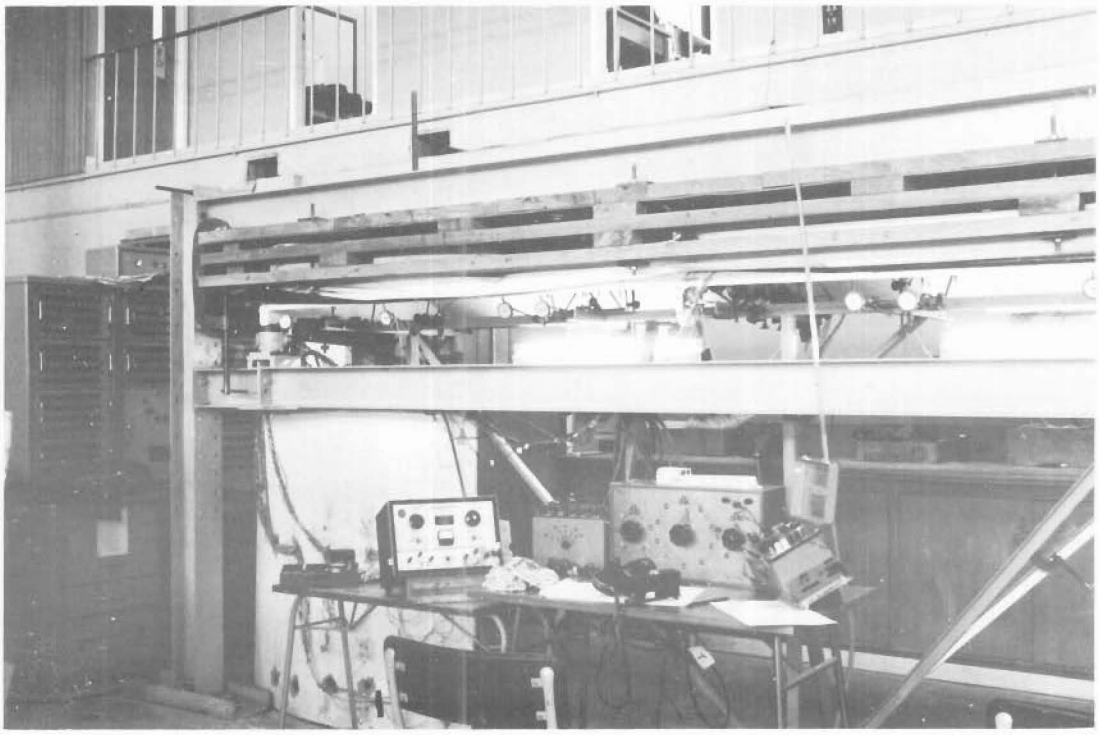

FIG 4.8 REACTION FRAME USED FOR SHELLS 1,2 & 3.

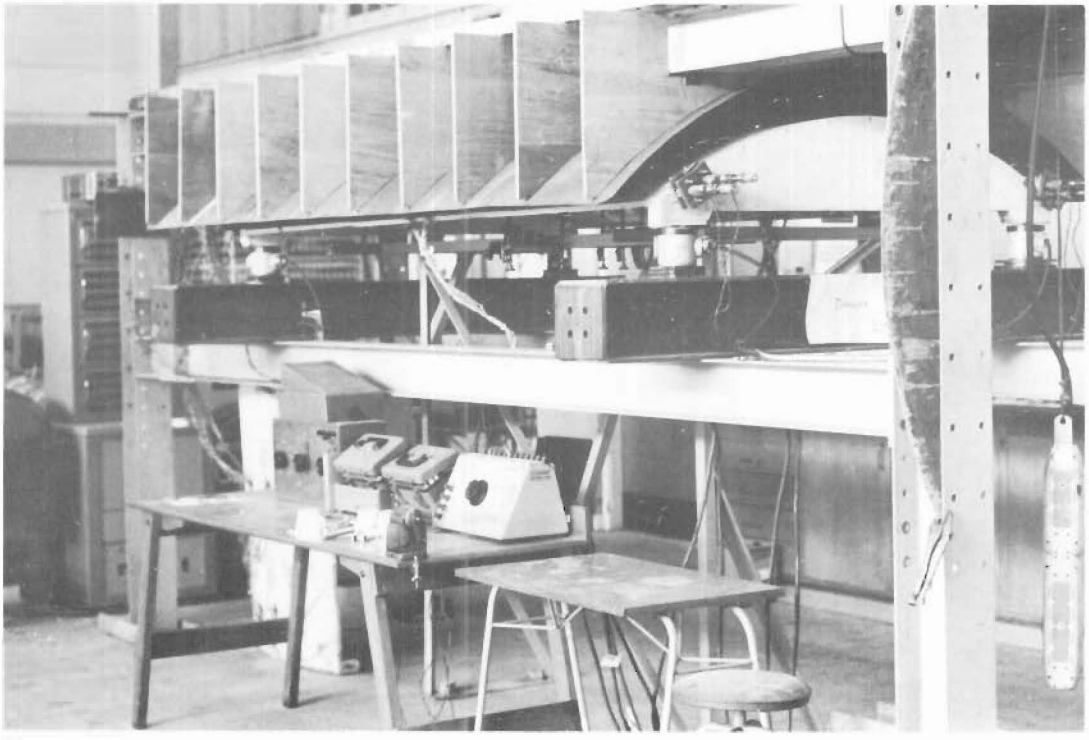

FIG.4.9 REACTION FRAME USED FOR SHELLS 4&5.

reaction deck and could be moved in and out as required.

For shells 4 and 5, with larger included angles, a flat reaction deck was not practicable and so a curved reaction deck and 6" deep rectangular airbags were used. The reaction deck was positioned 3" above the shell extrados and no side restraints were necessary.

All airbags were constructed from a rubberized apron material and the joints joined with Ados D2 adhesive, a one component contact cement. Each airbag had two ¼" diameter inlets with one leading to a water-air manometer and the other to the control board. Air was supplied to the control board from a compressor, through a reducing valve set at 10 psi. There were two valves on the inlet side of the control board to allow for very fine adjustment, and one valve on the outlet. By having a small amount of air going continually through the valves, pressure in the bag could be maintained to within ±.005' of the required pressure. A ½" diameter outlet plug was built into each airbag for rapid deflation.

In order to check the load on the shell as calculated from the manometer readings, each corner of the shell was placed on a load cell. These were all 2 ton Philips PR9226/02 load cells and were connected through a 4-arm switch box to a Budd P-360 portable strain indicator. The load cells were arranged with fixed, roller or ball bearing supports so that unrestrained lateral and longitudinal movement of the shell could take place. A 2 ton load cell and a roller support are shown in Figure 4.6. ½" thick steel plates were attached to the bottom of each traverse as can be seen in Figure 4.6. Each of these had a hemispherical indentation made on it, into which a ½" diameter ball on top of the load cell fitted. Each

load cell was calibrated before and after each test on an Avery 25,000 lbs testing machine. Generally three calibration runs were made, with the agreement between calibration before and after the tests being within 15 lb over the whole range. These four load cells also served to show up any non-uniformity in the distribution of load over the shell.

4.14 TESTING PROCEDURE

Testing was carried out by three persons: one person reading the deflection gauges and operating the data logger, another person maintaining the airbag at the correct pressure, and the third person recording deflection gauge readings, obtaining and recording load cell readings, and coordinating the test.

Initially each shell was cycled to a load of 10-15 lb/ft^2 two or three times as preliminary dummy runs. Zero readings were then taken and the shell loading begun. At each increment, once the correct load had been applied, the deflection readings were read and recorded. This took approximately five minutes. Strain measurements were then recorded by the data logger on both the typewriter and on paper tape. During this time the load cell readings were recorded. The shell was then inspected, any cracks or crack extensions being marked and labelled. The load cycles to which the shells were subjected are given in Figure 4.10. Each shell was tested over a period of approximately one week.

Deflection gauges were removed when they ran out of travel or when failure of the shell appeared imminent.

4.15 EVALUATION OF YOUNG's MODULUS

Experimental values of Young's modulus, E, for the micro

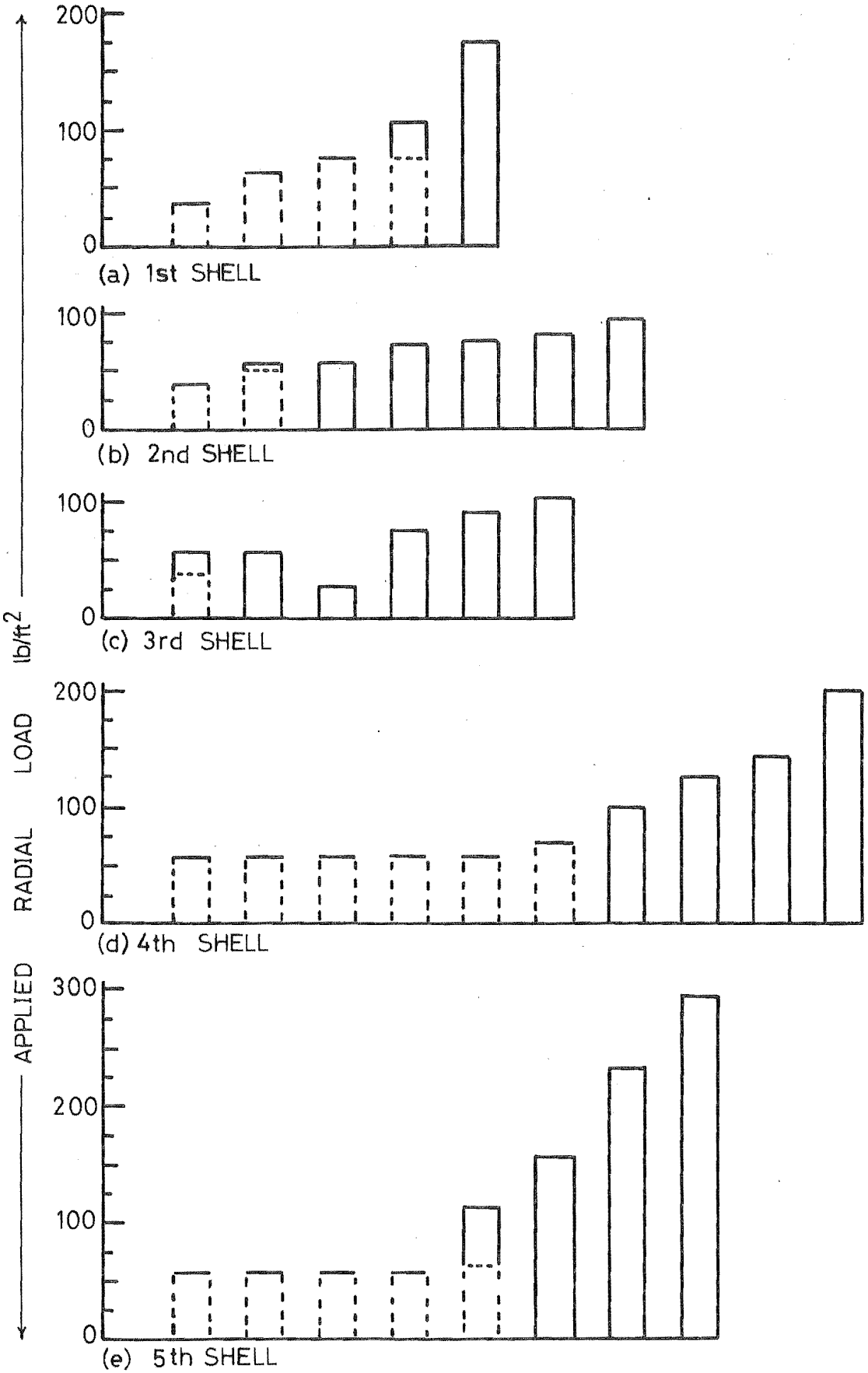

FIG. 4·10 LOADING SEQUENCE FOR SHELLS.

concrete shells were obtained by testing 24" x 6" x 0.6" reinforced slabs in bending. These slabs were supported at their ends and loaded equally at their $^1/_3$ points. Both deflection and strain measurements were taken at midspan and used to calculate E. A more detailed description of the testing technique and the method used for calculating E is given in Appendix B.2. Values of E obtained are given in Table B.5.

From these results it can be seen that for both micro-concrete mixes a lower average E was obtained when calculated from deflection measurements (E_D = 4.1 x 10^6 lb/in^2, and 5.1 x 10^6 lb/in^2) than from strain measurements (E_S = 4.5 x 10^6 lb/in^2 and 5.7 x 10^6 lb/in^2). Hence in reducing experimental strains to stresses, the average E_D for that particular mix was used; and for calculating theoretical deflections for a shell, the average E_S for that particular shell mix was used.

Also included in Table B.5 are the values of E_D and E_S obtained for two slabs which were prestressed longitudinally to an average prestress of 500 psi. These results show that while E_S remained similar to the value obtained for the non-prestressed slabs, E_D increased and approached the value of E_S.

Neuman[27], using a similar testing technique to the author, also found that E_D was lower than E_S. He postulated that E_D was lower due to micro-cracking reducing the stiffness of the slab. Whereas E_D depends on the stiffness of the whole slab, E_S depends only on the stiffness of the slab at the strain gauge. It would be reasonable to expect that the glue layer and strain gauge would delay the formation of micro-

GAUGE No.	5TH SHELL STRAIN READINGS (μ STRAINS) FOR CONSECUTIVE LOAD CYCLES AT AN APPLIED LOAD OF 56 lb/ft^2.					AVERAGE	STANDARD DEVIATION
1	-2	-3	1	0	-3	-1.4	1.6
2	-59	-66	-57	-56	-58	-59.2	3.5
3	-104	-100	-95	-94	-96	-97.8	3.7
4	-124	-133	-112	-118	-115	-120.4	7.4
5	5	11	12	13	13	10.8	2.9
6	-13	-21	-12	-12	-14	-14.4	3.3
7	-73	-79	-68	-67	-71	-71.6	4.2
8	-106	-110	-97	-99	-105	-103.4	4.7
9	-119	-119	-107	-109	-114	-113.6	4.9
10	-118	-112	-104	-105	-112	-110.2	5.1
11	-89	-93	-82	-90	-87	-88.2	3.6
12	-13	-15	-7	-12	-8	-11.0	3.0
13	9	8	16	15	15	12.6	3.3
14	-136	-135	-127	-127	-132	-131.4	3.8
15	-57	-49	-41	-42	-49	-47.6	5.7
16	48	46	52	55	53	50.8	3.3
17	27	49	52	53	50	46.2	9.7
18	226	254	295	273	-101	189.4	146.9
19	-22	-19	-4	-18	-20	-16.6	6.4
20	0	3	3	2	5	2.6	1.6
21	-1	-1	-1	-2	2	-0.8	1.4
22	43	48	48	48	48	47.0	2.0
23	-54	-53	-55	-59	-50	-54.2	2.9
24	-131	-122	-119	-127	-119	-123.6	4.7
25	-127	-121	-119	-123	-119	-121.8	2.9
26	-117	-112	-115	-118	-113	-115.0	2.2
27	-61	-55	-58	-60	-59	-58.6	2.0
28	-83	-78	-81	-84	-77	-80.6	2.7
29	100	116	114	115	120	113.0	6.8
30	-131	-126	-123	-129	-121	-126.0	2.6
31	-190	-188	-184	-191	-182	-187.2	3.1
32	-217	-204	-200	-209	-203	-206.6	5.9
33	3	10	17	14	14	11.6	4.8
34	7	13	8	2	12	8.4	3.9
35	58	63	65	65	67	63.6	3.0
36	101	105	101	102	105	102.8	1.8
37	109	113	110	112	112	111.2	1.4
38	35	93	87	90	90	79.0	22.0
39	65	83	78	77	76	75.8	5.9
40	2	17	10	10	8	9.4	4.8
41	-2	-2	0	3	3	0.4	2.2
42	-243	-238	-233	-240	-234	-237.6	3.7
43	-136	-135	-130	-133	-131	-133.0	2.2
44	-14	-10	-8	-9	-11	-10.4	2.0
45	25	39	32	32	31	31.8	4.4
46	13	18	14	14	16	15.0	1.7
47	6	5	6	2	7	5.2	1.7
48	12	12	15	16	14	13.8	1.6
49	-14	16	20	23	19	12.8	13.5
50	-25	-10	-9	-10	-11	-13.0	6.0
51	-132	-135	-127	-132	-130	-131.2	2.6
52	-212	-44	-121	-91	444	-4.8	231.0
53	-247	-234	-224	-234	-237	-235.2	7.3
54	-186	-178	-173	-181	-180	-179.6	4.2
55	-136	-126	-125	-136	-133	-131.2	4.7
56	88	91	91	94	91	91.0	1.8
57	-78	-72	-73	-76	-73	-74.4	2.2
58	36	47	44	47	45	43.8	4.0
59	4	16	18	16	16	14.0	5.0
60	4	4	7	8	5	5.6	1.6

Note: Results from all gauges have been included even though results from some gauges (e.g. 18,52) are obviously in error.

TABLE 4.4 TYPICAL REPEATABILITY OF STRAIN MEASUREMENTS

cracks at the strain gauge location and thus the strain measurement would give a higher E value than that calculated from deflection measurements. The tests performed by the author on prestressed slabs support this argument. Under prestress load, micro-cracking is delayed everywhere, thus increasing E_D but leaving E_S unchanged. A higher E_D for theoretical deflection calculations has not been used due to the tentative nature of the above argument and the variation of compressive stress throughout the shells.

4.16 ANALYSIS OF STRAIN DATA

4.16.1 Prestressing

Generally three sets of strain readings were taken before and after the prestressing force was applied to a shell. For each gauge the average strain, both before and after prestressing, was calculated, and the difference of these averages was taken as the strain due to the particular force being applied. The majority of gauge readings fell within ±2 μ strains of the average reading.

For the four segmented shells, the readings obtained during the joining process were almost meaningless. This was because the timber formwork upon which they were joined greatly influenced the strain distribution in the shells by resisting movement of the shells.

4.16.2 Surface Loading

The experimental strain data obtained during surface loading was analysed to obtain accurate strain results for the elastic behaviour of each shell at design working load (56 lb/ft^2).

Initially the strain results for each shell were checked to see for which load cycles strain was linear with load. These cycles are shown dashed on Figure 4.10. When strain increase was linear with load, the scatter of strain readings from the line of best fit was normally less than ±5 μ strains for each gauge.

When three or more load cycles were linear to 56 lb/ft^2, the strains for each gauge due to this load were averaged and used to obtain experimental stresses for comparison with theory. Typical values are shown in Table 4.4, for the 5th shell. Results for which the standard deviation was greater than 10 μ strains were discarded. The linearity of the results was then checked for each gauge by considering the average reading at both 18.67 lb/ft^2 and 37.33 lb/ft^2. If, when one of these averages was scaled up to 56 lb/ft^2, it did not agree to within 10 μ strain of the 56 lb/ft^2 average value, results from that gauge were discarded. Generally agreement was to within ± 3 μ strain.

If three linear cycles to 56 lb/ft^2 were not available, the 56 lb/ft^2 results for comparison with theoretical results were obtained by extrapolating each linear cycle to 56 lb/ft^2, using results from each increment of the load cycle. The results obtained were then averaged. For the 2nd shell there were two linear load cycles. Any gauges not agreeing to within 10 μ strains, when their readings were extrapolated to a load of 56 lb/ft^2, were discarded. In the case of the 3rd shell, no accurate check on the strain repeatability could be made as cracking occurred in the first load cycle.

4.16.3 Symmetry and Reliability

Readings from symmetrical gauge positions showed that

all shells behaved symmetrically during prestressing and elastic surface loading.

No attempt was made to repeat the prestressing of any shell due to the possibility of damaging the shell or losing the calibration of the prestressing load cells. However, one indication that the repeatability of strain readings was good is given by the 1st shell results (see Figures 5.1 and 5.2) where two of the sets of results are for similar loads. More than one set of results was obtained for the 1st shell due to slipping of prestress cables during stressing. Also during prestressing of the 5th shell, an outside cable failed at full load, and upon restressing the strains were to with ±10 μ strain of their former values.

For surface loading, the repeatability of the strain readings was excellent in the elastic range. At each load increment, the agreement between the load on the shell indicated by the manometer readings and the 2 ton load cell readings was checked. Except at low loads (up to 15 lb/ft^2) the maximum variation for any shell was 7%, the agreement often being better than 1%. Within the elastic range for all shells, the loads recorded on each of the 2 ton load cells were normally within 20 lb of the average load. Strain results were discarded from any load increment where the agreement between manometer and corner load cells was greater than 5%, or where the load recorded by any of the corner load cells was more than 20 lb from the average.

4.17 ANALYSIS OF DEFLECTION DATA

All deflection readings were corrected for the movement of the shells on their supports.

4.17.1 Prestressing

Deflection readings were taken before and after prestressing. The difference of the corrected readings was taken as the displacement due to that particular prestress force.

4.17.2 Surface Loading

Deflection results were repeatable and linear before the shells cracked. The variation between readings from different cycles, for the same gauge, at a load of 56 lb/ft^2 was generally less than 0.005".

In calculating the 56 lb/ft^2 deflections for comparison with experimental results, the 56 lb/ft^2 results from two linear elastic cycles, when available, were averaged. For the 2nd shell, the deflections were calculated by extrapolating to 56 lb/ft^2 from linear results of the first two load cycles. Extrapolation was also used for the 3rd shell, on the first load cycle, to obtain the 56 lb/ft^2 deflection. However no accurate check on the repeatability of the 3rd shell results was possible as cracking occurred during the first load cycle.

4.17.3 Symmetry and Reliability

There was a slight degree of non-symmetry in all shells. The shells behaved more symmetrically in the longitudinal direction than transversely; however in both directions, symmetrically located gauges showed similar trends.

As prestressing was not repeated no indication of the repeatability of the deflection readings was obtained. However for surface loading, the repeatability of the deflection measurements was excellent, despite movement of the shells on their supports.

CHAPTER FIVE

EXPERIMENTAL AND THEORETICAL RESULTS

5.1 ELASTIC BEHAVIOUR

From the experimental elastic strains, moments and normal forces were calculated assuming linear elastic behaviour across the shell thickness. In addition, for the 1st shell, in-plane shear forces and twisting moments were also calculated at the rosette gauge locations. Values of actions were averaged for symmetrical gauge locations on each shell.

Elastic theoretical results were obtained by use of the D.K.J. computer program, described in Appendix A, and run on the University of Canterbury's I.B.M. 360/44 computer. Three Fourier terms were used in applying the radial surface loading. The prestress anchorage forces were applied as rectangular shear blocks extending 0.05L into each shell, with the simplified beam on elastic foundation method of Section 2.5.5 being used to calculate the distribution of prestress force on the end of the shell. Line loads along the cables were considered by dividing half of shell length into 20 transverse strips and considering generators spaced at 1½" to 3". All prestressing terms were expanded as the sum of the first 10 Fourier terms.

5.1.1 Prestressing

Figures 5.1 to 5.7 show comparisons of the experimentally determined actions and deflections with theoretical results.

Longitudinal Normal Force. This was the dominant action in all shells. Agreement between experimental and theoretical

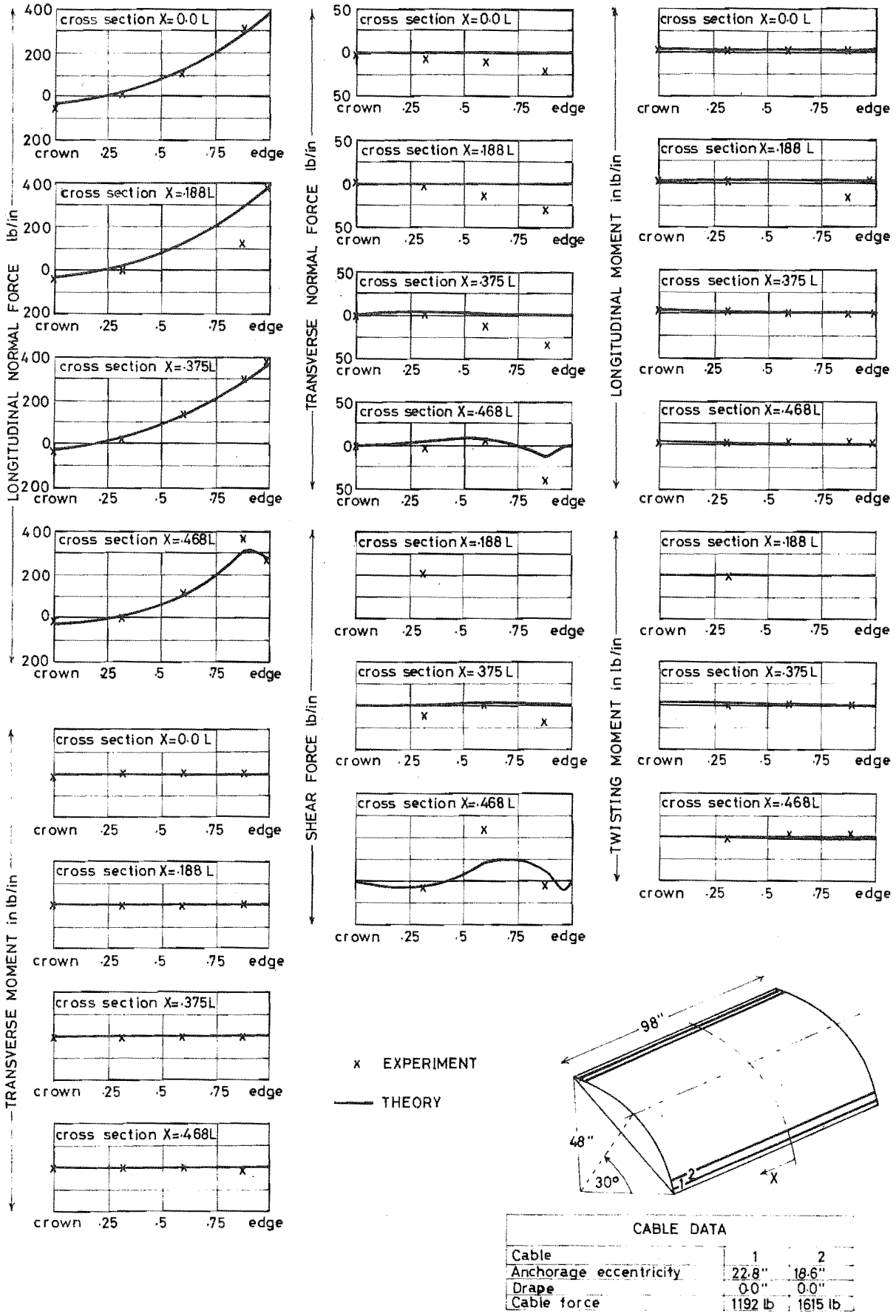

CABLE DATA		
Cable	1	2
Anchorage eccentricity	22·8"	18·6"
Drape	0·0"	0·0"
Cable force	1192 lb	1615 lb

FIG. 5.1 1st SHELL PRESTRESSING ACTIONS AND DISPLACEMENTS

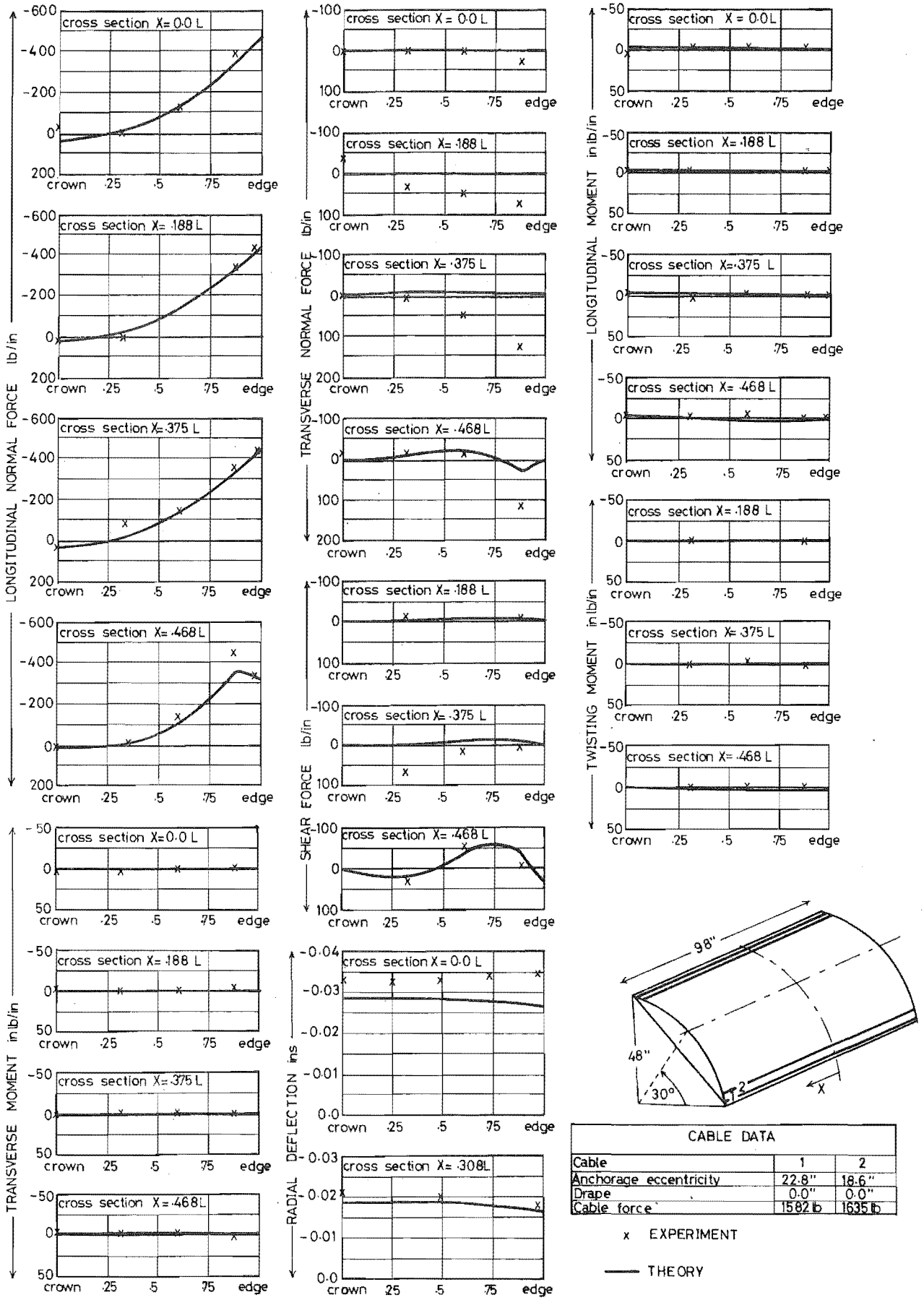

FIG. 5.2 1st SHELL PRESTRESSING ACTIONS AND DISPLACEMENTS

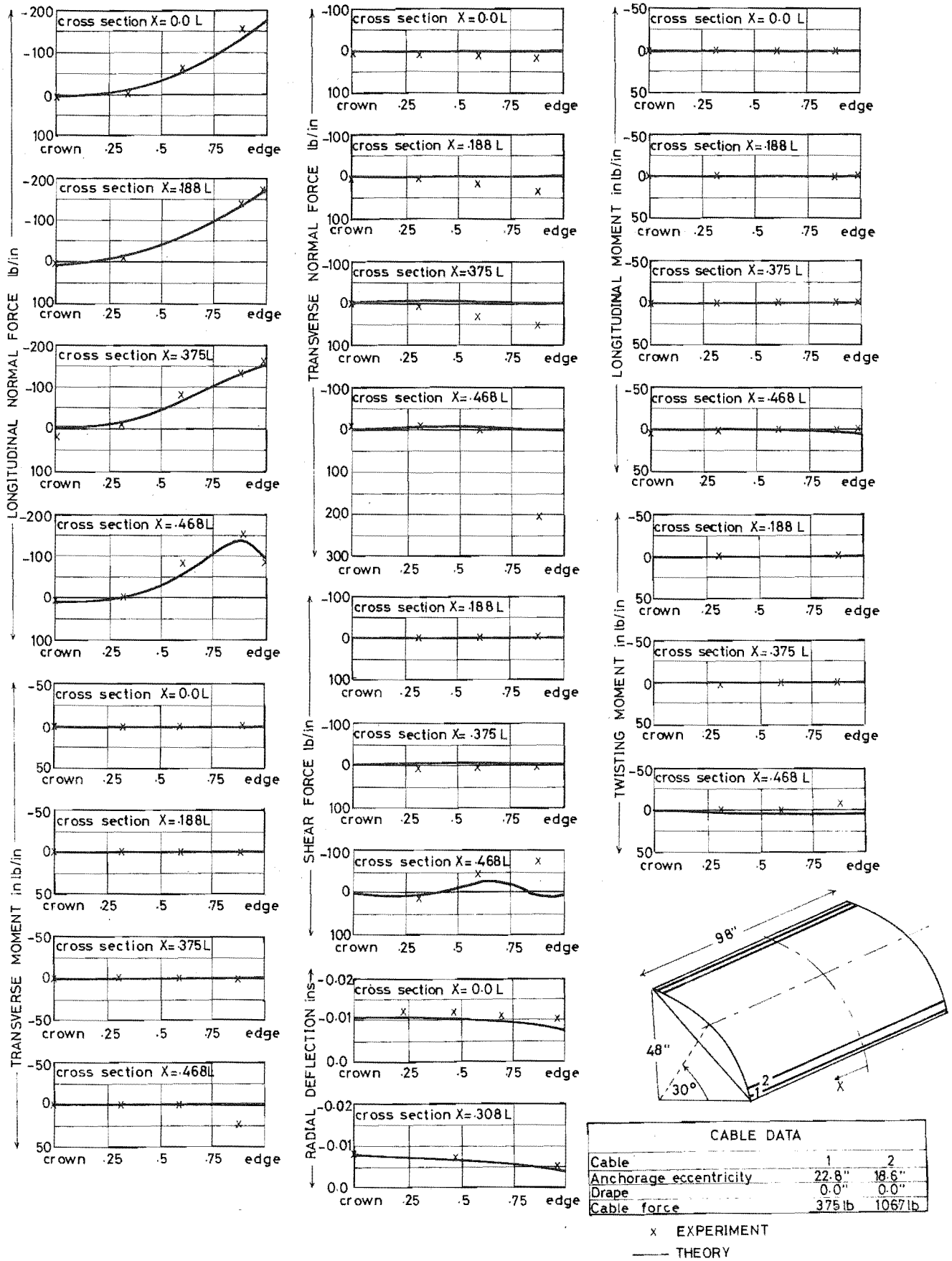

FIG. 5.3 1st SHELL PRESTRESSING ACTIONS AND DISPLACEMENTS

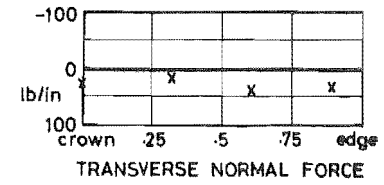

TRANSVERSE NORMAL FORCE

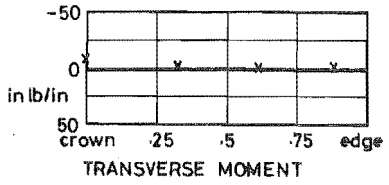

TRANSVERSE MOMENT

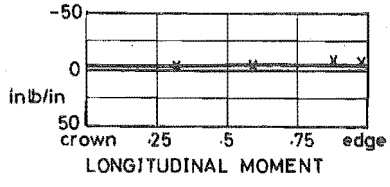

LONGITUDINAL MOMENT

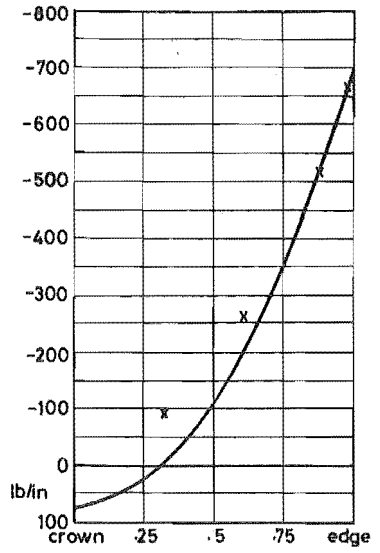

LONGITUDINAL NORMAL FORCE

CROSS SECTION X = 0.0

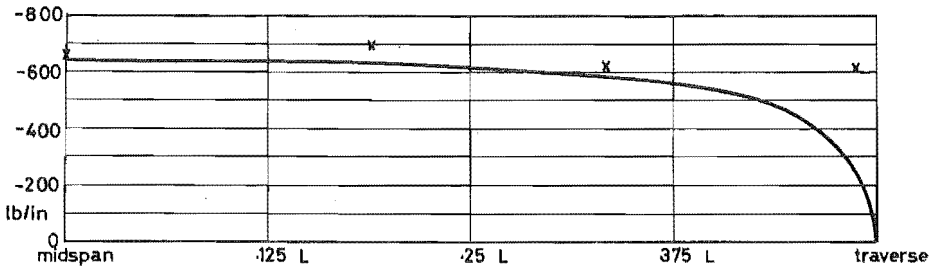

LONGITUDINAL NORMAL FORCE

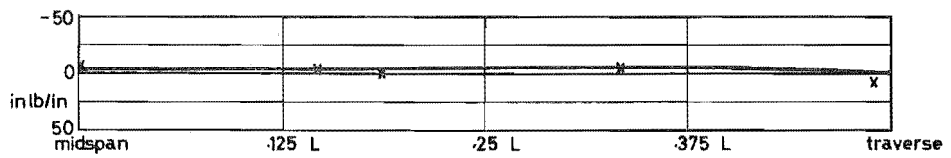

LONGITUDINAL MOMENT

LONGITUDINAL EDGE

x EXPERIMENT

— THEORY

CABLE DATA			
Cable	1	2	3
Anchorage eccentricity	22·8"	20·4"	18·0"
Drape	0·0"	0·0"	0·0"
Cable force	410 lb	2160 lb	2160 lb

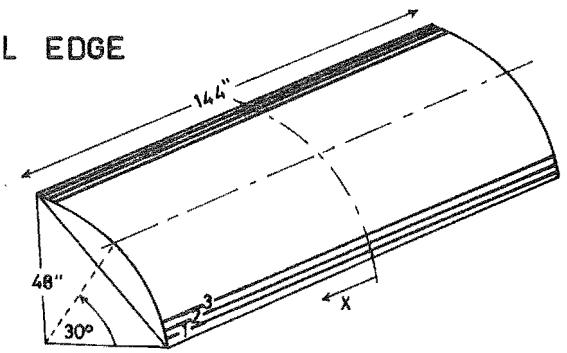

FIG.5.4 2nd SHELL PRESTRESSING ACTIONS AND DISPLACEMENTS

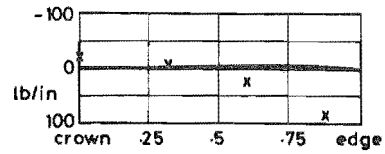

TRANSVERSE NORMAL FORCE

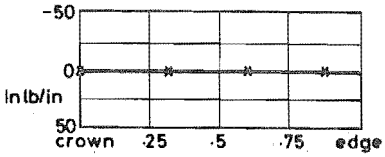

TRANSVERSE MOMENT

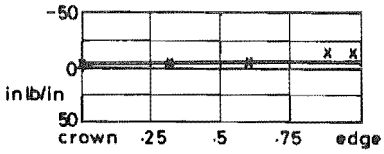

LONGITUDINAL MOMENT

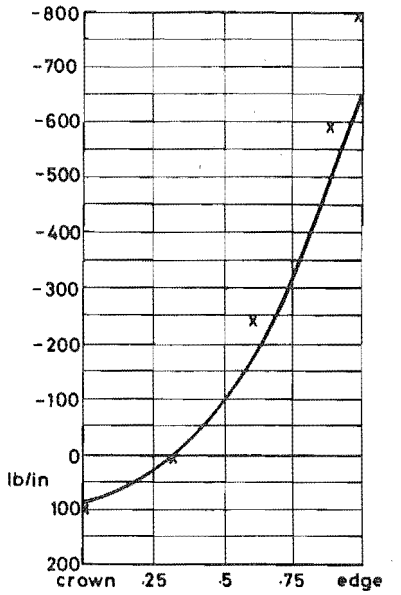

LONGITUDINAL NORMAL FORCE

CROSS SECTION

X = 0.0

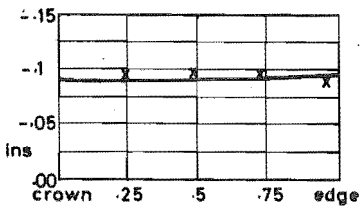

RADIAL DEFLECTION

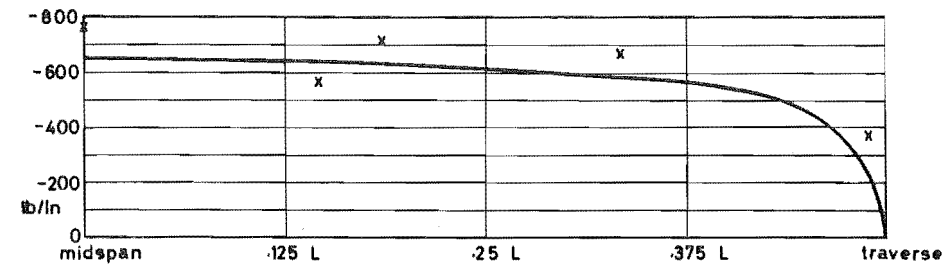

LONGITUDINAL NORMAL FORCE

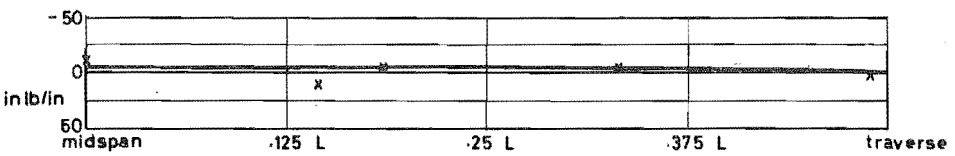

LONGITUDINAL MOMENT

LONGITUDINAL EDGE

x EXPERIMENT

— THEORY

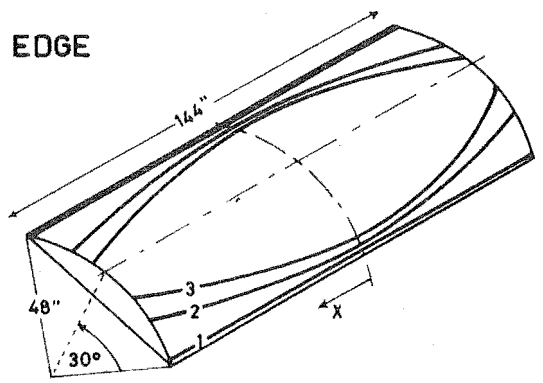

CABLE DATA			
Cable	1	2	3
Anchorage eccentricity	22·8"	15·9"	9·0"
Drape	0·0"	4·5"	9·0"
Anchorage force	2160 lb	2160 lb	2160 lb

FIG.5.5 3rd SHELL PRESTRESSING ACTIONS AND DISPLACEMENTS

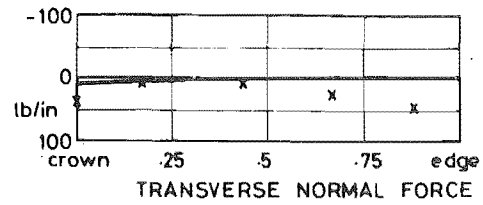

TRANSVERSE NORMAL FORCE

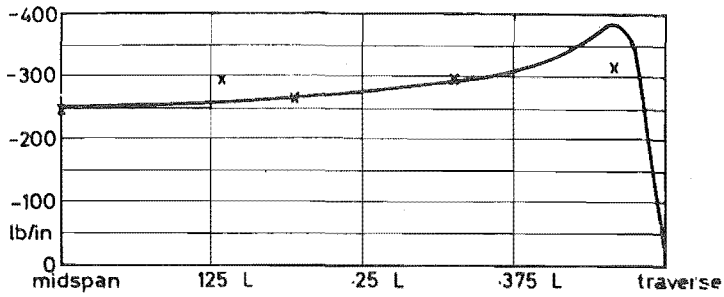

LONGITUDINAL NORMAL FORCE

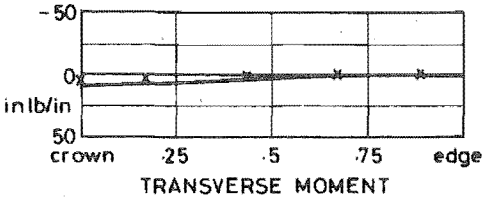

TRANSVERSE MOMENT

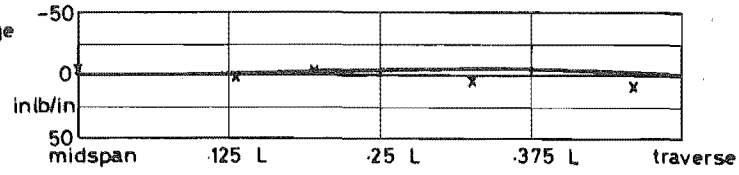

LONGITUDINAL MOMENT

LONGITUDINAL EDGE

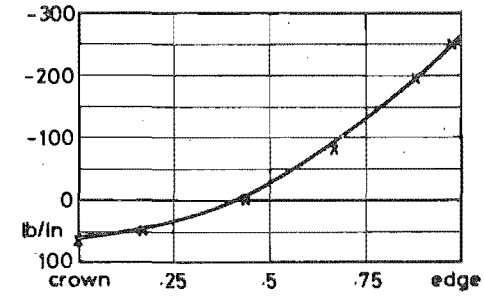

LONGITUDINAL NORMAL FORCE

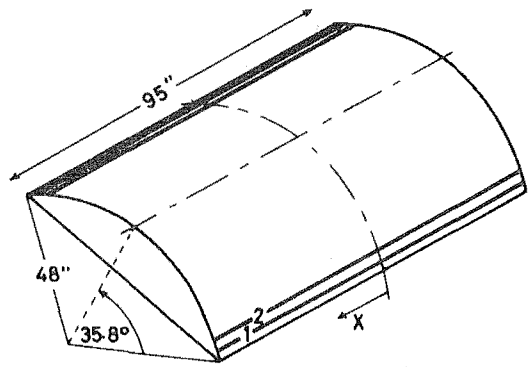

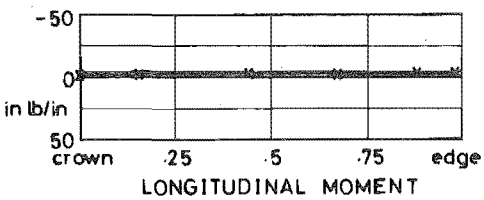

LONGITUDINAL MOMENT

CABLE DATA		
Cable	1	2
Anchorage eccentricity	28"	26"
Drape	0"	0"
Anchorage force	1600 lb	0 lb

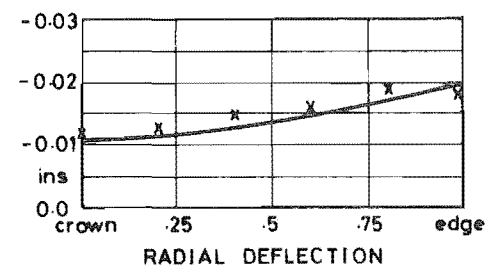

RADIAL DEFLECTION

× EXPERIMENT

— THEORY

CROSS SECTION X = 0.0

FIG. 5.6 4th SHELL PRESTRESSING ACTIONS AND DISPLACEMENTS

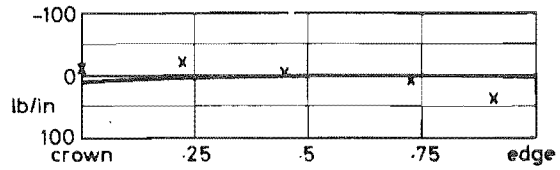

TRANSVERSE NORMAL FORCE

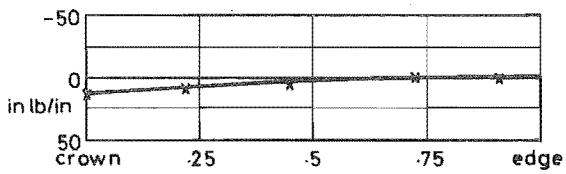

TRANSVERSE MOMENT

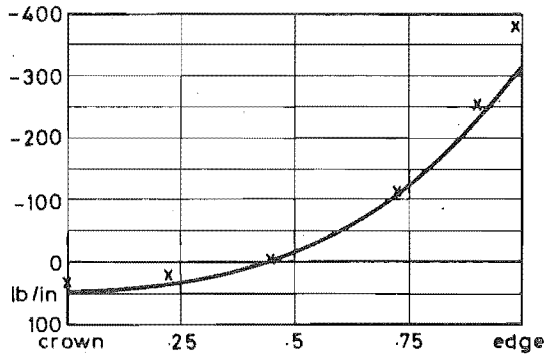

LONGITUDINAL NORMAL FORCE

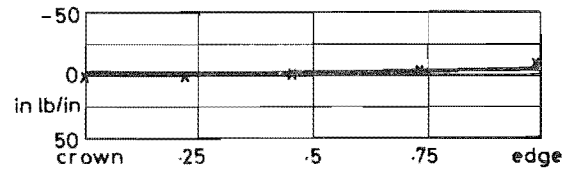

LONGITUDINAL MOMENT

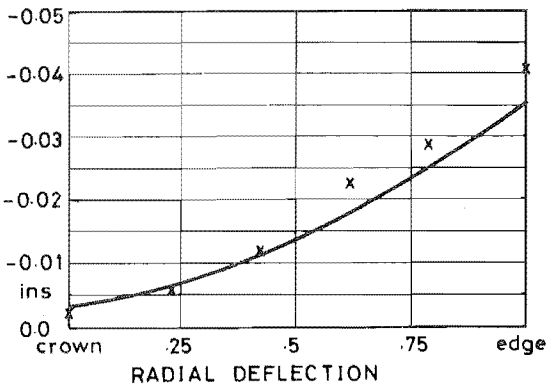

RADIAL DEFLECTION

CROSS SECTION X = 0.0

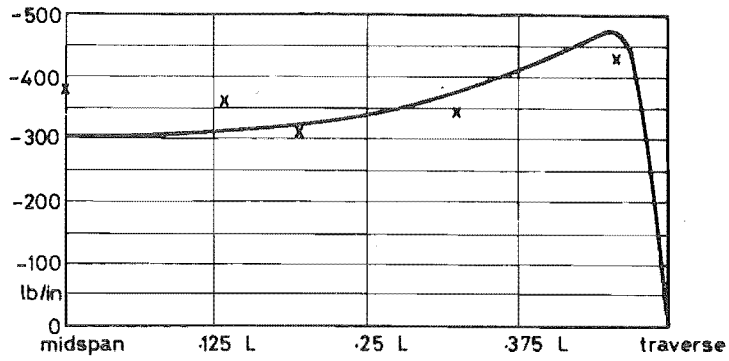

LONGITUDINAL NORMAL FORCE

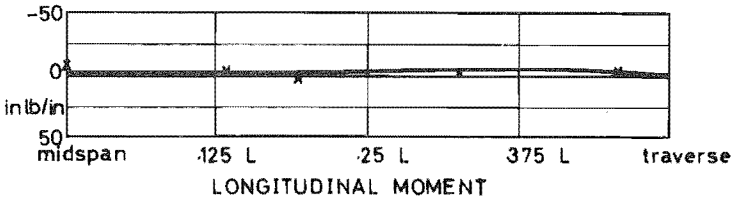

LONGITUDINAL MOMENT

LONGITUDINAL EDGE

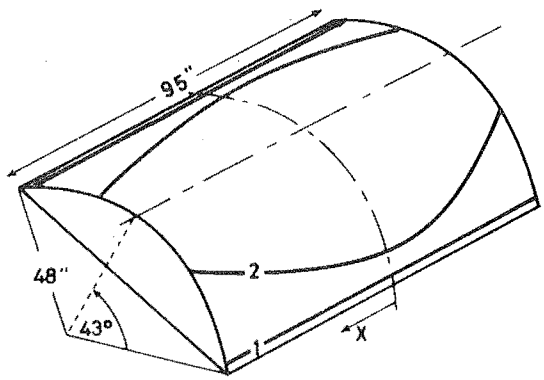

CABLE DATA		
Cable	1	2
Anchorage eccentricity	34"	20"
Drape	0"	10"
Anchorage force	2000 lb	0 lb

x EXPERIMENT

—— THEORY

FIG. 5.7 5th SHELL PRESTRESSING ACTIONS AND DISPLACEMENTS

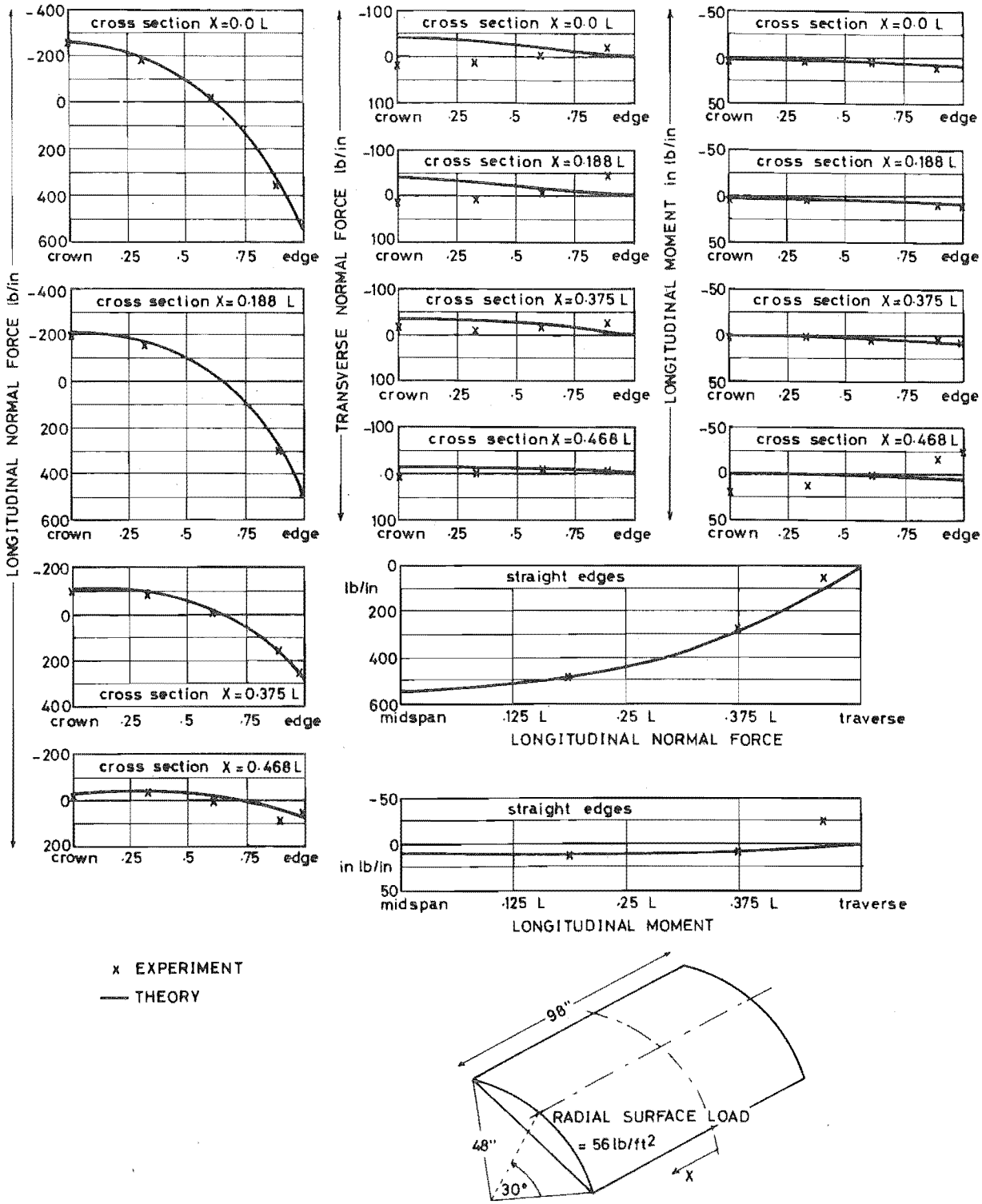

FIG.5.8(a) 1st SHELL SURFACE LOADING ACTIONS AND DISPLACEMENTS

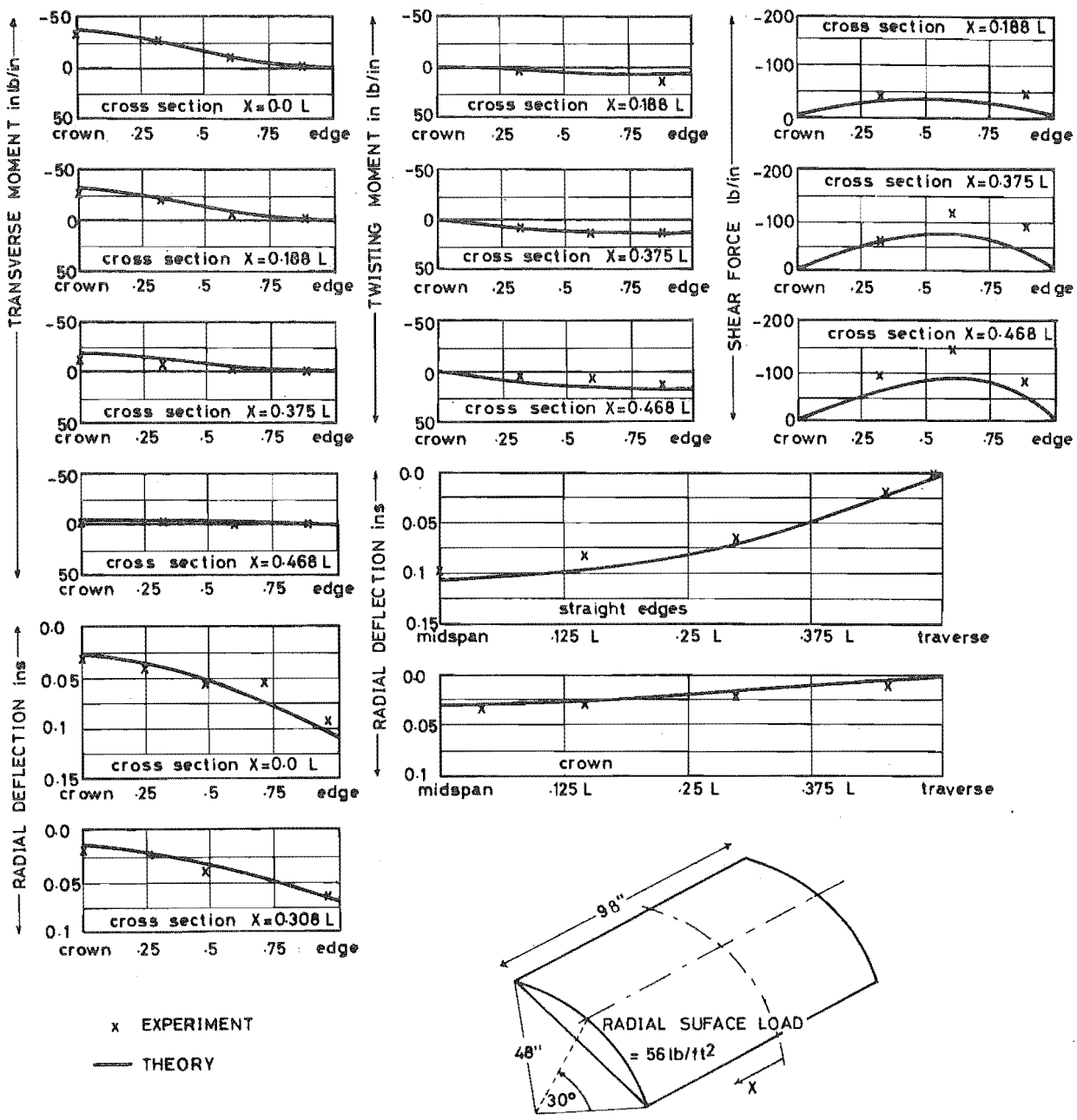

FIG. 5.8(b) 1st SHELL SURFACE LOADING ACTIONS AND DISPLACEMENTS

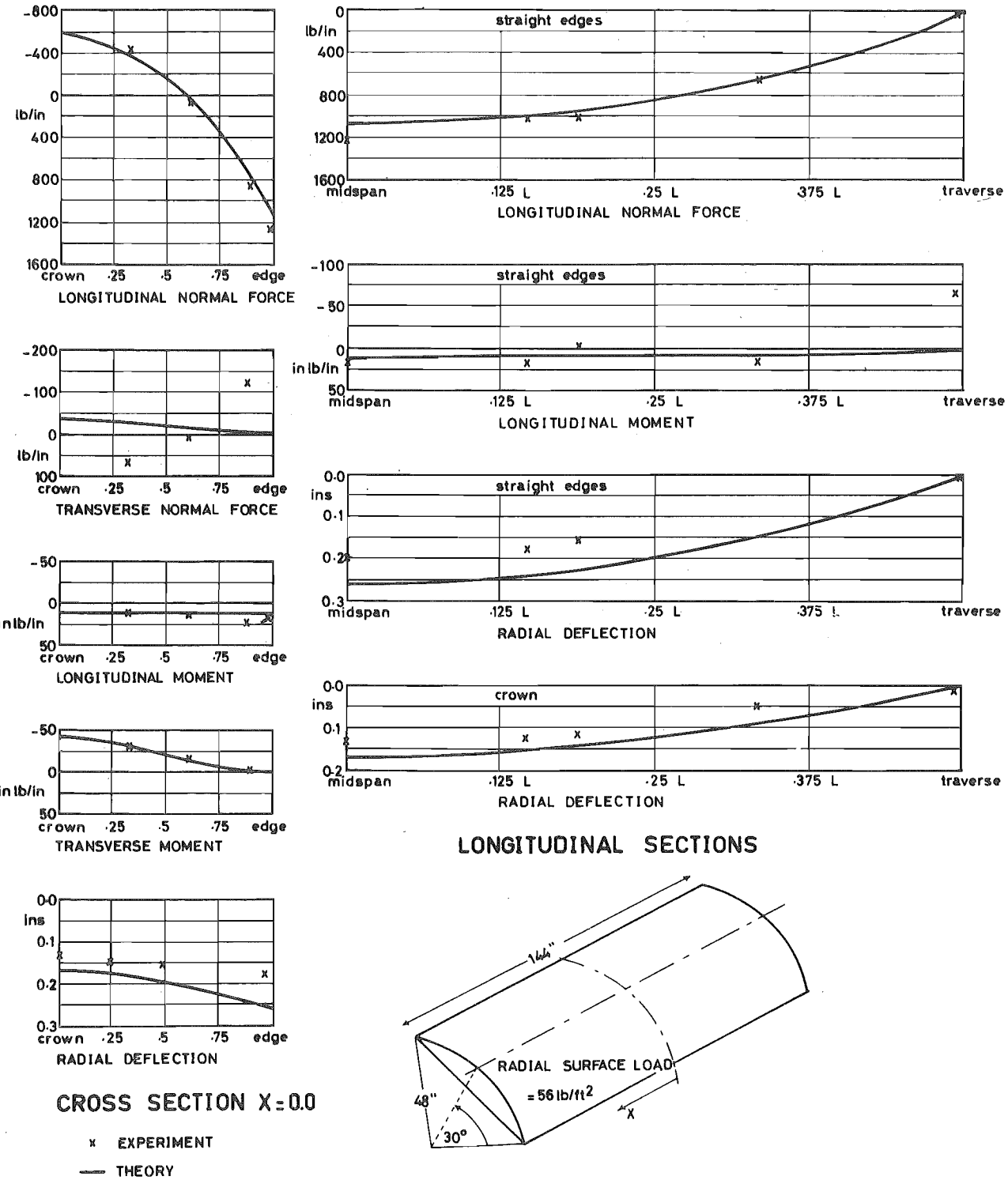

FIG. 5.9 2nd SHELL SURFACE LOADING ACTIONS AND DISPLACEMENTS

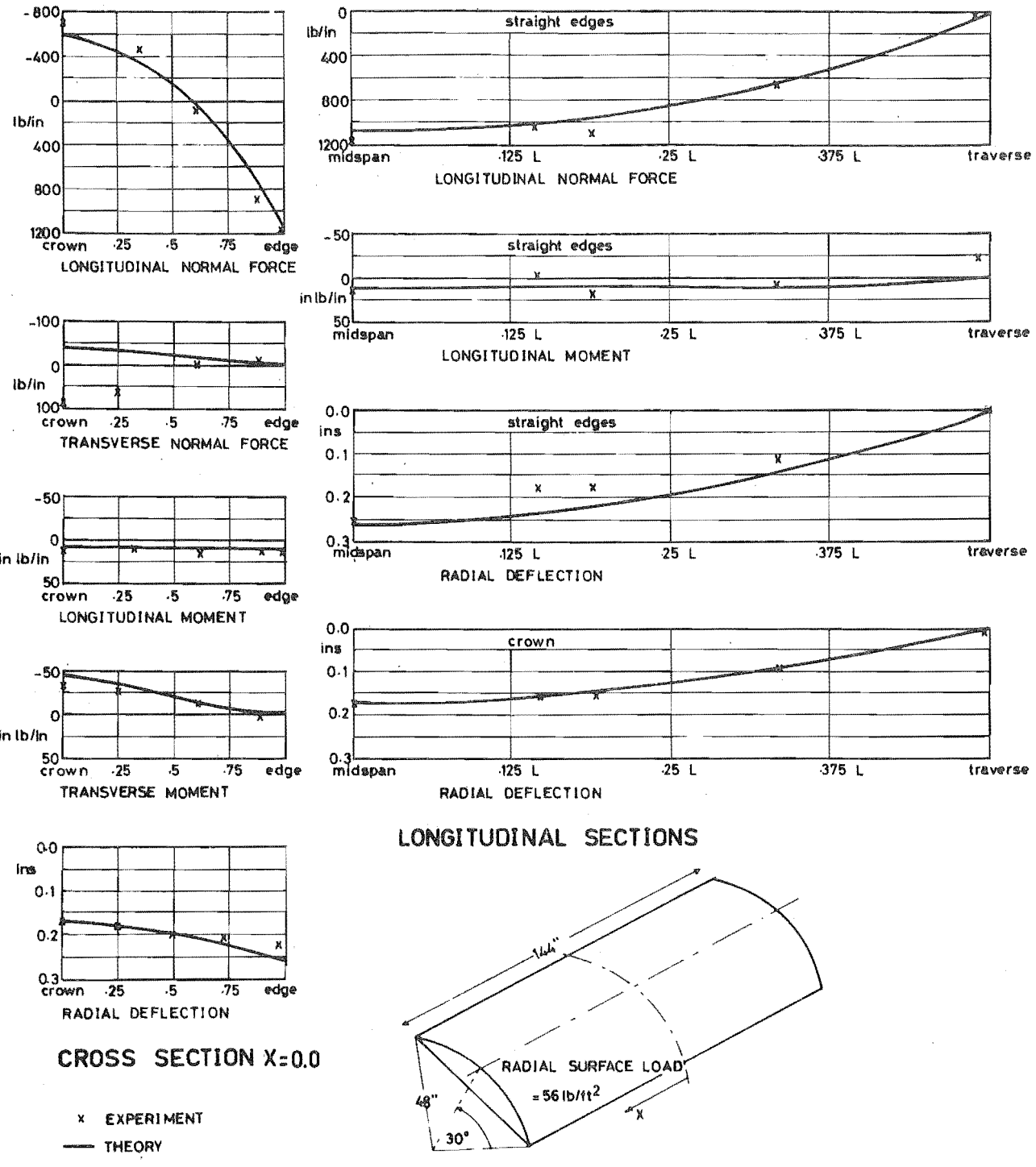

FIG. 5.10 3rd SHELL SURFACE LOADING ACTIONS AND DISPLACEMENTS

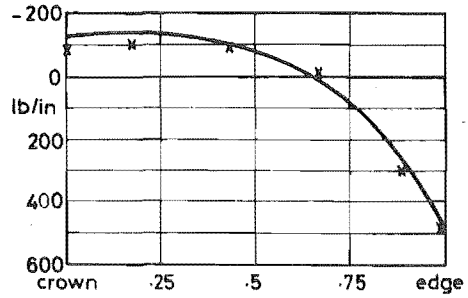

LONGITUDINAL NORMAL FORCE

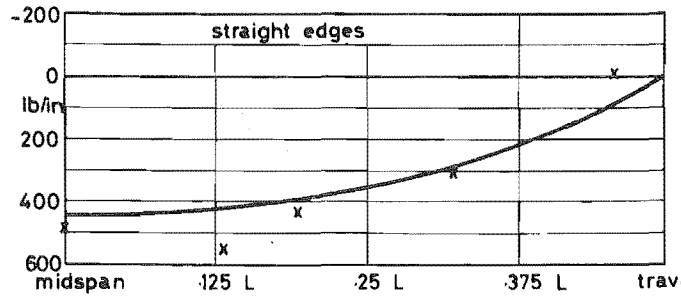

LONGITUDINAL NORMAL FORCE

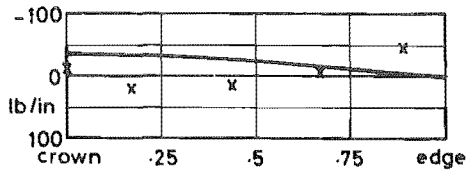

TRANSVERSE NORMAL FORCE

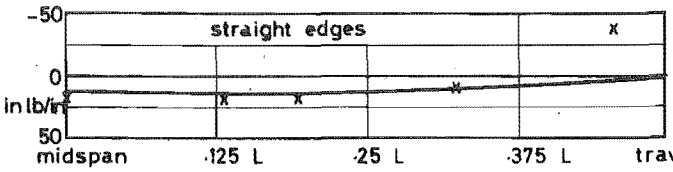

LONGITUDINAL MOMENT

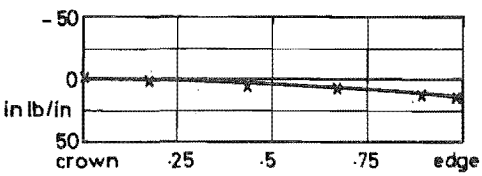

LONGITUDINAL MOMENT

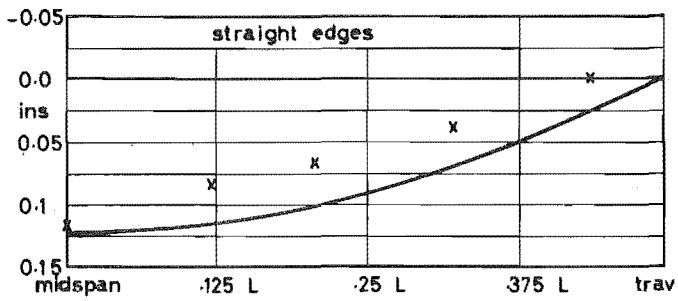

RADIAL DEFLECTION

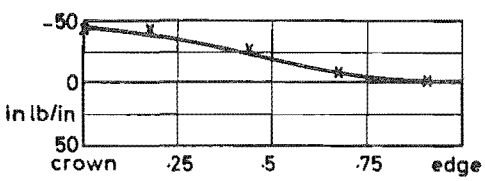

TRANSVERSE MOMENT

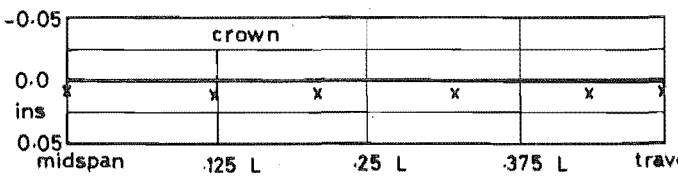

RADIAL DEFLECTION

LONGITUDINAL SECTIONS

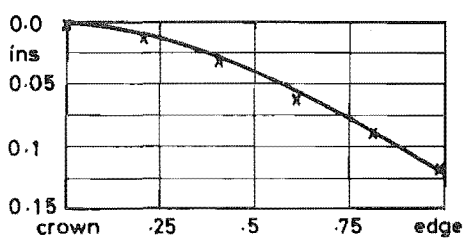

RADIAL DEFLECTION

CROSS SECTION X = 0·0

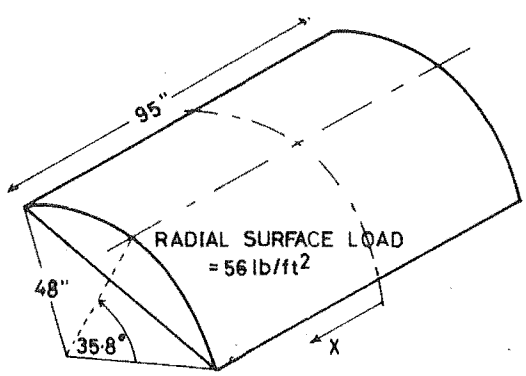

x EXPERIMENT

— THEORY

FIG. 5.11 4th SHELL SURFACE LOADING ACTIONS AND DISPLACEMENTS

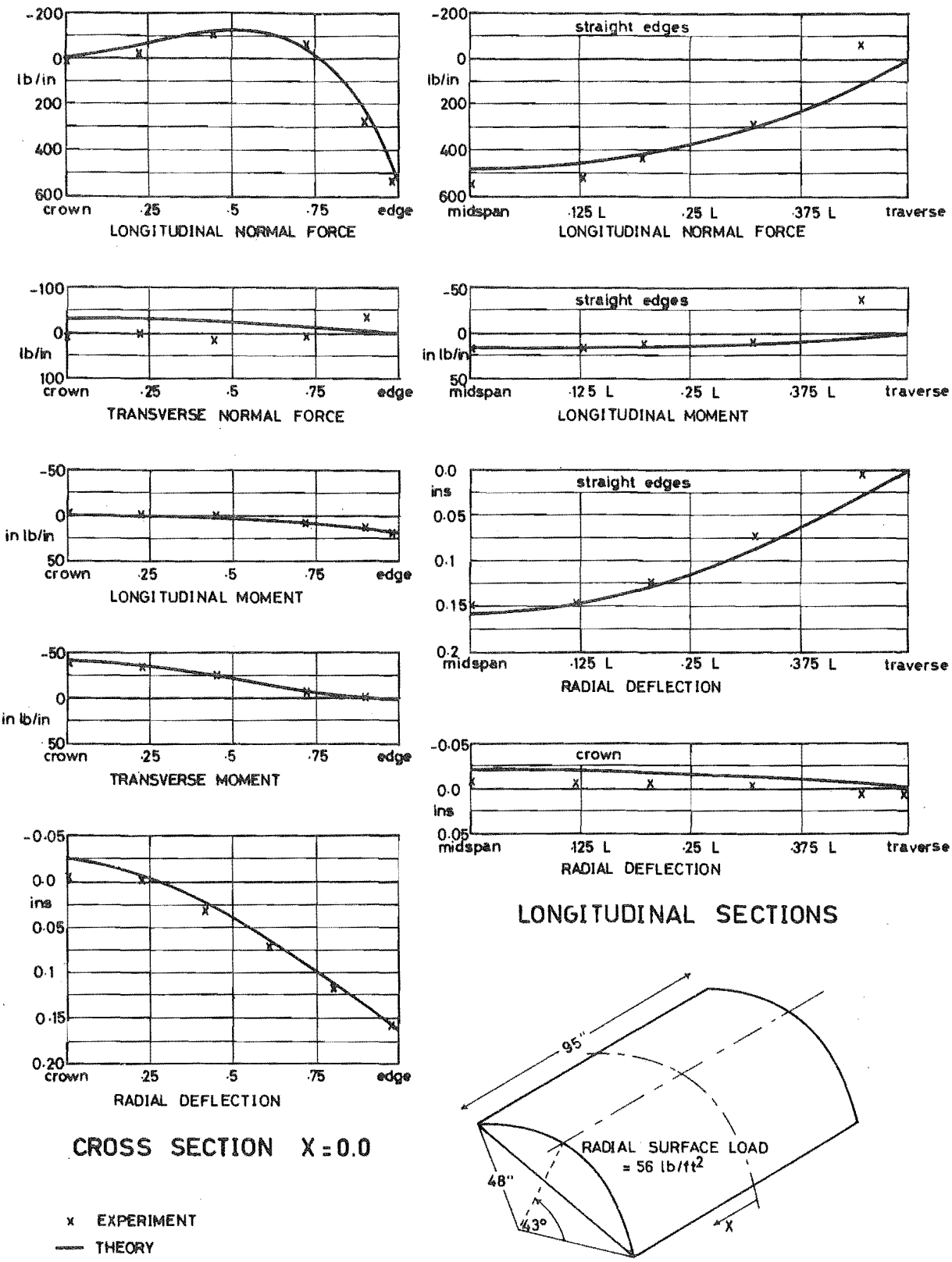

FIG. 5.12 5th SHELL SURFACE LOADING ACTIONS AND DISPLACEMENTS

results was generally good, both along the longitudinal edge and across the midspan cross-section.

For the 1st shell where experimental results were obtained for other transverse cross-sections, experimental and theoretical results also showed good agreement. Near the traverse it can be seen that the theoretical solution underestimates the peak values. This is due to the method of applying the anchorage force over a finite distance. (0.05L).

Longitudinal and Transverse Moments. For both the longitudinal and transverse moments there was considerable experimental scatter because the moments were calculated from the difference of two relatively large numbers (i.e. strains). However, both theory and experiment show the same trends and indicate that the moments are small for most of the strain gauged positions.

Transverse Normal Force. Both theoretical and experimental forces are small. Except for this, there is little agreement between the results. Theory predicts negligible N_2 across the midspan cross-section, while experimental results indicate a small positive transverse force near the edge.

In Plane Shear Force and Twisting Moment. Experimental values of both N_{12} and M_{12} are calculated from the strains of six separate strain gauges and thus are very susceptible to error.

Except at midspan where N_{12} is zero, the agreement between theoretical and experimental results is not good, especially as the traverse is approached.

M_{12} is given as being negligible by both theoretical and experimental results over most of the 1st shell. However where twisting moments do occur, theory and experiment often give a

different sign for the moment. Moments are small in both cases.

Deflections. Experimentally determined radial deflections show the same trends as theoretical values, although for shells 1 and 5 experimental deflections tend to be greater. This could well be due to incorrect determination of Young's modulus.

5.1.2 Surface Loading

Experimentally determined actions and displacements for surface loading are compared with theoretical values in Figures 5.8 to 5.12.

Longitudinal Normal Force. As in the case of prestressing, N_1 was the dominant action in all shells during surface loading. There is good general agreement between experimental and theoretical results. At the midspan edge experimental results tend to be about 10% higher than theoretical values.

Longitudinal Moment. There was good agreement between theoretical and experimental values of M_1 except near the traverse, where the stiffening effect of the traverse is clearly evident in the experimental results. In the theoretical solution the shell is assumed to be free to rotate about the traverse and thus the theoretical M_1 is zero along the traverse. However, in the actual shells, the traverse stiffened the shells, resulting in a relatively large negative M_1 at the corners which progressively changed around the arc to a positive moment at the crown.

Transverse Moment. Across the transverse centre line there is good agreement between theoretical and experimental results for M_2. From the 1st shell results, there is a tendency for the experimental results to be slightly lower than theory as

the traverse is approached.

Transverse Normal Force. As for the prestress loading results, there is little similarity between theoretical and experimental results for N_2, except that both are small. However, general trends are clear. Theoretical N_2 values across the midspan centre line indicate a compressive force near the crown which diminishes to zero at the edge. Experimentally N_2 is given as tensile near the crown and progressively changes to compression at the edge.

The difference between theory and experiment would appear to be due to the effect of skin friction on the shell as the airbag expanded. This is supported by the fact that the difference was reduced in shells 4 and 5 when a shaped reaction deck was used which results in the airbag requiring less expansion to conform to the shell shape. Also, in the 1st shell the difference lessens as the traverse is approached due to the restraining influence of the bag end.

In Plane Shear Force and Twisting Moment. Experimental N_{12} and M_{12} actions were only obtained for the 1st shell and these show the same trends as theoretical results. For N_{12}, experimental values tend to be 50% higher than theoretical results. At midspan, M_{12} experimental values are higher than theory, however, at the traverse the situation is reversed. Agreement between theory and experiment for N_{12} and M_{12} is better for surface loading than for prestressing.

Deflections. The agreement between theoretical and experimental radial deflections is good except for shells 2 and 3 where experimental deflections are greater than theoretical values. Across the midspan cross-section of these two shells

experimental deflections indicate that the shells are flattening towards the edge, a trend which is not shown by theory.

As the deformation of the traverse itself was not considered, experimental deflections along the longitudinal centre line tend to be greater than theory.

5.2 POST ELASTIC BEHAVIOUR

With increasing surface load, cracking of the shells began, causing strain and deflection non-linearly. Strain measurements taken in tensile zones were particularly influenced by cracking.

5.2.1 Change in Neutral Axis Position

Using the strain measurements from strain gauges in compression along the transverse centre line the position of the neutral axis (position of zero longitudinal strain) at midspan could be plotted, almost up to failure, for each shell. For the final load cycle of each shell, the movement of the neutral axis can be seen in Figure 5.13, where the midspan longitudinal compressive strain has been plotted against depth below the top of the crown. It can be seen that for all shells the neutral axis depth decreased with increase in load as would be expected in beam like behaviour. Figure 5.13 also shows that for shells 1, 2 and 3, ($\phi_k = 30^o$), the strain above the neutral axis is linear with distance above the neutral axis. For the 4th shell ($\phi_k = 35.8^o$), the initially non-linear curve becomes linear towards ultimate load. However for the 5th shell ($\phi_k = 43^o$) the strain remains non-linear with distance above the neutral axis throughout the whole load cycle.

5.2.2 Cracking Patterns

The progression of cracking in the model shells is

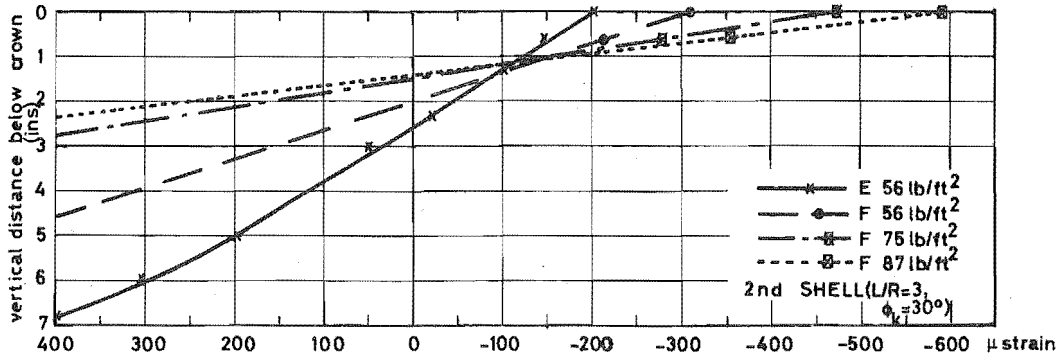

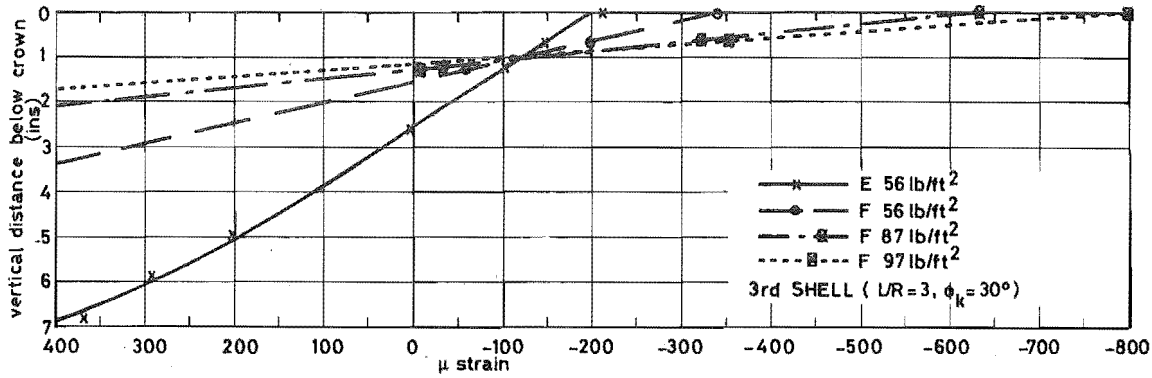

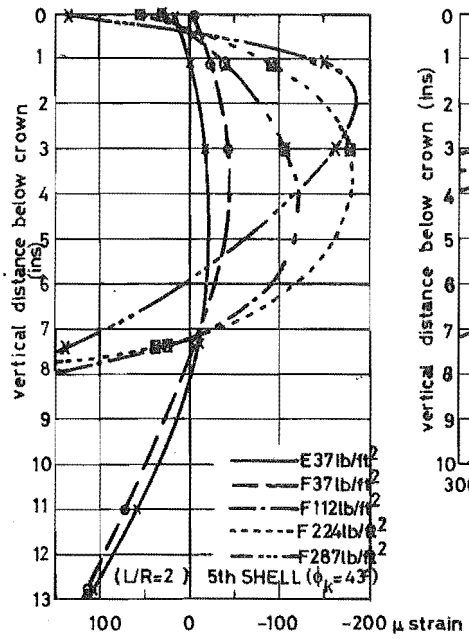

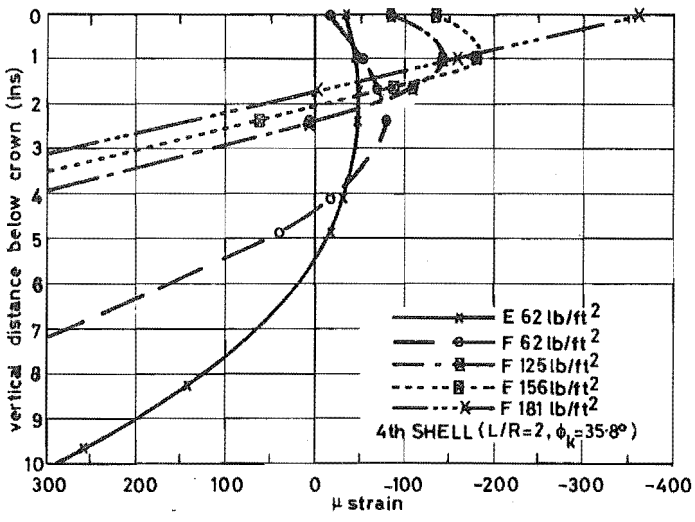

E - shells uncracked

F - final load cycle all shells cracked

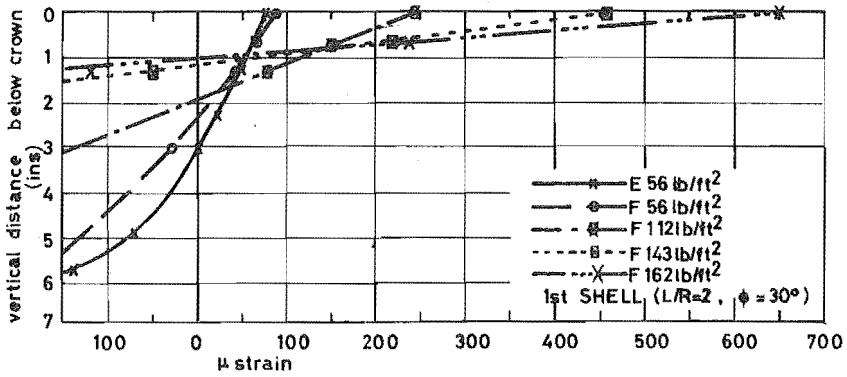

FIG. 5.13 MIDSPAN VARIATION OF LONGITUDINAL STRAIN WITH DEPTH BELOW CROWN

shown in Figure 5.14.

Cracking of all shells began at the edge in a transverse direction, near midspan, at approximately design working load. These cracks, particularly in the 1st shell, tended to start at and follow the transverse reinforcing steel.

At approximately working load in the segmented shells, cracking also began at the joints between the curved segments due to the lack of tensile reinforcement at the joints. These cracks occurred in the mortar rather than the epoxy resin and were the only cracks to continue to open noticeably once formed. This was because of the lack of effective grout in the joint region due to the metal tube used to prevent epoxy resin from flowing into the prestress duct during joining.

On unloading from a load of three times design load during the 5th shell test, longitudinal cracks along the crown of the shell occurred on the intrados. As the moment due to prestressing was a sagging moment, these cracks would be expected if the bending resistance of the shell section to sagging moments was sufficiently reduced. This reduction was presumably caused by longitudinal cracking on the extrados.

5.2.3 Recoverability from Overloads

No significant permanent set was observed in any of the shells on unloading from any of the loads. The shells were loaded to and unloaded from the following percentages of their ultimate loads; 1st, 64%; 2nd, 87%; 3rd, 88%; 4th, 75%; 5th, 58%. Only in the 4th shell at 90% of ultimate load was there any noticeable yielding of a shell.

5.2.4 Deflections

Deflections were linear and repeatable until approx-

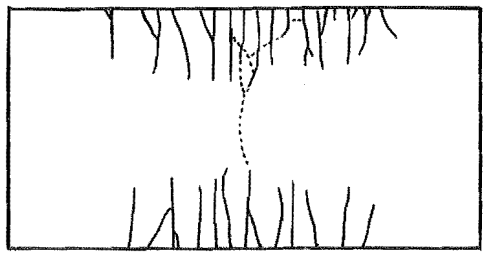

——— before failure
- - - - - during failure

a) 1st SHELL INTRADOS - extrados similar AT FAILURE

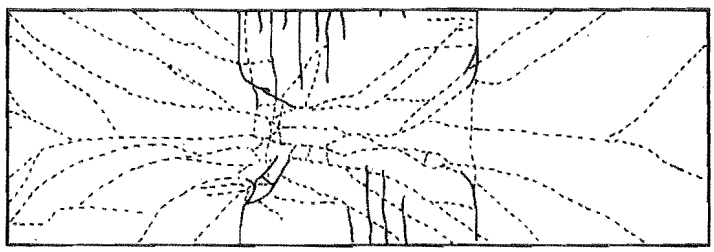

——— before failure
– – – – during failure

INTRADOS

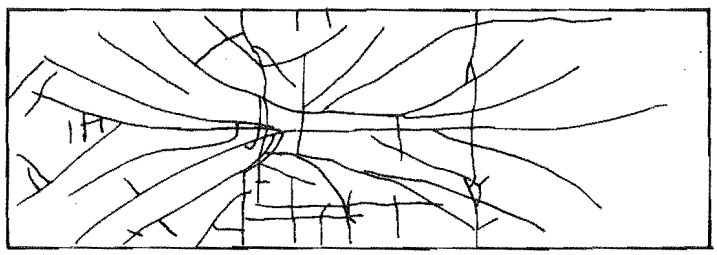

——— before & during failure

EXTRADOS

b) 2nd SHELL AT FAILURE

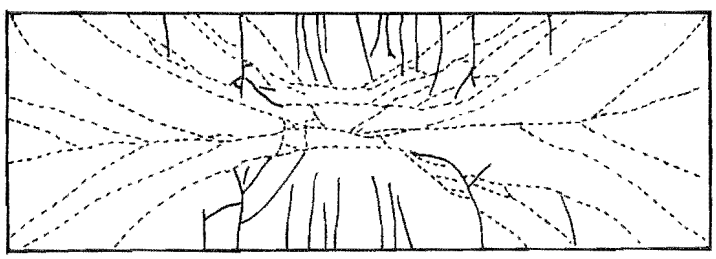

——— before failure
- - - - - during failure

INTRADOS

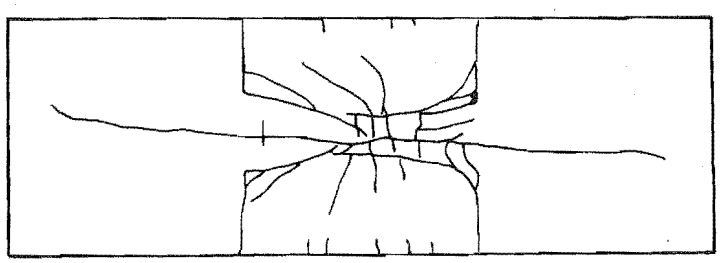

——— before & during failure

EXTRADOS

c) 3rd SHELL AT FAILURE

FIG. 5.14 CRACK PATTERN OF FAILED SHELLS

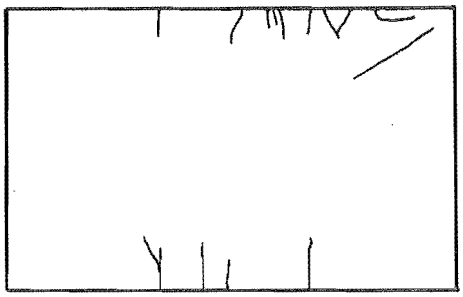

INTRADOS AT 124 lb/ft^2

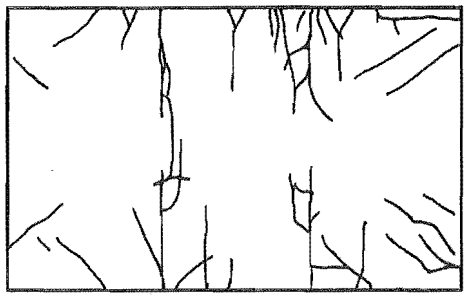

INTRADOS AT 187 lb/ft^2

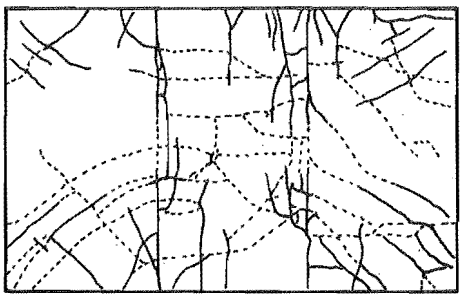

INTRADOS AT FAILURE

——— before failure; ------ during failure

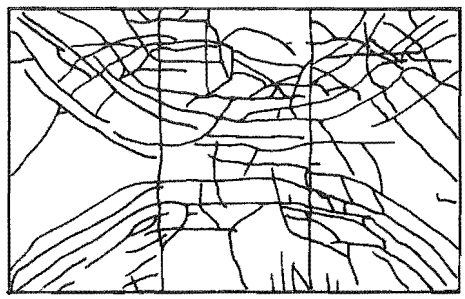

EXTRADOS AT FAILURE

d) 4th SHELL

INTRADOS AT 156 lb/ft^2

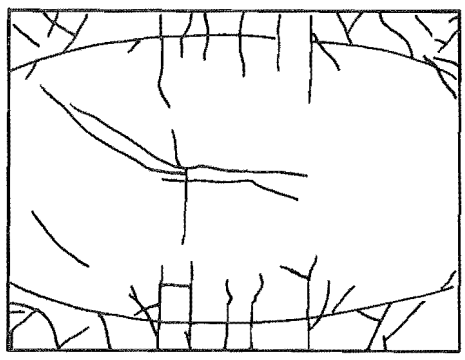

INTRADOS AT 250 lb/ft^2

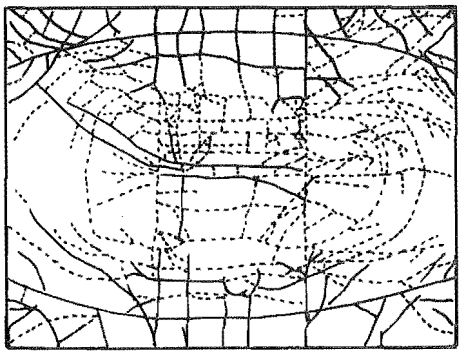

INTRADOS AT FAILURE

——— before failure

..... during failure

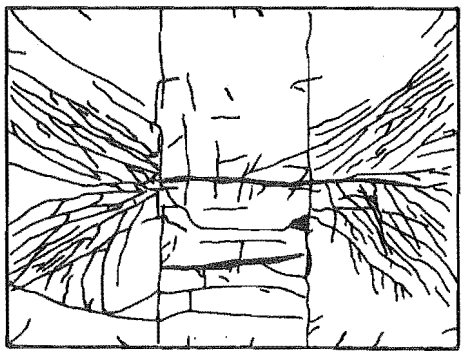

EXTRADOS AT FAILURE

e) 5th SHELL

FIG. 5.14 CRACK PATTERNS OF FAILED SHELLS

imately the onset of cracking after which shell stiffnesses reduced. A typical load versus deflection graph is shown in Figure 5.15. On reloading the shells after cracking had occurred in a previous load cycle, the load-deflection curve was linear and the same as for the uncracked cycles until the cracks began opening. From this position on the load-deflection plot, the curve took a linear path to the highest load deflection position reached in a previous load cycle. With further increase in load the curve became non-linear and extended the non-linear curve from previous load cycles.

The deflection of the transverse centre line cross-section for each shell is given in Figure 5.16 for increasing loads during the final cycle of each shell. It can be seen that even at high loads the deflection across the midspan centre line remained reasonably symmetrical. More detailed discussion of these graphs is given in Sections 5.2.6 and 5.2.7.

Along longitudinal sections, the radial deflection was symmetrical. There was a relative flattening of the central portion for all shells which was due, in part, to the inward rotation of the traverses towards each other.

Horizontal deflections at the midspan edge for shells 3, 4 and 5 are shown in Figure 5.17. Initially all shells deflected inwards and for shells 4 and 5 continued inwards once cracking began. However for the 3rd shell (smallest ϕ_k), with the onset of cracking horizontal movement occurred outwards.

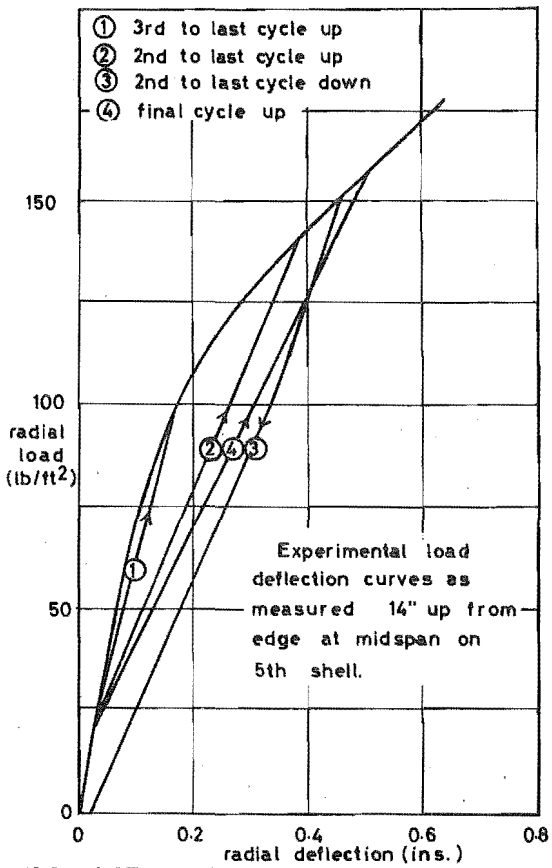

FIG. 5.15 TYPICAL SURFACE LOAD VERSUS DEFLECTION CURVE

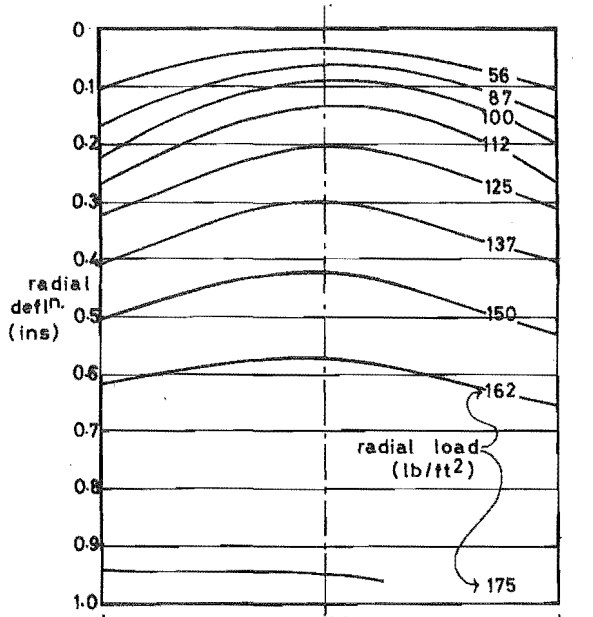

FIG. 5.16 (a) 1st SHELL

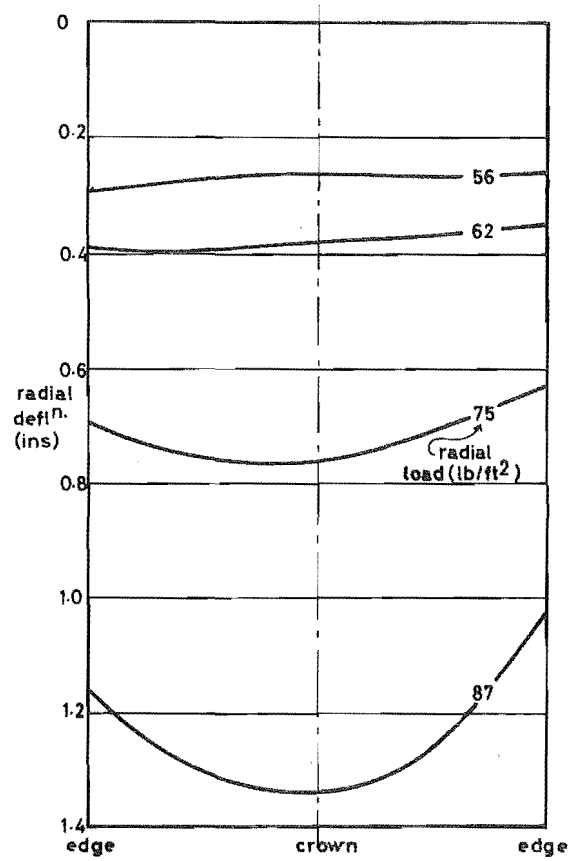

(b) 2nd SHELL

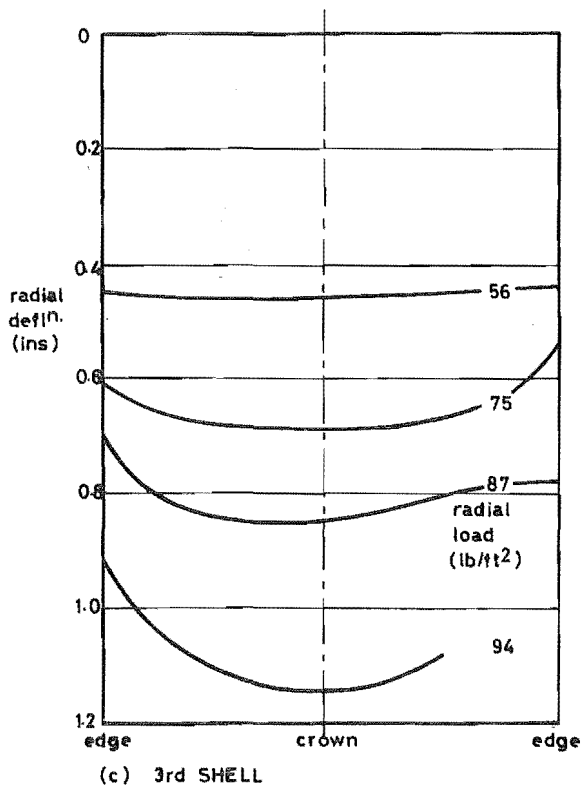

(c) 3rd SHELL

FIG. 5.16 RADIAL DEFLECTION ACROSS TRANSVERSE CENTRE LINE (final load cycles)

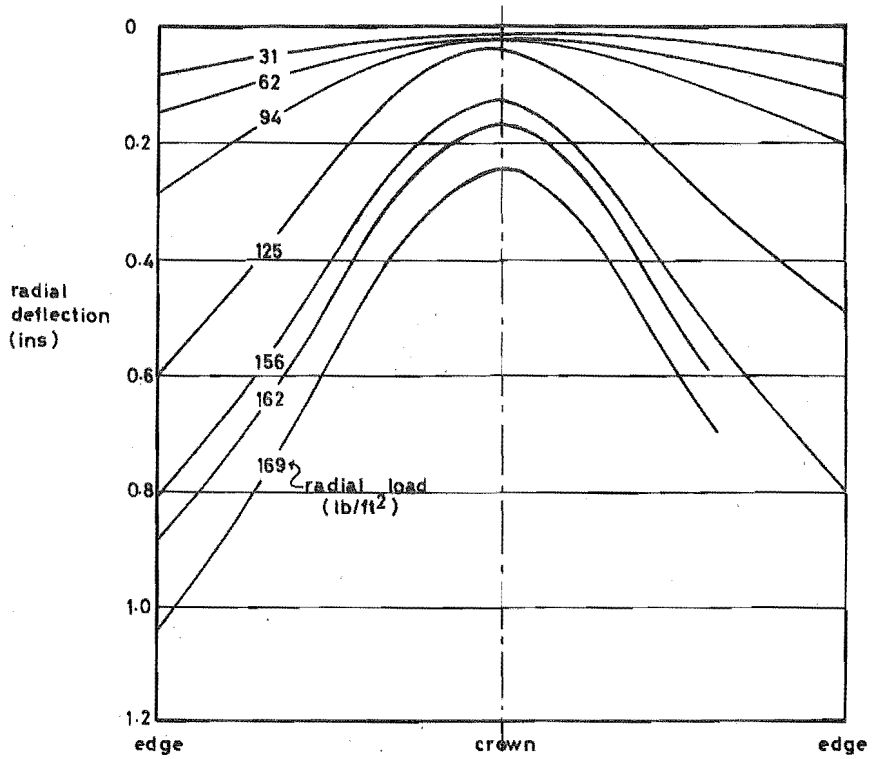

(d) 4th SHELL

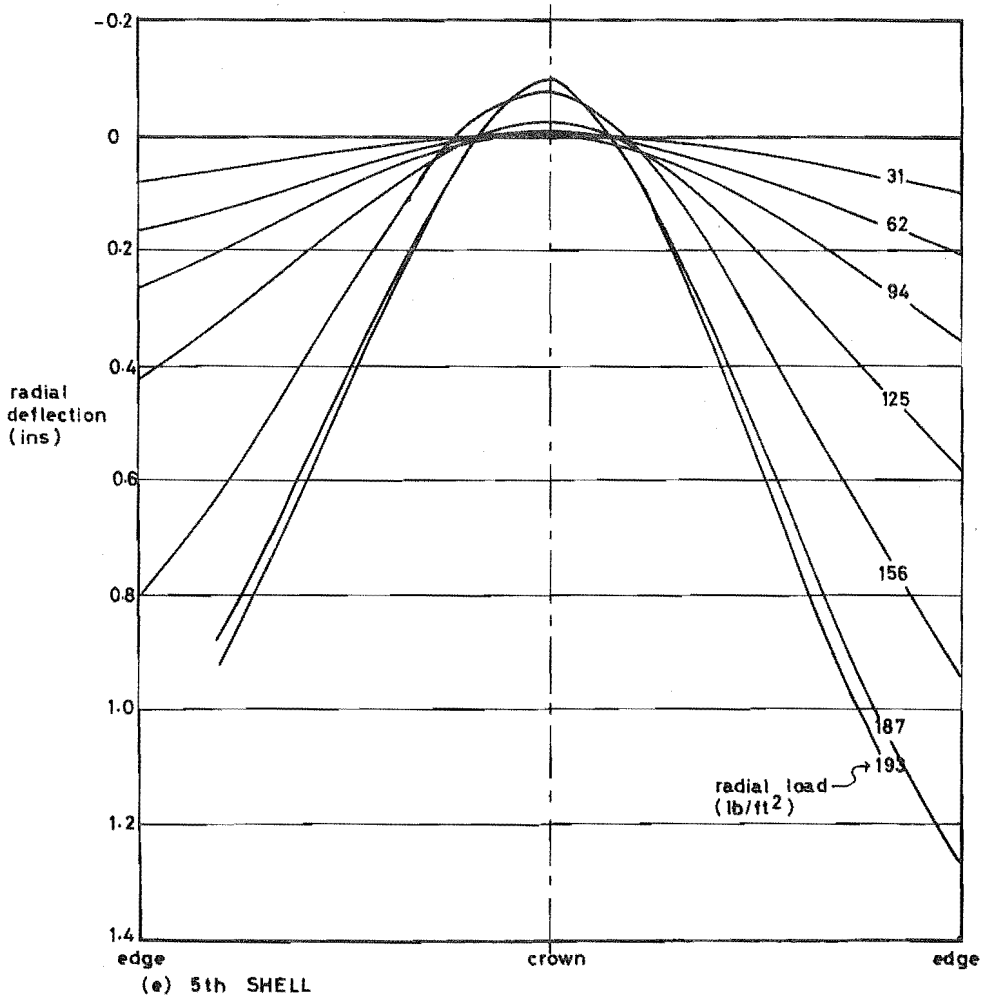

(e) 5th SHELL

FIG. 5.16 RADIAL DEFLECTION ACROSS TRANSVERSE CENTRE LINE

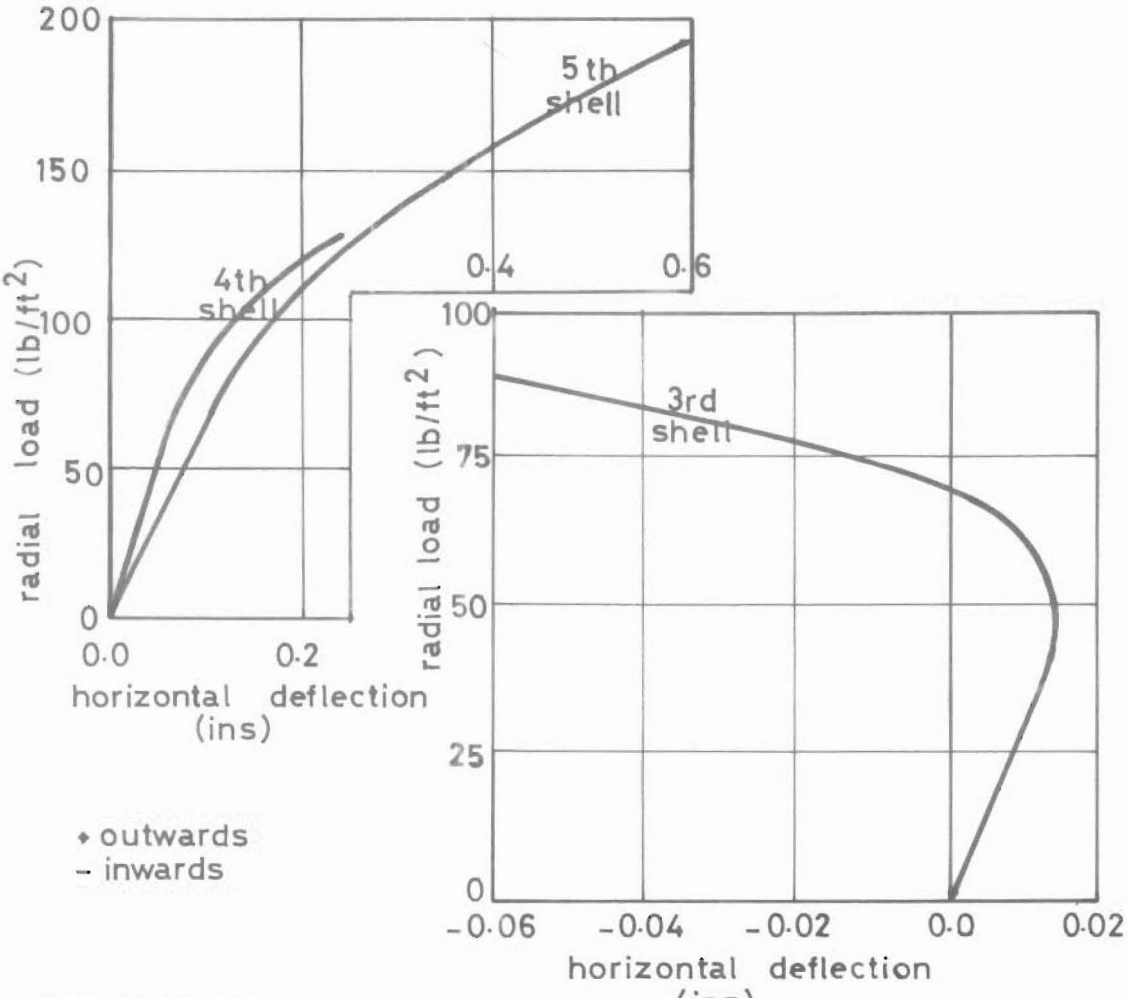

FIG. 5.17 HORIZONTAL DEFLECTIONS (at midspan edge)

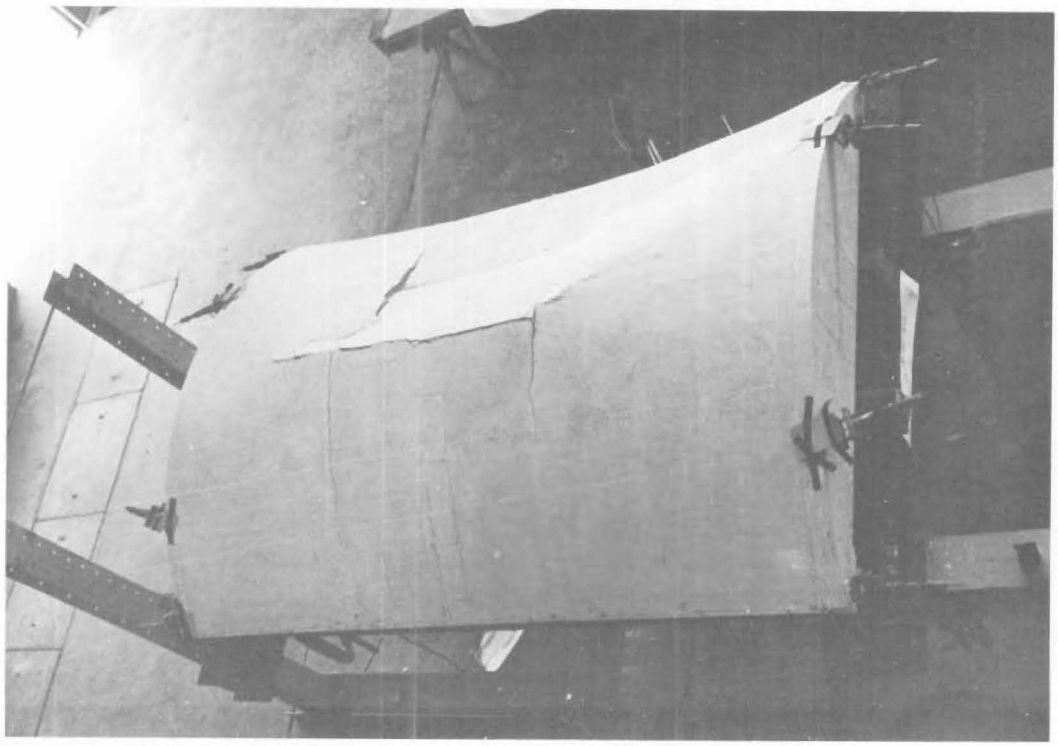

FIG. 5.18 FAILED 5th SHELL

5.2.5 Experimental Failure Mechanisms

1st Shell ($\phi_k = 30^o$, L/R = 2). The 1st shell failed suddenly and without warning at a load of 175 lb/ft^2, by fracture of the prestress wires at midspan on one side.

Prior to failure, transverse cracking had extended into the shell, leaving only the central third uncracked. However no cracks had opened appreciably. No cracking of the traverse occurred during the test.

2nd Shell ($\phi_k = 30^o$, L/R = 3). Failure in the 2nd shell occurred gently over 10-15 seconds at a load of 94 lbs/ft^2, by flattening of the cross-section midway between midspan and one joint ($^L/_3$), followed by diagonal cracks radiating towards the traverse from the failure region. The crown of the shell came down almost to the level of the edges, and on examination crushing was evident on the extrados above the failure region. Neither prestress steel nor reinforcing steel had fractured.

At failure vertical cracks appeared at approximately 6" centres in the traverse nearest the failure region. Also at this traverse a small crack developed at the joint between the traverse and shell surface as shown in Figure 5.14(b).

It is interesting to note that as the reaction deck was being removed the shell was knocked slightly, resulting in a large bang and the shell assuming its original shape. This would indicate that little or no yielding of the prestressing cables had taken place.

3rd Shell ($\phi_k = 30^o$, L/R = 3). The failure mechanism in the 3rd shell was similar to that of the 2nd shell. Failure occurred slowly at 103 lb/ft^2 by flattening of the cross-section at midspan. Crushing of the extrados above the failure region

was evident.

Before failure vertical cracks at approximately 6" centres had been observed in both traverses.

4th Shell ($\phi_k = 35.8^o$, $L/R = 2$). The 4th shell was the only shell where noticeable yielding occurred. Yielding began at a load of 181 lb/ft^2. At a load of 200 lb/ft^2 the shell continued to deflect without taking any increase in load, resulting in the joint cracks opening up until the prestressing wires failed at a joint. There was no apparent crushing anywhere on the shell surface.

Vertical cracks appeared in the traverses at 180 lb/ft^2 and by maximum load had spread across the traverses.

5th Shell ($\phi_k = 43^o$, $L/R = 2$). Failure of the 5th shell occurred suddenly at a load of 293 lb/ft^2 by a transverse bending failure of one half of the centre shell segment as shown in Figure 5.18. Prior to failure the shell had deflected approximately 3" vertically at the edge in the centre section.

Vertical cracking of both traverses began at 130 lb/ft^2.

5.2.6 Comparison Between $\phi_k = 30^o$ Shells

Across the midspan transverse cross-section (see Figure 5.16) all three shells deflected more at the edges than the crown under low loads. However, once cracking had occurred during previous load cycles, the 12'-0" shells regained their original shape at approximately 60 lb/ft^2 load and from this

load until failure the crown deflected more than the edges. For the 8'-0" shell however, deflection at the edges was always greater than the crown until failure, when the shell regained its original shape.

The two 12'-0" shells were identical except that one, the 2nd shell, had straight cables and the other, the 3rd shell, had draped cables. Close similarity in behaviour between the two shells occurred. The 2nd shell, however, was stiffer at low loads due to it having a greater prestress force near the edge. At higher loads the 3rd shell was stiffer due to the draped cables retarding the development of cracks and also because of the lack of effective grout in the 2nd shell. This caused fewer but wider cracks to occur in the shell as can be seen in Figure 5.14(b).

In the 12'-0" shells the prestress steel at midspan was positioned at the same effective depth. This resulted in the shells having very similar ultimate loads.

5.2.7 Comparison Between 8'-0" Shells

For similar loads, the largest deflection at the midspan crown for the three 8'-0" shells tested occurred in the 1st shell ($\phi_k = 30^o$), which had the smallest half included angle. For the 4th shell ($\phi_k = 35.8^o$) with increased ϕ_k the deflection was less and for the 5th shell ($\phi_k = 43^o$) with even larger ϕ_k the crown actually rose. At low loads the greatest deflection across the midspan centre line was at the edge for all shells. This trend continued at high loads for shells 4 and 5 but not for the 1st shell which regained its original shape at failure.

With increasing ϕ_k there was an increase in the ultimate load per unit area (and hence also the ultimate load per unit

length along the shell). This was mainly due to the increase in effective depth of the prestress tendons.

By comparing shells 4 and 5 it appears that corner diagonal cracks are delayed by draped cables.

5.2.8 Comparison of Shells With and Without Edge Beams

In order to counter high tensile forces near the shell edges, reinforced concrete cylindrical shells are built with relatively large edge beams. These edge beams also serve to reduce deflections to an acceptable level. Concern has been expressed that in prestressed cylindrical shells where edge beams are eliminated, excessive deflections may occur.

Although larger deflections will occur for a prestressed shell without edge beams, than for a similar size reinforced shell with edge beams, the difference may not be as large as an elastic analysis would indicate. This is because for prestressed shells, the cable layout can be designed to prevent cracking up to working load, and thus the whole cross-section will be effective in resisting deflections. For reinforced shells with edge beams, however, cracking will occur before working load is reached and thus the effective stiffness is not that of the whole cross-section. Figure 5.19 shows a comparison of theoretical and experimental results for the 3rd shell (L = 8'-0", R = 4'-0", $\phi_k = 30^o$), a prestressed shell without edge beams, with a similar size reinforced shell tested by Scrivener[23] which had 1.3" x 3.25" reinforced edge beams. The theoretical results would indicate that under surface loading the shell without edge beams deflects three times that of the shell with edge beams. However, experimental results show that at working load, the prestressed shell deflection is only $^4/_3$ of the reinforced shell deflection. If

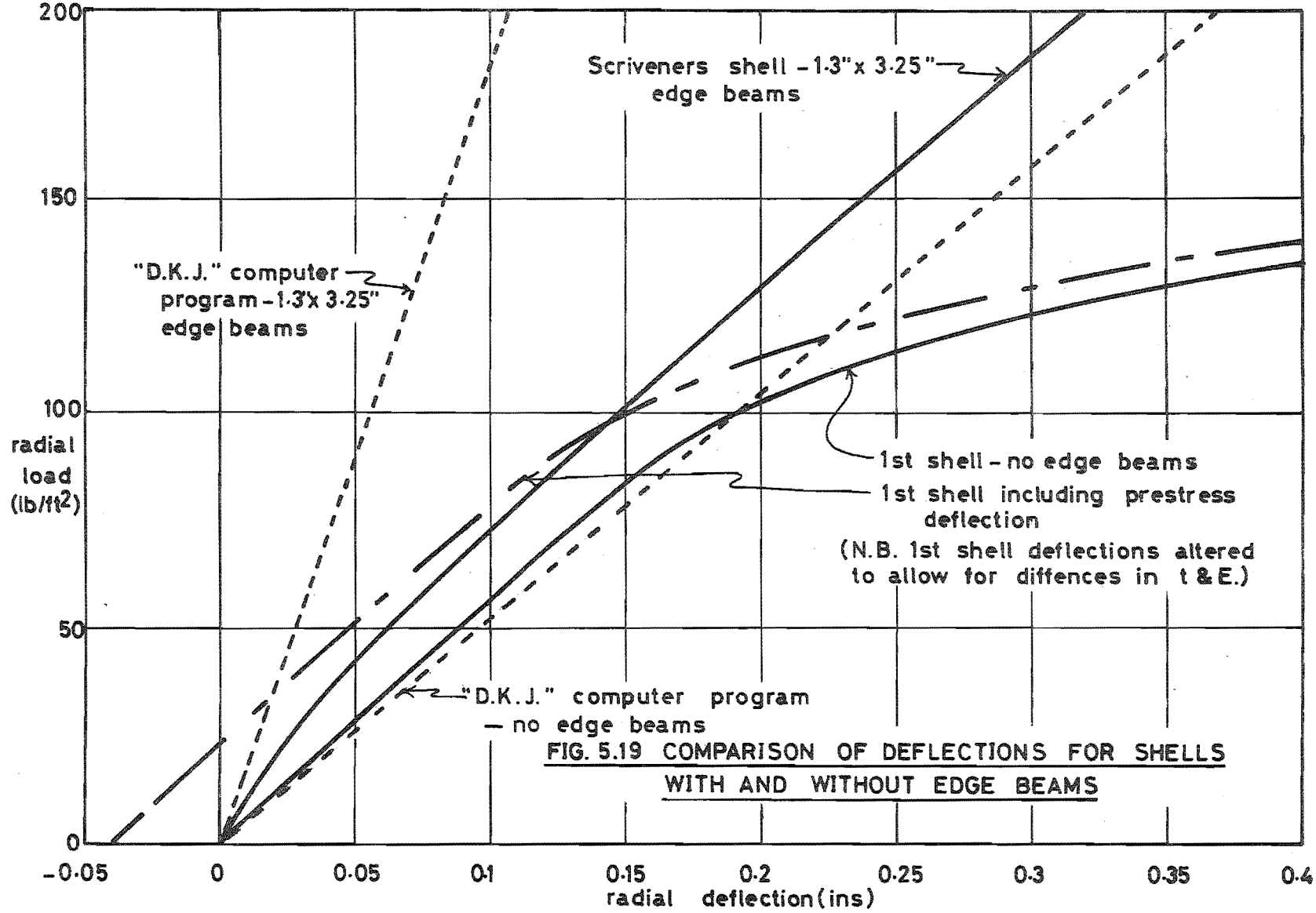

FIG. 5.19 COMPARISON OF DEFLECTIONS FOR SHELLS WITH AND WITHOUT EDGE BEAMS

Shell		1	2	3	4	5
	A_s in^2	.034	.077	.077	.034	.051
min.	A_s (Section 3.1.7)	.45	.037	.035	.078	.139
max.	A_s (Section 3.1.6)	.289	.253	.242	.318	.422
	d ins	4.71	4.56	4.56	7.74	10.63
	t ins	.614	.625	.625	.680	.669
	f'_c psi	9,300	7,690	7,350	6,200	8,050
	f_c psi	7,900	6,540	6,250	5,270	6,840
	T_t lbs	10,000	20,800	20,800	10,000	13,920
	A_t in^2	1.27	3.18	3.33	1.90	2.03
	a' ins	.10	.26	.27	.18	.20
	d' ins	4.61	4.3	4.29	7.56	10.43
M_{uL} -	lb ins (prestress steel only)	46,000	89,000	89,000	76,000	145,000
M_{uL} -	lb ins (total)	63,000	111,000	111,000	119,000	212,000
	kd ins	1.0	.6	.6	.4	.7
	e_{sp}	.0091	.0057	.057	.0075	.0055
	e_{sL}	.00256	.0228	.0228	.058	.064
	$e_T = e_{sp} + e_{sL}$	.0117	.0285	.0285	.0655	.0695
	f_{su} psi	266,000	270,000	270,000	288,000	270,000

TABLE 5.1 DATA USED IN CALCULATING THE THEORETICAL MOMENT RESISTANCE OF THE SHELLS

the upward deflection due to prestressing is considered, the total prestressed shell deflection is less at working load than that of the reinforced shell.

5.3 ULTIMATE LOAD BEHAVIOUR

Using the method presented in Section 3.1, an ultimate load analysis was carried out on all five shells. Using the notation given in Section 3.1, a summary of the data used is given in Table 5.1. The prestressing steel content, A_s, in all shells was relatively low and the prestressing steel strain, e_{sp}, high. Thus the ultimate stress, f'_s, of the tendons was used as an initial estimate of the tendon stress f_{su} for calculating the ultimate moment of the shells. Subsequent calculations showed that in all shells, the tendon strain was such that f_{su} was close to f'_s. However the actual experimental f_{su} could not be calculated as the stress strain curves of the tendons could not be obtained accurately near ultimate load.

Comparison between the experimental failure moment along the shells (i.e. the moment obtained by considering the shell as a simply supported beam) and the theoretical moments of resistance are given in Figure 5.20. Reduced theoretical moments of resistance occur at the joints due to the absence of non-prestressed steel.

5.3.1 1st Shell

The 1st shell had a prestressing steel content below the minimum required to prevent failure by fracture of the prestressing tendons. However, there was sufficient non-prestressed steel to raise the effective steel content above the minimum and hence failure by elongation of the longitudinal

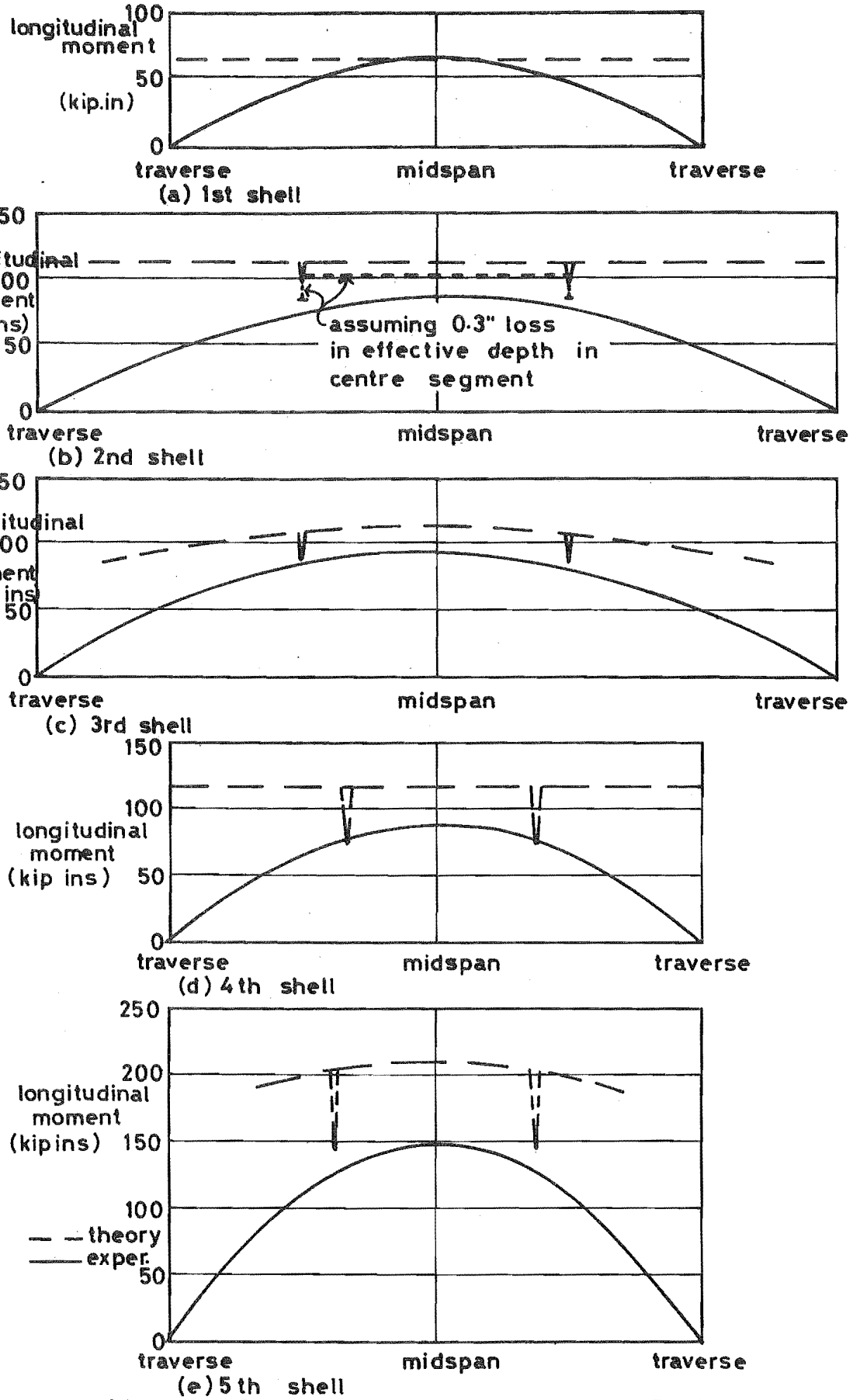

FIG. 5.20 COMPARISON OF THEORETICAL MOMENT RESISTANCE AND EXPERIMENTAL FAILURE MOMENT

steel and subsequent crushing of the concrete would be expected. However, failure actually occurred without warning by fracture of the non-prestressed steel, resulting in failure of the prestressing steel. Subsequent investigation showed that the reason for the sudden failure was due to the relatively low ultimate tensile strength (35,000 psi) at midspan of the bronzed joints with which the reinforcing meshes had been joined. The low strength prevented the reinforcing steel from reaching a sufficiently high stress to elongate noticeably, and thus give warning of imminent failure.

A theoretical analysis, including the effects of the reinforcing steel, was carried out using the neutral axis depth, 1" , and maximum crown concrete strain, 690 μ strain, found experimentally at the load increment before failure. As the concrete was still in the elastic range a linear stress strain relationship was assumed for the concrete in compression, and the resultant longitudinal compressive force and line of action were found by integration. The results of the analysis are given in Table 5.1. The agreement between the experimental load, 162 lb/ft^2, and theoretical load, 156 lb/ft^2 is good. This analysis showed that immediately prior to failure the reinforcing had been taking approximately one third of the tensile forces across midspan at a stress of approximately 35,000 psi. Hence failure at the next load increment, as occurred, would not be unexpected.

Thus, although the reinforcement raised the ultimate moment by 30%, the bronzed joint resulted in a sudden unexpected failure.

5.3.2 Shells 2 and 3

The prestressing steel contents of shells 2 and 3 fall

between the limits to prevent sudden failure by crushing of the concrete and fracture of the prestressing tendons. Thus by considering Figure 5.20 (b) & (c), failure would be expected to occur at the joints by elongation of the tendons and subsequent crushing of the concrete at the crown.

However, from Figure 5.16 (b) & (c) showing radial deflection across the midspan cross-section, it can be seen that the transverse cross-sections of both shells are flattening near ultimate load. Hence once yielding began at the joints, the shells would be able to flatten even more, causing the resulting failure mechanism.

5.3.3 4th Shell

The 4th shell failed by fracture of the prestressing tendons at the joint. This would be expected as the prestress steel content at the joints was approximately half that required theoretically to prevent this type of failure. Prior to failure, the joint cracks had opened up to approximately .45", and thus adequate warning of imminent failure was given.

It appears, Figure 5.20(d), that the theoretical moment of resistance of the shell is exceeded experimentally. This is due to the shell cross-section "closing up", see Figure 5.16(d), causing an increase in effective depth and hence in ultimate moment.

5.3.4 5th Shell

Theoretically, by the method of Section 3.1, failure at the joints by fracture of the prestressing tendons at an ultimate moment near the experimental value is predicted. However, before this could happen, the shell failed in transverse bending in the centre element.

A simple analysis was carried out on the centresection by equating the internal and external virtual work. Referring to Figure 5.21, a negative yield line was assumed along A and a positive yield line along B. These were chosen by considering the crack pattern and rotation of the failed shell. It was also assumed that there was no restraint along the transverse boundary, i.e. between the centre segment and the outer shell segments. This analysis indicates that failure would occur at 110 lb/ft^2 compared with the actual failure load of 293 lb/ft^2. However, these boundary conditions would apply only when the prestressing cables have elongated to open up the joint cracks sufficiently to remove the restraint between segments. This would occur when the neutral axis depth is small near ultimate moment. Thus a transverse bending failure as occurred would be expected.

Moore[28] has carried out a more detailed analysis of this shell by considering the cracks in one quarter of the shell and idealizing yield lines. Using the kinematic limit approach of Olzak and Sawczuk[29] good agreement was obtained between theoretical (284 lb/ft^2) and experimental (293 lb/ft^2) ultimate loads. Unfortunately this technique is not a design method, as it is extremely difficult to minimize the equations for generalized yield lines when the failure pattern is not known from experiment.

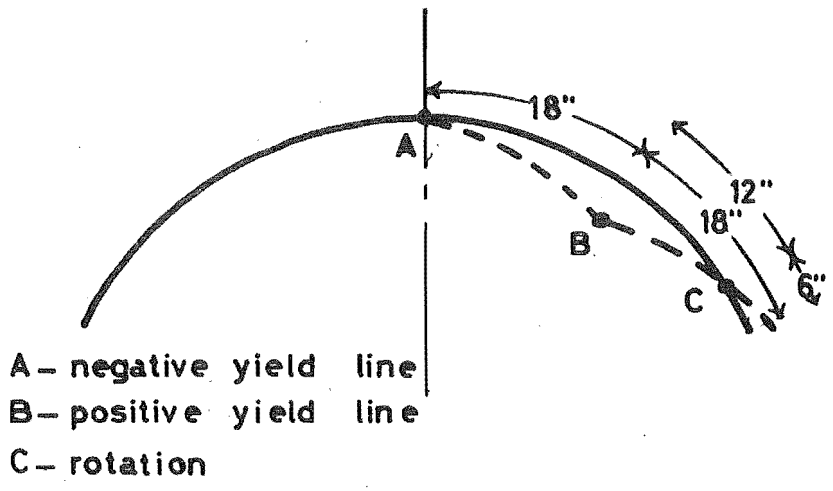

FIG. 5.21 FAILURE MECHANISM OF 5th SHELL IN CENTRE SEGMENT

CHAPTER SIX

APPROXIMATE METHODS FOR THE ELASTIC DESIGN OF PRESTRESSED CYLINDRICAL SHELLS

The primary aim in the analysis of prestressed cylindrical shells is to obtain the longitudinal normal force, N_1 , so that N_1 due to the applied load and dead load may be fully or partly counteracted. Hence a simple, quick method of calculating N_1 is desirable. The magnitude and distribution of transverse bending moments, M_2 , is also required as these may be critical. Wind loading and earthquake loading have not been considered in this thesis as these effects are generally much less severe than the effects of dead weight and uniformly distributed live load such as snow.

Within this chapter limits are put on the range of applicability of beam theory for the analysis of prestressed cylindrical shells. Other simplified analysis methods are developed so that initial design can be undertaken, without the need for electronic computers. They also enable the designer to see in general terms the effect that an alteration in cable position will have on the shell.

For straight cables, the only force considered is that at the anchorage, line losses being neglected. As these are generally small for straight cables, this is not a serious restriction. In the case of draped cables the anchorage force and line loads are dealt with separately. Only symmetrical shells and cable layouts are considered.

6.1 DEAD AND LIVE LOADS

In order that the feasibility of a particular design may be quickly determined, it is helpful to have a simple method of calculating the critical normal force distribution. Once this is done a fuller analysis[13,22] can be carried out if required, to find the magnitude and distribution of significant shell actions due to dead and live loading, namely longitudinal normal force, transverse normal force, in-plane shear force and transverse bending moment.

A commonly used method for calculating the longitudinal normal force for the surface loads is to assume that the shell spans longitudinally as a beam, simply supported between the traverses. This technique[34] is simple and has the advantage that the loading can be of any distribution and the shell of any thickness. Also any cylindrical shape may be considered.

The distribution of normal force according to the beam theory is given by:

$$N_1 = \frac{M y t}{I}$$

where M = the applied moment ($= \frac{WL}{8}$ at midspan if W is the total uniformly distributed load).

t = thickness of shell.

y = vertical distance above the neutral axis, where the depth below the crown of the neutral axis is given by $R(1 - \frac{\sin \phi_k}{\phi_k})$

I = moment of inertia of shell cross-section

$$= R^3 t \left[\phi_k + \sin \phi_k \left(\cos \phi_k - \frac{2 \sin \phi_k}{\phi_k} \right) \right]$$

In calculating the moment of inertia the difference of two

similar numbers must be found, and hence to obtain it accurately a reasonable number of significant figures, say 7, must be used.

As the L/R ratio is decreased, the difference between beam theory results and those calculated by an exact method increase. Figure 6.1 shows where the results from beam theory, for the maximum midspan values of N_1, differ by less than 5% from those obtained from the D.K.J. program using 3 Fourier terms. For these shells the N_1 distribution across the whole cross-section is similar to the linear distribution given by beam theory. The comparison was for a uniform dead load.

To calculate the N_1 distribution for dead load for shells where actions are not well predicted by beam theory, Figure 6.2 can be used. These curves have been plotted from results obtained from the D.K.J. program, again using 3 Fourier terms.

6.2 ANCHORAGE LOAD

For straight cables the anchorage load is taken as the actual prestressing force and for draped cables it is taken as the component of the anchorage force parallel to the shell generators. For draped cables, the remaining component of anchorage force is considered to be taken directly by the traverse. Maximum values of N_1 due to anchorage load occur at midspan or near the traverse.

6.2.1 N_1 at Midspan

At midspan, for a large range of shells, the magnitude and distribution of N_1 can be accurately determined by use of the beam theory approach.

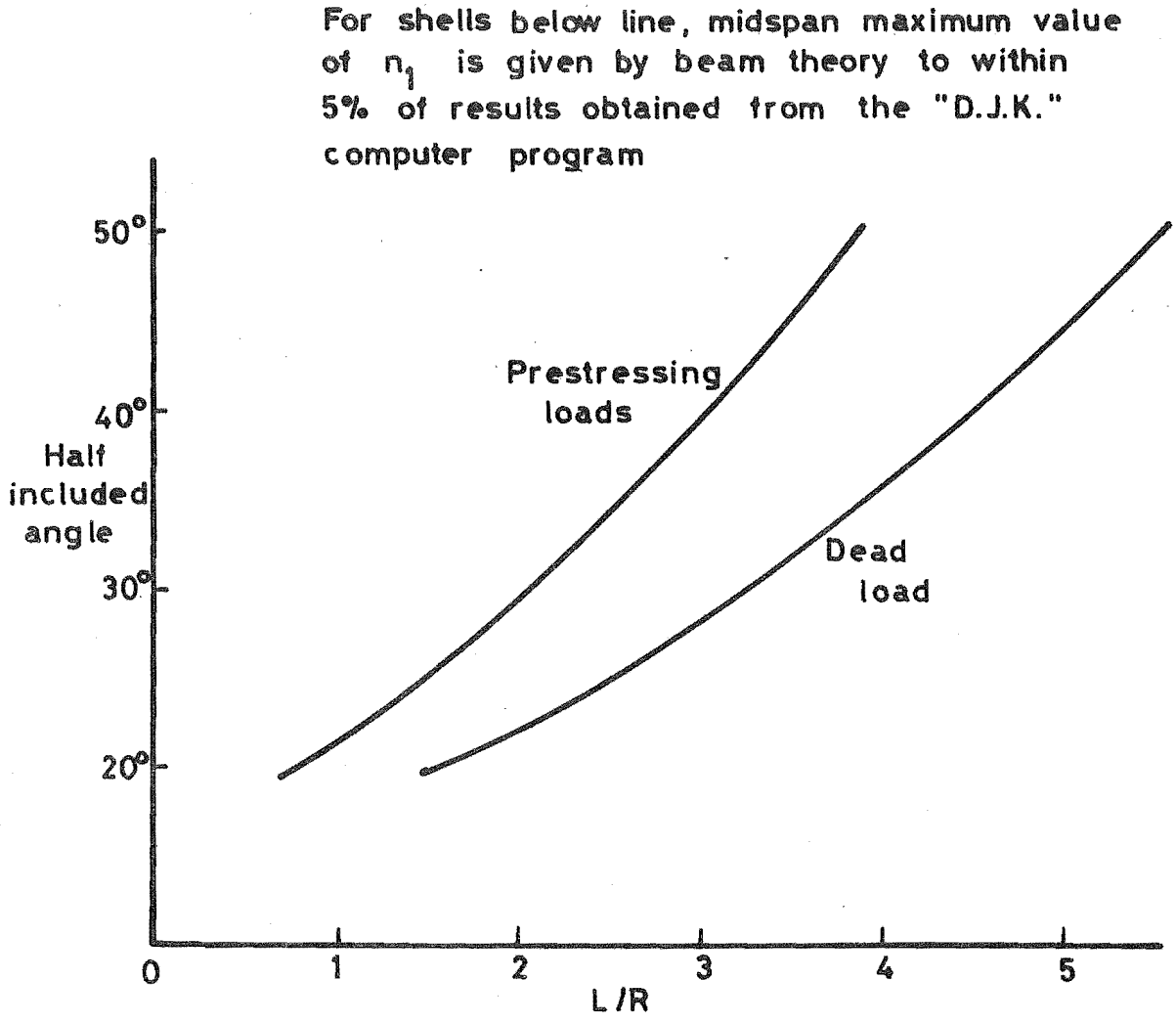

FIG. 6.1 ACCURACY OF BEAM THEORY RESULTS

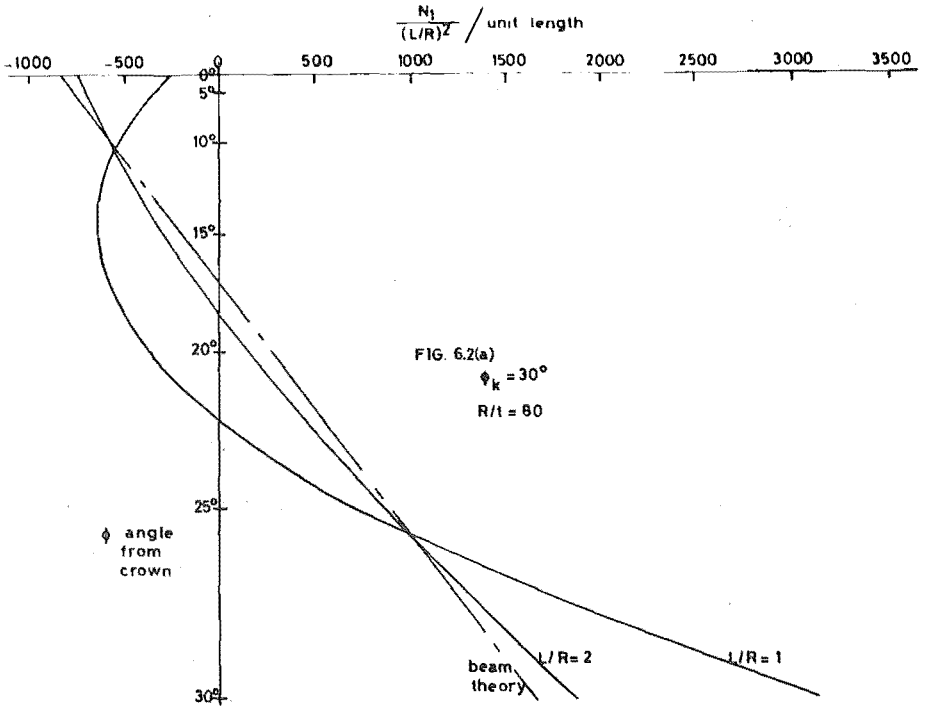

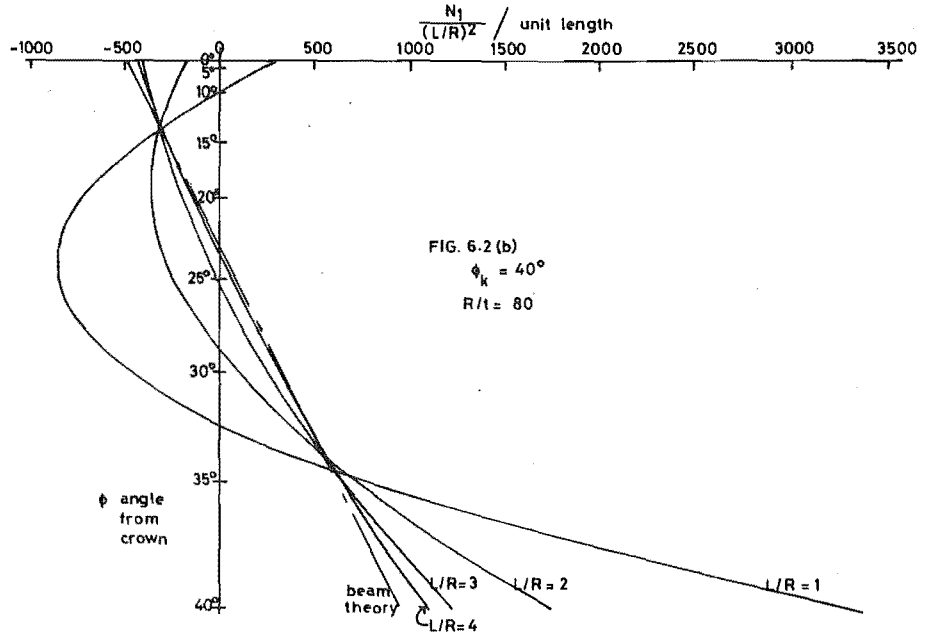

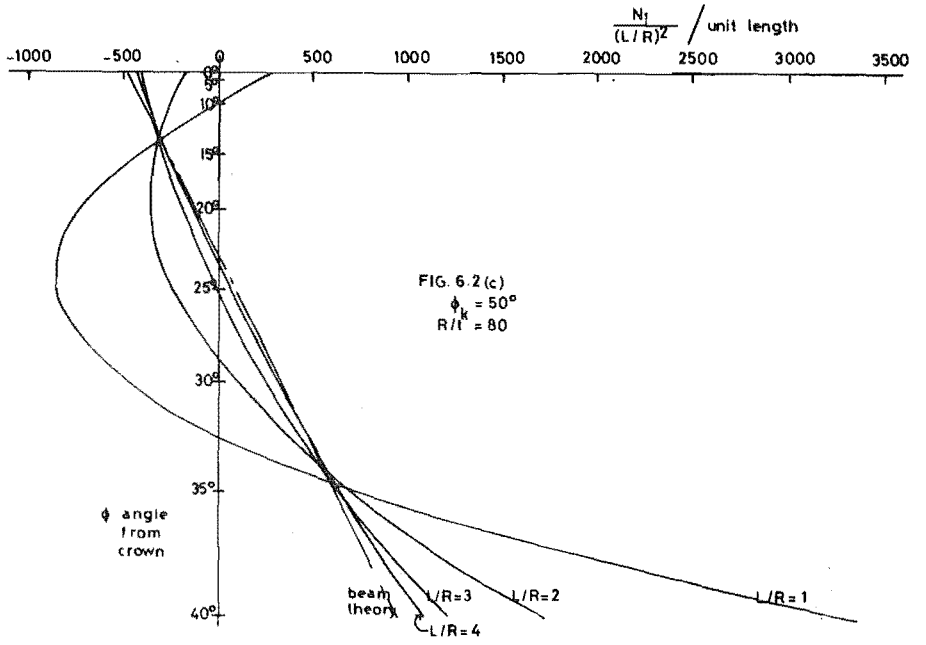

FIG. 6.2. N_1 AT MIDSPAN DUE TO UNIT DEAD LOAD

i.e. $N_1 = \frac{M y t}{I}$ where $M = 2 P_a y_p$

and y_p = vertical distance of anchorage above neutral axis

P_a = anchorage load.

Beam theory has the advantage that the effect of a change in cable position can be readily seen. Figure 6.1 indicates the range of shells for which beam theory gives results for maximum N_1 values to within 5% of results calculated by the D.K.J. program using 10 Fourier terms.

The range of L/R for which beam theory gives reliable results is larger for prestress loads than dead load. This is due to the assumption inherent in the beam theory method that the transverse cross-section does not change shape. As prestress loads cause a lower order of M_2 (and thus smaller change in cross-sectional shape) than dead load, this assumption is more valid for prestress loads than for dead load.

For shells where beam theory does not give satisfactory results, the distribution and magnitude of N_1 at midspan due to anchorage load can be obtained by interpolation from Figures 6.3-6.5. These were plotted from results from the D.K.J. program, using 10 Fourier terms and two symmetrical prestress forces of 10,000 force units each.

Although for prestress anchorage loads beam theory would indicate that there is no change in N_1 distribution along the shell, there is in fact a change due to the influence of the traverse. However, the distribution and magnitude of N_1 at any particular cross-section is similar to that at midspan for a considerable portion of the shell

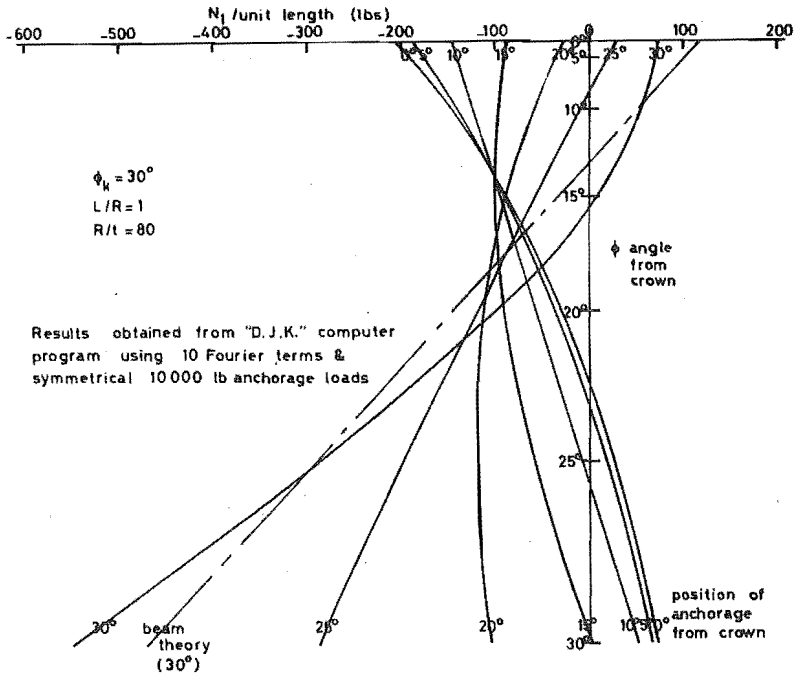

FIG. 6.3 MIDSPAN N_1 DUE TO ANCHORAGE LOAD— $\phi_k = 30°$

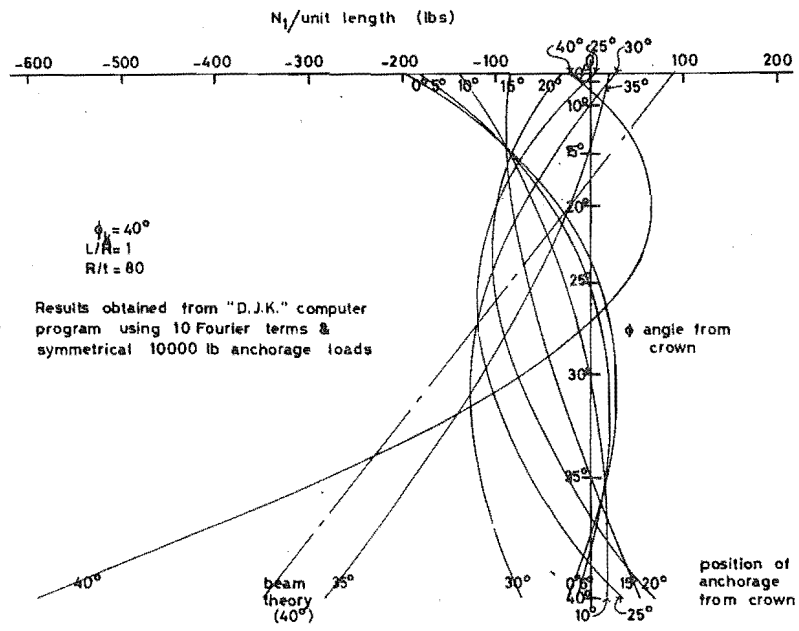

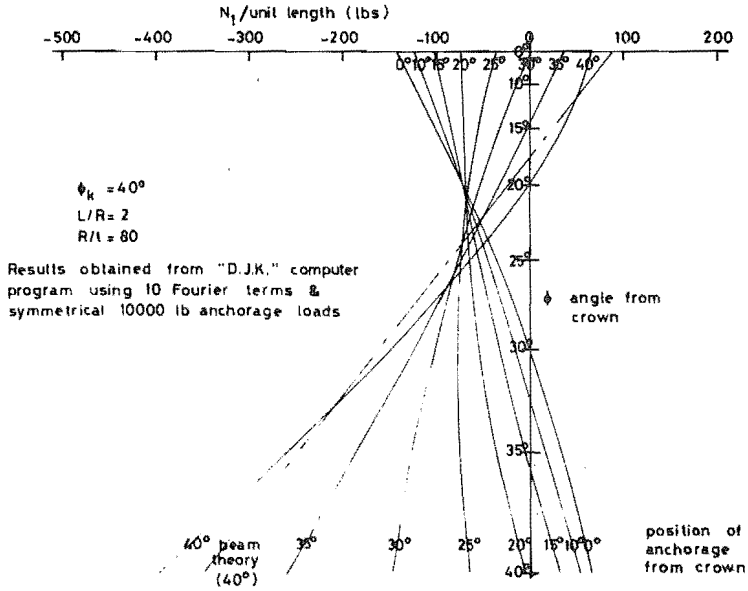

FIG. 6.4 MIDSPAN N_1 DUE TO ANCHORAGE LOAD- $\phi_k = 40°$

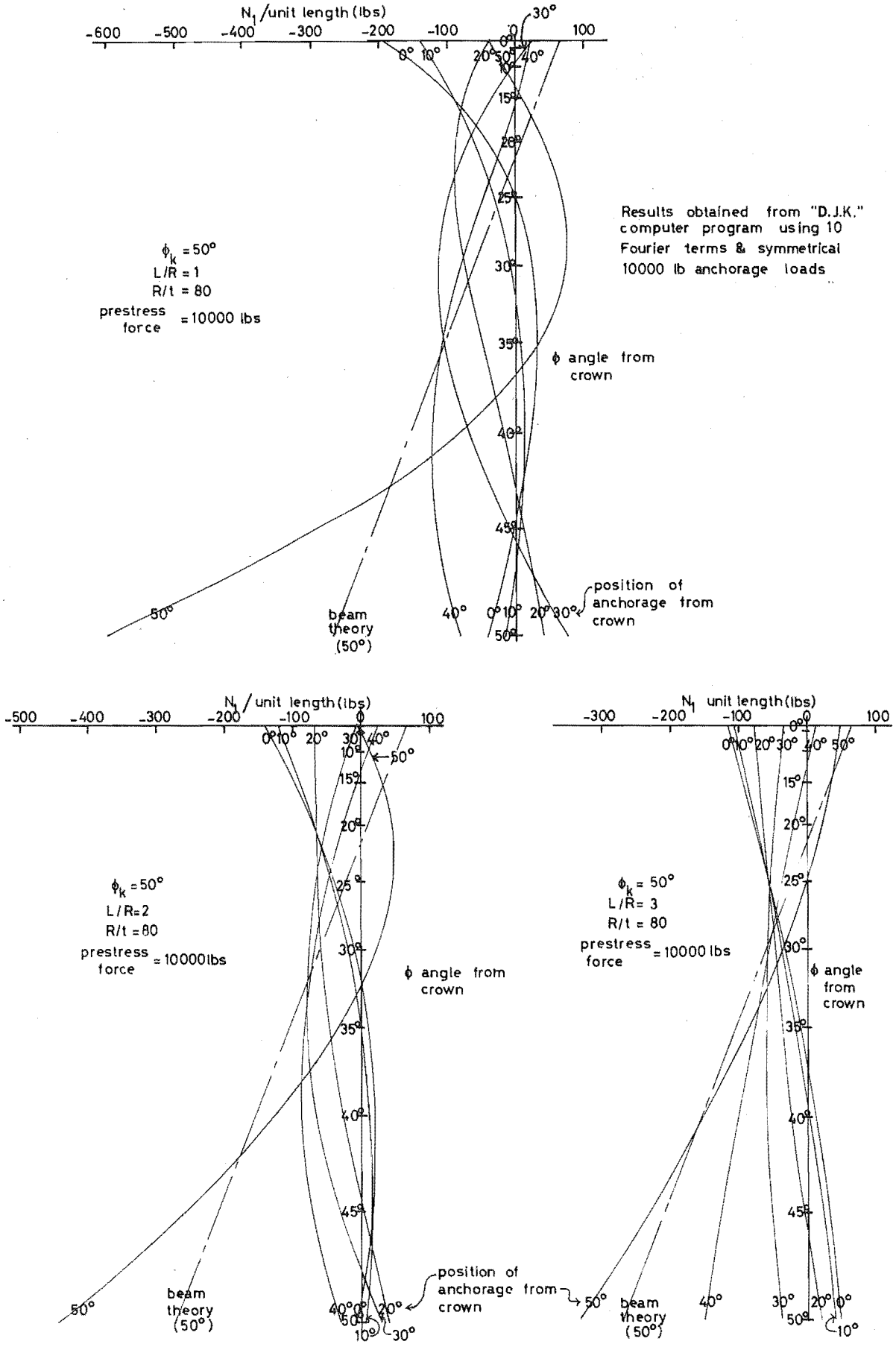

FIG. 6.5 MIDSPAN N_1 DUE TO ANCHORAGE LOAD $-\phi_k = 50°$

length, even for some of those shells whose midspan distribution of N_1 is not given correctly by beam theory. Table 6.1 indicates the approximate distances from the traverse where the maximum values of N_1 change by more than 10% from those at midspan.

L/R	1	2	3	4
$\phi_k = 20^o$	$\frac{5}{16}L$	$\frac{1}{8}L - \frac{1}{16}L$	$\frac{1}{8}L - \frac{1}{16}L$	$\frac{1}{8}L - \frac{1}{16}L$
$= 30^o$	$\frac{5}{16}L$	$\frac{5}{16}L$	$\frac{1}{4}L$	$\frac{1}{8}L$
$= 40^o$	$\frac{5}{16}L - \frac{3}{8}L$	$\frac{5}{16}L$	$\frac{5}{16}L$	$\frac{1}{4}L$
$= 50^o$	$\frac{5}{16}L - \frac{3}{8}L$	$\frac{5}{16}L$	$\frac{5}{16}L$	$\frac{5}{16}L$

Distance from traverse where maximum N_1 values, due to prestress anchorage force, differ by more than 10% from midspan values.

TABLE 6.1 INFLUENCE OF TRAVERSE ON MAXIMUM N_1 VALUES

It was found that for shells where the midspan distribution of N_1 was generally not linear, there were for each particular ϕ_k two anchorage eccentricities which did however give linear distribution for all L/R in the range 1 - 4. For these anchorage eccentricities, the distribution of N_1 around the arc remained similar to that at the midspan arc till nearer the traverse and transverse moments were minimal.

Variation of R/t. With an increase in R/t the range of applicability of beam theory decreases due to the shell being more flexible in the transverse direction, and thus

the assumption of no change in cross-sectional shape is less valid. However for an increase in R/t from 80 to 120 the decrease in the range of applicability of beam theory is small, and for shells which lie within this range there is negligible change in the N_1 distribution. For other shells outside this range slight differences do occur as illustrated in Figure 6.6 for a shell with $\phi_k = 40^o$ and $L/R = 2$. Generally the N_1 distribution departs further from the linear distribution given by beam theory.

6.2.2 N_1 near Traverse

The N_1 distribution near the traverse can be calculated approximately using the beam on elastic foundation technique presented in Section 2.5, using a value of β calculated at the shell-traverse junction, and assuming that this distribution continues a short ($L/8$) distance into the shell. This technique, which only applies close to the traverse, indicates that the N_1 distribution about the anchorage as origin is independent of the anchorage eccentricity except when it is close to the edge. Computer results from the D.K.J. program give the same trend, but do not predict the magnitude of the peaks quite as well. (See Figure 2.14).

Thus by means of beam theory or Figures 6.3 - 6.5 at midspan, and the beam on elastic foundation technique near the traverse, critical N_1 forces due to prestress anchorage loads can be calculated. For parts of the shell further than $L/8$ from the traverse and lying within the limits of Table 6.1, interpolation between known results can be used to obtain sufficiently accurate results for design purposes.

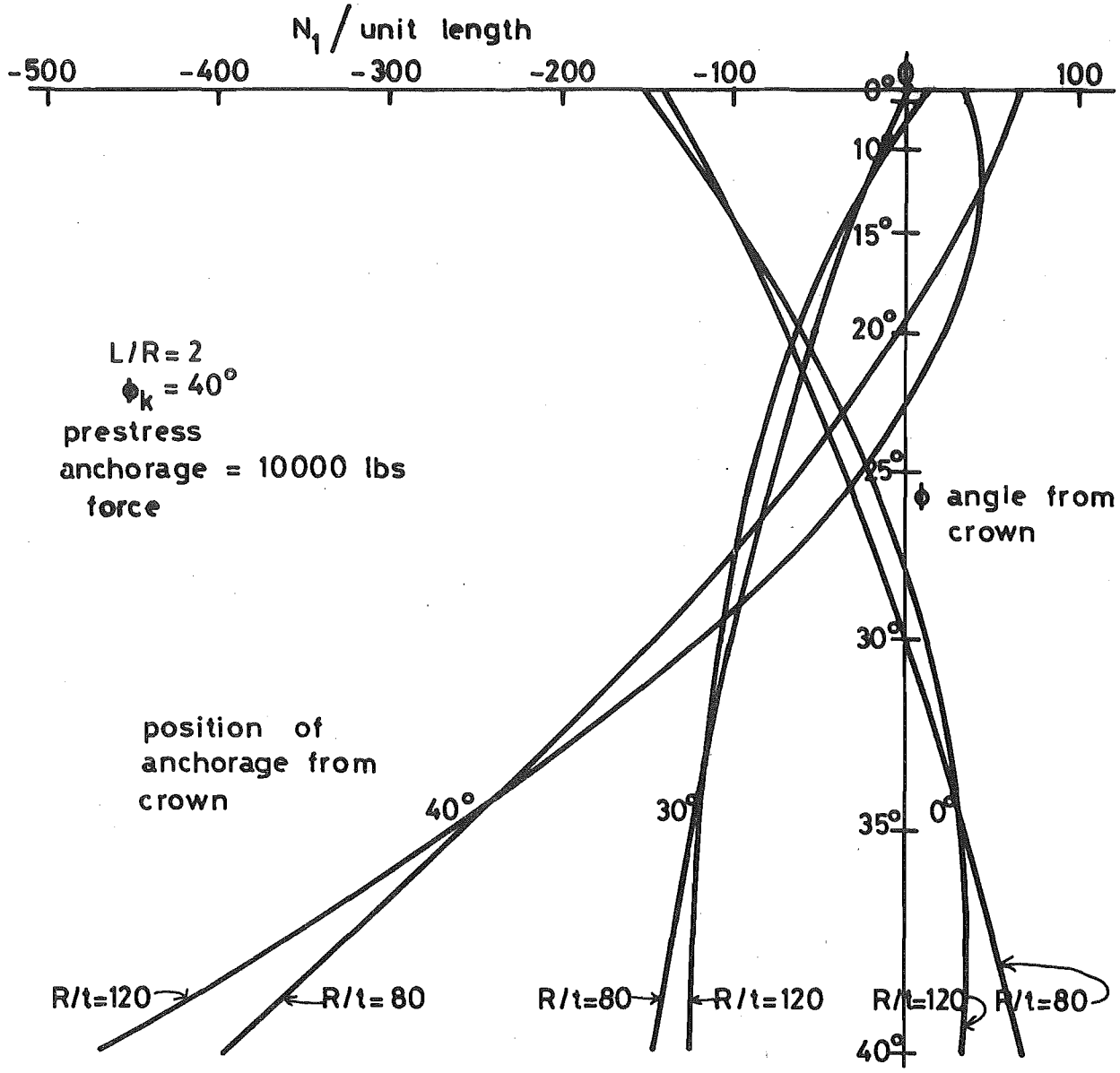

FIG. 6.6 VARIATION OF MIDSPAN N_1 WITH CHANGE IN R/t

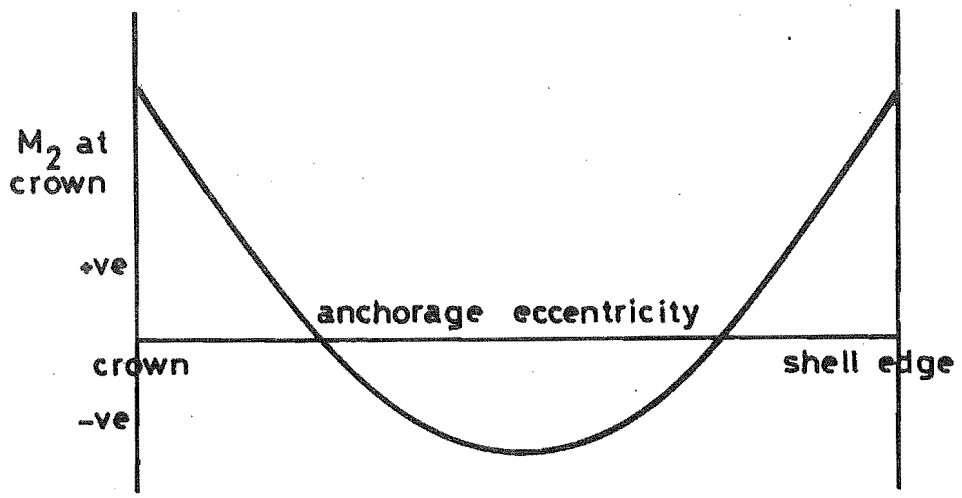

FIG.6.7 VARIATION OF M_2 AT CROWN FOR CHANGE IN ANCHORAGE ECCENTRICITY

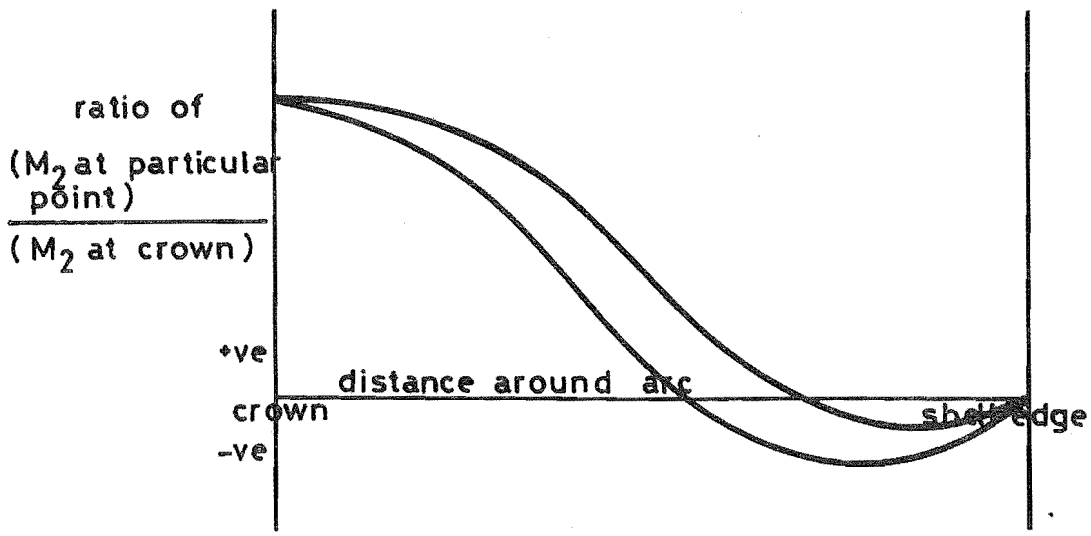

FIG.6.8 M_2 RATIO ENVELOPE

6.2.3 M_2 Due to Anchorage Load

Using the D.K.J. computer program, a systematic study was made of changes in M_2 as L/R, ϕ_k and anchorage eccentricity were altered. R/t (=80) was kept constant. General trends in distribution and magnitude were found for changes in ϕ_k and anchorage eccentricity. These trends degenerate as the L/R ratio is decreased.

The loading terms in the D.K.J, computer program are based on the assumption that the traverse is infinitely stiff in its own plane and has zero stiffness perpendicular to its plane. If an actual traverse differs from this, the general trends outlined and discussed in this section will still hold, but numerical values will be different.

Near the traverse (within $L/8$), relatively large oscillations in the magnitude of M_2 occur, due to the influence of the traverse. In this region, M_2 depends very much on the actual properties of the traverse and few trends or generalisations can be stated. The following discussion only deals with M_2 in the shell between midspan and $L/8$ from the traverse.

At midspan the maximum transverse moment usually occurs at the crown, and the largest moment of opposite sign a short distance up from the edge. As the traverse is approached the positions of maximum positive and negative moments do not alter greatly from those at midspan (until the last $L/8$ from traverse), but the magnitude may increase or decrease, by a factor of up to 20, as shown in Table 6.2.

L/R	1	2	3	4
$\phi_k = 20^o$	I	I	I	I
$= 30^o$	D	I,D	I	I
$= 40^o$	D	I,D	I	I
$= 50^o$	D	D	D	I,D

I - Increase) in maximum M_2 value at $L/8$ from traverse,
D - Decrease) from maximum midspan M_2 value. ($R/t = 80$).
I,D - Increase or Decrease; depending upon anchorage position.

TABLE 6.2 VARIATION OF MAXIMUM M_2 VALUES ALONG SHELL DUE TO ANCHORAGE LOAD

Maximum values of M_2 generally occur at midspan or about $L/8$ from the traverse. For design, once these extreme values are known other values at different cross-sections may be obtained by interpolation.

The behaviour of M_2 around an arc can be explained by means of Figures 6.7 and 6.8, drawn for an arbitrary L/R, R/t and ϕ_k. The sign convention used is that positive moments cause sagging.

Figure 6.7 shows that the sign of the crown moment depends on the position of the anchorage. If the anchorage is near the crown or edge of the shell, the crown moment is positive and for most shells would oppose the moment due to surface loading. If the anchorage is in the centre portion of the shell arc, the crown moment is negative.

As L/R is varied for a particular ϕ_k, the magnitude of the crown moments alter, although the general distribution

does not alter greatly, as shown in Figures 6.9 and 6.11. Generally as $^{L}/R$ is increased the magnitude of the crown moment decreases. As the traverse is approached the rate of decrease reduces. It is interesting to note that for each ϕ_k the average positions of anchorage eccentricity for zero moment, for all $^{L}/R$ shown ($^{L}/R$ = 1 to 4), are approximately equidistant around the arc from the neutral axis position. Also the average distances around the arc from the neutral axis increase linearly with increase in ϕ_k. These anchorage eccentricities are the same as those that were found in Section 6.2.1 to give linear midspan N_1 distribution for all $^{L}/R$. No apparent reason could be found for this phenomenon.

For a particular ϕ_k, $^{L}/R$ and $^{R}/t$ it was found that the ratio, (M_2 at any particular position on the cross-section being considered)/(M_2 at the crown), was similar for all anchorage eccentricities. By considering all anchorage eccentricities an envelope of ratios can be drawn as shown in Figure 6.8. The actual ratio for any particular cable position will be between the two extremes of the envelopes. As a general rule, the actual M_2 ratio moves from the top of the M_2 ratio envelope to the bottom, as the cable anchorage position is varied from the edge to the crown of the shell.

Numerical Results. Using a 10,000 unit anchorage load, Figures 6.9-6.12 have been drawn, so that M_2 at midspan and M_2 at $^{L}/8$ from the traverse can be calculated. In some cases of large ϕ_k and short shell, the envelopes are so wide as to be of little use for design, however the general behaviour can be seen. In drawing the M_2 ratio

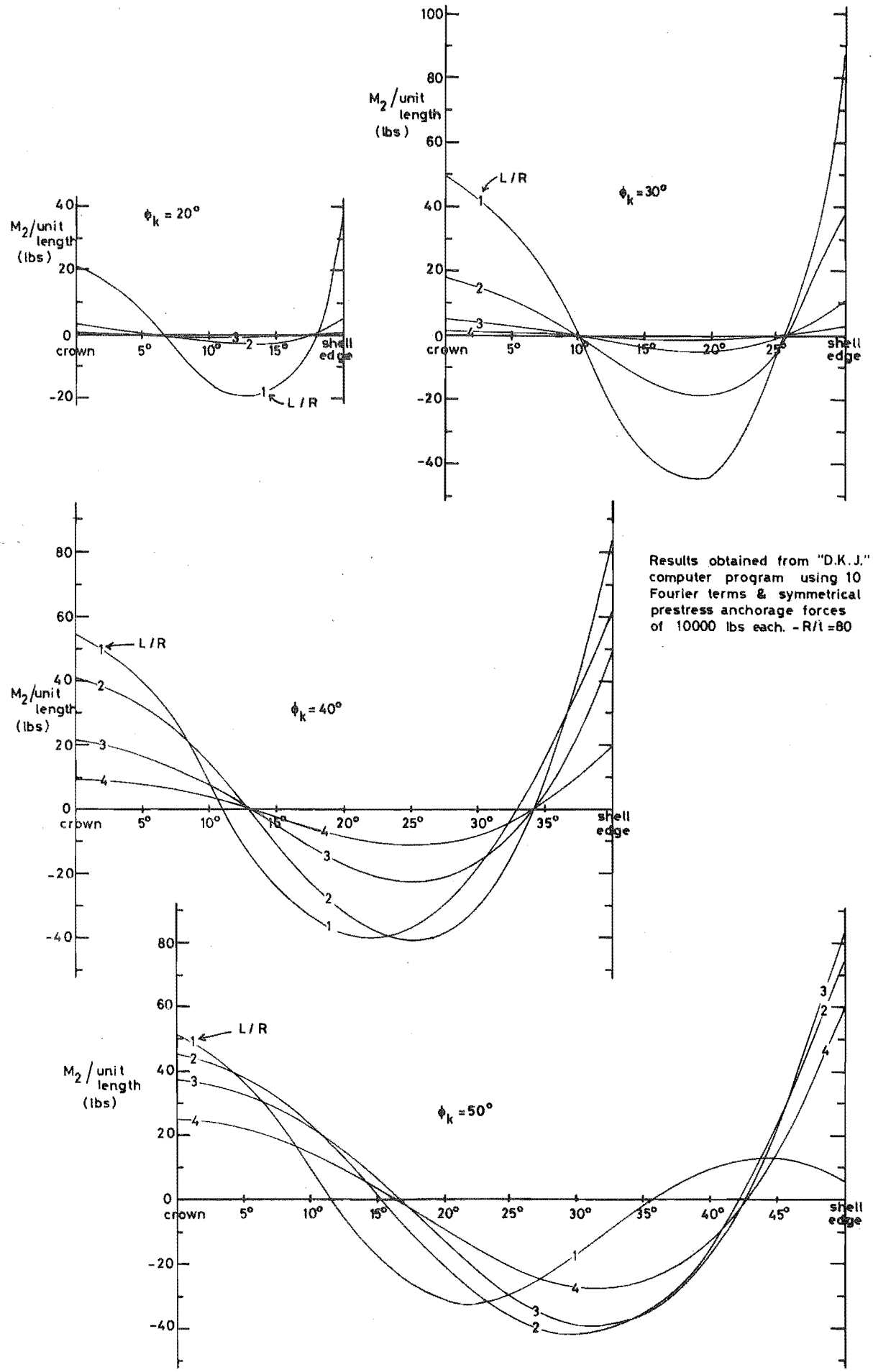

FIG. 6.9 VARIATION OF CROWN M_2 AT MIDSPAN FOR CHANGE IN ANCHORAGE ECCENTRICITY AND L/R RATIO

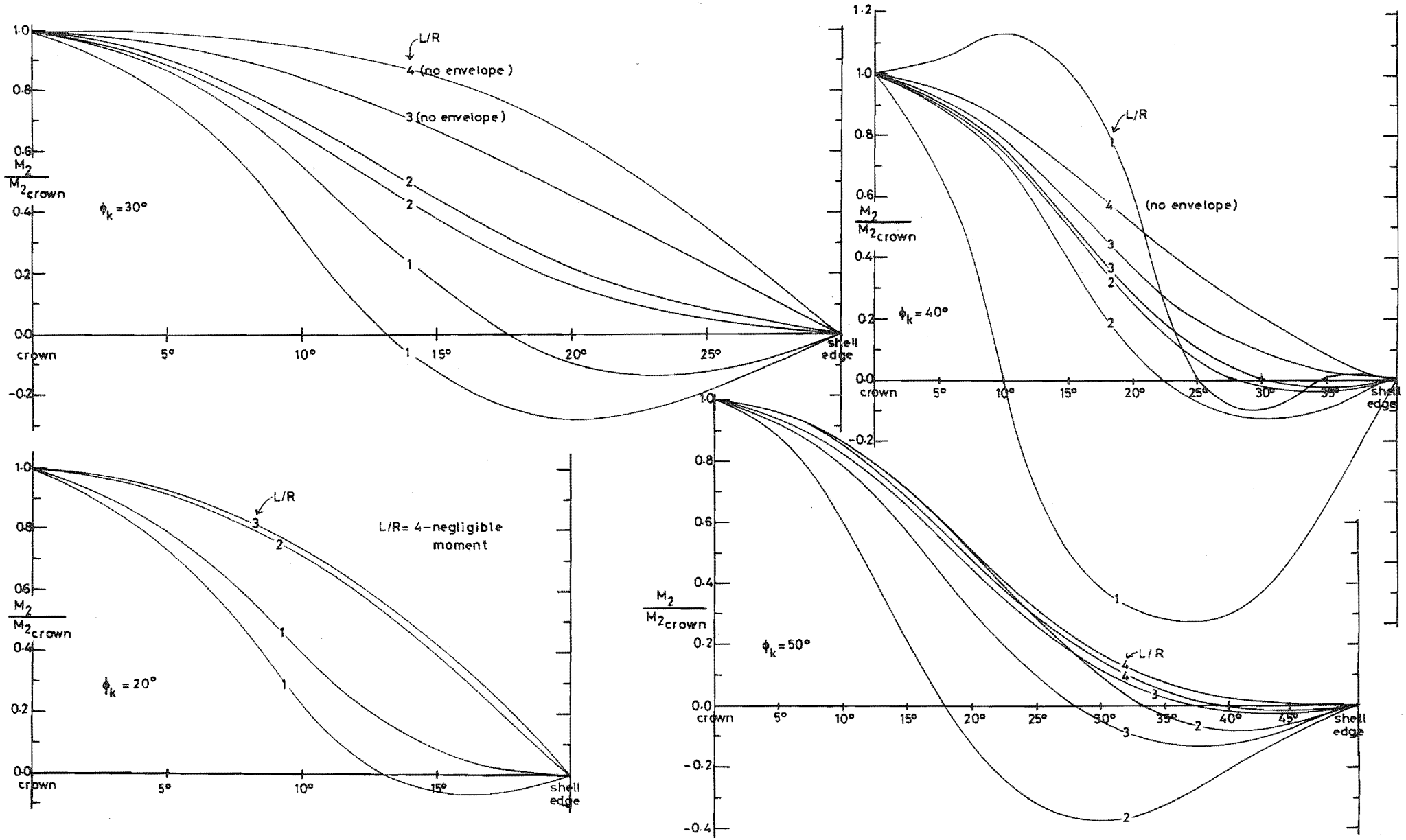

FIG. 6.10 MIDSPAN M_2 RATIO ENVELOPES

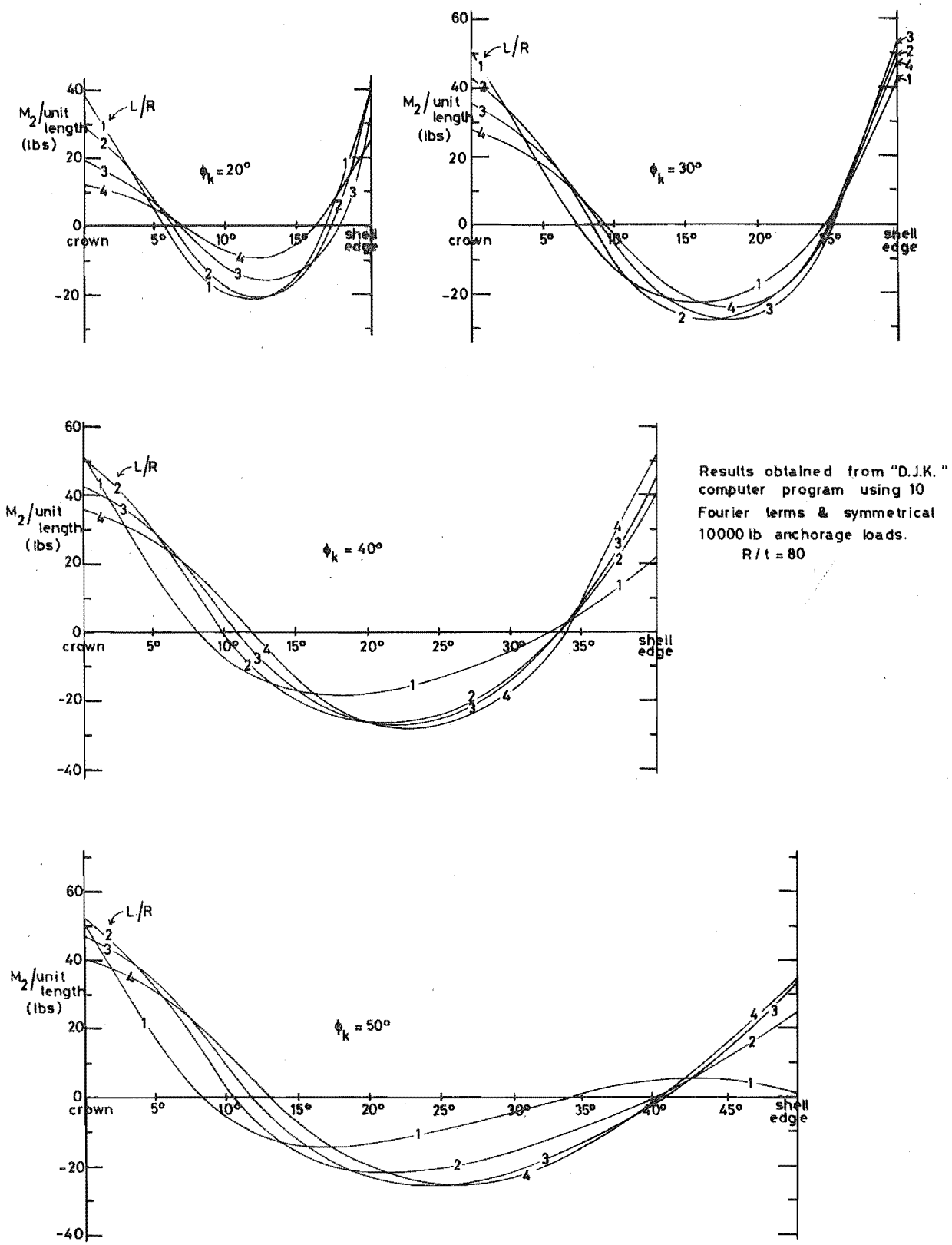

FIG. 6.11 VARIATION OF CROWN M_2 AT L/8 FROM TRAVERSE FOR CHANGE IN ANCHORAGE ECCENTRICITY AND L/R RATIO

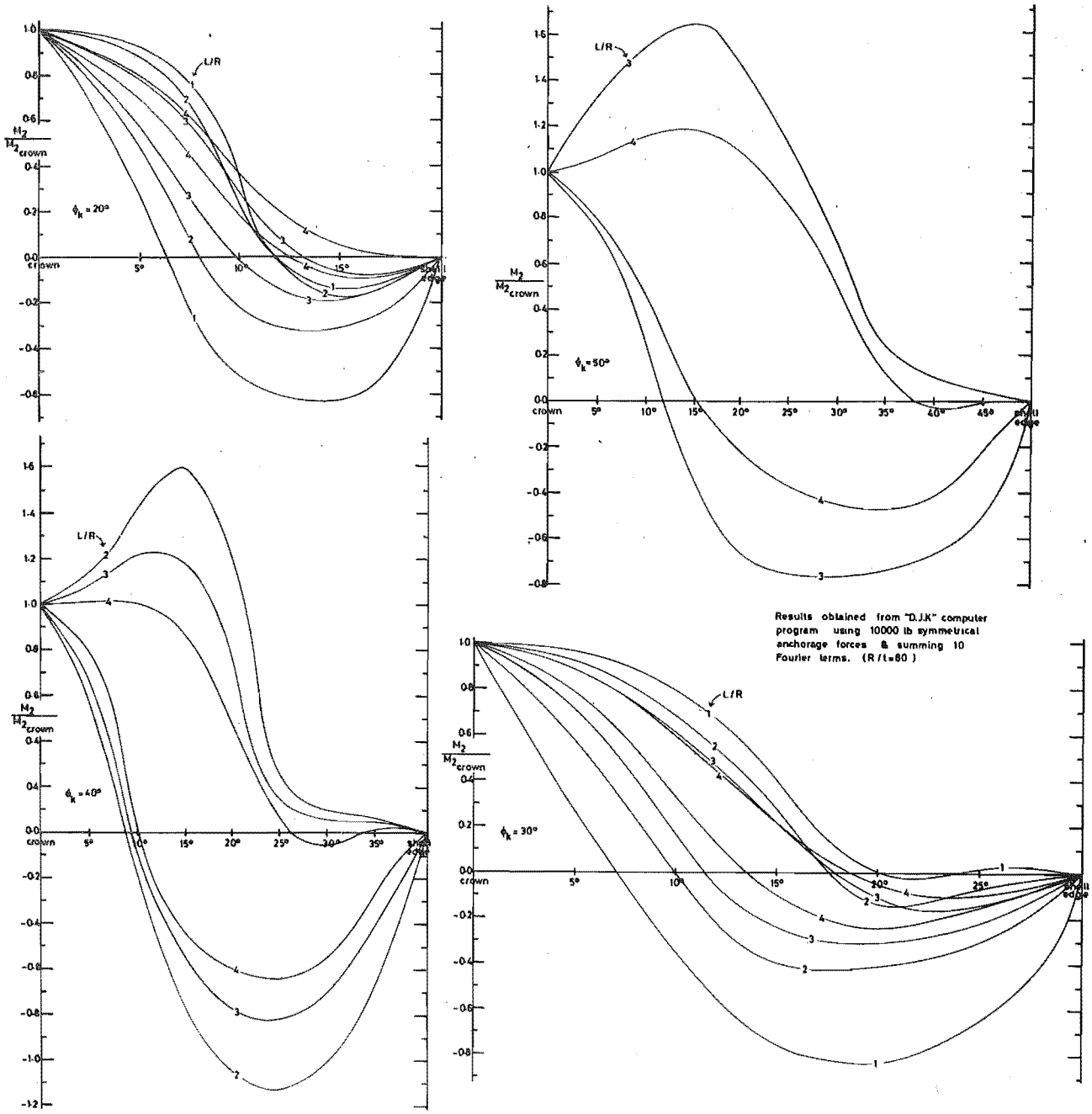

FIG. 6.12 M_2 RATIO ENVELOPES AT L/8 FROM TRAVERSE

envelopes, anchorage eccentricities within $2\frac{1}{2}^{o}$ on either side of the crown zero moment anchorage eccentricity have been ignored. This is because within this range, large M_2 ratios can occur for relatively small moments due to the crown moments themselves being small. For these cable positions the value of M_2 is small over the entire cross-section and is less than the values calculated for anchorage at $2\frac{1}{2}^{o}$ away from the crown zero moment anchorage eccentricity.

Variation of R/t. For an increase in R/t, from 80 to 120, the effect is to give slight variations in the magnitude of the crown moments, the actual distribution across any cross-section remaining similar. For small included angles, (20^{o} and 30^{o}), there is generally an increase in M_2 at midspan and a decrease at the traverse. For larger ϕ_k (40^{o} and 50^{o}), a decrease everywhere generally occurred. Figure 6.13 illustrates these trends for a shell ($\phi_k = 30^{o}$, $L/R = 2$), for an increase in R/t from 80 to 120.

6.3 DRAPED CABLE LOADS

6.3.1 N_1 Due to Cable Drape

At any cross-section, for a symmetrical shell and cable layout, the resultant external forces on the section are a normal force P due to the anchorage load (considered in Section 6.2), and a moment M due to the cable drape, where

$$M = 2P'e'$$

and P' = component of anchorage force parallel to the shell generators less line losses up to cross-section being considered.

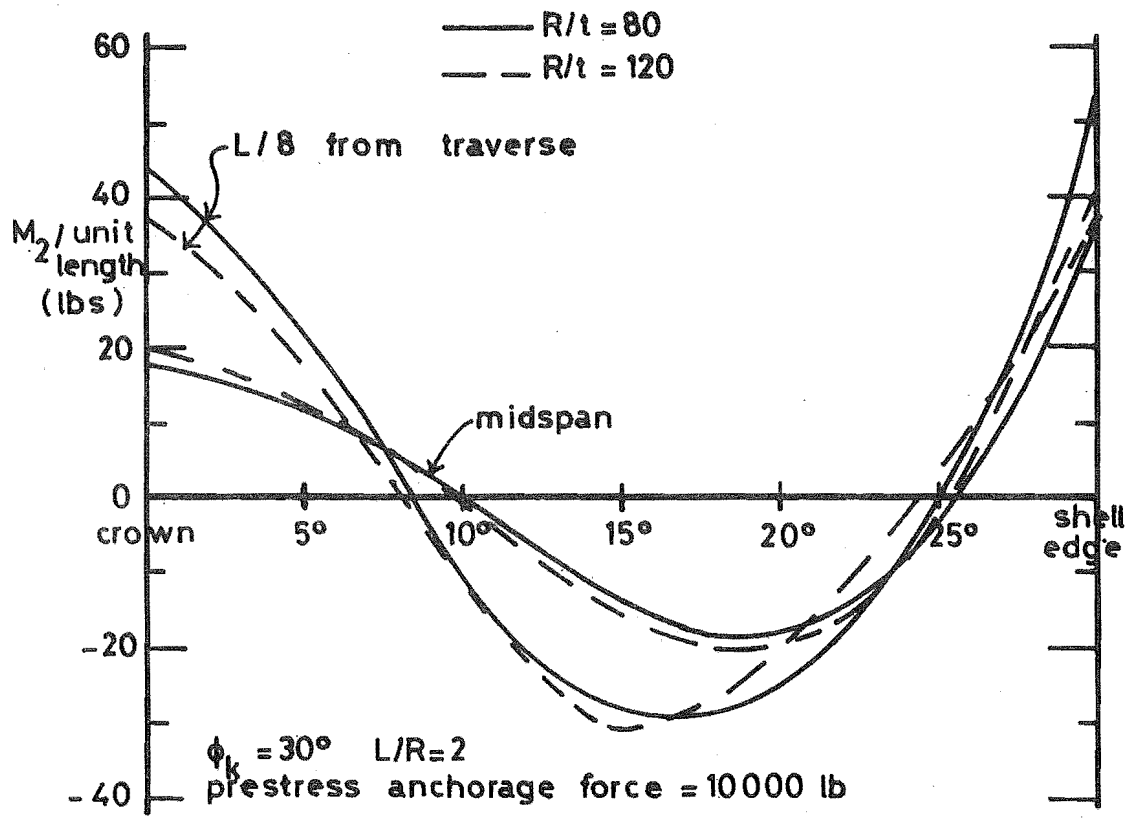

FIG. 6.13 VARIATION IN M_2 DISTRIBUTION FOR CHANGE IN R/t.

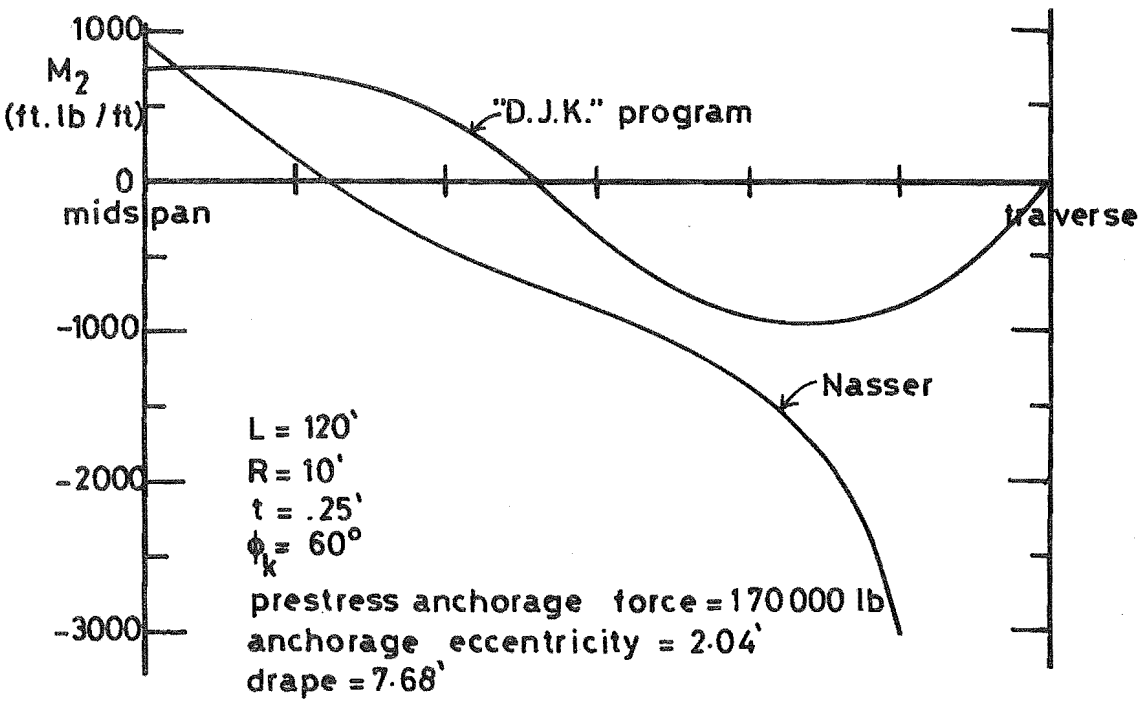

FIG. 6.14 COMPARISON OF RESULTS FROM "D.J.K" PROGRAM AND NASSERS TECHNIQUE

e' = vertical distance from the anchorage to the cable position.

N_1 due to the cable drape can then be calculated accurately for a large range of shells by the simple beam equation,

$$N_1 = \frac{M y t}{I}, \quad M = 2 P' e' \quad \text{and} \quad y, t, I \quad \text{as defined in Section 6.2.}$$

From the small number of results obtained by the author, mainly for cables near the edge with small drape, Figure 6.1 appears to give a good guide to the range for which beam theory, for draped cable effects, gives reliable results.

6.3.2 M_2 Due to Cable Drape

Due to curvature and friction, draped cables exert line loads on the shell which result in transverse bending moments, with maximum values generally occurring at the crown. The vertical component of the line loads, F_V, normally results in a moment at the crown which opposes the moment due to dead and live loads, while the moment resulting from the horizontal line load component, F_H, adds to the dead and live load moments. For most shells the cable will be near the edge at midspan and the resultant crown moment due to the cable drape will counter that due to dead and live loads. Near the traverse the transverse bending moments at the crown due to surface loading and prestress loading will also generally be opposed if the anchorage is near the edge. However this may not be the case if the anchorage is nearer the crown.

For long shells, Nasser[30,31,32] has developed a method for calculating the transverse bending moments. Lin[33]

suggests a similar method using his load balancing technique, but does not develop it so fully. In essence, this method assumes that M_2 at any point on a cross-section is equal to the moment of the line loads acting on the cross-section taken about the point being considered. This is most easily done by calculating the vertical and horizontal components of the line loads, F_V and F_H. Then, M_2/unit length, at any position A can be calculated from,

$$M_A = F_V h_a - F_H v_a$$

where h_a and v_a are the horizontal and vertical distances from the prestressing cable to the point A being considered.

Nasser approximated the line loads by assuming that the cable was draped in a vertical plane. This may give incorrect results, particularly near the end of the shell, and hence accurate calculation of line loads (see Section 2.3.8) would be better, especially as it involves little, if any, extra effort.

For the long shell ($L/R = 12$, $\phi_k = 60^\circ$, $R/t = 40$) analysed by Nasser, Figure 6.14 shows a comparison between transverse bending moments calculated by the D.K.J. program and by using Nasser's technique, accurate line loads being used for both methods. Reasonable agreement is obtained between results near midspan, however at other cross-sections the agreement is lower. Except near the traverse, the general range of magnitude of M_2 is predicted correctly by Nasser's method although the accuracy is not as good as it is at midspan.

For shorter shells Nasser's technique gives moments that are much too large. This is due to the assumption

in Nasser's technique that the total line loads at any cross-section contribute to the transverse bending moment, whereas in fact a portion of the line loads are countered directly by in-plane shear force. A similar limitation occurs for surface loading in Lundgren's beam-arch method. Nasser's method gives an upper bound limit to the moment but the correct moment may be only a small percentage of this, e.g. for the 3rd shell tested by the author, $^{L}/R = 3$, $\phi_k = 30^{o}$, $^{R}/t = 77$, the correct values of maximum transverse moments are approximately 7% that given by Nasser's technique. As the ratio of transverse bending stiffness (a function of ϕ_k, t^3) to longitudinal shear stiffness (a function of L^2, ϕ_k, t) decreases, a greater proportion of the line loads are taken by in-plane shear. No simple relation to calculate the proportion of load carried by each action is apparent.

For small cable drapes the line loads will be small and thus the resulting transverse bending moment will also be small. However for large cable drapes significant moments may occur and a detailed analysis, such as by a computer program similar to that used by the author, should be carried out.

6.4 DISCUSSION

The primary aim in the design of prestressing cable layouts is to counter N_1 at the midspan edge due to dead and live loads. This is achieved by having the cables as near the edge as possible at midspan. For a given anchorage force a straight cable is more efficient than a draped cable as line losses will be less and thus there will be a larger N_1 at midspan to oppose the normal force due to surface loading.

Although the magnitude of M_2 caused by prestressing will normally be lower than that resulting from dead load and live load, it is desirable that the prestressing moments oppose the dead and live load moments. The moments due to prestressing can be considered in two parts, namely the moments due to the anchorage force, M_2^a , and the moments due to cable drape, M_2^d . For the anchorage force, the nearer the edge of the shell the anchorage is, the larger are the transverse bending moments opposing those of dead and live loads. Moments due to the cable drape generally also oppose dead load and live load moments, however these will be small unless there is significant cable drape, in which case the anchorage will be away from the shell edge and thus M_2^a will be reduced. For most shells the increase in M_2^d will be less than the decrease in M_2^a and thus the total transverse bending moment opposing dead and live load moment will be less than for a straight cable with the same cable eccentricity at midspan. If friction losses are high, relatively large moments will occur for cables with small drape. However in this case the normal force at the midspan edge to oppose the tensile force due to dead load and live load will be considerably reduced.

Thus in the author's opinion there is little to be gained by the use of draped cables for prestressing cylindrical shells, excepting practical difficulties of minimum anchorage spacings, stress concentrations in the vicinity of the anchorage etc.

CHAPTER SEVEN

SUMMARY AND CONCLUSIONS

7.1 MODEL TESTS

The method used for constructing the model shells proved to be very satisfactory. By use of a mesh and mortar packing blocks the reinforcement could be accurately placed in the shell surface. This in turn enabled the prestressing cables to be accurately positioned by tying the P.V.C. cable duct to the mesh. When the micro-concrete had set, the P.V.C. duct was easily withdrawn, leaving a perfectly clean hole for the prestress cable.

With the prestressing system developed, the loads on the prestress cables could be set to within 20 lbs of the desired load. Despite the thin shell section (.6") full grout penetration of the cables was achieved in all but one of the shells.

Segmented shells were successfully joined by coating the surfaces to be joined with an epoxy resin and applying a prestress force to the shell. The segmented shells behaved satisfactorily through all loading stages. Cracking generally initiated in the joint region due to lack of tensile reinforcement across the joint.

The method of applying radial surface load to the shells by means of an airbag was generally satisfactory although some effects of skin friction between the airbag and shell were detected. This affected the transverse normal force results particularly.

Reliable results for actions and displacements were obtained for both prestressing and surface loading of the shells. Before cracking of the shells occurred strain readings were repeatable to within ±5 μ strains and deflection measurements were repeatable to with ±.005 inches. All five shells behaved symmetrically.

Young's modulus, E , was calculated by testing reinforced concrete slabs in bending and measuring deflection and strain at midspan. It was found that due to the influence of micro-cracking, a different value of E was obtained depending upon whether E was calculated from strain or deflection measurements.

7.2 ELASTIC BEHAVIOUR

Theoretical elastic results for both prestress and surface loading were obtained by use of the D.K.J. computer program described in Appendix A. This program extended an existing program to enable circular cylindrical shells, with or without edge beams to be analysed for surface loading and symmetrical prestress loading in either the edge beams or in the shell surface itself. Prestressing can be from either straight or draped cables.

7.2.1 Prestressing

For cables in the shell surface, the D.K.J. computer program used the generator line load technique developed by Bryant and Scrivener. An attempt was made to increase the convergence of the technique by modifying the Fourier coefficients but little improvement in convergence could be obtained. However the generator line load method was successfully modified to include the effects of the traverse

on the distribution of prestress anchorage force on the end of the shell. This is particularly important when the anchorage is near the edge of the shell as small changes in the distribution of anchorage force can have significant effects on the transverse bending moments and radial deflections.

The dominant action for all the models was the longitudinal normal force, N_1 , and for this action there was good agreement between theory and experiment, except near the traverse. This is due to the method of feeding in the anchorage force over a finite length (.05L) in the theoretical solution. However near the traverse the magnitude and distribution of N_1 can be obtained by means of the beam on an elastic foundation technique given in Chapter 2 (Equation 2.5). There was also good agreement between theory and experiment for the radial deflection and longitudinal and transverse bending moments. The agreement for other actions, particularly the transverse normal force was not as good.

7.2.2 Surface Loading

As was the case for prestressing the dominant action for the surface loading of all shells was N_1 . This action was predicted well by the theoretical analysis. Again, radial deflection and longitudinal and transverse moments were also predicted well by the theoretical analysis, except near the traverse where the stiffening effect of the traverse is clearly evident in the experimental results. Although both theory and experiment indicate small N_2 , experimental results were influenced by skin friction between the airbag and shell.

7.2.3 Simplification of Analysis

The most important actions in the design of prestressed cylindrical shells are N_1 and M_2. By means of the approximate hand techniques given in Chapter 6 (simple beam theory for N_1 and moment design curves for M_2) these actions can be calculated with sufficient accuracy for initial design purposes, for a large range of shells.

For both prestress and surface loading it has been shown that by considering the shell as a beam, simply supported between the traverses, the midspan N_1 can be predicted to within 5% of results calculated by use of the D.K.J. bending theory, providing the shell geometry is outside certain limits. The limits on the range of shells is less restrictive for prestressing than for surface loading. The general trend is that for a larger included angle, a larger L/R is required to ensure reasonable accuracy of the beam theory. For long narrow shells, the N_1 distribution remains similar to that at midspan till near the traverse, whereas for shorter broader shells the distribution changes more rapidly.

7.2.4 General

The model tests show that by means of an elastic analysis, prestressed concrete cylindrical shells can be designed so that no cracking occurs until a considerable working load is applied. Thus the need for a waterproofing membrane over the extrados can be eliminated. Also the lack of cracking means that unlike reinforced concrete edge beamed cylindrical shells, the effective stiffness of the shell is that of the whole cross-section. Thus, although an elastic analysis would indicate that a prestressed cylindrical shell would deflect considerably more than an equivalent

reinforced concrete cylindrical shell, the actual difference in deflection at design working load may be small.

With regard to M_2 , if the anchorage is near the shell edge, M_2^a caused by the anchorage force will normally oppose that resulting from dead and live loads. If the anchorage is moved away from the edge, M_2^a is reduced until at a relatively small distance from the edge, M_2^a begins to add to that of dead and live loads. The forces resulting from the draping of a prestressing cable will also generally produce M_2^d which oppose those of dead and live loads. However by draping the cable the anchorage will be nearer the crown and thus M_2^a opposing surface loads will be less. The gain in M_2 by draping the cable will normally be less than the loss due to the anchorage being nearer the crown. In the author's opinion there is little to be gained by the use of draped cables except that they tend to retard the development of corner diagonal cracks.

7.3 POST ELASTIC BEHAVIOUR

With the onset of cracking, stress and deflection non-linearity occurred. However for all shells tested excellent recoverability from overloads of up to 90% of ultimate load was achieved.

Cracking in all shells began near midspan with transverse flexural cracks. Diagonal cracking near the corners occurred at a load considerably in excess of that which would be needed to cause similar cracking in non-prestressed shells. In the segmented shells, the only cracks to open appreciably were those occurring at the centre-most joints between elements.

At midspan, where maximum radial displacements occurred for all shells, the greatest radial deflection during elastic behaviour occurred at the edge. Once cracking had occurred this trend continued for the shells with large included angle ϕ_k ; however for the longer, narrower shells cracking resulted in the shells opening, (i.e. decreasing in curvature).

For the shells with small ϕ_k , the longitudinal compression strain at midspan was linear with distance above the neutral axis right up to failure while for shells with large ϕ_k the strain was non-linear. For shells whose ϕ_k lay between these two extremes, an initially non-linear strain versus distance distribution became linear near ultimate load.

7.4 ULTIMATE LOAD BEHAVIOUR

A method is given for the flexural beam type ultimate load design of prestressed cylindrical shells. This method accurately predicted the failure loads of four of the five model shells tested by the author (L/R = 2 or 3, $\phi_k = 30^o - 35.8^o$). The other shell failed in a yield line type failure.

In the beam type ultimate load analysis the shell is assumed to span between the traverses as a simply supported beam. The change in shape of the shell cross-section is ignored. However this is of real concern only when the shell reduces its curvature under applied loads. Limits are given for the range of shells for which this happens. Also in the analysis it is assumed that the strain distribution is linear with distance above and below the neutral axis. The author's experiments show that this assumption is valid for all but short wide shells (e.g. $L/R = 2$, $\phi_k = 43^o$). A method is given

to include the effects of non-prestress steel and the method was shown to give accurate results on the 1st shell tested by the author. In this shell there was a significant amount of non-prestress steel which raised the ultimate load 30% above that of the prestress steel ultimate load. Ultimate load of segmented shells would have been raised if there had been non-prestress steel across the joints.

Limits are put on the minimum steel content to prevent failure by fracture of the tendons, and on maximum steel content to prevent a brittle fracture of the shell. The four shells tested by the author which failed in a beam type manner conformed to these limits.

7.5 MAJOR CONCLUSIONS

From the results of this thesis it is concluded that:

i) Precast, prestressed cylindrical shells can be designed to behave satisfactorily at all loading stages. Cracking can be avoided until a considerable surface load has been applied.

ii) The elastic behaviour for both prestress and surface loads can be accurately predicted.

iii) The ultimate load and failure mechanism can be accurately predicted for shells which fail in a flexural beam type manner.

iv) There is little to be gained by the use of draped prestressing cables.

v) The approximations presented provide a simple method for the initial design of prestressed cylindrical shells, and in general terms show the behaviour of the critical actions N_1 and M_2 as L/R and ϕ_k are varied.

REFERENCES

1. de Sitter, W.R., "Theoretisch en experimenteel onderzoek naar het gedrag van een voorgespannen tonschaal". Heron, Jaargang 11, No.1, 1963, pp.28-47. ("Theoretical and Experimental Investigation into the Behaviour of a Prestressed Cylindrical Shell". Translation, University of Canterbury, 1964).

2. Berndt, E., "Die Wirkungsweise von Gekrummt und Gerade Geführten Spanngliedern in langen Tonnenschalen". Symposium über die Probleme des Zusammenhängen Zwischen Entwerfen und Bauausführung von weitgespannten Schalen. USSR, Leningrad, September 1966. ("The Effect of Draped and Straight Prestressing Cables in Long Cylindrical Shells". Translation, University of Canterbury, 1970).

3. Bryant, A.H., and Scrivener, J.C., "Cylindrical Shell Roofs With Draped Prestressing". Journal of the Structural Division, Proceedings of the American Society of Civil Engineers, Vol.95, No.ST4, April 1969, pp.611-634.

4. Bouma, A.L., van Riel, A.C., van Koten, H., and Beranek, W.J., "Investigations on Models of Eleven Cylindrical Shells Made of Reinforced and Prestressed Concrete". Proceedings of the Symposium on Shell Research, Delft, August 1961, pp.79-101.

5. Scrivener, J.C., and Megget, L.M., "Post-Tensioned Concrete Cylindrical Shell Roof", Civil Engineering Transactions of the Institution of Engineers, Australia, Vol.CE12, No.1, April 1970, pp.7-10.

6. Bryant, A.H., "A Theoretical and Experimental Investigation of Prestressed Cylindrical Shell Roofs". Ph.D. Thesis, University of Canterbury, 1966.

7. Jenkins, R.S., "Theory and Design of Cylindrical Shell Structures". Ove Arup and Partners, London, 1947.

8. McNamee, J., "Analysis of Symmetric Cylindrical Shells". G.B.D.S.I.R., 1955.

9. Billington, D.P., "Thin Shell Concrete Structures". McGraw Hill Book Co., New York, 1965.

10. Gibson, J.E., "The Design of Cylindrical Shell Roofs". Spon, London, 2nd. ed., 1961.

11. Ramaswamy, G.S., "Design and Construction of Concrete Shell Roofs", McGraw Hill Book Co., 1968.

12. Holand, I., "Design of Circular Cylindrical Shells". Oslo University Press, 1957.

13. A.S.C.E., "Design of Cylindrical Concrete Shell Roofs". The American Society of Civil Engineers Manual of Engineering Practice, No.31, 1952.

14. Haas, A.M., "Prestressed and Precast Shells". Proceedings 2nd Symposium on Concrete Shell Roof Construction, Oslo, July 1957.

15. Dehousse, N.M., "Discussion on Prestressed and Precast Shells". Proceedings, 2nd Symposium on Concrete Shell Roof Construction, Oslo, July 1957.

16. Bieger, K.W., "Model Tests on Prestressed Cylindrical Shells". R65-34, Department of Civil Engineering Massachusetts Institute of Technology, Cambridge Mass., 1965.

17. Lanczos, C., "Linear DifferentialOperators". D. Van Nostrand Co., London, 1961.

18. Bary, N.K., "A Treatise on Trigonometric Series". Vol.1, Pergamon Press, 1964.

19. Rish, R.F., "Some Studies in Elastic Shell Structures". Section B, "The Analysis of Cylindrical Shell Roofs with Post Tensioned Edge Beams", Ph.D. Thesis, University of Tasmania, 1971.

20. Kreyszig, E., "Advanced Engineering Mathematics". John Wiley and Sons, 2nd ed., 1968.

21. Timoshenko, S., "Strength of Materials". Part II, D. Van Nostrand Company, 3rd ed., 1956.

22. Gibson, J.E. "Computer Analysis of Cylindrical Shells", Spon, 1961.

23. Scrivener, J.C., "The Testing and Analysis of Reinforced Concrete Cylindrical Shell Roof Models". M.E. Thesis, University of Canterbury, 1958.

24. "Shell Roof". Information Pamphlet, Concrete Technology Corporation, Tacoma, Washington.

25. Rowe, R.E., "Model Analysis and Testing - its Relation to Established Methods of Design and its Accuracy in Predicting the Behaviour of the Actual Structure". Proceedings of a One-Day Meeting on Model Testing, Organized by the Cement and Concrete Association, London, March 1964.

26. Carmichael, A.J., "The Use of Wire Resistance Strain Gauges for Measuring Surface Strains in Concrete Members". Construction Review, December 1959.

27. Neuman, W.M., "Shear Failure Mechanisms of Cylindrical Concrete Shells". Ph.D. Thesis, University of New South Wales, 1965.

28. Moore, B.C., "Limit Analysis of Reinforced Concrete Shells". M.E. Report, University of Canterbury, 1972.

29. Olszak, W., and Sawczuk, A., "Inelastic Behaviour in Shells". P. Noordhoff, Groningen, Netherlands, 1967.

30. Nasser, A.R., and Johnson, C.B., "Semigraphical Analysis of Long Prestressed Concrete Vaulted Shells". Proceedings of the American Concrete Institute, Vol.59, No.5, May 1962, pp.659-671.

31. Nasser, G.D., "Designing Long Prestressed Vaulted Shells". Consulting Engineer, November 1966, pp.116-110.

32. Nasser, G.D., "The Design of Long Prestressed Parabolic Shells". Concrete, April 1966, pp.161-166.

33. Lin, T.Y., and Kulka, F., "Concrete Shells Prestressed for Load Balancing". Proceedings of the World Conference on Shell Structures, San Francisco, October 1962, pp.423-430.

34. Lundgren, H., "Cylindrical Shells". Vol.1, Danish Technical Press, 1960.

35. Baker, A.L.L., "A Plastic Design Theory for Reinforced and Prestressed Concrete Shell Roofs". Magazine of Concrete Research, No.4, July 1950.

36. Baker, A.L.L., "Ultimate Strength Theory for Short Reinforced Concrete Cylindrical Shell Roofs". Magazine of Concrete Research, No.10, July 1952.

37. Gouda, M.A., "Experimental and Analytical Investigation of Stresses in Reinforced Concrete Cylindrical Shell Roofs". Ph.D. Thesis, University of London, 1951.

38. Ernst, G.C., Marlette, R.R., and Berg, G.V., "Ultimate Load Theory and Tests of Long Cylindrical Shell Roofs". Proceedings of the American Concrete Institute, Vol.51, No.3, November 1954, pp. 257-271.

39. Sawczuk, A., "On experimental Foundations of the Limit Analysis Theory of Reinforced Concrete Shells". Proceeding of the Symposium on Shell Research, Delft, August 1961, pp.217-231.

40. A.C.I., Committee 318. "Building Code Requirements for Reinforced Concrete", American Concrete Institute, 1971.

41. Chronowicz, A., "The Design of Shells". Crosby Lockwood, London, 3rd ed., 1968 .

42. Lin, T.Y., "Design of Prestressed Concrete Structures". John Wiley & Sons, 2nd ed., 1963.

43. Mattock, A.H., and Kriz, L.B., "Ultimate Strength of Nonrectangular Structural Concrete Members", Proceedings of the American Concrete Institute, Vol.57, No.7, January 1961, pp.737-766.

44. Harris, H.G., and White, R.N., "Inelastic Behaviour of Reinforced Concrete Cylindrical Shells". Journal of the Structural Division, Proceedings of the American Society of Civil Engineers, Vol.98, No.ST7, July 1972, pp.1633-1653.

45. Hedgren, A.W., "A Numerical and Experimental Study of Translational Shell Roofs". Ph.D. Thesis, Princeton University, 1965.

46. Darvall, P. Le P., Billington, D.P., and Mark, R., "Model Analysis of a Continuous Microcrete Cylindrical Shell". Proceedings of the American Concrete Institute, Vol.68, No.11, November 1971, pp.832-843.

47. Mileykovsky, I.E., "Some Problems of Analysis of Reinforced Concrete Cylindrical Shell Roofs Taking Into Account Crack Formation". Proceedings of the Symposium on Non-Classical Shell Problems, Warsaw, 1963, North Holland Publishing Company, Amsterdam, pp.1126-1139.

48. Rzhanitsyn, A.R., "The Design of Plates and Shells by the Kinematic Method of Limit Equilibrium". IX International Congress of Applied Mechanics, Brussels, 1956, Vol.6, pp.331-340.

49. Darvall, P. Le P., and Billington, D.P., "Correlation Study of the Behaviour of Concrete Thin Shells to Collapse". International Association for Shell and Spatial Structures Bulletin, No.49, June 1972, pp.59-63.

50. Gerard, G., and Becker, H., "Handbook of Structural Stability: Part III, Buckling of Curved Plates and Shells". National Advisory Committee for Aeronautics, Technical Note 3783, 1957.

51. A.C.I. Committee 334. "Concrete Shell Structures Practice and Commentary". Proceedings of the American Concrete Institute, Vol.61, No.9, September 1964, pp.1091-1107.

52. Bryant, A.H., "Model Tests of Prestressing of a Concrete Cylindrical Shell Roof". Proceedings of the 3rd Australasian Conference on the Mechanics of Structures and Materials. Auckland, August 1971, Vol.II.

APPENDIX A

"D.K.J." COMPUTER PROGRAM

Two programs, both using the D.K.J. equation as the characteristic shell equation, were written in Fortran IV for the University of Canterbury's I.B.M. 360/44 computer. The first program is for analysing single circular cylindrical shells without edge beams subject to surface loads and prestress loads from both straight and draped cables. The second program is for analysing single circular cylindrical shells with edge beams subject to surface loading or prestress loading in the edge beams. Both programs use many of the same subroutines and input data decks are similar for each program.

For prestressing loads in the shell surface, the method described in Sections 2.3.2 and 2.3.4 has been used. As Bryant's[6] program, written in Fortran II for the University of Canterbury's I.B.M. 1620 computer was available, as much use as possible was made of this program. Surface loading is distributed to the shell as given in Section 2.2 and prestress edge beam loading as given in Section 2.4. The torsional resistance of the edge beam has been included as this involves little extra computer computation time and thus there is no reason to neglect it.

An indication that the accuracy of the "D.K.J." program is good is given in Figures A.1 and A.2 where results from the computer program are compared with results given by Billington[9] and Gibson[22]. These results were

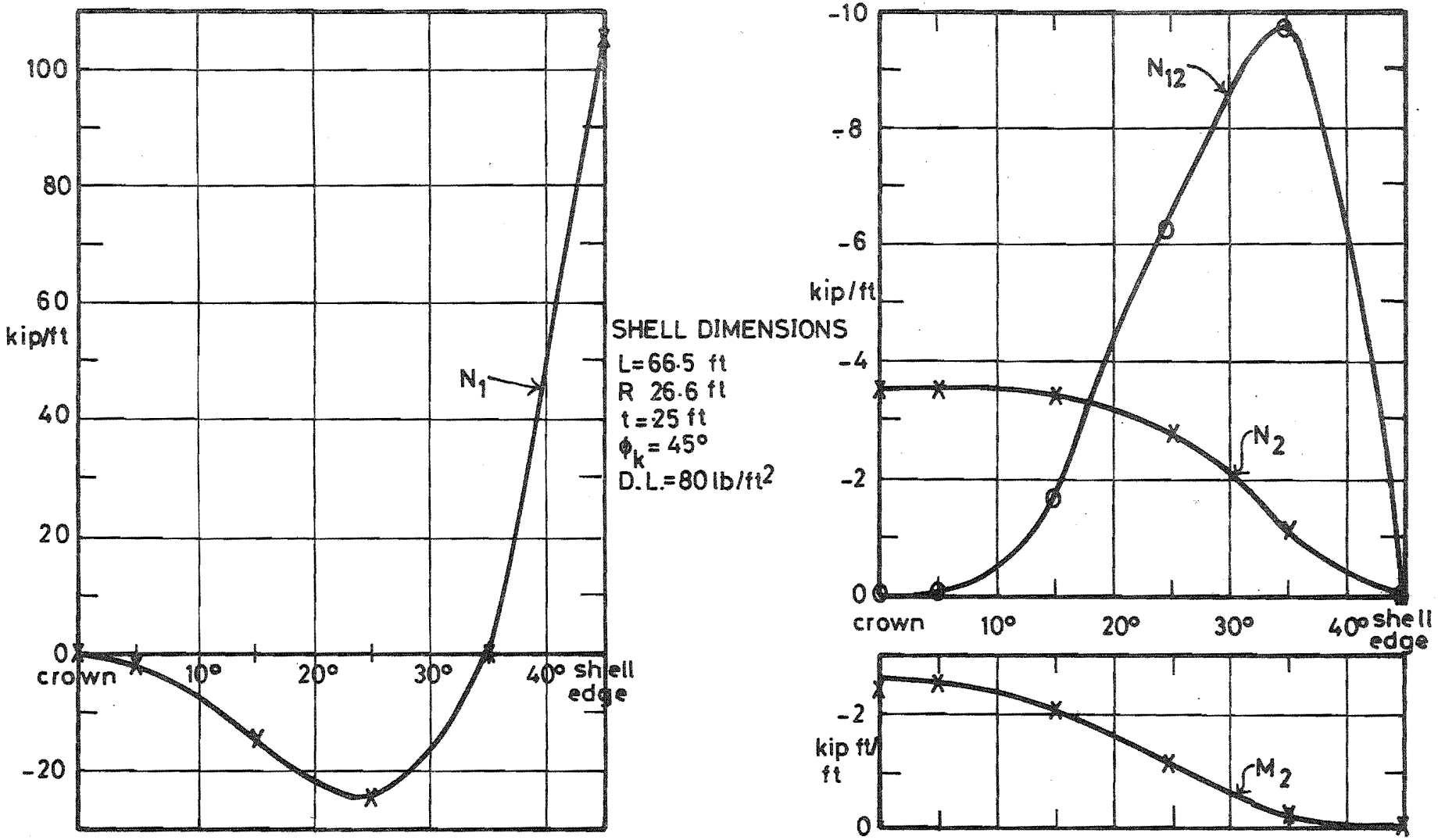

FIG. A.1 COMPARISON OF "D.J.K." COMPUTER PROGRAM RESULTS WITH RESULTS GIVEN BY BILLINGTON

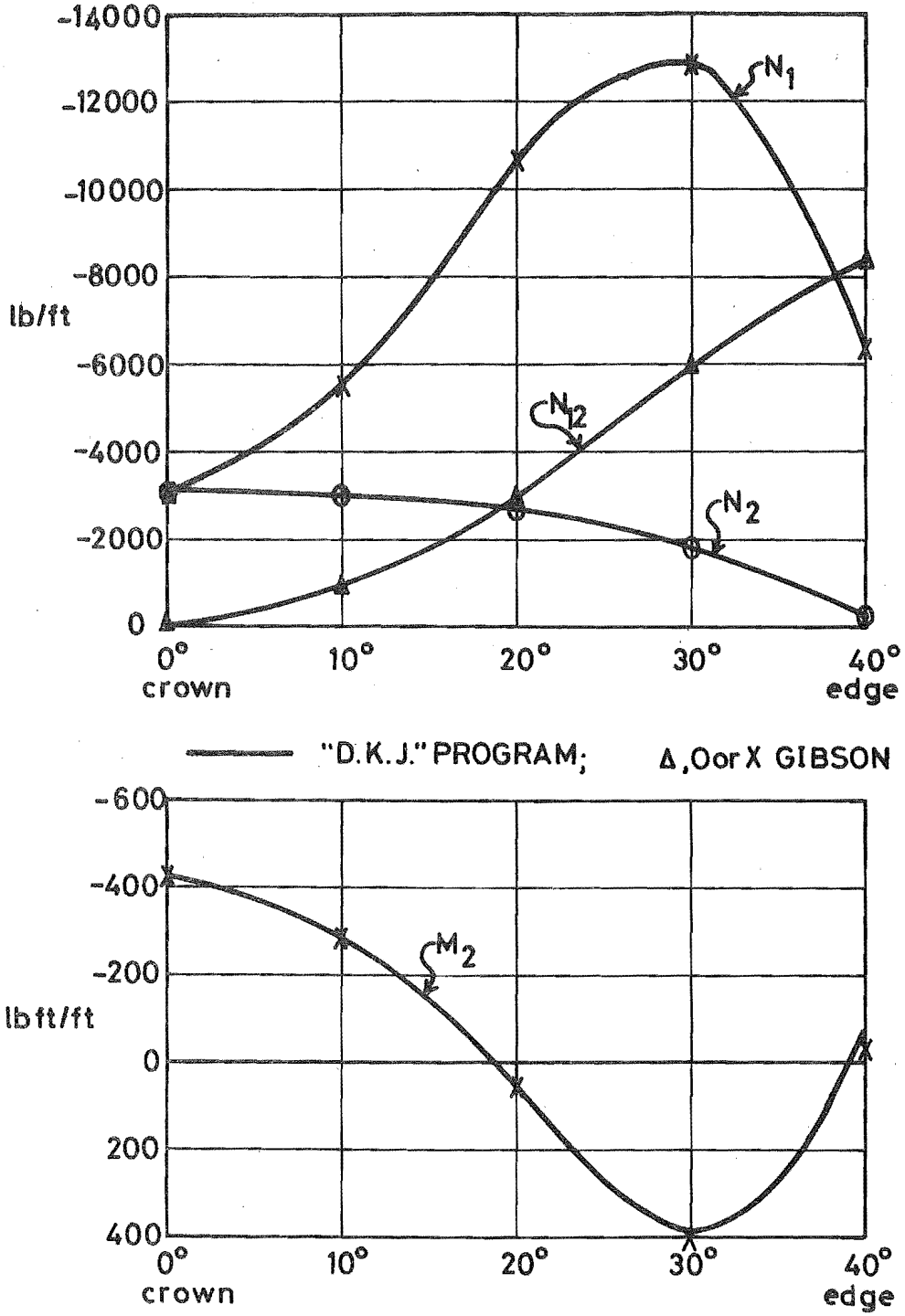

EDGE BEAM ACTIONS	GIBSON	"D.K.J." PROG.
Longitudinal force (lbs)	2.46×10^5	2.5×10^5
Longitudinal moment (lbft)	3.20×10^5	3.2×10^5
Lateral moment (lbft)	4.63×10^3	4.5×10^3

SHELL DIMENSIONS (Gibson shell S92): L = 90'-0", R = 40'-0", $\phi_k = 40°$, t = 0·25', D.L. = 56 lb/ft^2, edge beam 5'-0" x 0·82', weight = 625 lb/ft

FIG. A.2 COMPARISON OF "D.K.J." COMPUTER RESULTS WITH RESULTS GIVEN BY GIBSON

obtained by use of equations of similar formulation to that used in the "D.K.J." program. Figure A.1 shows a comparison with Billington's results for the dead + live load analysis of a cylindrical shell without edge beams ($^{L}/_{R} = 2.5$, $\phi_k = 45^{o}$) and Figure A.2 shows a comparison with Gibson's results for a shell with edge beams ($^{L}/_{R} = 2.25$, $\phi_k = 40^{o}$).

The imput data required for the two programs is given below. Any of the data not required by the particular program being used is ignored.

Card 1. Title (20 A4)

Any alphanumeric characters. Leave first column blank.

Card 2. R, G, T, PHIK, E, PR, SRN, EDGB (8G 10.0) - Shell properties

R = radius G = length

T = thickness PHIK = half included anlge (ϕ_k)

E = Young's modulus PR = Poisson's ratio (ν)

SRN = reference number, for identifying output only

EDGB = 0.0 if no edge beams

Card 3. TL1, TL2, DWEI, PRESF, BAE, BDR, BETG2 (8F10.2) - Edge beam properties. This card is omitted if there are no edge beams

TL1 = depth, D TL2 = breadth, b

DWEI = density PRESF = prestress force

BAE = anchorage eccentricity above centroid

BDR = drape at centre-line (+ve below anchorage)

BETG2 = β for calculating torsional stiffness ($I_r = \beta b^3 D/2(1+\nu)$) (a default value of $\beta = 0.333$ is taken if BETG2 left blank

Card 4. NSECT, NP, NDO (8I10)

NSECT = number of transverse cross-sections (≤ 9) output required for.

NP = number of points on cross-section (≤ 12) output required for.

NDO = type of printout required

= 1 actions

= 2 actions and displacements

= 3 actions, displacements and surface stresses

Card 5. C(I) ; I = 1, NSECT (8G10.0) Positions of cross-sections from centre-line where results required.

C(1) = 0.0)
) Set automatically in program
C(NSECT) = half shell length)

Card 6. P(I) ; I = 1, NP (8G10.0) Position on each cross-section from crown where results required

P(1) = $R\phi_k$ - Set automatically in program

Card 7. VAR (A4) Control card to determine next computation step.

If VAR = D.L. or VAR = RADL, the dead load or radial load routine is utilized and next card is read as:

Card 8. KϕDE, FLϕAD, NFX (I10, F10.2, I10)

KϕDE = Code number of loading - used for reference only.

FLϕAD = load/unit area

NFX = number of Fourier terms to be considered

If VAR = GENL, a general surface loading is considered and next card read as:

Card 8. KϕDE, X,Y,Z,NFX (I10, 3F10.2, I10)

X,Y,Z = Load/unit area in x,y,z direction respectively.

If VAR = P.L., prestress loading in the shell surface is considered and next card is read as:

Card 8. KϕDE, P, FA, F, FR, NN, NB, NS, NC, NSH, PXU, WK

(I5, 4 F10.2, 5I5, 2F5.5)

P = prestress force

FA = anchorage eccentricity around arc from crown

F = cable drape around arc from anchorage

FR = friction loss along half cable length- numerical integration is used to distribute the friction loss along the cable using the equations given at the end of Section 2.3.8.

NN = number of Fourier terms to be considered.

NB = number of transverse strips half the shell is to be divided equally into for Fourier analysis.

NS = number of loaded generators to be considered.

NC = 1: straight cable, 1 anchorage force

= 2: draped cable, 1 anchorage force

= 3: draped cable, no anchorage force

= 4: straight cable, 2 anchorage forces

= 5: draped cable, 2 anchorage forces

N.B. for NC = 4 or 5, anchorage forces of $P/2$ are considered acting at anchorage eccentricity $\pm R/100$.

NSH = anchorage force-is considered as a rectangular shear block spread a distance of $\frac{\text{shell length}}{4\ \text{NSH}}$ into the shell

PXU = coefficient of friction between cable and shell

WK = wobble factor.

N.B. for draped cables, if FR = 0.0, PXU and WK are used to calculate the line loads. Straight cables may be considered by using NC = 2,3 or 5 with F = 0.0

If VAR = SUML, the results for the KϕDE numbers specified on the next card are summed and then printed out.

Card 8. NPO(I) I = 1,8 (8I10)

NPO(I) KϕDE numbers of results to be added and outputed.

After reading any of the above VAR control cards and following card, the program returns to read a new VAR control card.

If VAR = NEWC, the program goes to Card 1 and repeats for a new shell.

If VAR = END. the program terminates execution.

```
C     ******************************************************************************
C
C     D.K.J. - MAINLINE PROGAM - EDGE BEAMS
C     TO FIND ACTIONS AND DISPLACEMENTS IN A CIRCULAR CYLINDRICAL
C     SHELL SUBJECT TO SURFACE LOADS, OR PRESTRESSING LOADS IN
C     THE EDGE BEAMS
C
C     ******************************************************************************
C
      COMMON/SHELL/R,G,T,PHIK,E,PR,NSECT,NP,SRN,NDNP,PI,NDO,EDGB
      COMMON/STRESS/AN(7,9,12),AU(6,9,12),AS(6,9,12)
      COMMON/SICOS/SIX(9),SIY(12), COX(9),COY(12)
      COMMON/CS/C(9),P(12),ANM(4),AUM(4)
      COMMON/UCN/CCN(7,12),CCU(4,12)
      COMMON/COEFS/AL,GAM
      COMMON/EDGEE/TL1,TL2,WEI,PRESF,PE,VP,BI1,BI3,BG2,BA
      COMMON/BEAM/BU(4,9),BN(4,9),BCU(4),BCN(4)
      COMMON/BEAM1/ACCN(4),ACCU(4),FPIS(4),UCPS(4),UPIB(4),UPIT(4),UCFS(
     14),FLEX(4,4)
      COMMON /ABCON/ AJ,AK,AJ1,AK1,ALM,V
      COMMON/NPO/NPC(8)
      COMMON/XBY/XUI,BETA,YMAX ,PXU,WK
      COMMON/KO/KODE,A,FA,F,FR,NN,NB,NS,NC,NSH
      COMMON/FOURT/H(5,12,4)
      COMMON/GENY/Y(5)
      DATA T1/'D.L.'/,T2/'L.L.'/,T3/'P.L.'/,T4/'SUML'/,T5/'NEWC'/,T6/'EN
     1D.'/,T7/'RADL'/,T8/'GENL'/
      DIMENSION TITLE(20)
      CALL MASKO
      PI=3.1415927
    5 READ(5,110)(TITLE(I),I=1,20)
       WRITE(6,110)(TITLE(I),I=1,20)
C     REWIND1
C     REWIND3
C     REWIND8
  110 FORMAT(20A4)
      READ(5,100)R,G,T,PHIK,E,PR,SRN,EDGB
  100 FORMAT(8G10.0)
  101 FORMAT(4H1SRN,T6,1H=,F10.3,22H(SHELL REFERENCE NO. )/2H R,T6,1H=,
     5F10.3,
     1    8H(RADIUS)/2H G,T6,1H=,F10.3,17H(LENGTH OF SHELL)/2H T,T6,2H =
     2,F10.3,20H(THICKNESS OF SHELL)/5H PHIK,T6,1H=,F10.5,33H(HALF INCLU
     3UDED ANGLE IN RADIANS)/2H E,T6,1H=,F10.0,16H(YOUNGS MODULUS)/4H PR
     4 ,T6,1H=,F10.5,16H(POISSONS RATIO))
      WRITE(6,101)SRN,R,G,T,PHIK,E,PR
      IF(EDGB.NE.0.0)CALL EPROP
      READ(5,102) NSECT,NP,NDO
      IF(NDO.GT.3)NDO=3
      IF(NP.GT.12)NP=12
      IF(NSECT.GT.9)NSECT=9
       NDNP=NSECT*NP
  102 FORMAT(8I10)
      WRITE(6,103) NSECT,NP,NDO
  103 FORMAT(6H NSECT,T6,1H=,I10,23H(NO. OF CROSS-SECTIONS)/3H NP,T6,
     11H=,I10,32H(NC. OF POINTS ON CROSS-SECTION)/4H NDO,T6,I10,25H(TYPE
     1 OF OUTPUT REQUIRED))
      READ(5,100) (C(I),I=1,NSECT)
      C(1)=0.0
      C(NSECT)=G/2.0
      WRITE(6,105) (C(I),I=1,NSECT)
  105 FORMAT(58H POSITIONS OF CROSS-SECTIONS MEASURED FROM CENTRE OF SHE
     1LL/1H ,9F12.4)
      READ(5,100) (P(I),I=1,NP)
       P(1)=R*PHIK
      WRITE(6,104) (P(I),I=1,NP)
  104 FORMAT(91H POSITIONS OF POINTS ON CROSS-SECTIONS , MEASURED FROM C
     1ENTRE-LINE OF SHELL AS ARC DISTANCE/1H ,5F12.4)
    8 READ(5,110) VAR
   11 DO 300I=1,12
      DO300J=1,9
      DO303K=1,6
  302 AU(K,J,I)=0.0
  303 AS(K,J,I)=0.0
      DO300K=1,7
  300 AN(K,J,I)=0.0
      IF(VAR.EQ.T1.OR.VAR.EQ.T2) GO TO 2
C     IF(VAR.EQ.T3) GO TO 9
C     IF(VAR.EQ.T4) GO TO 18
      IF(VAR.EQ.T5) GO TO 5
      IF(VAR.EQ.T6) GO TO 25
      IF(VAR.EQ.T7) GO TO 2
      IF(VAR.EQ.T8) GO TO 2
      WRITE(6,10)
   10 FORMAT('MISTAKE IN LOADING FORMAT')
      STOP
    2 CALL SURFLD (VAR)
      GO TO 8
C    9 CALL PRESLD
C     GO TO 8
C   18 CALL SUMLD
C     GO TO 8
   25 WRITE(6,109)
  109 FORMAT(14H JOB COMPLETED)
      END



C
      SUBROUTINE ROTMLT (B,A,ANG)
C
      DIMENSION A(4,4),B(4,4)
C     B=LT*A
      C=COS(ANG)
      S=SIN(ANG)
      DO 1 J=1,4
      B(1,J)=A(1,J)
      B(2,J)=A(2,J)*C-A(3,J)*S
      B(3,J)=A(2,J)*S+A(3,J)*C
    1 B(4,J)=A(4,J)
      RETURN
      END
```

```
C
      SUBROUTINE PARTI(NFX,X,Y,Z,VAR)
C
C     PARTICULAR INTEGRAL SUBPROGRAM
C     LOADING IS TAKEN IN FORM
C     X=XSIN(X)COS(Y),Y=YCOS(X)SIN(Y),Z=ZCOS(X)COS(Y)
C
      COMMON/SHELL/R,G,T,PHIK,E,PR,NSECT,NP,SRN,NONP,PI,NDC,EDGB
      COMMON/STRESS/AN(7,9,12),AU(6,9,12),AS(6,9,12)
      COMMON/SICOS/SIX(9),SIY(12), COX(9),COY(12)
      COMMON/CS/C(9),P(12),ANM(4),AUM(4)
      COMMON/UCN/CCN(7,12),CCU(4,12)
      COMMON/COEFS/AL,GAM
      COMMON/BEAM/BU(4,9),BN(4,9),BCU(4),BCN(4)
      COMMON/EDGEE/TL1,TL2,WEI,PRESF,PE,VP,BI1,BI3,BG2,BA
      COMMON/BEAM1/ACCN(4),ACCU(4),FPIS(4),UCPS(4),UPIB(4),UPIT(4),UCFS(
     14),FLEX(4,4)
      COMMON /ABCON/ AJ,AK,AJ1,AK1,ALM,V
      COMMON /SMAT/ A(4,4),B(4,4),AA(4,4),BS(4,4),FSH(4,4),FZ(4,2),FY(4,
     12),AS1(4,4),AC(4),ACC(4)
      COMMON/NPO/NPO(8)
      DIMENSION S(4,4)
      DATA T1/'D.L.'/,T2/'L.L.'/,T3/'P.L.'/,T4/'SUML'/,T5/'NEWC'/,T6/'EN
     1D.'/,T7/'RADL'/,T8/'GENL'/
  150 FORMAT (1H ,8E10.3)
C     INITIALIZE REQUIRED CONSTANTS
      DO10J=1,9
      DO10I=1,4
      BN(I,J)=0.0
   10 BU(I,J)=0.0
      NPCO=1
      XSI=-1.0
      BL1=TL1/2.
      BL2=TL2/2.
      PI=3.1415927
      GAM=1.0/R
      BE4=3*(1-PR*PR)/(R*R*T*T)
      BT=BE4**.25
      D=(T**3)/(12.0*(1-PR*PR))
      DO 4 IJ=1,NP
        GAMY=P(IJ)/R
      SIY(IJ)=SIN(GAMY)
    4 COY(IJ)=COS(GAMY)
C     DO LOOP FOR CARRYING OUT FOURIER DISTRIBUTION IN X DIRECTION
      DO 1 J=1,NFX
C     ESTABLISH COEFFICIENTS DEPENDENT ON PARTICULAR FOURIER
C     TERM BEING CONSIDERED
      AM=2*J-1
      AL=(AM*PI)/G
      AL2=AL*AL
      ALM=SQRT(AL*BT)
      V=AL/BT
      AJ1=SQRT((SQRT(1.0+(1.0-V)**2)-1.0+V)/2.0)
      AJ=SQRT((SQRT(1.0+(1.0+V)**2)+1.0+V)/2.0)
      AK=1.0/(2.0*AJ)
      AK1=1.0/(2.0*AJ1)
      V4=(AL**4/BE4)/4.0
      DO 2 IJ=1,NSECT
      ALX=AL*C(IJ)
      COX(IJ)=COS(ALX)
      IF(C(IJ).EQ.(G/2.0)) COX(IJ)=0.0
    2 SIX(IJ)=SIN(ALX)
      GA=GAM/AL
      GA2=GA**2
      FAC=(1.0+GA*GA)**2
      DEN=1.0+V4*FAC**2
      XSI=-XSI
      FOCEX=(4.0*XSI)/(PI*AM)
      X1=X*FOCEX
      Y1=Y*FOCEX
      Z1=Z*FOCEX
      HX=((R*(PR-GA2))/(AL*T*DEN))*X1
      HY=(R*GA*(GA2+2.0+PR)*Y1)/(AL*T*DEN)
      HZ=(R*R*FAC*Z1)/(T*DEN)
      FX=(V4*FAC*(GA2-PR)*X1)/(AL**3*DEN)
      YY=((V4*FAC*(1.0-PR*GA2)+1.0)*Y1)/(AL*AL*GAM*DEN)
      ZZ=(R*Z1)/(AL*AL*DEN)
      F=FX+YY+ZZ
      H=HX+HY+HZ
      ANM(1)=-AL*GAM*F
      ANM(2)=(-AL*AL*F+Y1/GAM)
      ANM(3)=(-D*AL**3)*(GA*GA2+GA*(2.0-PR))*H
      ANM(4)=(PR+GA2)*D*AL*AL*H
      AUM(1)=AL*(PR-GA2)*F/T+X1/(T*AL*AL)-PR*Y1/(T*AL*GAM)
      AUM(2)=AL*AL*(PR*G-1.0)*F/(T*GAM)-PR*X1/(T*AL*GAM)+Y1/(T*GAM*GAM)+
     1HY/(GAM*R)+HZ/(GAM*R)
      AUM(3)=H
      AUM(4)=GAM*H
      IF(VAR.EQ.T7) GO TO 3
      DO 7 K=1,NP
      CCN(1,K)=ANM(1)*SIY(K)
      CCN(2,K)=ANM(2)*COY(K)
      CCN(3,K)=ANM(3)*SIY(K)
      CCN(4,K)=ANM(4)*COY(K)
      CCU(1,K)=AUM(1)*COY(K)
      CCU(2,K)=AUM(2)*SIY(K)
      CCU(3,K)=AUM(3)*COY(K)
      CCU(4,K)=AUM(4)*SIY(K)
    7 CONTINUE
      DO 11K =1,4
   11 ACCN(K)=-CCN(K,1)
C     CALCULATE SHELL EDGE DEFLECTIONS DUE TO P.I. + C.F.
      CALL ABMAT(A,B)
      YE= 2.0*R*PHIK
      CALL COMFUN(YE,FY)
      CALL FMULT(S,FY,A)
      CALL JSUB(AA,S,A)
      CALL FMULT(S,FY,B)
      CALL JADD(BS,S,B)
      CALL INVER(AA,AS1,KO)
C     REESTABLISH MATRIX AA
      CALL COMFUN(YE,FY)
      CALL FMULT(S,FY,A)
      CALL JSUB(AA,S,A)
C     SHELL STIFFNESS MATRIX
      CALL MMULT (FSH,BS,AS1)
C     CALCULATE DEFLECTION OF SHELL DUE TO C.F.
      CALL RMULT (UCFS,FSH,ACCN)
C     CALCULATE ARBITARY CONSTANTS DUE TO C.F.
      CALL RMULT(AC,AS1,ACCN)
```

```
C     FIND TOTAL SUM AND CONVERT TO JUNCTION COORDINATES
      DO 13K=1,4
   13 ACCU(K) = CCU(K,1) + UCFS(K)
      CALL ROTATE(ACCU,UCPS,PHIK,1)
C     DEFLECTION OF BEAM AT JUNCTION DUE TO PRESTRESS + D.L.
      ZM=(PE+(WEI-VP)/AL2)*FOCEX
      PP = -PRESF*FOCEX
      UPIB(1)=(PP/BA-ZM*BL1/BI1)/AL
      UPIB(2)=0.0
      UPIB(3)=ZM/(BI1*AL2)
      UPIB(4)=0.0
C     CALCULATE DIFFERENCE IN P.I. DEFLECTIONS
      DO 6 K=1,4
    6 UPIT(K)=UPIB(K)-UCPS(K)
C     CALCULATE TOTAL STIFFNESS MATRIX
C     FIND ARBITARY CONSTANTS FOR SHELL AND EDGE BEAM
      CALL ARBSE
      CALL SYCFS
      DO 8 K=1,NP
      CCN(5,K)=AL*T*CCU(1,K)+PR*CCN(2,K)
      CCN(6,K)=PR*CCN(4,K)+AL*AL*T**3*CCU(3,K)/(12.0*(1.0-PR*PR))
      CCN(7,K)=-AL*T**3*CCU(4,K)/(12.0*(1.0+PR))
    8 CONTINUE
C     CALCULATE (N) AND (U) FOR BEAM MIDSPAN
      DO 9 K=1,4
    9 ACCN(K)=-CCN(K,1)
      CALL ROTATE (ACCN,FPIS,PHIK,1)
      BCN(1)=FPIS(1)/AL+PP
      BCN(2)=(FPIS(3)-AL*BL1*FPIS(1))/AL2+ZM
      BCN(3)=(FPIS(2)-AL*BL2*FPIS(1))/AL2
      BCN(4)=(BL1*FPIS(2)-FPIS(4)-BL2*FPIS(3))/AL
      BCU(1)=BCN(1)/(AL*BA)
      BCU(2)=BCN(3)/(AL2*BI3)
      BCU(3)=BCN(2)/(AL2*BI1)
      BCU(4)=-BCN(4)/(AL*BG2)
C     DO LOOP TO CALCULATE VECTORS N,U AND LOADING AT EACH POINT FOR PAR
C     TICULAR FOURIER TERM BEING CONSIDERED.
C     RESULTS ARE ADDED ONTO RESULTS FROM PREVIOUS TERMS.
      DO 5 L=1,NSECT
      CC=COX(L)
      SS=SIX(L)
      BN(1,L)=BN(1,L)+BCN(1)*CC
      BN(2,L)=BN(2,L)+BCN(2)*CC
      BN(3,L)=BN(3,L)+BCN(3)*CC
      BN(4,L)=BN(4,L)+BCN(4)*SS
      BU(1,L)=BU(1,L)+BCU(1)*SS
      BU(2,L)=BU(2,L)+BCU(2)*CC
      BU(3,L)=BU(3,L)+BCU(3)*CC
      BU(4,L)=BU(4,L)+BCU(4)*CC
      DO 5 K=1,NP
      AN(1,L,K)=AN(1,L,K)+CCN(1,K)*SIX(L)
      AN(2,L,K)=AN(2,L,K)+CCN(2,K)*COX(L)
      AN(3,L,K)=AN(3,L,K)+CCN(3,K)*COX(L)
      AN(4,L,K)=AN(4,L,K)+CCN(4,K)*COX(L)
      AN(5,L,K)=AN(5,L,K)+CCN(5,K)*COX(L)
      AN(6,L,K)=AN(6,L,K)+CCN(6,K)*COX(L)
      AN(7,L,K)=AN(7,L,K)+CCN(7,K)*SIX(L)
      AU(1,L,K)=AU(1,L,K)+CCU(1,K)*SIX(L)
      AU(2,L,K)=AU(2,L,K)+CCU(2,K)*COX(L)
      AU(3,L,K)=AU(3,L,K)+CCU(3,K)*COX(L)
      AU(4,L,K)=AU(4,L,K)+CCU(4,K)*COX(L)
    5 CONTINUE
    1 CONTINUE
      RETURN
    3 DO12 K=1,NP
      CCN(1,K)=0.0
      CCN(2,K)=ANM(2)
      CCN(3,K)=0.0
      CCN(4,K)=ANM(4)
      CCU(1,K)=AUM(1)
      CCU(2,K)=0.0
      CCU(3,K)=AUM(3)
   12 CCU(4,K)=0.0
      GO TO 7
      END



C
      SUBROUTINE EPROP
C
C     TO CALCULATE PROPERTIES OF EDGE BEAM
C
      COMMON/EDGEE/TL1,TL2,WEI,PRESF,PE,VP,BI1,BI3,BG2,BA
      COMMON/SHELL/R,G,T,PHIK,E,PR,NSECT,NP,SRN,NDNP,PI,NDO
      READ(5,100)TL1,TL2,DWEI,PRESF,BAE,BDR,BETG2
  100 FORMAT(8F10.2)
      BA=TL1*TL2
      WEI=DWEI*BA
      B=TL2
      D=TL1
      IF(TL1.LT.TL2)B=TL1
      IF(TL1.LT.TL2)D=TL2
      IF(BETG2.EQ.0)BETG2=.3333333
      BG2=BETG2*(B*B*B*D)/(2.*(1.0+PR))
      PE=PRESF*BAE
      VP=8.*PRESF*BDR/(G*G)
      BI1=TL2*TL1**3/12.
      BI3=TL1*TL2**3/12.
      WRITE(6,101)TL1,TL2,BA,WEI,DWEI
  101 FORMAT(//T10,'PROPERTIES OF EDGE BEAM'//' DEPTH =',T25,F10.2   /'
     1BREADTH =',T25,F10.2/' AREA =',T25,F10.2/' WEIGHT/UNIT LENGTH =',T
     225,F10.2,'DENSITY =',F10.2)
      WRITE(6,102)BI1,BI3,BG2,BETG2
  102 FORMAT(' IXX =',T25,F10.2/' IYY =',T25,F10.2/' IZZ =',T25,F10.2,5X
     1,'BETA =',F10.2)
      WRITE(6,103)PRESF,BAE,BDR,VP,PE
  103 FORMAT(' PRESTRESS FORCE =',T25,F10.2/' ANC. ECC. =',T25,F10.4/' D
     1RAPE =',T25,F10.4/' EQ. VERT. CABLE LOAD =',T25,F10.3/' ANC. MT. =
     2',T25,F10.2)
      RETURN
      END
```

```
C
      SUBROUTINE SURFLD(VAR)
C
      COMMON/SHELL/R,G,T,PHIK,E,PR,NSECT,NP,SRN,NDNP,PI,NDO,EDGB
      COMMON/STRESS/AN(7,9,12),AU(6,9,12),AS(6,9,12)
      COMMON/SICOS/SIX(9),SIY(12), COX(9),COY(12)
      COMMON/CS/C(9),P(12),ANM(4),AUM(4)
      COMMON/UCN/CCN(7,12),CCU(4,12)
      COMMON/COEFS/AL,GAM
      COMMON/EDGEE/TL1,TL2,WEI,PRESF,PE,VP,BI1,BI3,BG2,BA
      COMMON/BEAM/BU(4,9),BN(4,9),BCU(4),BCN(4)
      COMMON/BEAM1/ACCN(4),ACCU(4),FPIS(4),UCPS(4),UPIB(4),UPIT(4),UCFS(
     14),FLEX(4,4)
      COMMON/NPO/NPO(8)
      DATA T1/'D.L.'/,T2/'L.L.'/,T3/'P.L.'/,T4/'SUML'/,T5/'NEWC'/,T6/'EN
     1D.'/,T7/'RADL'/,T8/'GENL'/
  100 FORMAT(I10,F10.2,I10)
      IF (VAR.EQ.T8) GOTO 1
      READ(5,100) KODE,FLOAD,NFX
    1 IF(VAR.EQ.T1) GO TO 7
      IF(VAR.EQ.T2) GO TO 8
      IF(VAR.EQ.T7) GO TO 9
      IF(VAR.EQ.T8) GO TO 13
C
C     GENERAL LOAD CASE
C
   13 READ(6,101) KODE,X,Y,Z,NFX
  101 FORMAT(I10,3F10.2,I10)
      WRITE(6,14) KODE,X,Y,Z,NFX
   14 FORMAT('0GENERAL LOAD CASE'/' KODE NO = ',I5/' X =',F10.5/' Y =',F
     110.5/' Z =',F10.5/' NFX =',I5)
      CALL PARTI(NFX,X,Y,Z,VAR)
      GO TO 11
C
C     DEAD LOAD ROUTINE
C
    7 WRITE(6,12) FLOAD,KODE,NFX
   12 FORMAT('0DEAD LOAD = ',F10.5/' KODE NO = ',I5/' NFX =',I5///)
      X=0.0
      Y=FLOAD
      Z=FLOAD
      CALL PARTI(NFX,X,Y,Z,VAR)
      GO TO 11
C
C     RADIAL LOAD ROUTINE
C
    9 WRITE(6,10)FLOAD,KODE,NFX
   10 FORMAT('0RADIAL LOAD = ',F10.5/' KODE NO = ',I5/' NFX =',I5///)
      X=0.0
      Y=0.0
      Z=FLOAD
      CALL PARTI(NFX,X,Y,Z,VAR)
      GO TO 11
C
C     LIVE LOAD ROUTINE
C
    8 WRITE(6,16) FLOAD,KODE
   16 FORMAT('0LIVE LOAD = ',F10.5,'KODE NO = ',I5)
C
C  TO WRITE RESULTS ON DISC
C
   11 CALL OUTPUT
C  11 WRITE(1)KODE
C     WRITE(1)(((AN(J,I,K),J=1,7),K=1,NP),I=1,NSECT)
C     WRITE(1)(((AU(J,I,K),J=1,4),K=1,NP),I=1,NSECT)
      RETURN
      END
C
      SUBROUTINE SYCFS
C
      COMMON/SHELL/R,G,T,PHIK,E,PR,NSECT,NP,SRN,NDNP,PI,NDO,EDGB
      COMMON/STRESS/AN(7,9,12),AU(6,9,12),AS(6,9,12)
      COMMON/SICOS/SIX(9),SIY(12), COX(9),COY(12)
      COMMON/CS/C(9),P(12),ANM(4),AUM(4)
      COMMON/UCN/CCN(7,12),CCU(4,12)
      COMMON/COEFS/AL,GAM
      COMMON/EDGEE/TL1,TL2,WEI,PRESF,PE,VP,BI1,BI3,BG2,BA
      COMMON/BEAM/BU(4,9),BN(4,9),BCU(4),BCN(4)
      COMMON/BEAM1/ACCN(4),ACCU(4),FPIS(4),UCPS(4),UPIB(4),UPIT(4),UCFS(
     14),FLEX(4,4)
      COMMON /ABCON/ AJ,AK,AJ1,AK1,ALM,V
      COMMON /SMAT/ A(4,4),B(4,4),AA(4,4),BS(4,4),KSH(4,4),FZ(4,2),FY(4,
     12),BS1(4,4),AC(4),ACC(4)
      COMMON/NPO/NPO(8)
      DIMENSION A1(4,4),A2(4,4),B1(4,4),B2(4,4), EN(4),EU(4)
      P1=R*PHIK
      DO 1 I=1,NP
      Y=P1+P(I)
      Z=P1-P(I)
      CALL COMFUN(Z,FZ)
      CALL COMFUN(Y,FY)
      CALL FMULT(A1,FY,A)
      CALL FMULT(A2,FZ,A)
      CALL FMULT(B1,FY,B)
      CALL FMULT(B2,FZ,B)
      CALL JSUB(A1,A1,A2)
      CALL JADD (B1,B1,B2)
      CALL RMULT (EN,A1,AC)
      CALL RMULT (EU,B1,AC)
      DO 2K=1,4
      CCN(K,I)=CCN(K,I)+EN(K)
      CCU(K,I)=CCU(K,I)+EU(K)
    2 CONTINUE
    1 CONTINUE
      RETURN
      END
```

```
C
      SUBROUTINE OUTPUT
C
C     PRINTS OUT MATRIX AN(7,9,5),AU(6,9,5),AS(6,9,5)
C
      COMMON/SHELL/R,G,T,PHIK,E,PR,NSECT,NP,SRN,NDNP,PI,NDO
      COMMON/STRESS/AN(7,9,12),AU(6,9,12),AS(6,9,12)
      COMMON/SICOS/SIX(91),SIY(12), COX(9),COY(12)
      COMMON/CS/C(9),P(12),ANM(4),AUM(4)
      COMMON/UCN/CCN(7,12),CCU(4,12)
      COMMON/COEFS/AL,GAM
      COMMON/EDGEE/TL1,TL2,WEI,PRESF,PE,VP,BI1,BI3,BG2,BA
      COMMON/BEAM/BU(4,9),BN(4,9),BCU(4),BCN(4)
      COMMON/BEAM1/ACCN(4),ACCU(4),FPIS(4),UCPS(4),UPIB(4),UPIT(4),UCFS(
     14),FLEX(4,4)
      COMMON/NPO/NPO(8)
      DIMENSION DD(6)
      WRITE(6,200) SRN
  200 FORMAT(' RESULTS FOR SHELL',F10.5,T110,'BEAM ACTIONS')
      WRITE(6,208)
  208 FORMAT(40HOX IS MEASURED FROM CENTRE-LINE OF SHELL)
      WRITE(6,202)
  202 FORMAT(48H NP IS MEASURED AS ARC DISTANCE FROM CENTRE-LINE//T5,3H
     1NP,T15,3HN12,T29,2HN2,T41,2HR2,T53,2HM2,T65,2HN1,T77,2HM1,T89,3HM1
     22,T98,1HP,T107,2HM1,T116,2HM3,T125,2HM2)
      DO 3 JK=1,NSECT
      WRITE(6,201)C(JK),(BN(I,JK),I=1,4)
  201 FORMAT(31HOSTRESSES FOR CROSS-SECTION X =,F15.5,T95,4(E9.2    ) )
      DO 3 L=1,NP
      WRITE(6,203)P(L),(AN(I,JK,L),I=1,7)
  203 FORMAT(F10.3,T10,10(F12.4))
    3 CONTINUE
      IF(NO.EQ.1) GO TO 10
      WRITE(6,204) SRN
  204 FORMAT(24H1DISPLACEMENTS FOR SHELL,F15.5)
      WRITE(6,207)
  207 FORMAT(T5,3H NP,T17,1HU,T29,1HV,T41,1HW,T53,6HTHETA2,T65,5HHORIZ,T
     177,4HVERT,T98,1HU,T107,1HV,T116,1HW,T125,5HTHETA)
      ZED=6./(T*T)
      DO 9K=1,NP
      DO 9 J=1,NSECT
      AU(5,J,K)  =  -AU(3,J,K)*SIY(K) +  AU(2,J,K)*COY(K)
      AU(6,J,K)=(AU(3,J,K)*COY(K)+AU(2,J,K)*SIY(K))
      AS(1,J,K)=AN(5,J,K)/T+AN(6,J,K)*ZED
      AS(2,J,K)=AN(5,J,K)/T-AN(6,J,K)*ZED
      AS(3,J,K)=AN(2,J,K)/T+AN(4,J,K)*ZED
      AS(4,J,K)=AN(2,J,K)/T-AN(4,J,K)*ZED
      AS(5,J,K)=AN(1,J,K)/T+AN(7,J,K)*ZED
    9 AS(6,J,K)=AN(1,J,K)/T-AN(7,J,K)*ZED
      DO 8 JK=1,NSECT
      DO 1 I=1,4
    1 DD(I)=BU(I,JK)/E
      WRITE(6,205)C(JK),(DD(I),   I=1,4)
  205 FORMAT(36HODISPLACEMENTS FOR CROSS-SECTION X =,F15.5,T95,4(E9.2
     1))
      DO 8 L=1,NP
      DO 4 I=1,6
    4 DD(I)=AU(I,JK,L)/E
      WRITE(6,206) P(L),(DD(I),I=1,6)
  206 FORMAT(F10.3,T12,6(2X,F10.4))
    8 CONTINUE
      IF(NO.EQ.2) GO TO 10
C        PRINT OUT SURFACE SRESSES
      WRITE(6,210)SRN
  210 FORMAT('OSURFACE STRESSES FOR SHELL',F10.1)
      WRITE(6,211)
  211 FORMAT(T20,'LONG STRESS',T39,'TRANS STRESS',T59,'SHEAR STRESS'/T5,
     1'NP',T15,3('INT',7X,'EXT',7X))
      DO12JK=1,NSECT
      WRITE(6,201)C(JK)
      DO 12 L=1,NP
   12 WRITE(6,212)P(L),(AS(I,JK,L),I=1,6)
  212 FORMAT(F10.3,T15,6(F8.2,2X))
   10 RETURN
      END
C
      SUBROUTINE FLEXIB(A,AL)
C
      COMMON/EDGEE/TL1,TL2,WEI,PRESF,PE,VP,BI1,BI3,BG2,BA
      AL2=AL*AL
      DIMENSION A(4,4)
      A1=TL1/2.
      B1=TL2/2.
      A(1,1)=1./BA+A1*A1/BI1+B1*B1/BI3
      A(1,2)=-B1/(BI3*AL)
      A(1,3)=-A1/(BI1*AL)
      A(1,4)=0.0
      A(2,1)=A(1,2)
      A(2,2)=1./(AL2*BI3)+A1*A1/BG2
      A(2,3)=-A1*B1/BG2
      A(2,4)=-A1/BG2
      A(3,1)=A(1,3)
      A(3,2)=A(2,3)
      A(3,3)=1./(AL2*BI1)+B1*B1/BG2
      A(3,4)= B1/BG2
      A(4,1)=0.0
      A(4,2)=A(2,4)
      A(4,3)=A(3,4)
      A(4,4)= 1./BG2
      DO 1 J=1,4
      DO 1 I=1,4
    1 A(I,J)=A(I,J)/AL2
      RETURN
      END
```

```
C
      SUBROUTINE ABMAT(A,B)
C
      COMMON/SHELL/R,G,T,PHIK,E,PR,NSECT,NP,SRN,NDNP,PI,NDO,EDGB
      COMMON/COEFS/AL,GAM
      COMMON /ABCON/ AJ,AK,AJ1,AK1,ALM,V
      DIMENSIONA(4,4),B(4,4)
      AM1=T*AL**3/(2.0*R*ALM**3)
      A(1,1)=-AM1*AK
      A(1,2)=-AM1*AJ
      A(1,3)=+AM1*AK1
      A(1,4)=AM1*AJ1
      AM1=AM1*AL/ALM
      A(2,1)=0.0
      A(2,2)=-AM1
      A(2,3)=0.0
      A(2,4)=AM1
      AM1=AM1/(2.0*R*ALM)
      VPR=V*(1.0-PR)
      A(3,1)=AM1*(AJ*(1.0-VPR)-AK)
      A(3,2)=+AM1*(-AK*(1.0-VPR)-AJ)
      A(3,3)=AM1*(-AJ1*(1.0+VPR)-AK1)
      A(3,4)=AM1*(AK1*(1.0+VPR)-AJ1)
      AM1=AM1/ALM
      A(4,1)=AM1*(-1.0-VPR)
      A(4,2)=AM1
      A(4,3)=AM1*(1.0-VPR)
      A(4,4)=AM1
C     MATRIX B
      VPR=V*(1.0+PR)
      AM1=AL/(2.0*R*ALM*ALM)
      B(1,1)=AM1
      B(1,2)=AM1*(1.0+VPR)
      B(1,3)=-AM1
      B(1,4)=AM1*(1.0-VPR)
      AM1=1.0/(2.0*R*ALM)
      B(2,1)=AM1*(-AK*(1.0-VPR)-AJ)
      B(2,2)=AM1*(-AJ*(1.0-VPR)+AK)
      B(2,3)=AM1*(-AK1*(1.0+VPR)+AJ1)
      B(2,4)=AM1*(-AJ1*(1.0+VPR)-AK1)
      B(3,1)=1.0
      B(3,2)=0.0
      B(3,3)=1.0
      B(3,4)=0.0
      AM1=ALM
      B(4,1)=ALM*AJ
      B(4,2)=-ALM*AK
      B(4,3)=ALM*AJ1
      B(4,4)=-ALM*AK1
      RETURN
      END
```

```
C
      SUBROUTINE INVER(A,B,KO)
C
C     TO INVERT MATRICES
C
      DIMENSIONA(4,4),B(4,4)
      N=4
      DO 3 I=1,N
      DO 3 J=1,N
      IF(I-J)1,2,1
    1 B(I,J)=0.
      GO TO 3
    2 B(I,J)=1.
    3 CONTINUE
      DO 12 I=1,N
      BIG= ABS(A(I,I))
      JJ=I
      IF(I-N)14,15,15
   14 MM=N-1
      DO6J=I,MM
      IF(BIG- ABS(A(J+1,I)))7,6,6
    7 BIG= ABS(A(J+1,I))
      JJ=J+1
    6 CONTINUE
   15 IF(BIG-1.E-07)8,8,9
    8 WRITE(6,36)
   36 FORMAT('0 ILL CONDITIONED MATRIX')
      KO=1
      RETURN
    9 IF(JJ-I)18,4,18
   18 DO 10 K=1,N
      C=A(I,K)
      D=B(I,K)
      A(I,K)=A(JJ,K)
      B(I,K)=B(JJ,K)
      A(JJ,K)=C
   10 B(JJ,K)=D
    4 P=1./A(I,I)
      DO 11 L=1,N
   11 B(I,L)=P*B(I,L)
      DO16L=I,N
   16 A(I,L)=P*A(I,L)
      DO 12 L=1,N
      IF(L-I)13,12,13
   13 P=A(L,I)
      DO17M=I,N
   17 A(L,M)=A(L,M)-P*A(I,M)
      DO24M=1,N
   24 B(L,M)=B(L,M)-P*B(I,M)
   12 CONTINUE
      KO=2
      RETURN
      END
```

```
C
      SUBROUTINE ARBSE
C
      COMMON/SHELL/R,G,T,PHIK,E,PR,NSECT,NP,SRN,NDNP,PI,NDO,EDGB
      COMMON/COEFS/AL,GAM
      COMMON/BEAM1/ACCN(4),ACCU(4),FPIS(4),UCPS(4),UPIB(4),UPIT(4),UCFS(
     14),FLEX(4,4)
      COMMON /SMAT/ A(4,4),B(4,4),AA(4,4),BS(4,4),KSH(4,4),FZ(4,2),FY(4,
     12),BS1(4,4),AC(4),ACC(4)
      COMMON /ABCON/ AJ,AK,AJ1,AK1,ALM,V
      DIMENSION S(4,4),TOTF(4,4),TOTK(4,4)
      CALL ROTMLT(S,AA,PHIK)
      CALL FLEXIB(FLEX,AL)
      CALL MMULT (TOTF,FLEX,S)
      CALL ROTMLT (S,BS,PHIK)
C     SUM TO OBTAIN TOTAL FLEXIBILITY MATRIX TOTF(I,J)
      DO 3I = 1,4
      DO 3 J =1,4
    3 TOTF(I,J)  =  TOTF(I,J) + S(I,J)
      CALL INVER (TOTF,TOTK,KO)
C     FIND ARBITARY CONSTANTS FOR SHELL AND EDGE BEAM
      CALL RMULT(ACC,TOTK,UPIT)
C     FIND TOTAL ARBITARY CONSTANTS FOR SHELL AND EDGE BEAM
      DO 14 I = 1,4
   14 AC(I) = AC(I) + ACC(I)
      END
```

```
C
      SUBROUTINE ROTATE (A,B,ANG,K)
C
C     IF K=1, TO ROTATE FROM SHELL TO JUNCTION COORDINATES
C     IF K=2, TO ROTATE FROM JUNCTION TO SHELL COORDINATES
C     A=SHELL COORDS., B= JUNCTION COORDS.
C
      DIMENSION A(4),B(4)
      C=COS(ANG)
      S=SIN(ANG)
      IF(K.EQ.2) GOTO 2
    1 B(1)=A(1)
      B(2)=A(2)*C-A(3)*S
      B(3)=A(2)*S+A(3)*C
      B(4)=A(4)
  150 FORMAT(1H ,8E10.3)
      RETURN
    2 A(1)=B(1)
      A(2)=B(2)*C+B(3)*S
      A(3)=-B(2)*S+B(3)*C
      A(4)=B(4)
      RETURN
      END
```

```
C
      SUBROUTINE COMFUN(Y,F)
C
C     COMPLEMENTARY FUNCTION PROGRAM TO CORRECT FOR SYMMETRICAL
C     STRESSES AT EDGE.
C     TO OBTAIN MATRIX F FOR Y=Y
C
      COMMON/COEFS/AL,GAM
      COMMON /ABCON/ AJ,AK,BJ,BK,BM
      DIMENSION F(4,2)
      P=BM*Y
      Q1=EXP(-AJ*P)
      Q2=EXP(-BJ*P)
      P1=COS(AK*P)
      P2=SIN(AK*P)
      P3=COS(BK*P)
      P4=SIN(BK*P)
      F(1,1)=Q1*P1
      F(1,2)=Q1*P2
      F(2,1)=-Q1*P2
      F(2,2)=Q1*P1
      F(3,1)=Q2*P3
      F(3,2)=Q2*P4
      F(4,1)=-Q2*P4
      F(4,2)=Q2*P3
      RETURN
      END
```

```
C
      SUBROUTINE FMULT(B,F,A)
C
C     B=A*F
C
      DIMENSION B(4,4),F(4,2),A(4,4)
      DO 1 I=1,4
      DO 1 J=1,2
      B(I,J)=A(I,1)*F(1,J)+A(I,2)*F(2,J)
    1 B(I,J+2)=A(I,3)*F(3,J)+A(I,4)*F(4,J)
      RETURN
      END
```

```
C
      SUBROUTINE RMULT(C,A,B)
C
C     C=B*A
C
      DIMENSION C(4),A(4,4),B(4)
      DO 1 I=1,4
      S=0.
      DO 2 J=1,4
    2 S=S+A(I,J)*B(J)
    1 C(I)=S
      RETURN
      END
```

```
C
      SUBROUTINE MMULT(C,A,B)
C
C     C=A*B
C
      DIMENSION A(4,4),B(4,4),C(4,4)
      DO 1 I=1,4
      DO 1 J=1,4
      S=0.
      DO 2 K=1,4
    2 S=S+A(I,K)*B(K,J)
    1 C(I,J)=S
      RETURN
      END
```

```
C
      SUBROUTINE JADD(C,A,B)
C
C     C=A+J*B
      DIMENSION C(4,4),B(4,4),A(4,4)
      DO 1 I=1,3,2
      DO 1 J=1,4
      C(I,J)=A(I,J)+B(I,J)
    1 C(I+1,J)=A(I+1,J)-B(I+1,J)
      RETURN
      END
```

```
C
      SUBROUTINE JSUB(C,A,B)
C
C     C=A-J*B
C
      DIMENSIONA(4,4),B(4,4),C(4,4)
      DO 1 I=1,3,2
      DO 1 J=1,4
      C(I,J)=A(I,J)-B(I,J)
    1 C(I+1,J)=A(I+1,J)+B(I+1,J)
      RETURN
      END
```

```
C     ************************************************************************
C
C     D.K.J. - MAINLINE PROGAM - NO EDGE BEAMS
C     TO FIND ACTIONS AND DISPLACEMENTS IN A CIRCULAR CYLINDRICAL
C     SHELL SUBJECT TO SURFACE LOADS, OR PRESTRESSING LOADS IN
C     SHELL SURFACE
C
C     ************************************************************************
C
      COMMON/SHELL/R,G,T,PHIK,E,PR,NSECT,NP,SRN,NDNP,PI,NDO
      COMMON/STRESS/AN(7,9,12),AU(6,9,12),AS(6,9,12)
      COMMON/SICOS/SIX(9),SIY(12), COX(9),COY(12)
      COMMON/CS/C(9),P(12),ANM(4),AUM(4)
      COMMON/UCN/CCN(7,12),CCU(4,12)
      COMMON/COEFS/AL,GAM
      COMMON/NPO/NPO(8)
      COMMON/XBY/XU1,BETA,YMAX ,PXU,WK
      COMMON/KO/KODE,A,FA,F,FR,NN,NB,NS,NC,NSH
      COMMON/FOURT/H(5,12,4)
      COMMON/GENY/Y(5)
      DATA T1/'D.L.'/,T2/'L.L.'/,T3/'P.L.'/,T4/'SUML'/,T5/'NEWC'/,T6/'EN
     1D.'/,T7/'RADL'/,T8/'GENL'/
      DIMENSION TITLE(20)
      CALL MASKO
      PI=3.1415927
    5 READ(5,110)(TITLE(I),I=1,20)
       WRITE(6,110)(TITLE(I),I=1,20)
      REWIND1
      REWIND3
      REWIND8
  110 FORMAT(20A4)
      READ(5,100) R,G,T,PHIK,E,PR,SRN
  100 FORMAT(8G10.0)
  101 FORMAT(4H1SRN,T6,1H=,F10.3,22H(SHELL REFERENCE NO. )/2H R,T6,1H=,
     5F10.3,
     1    8H(RADIUS)/2H G,T6,1H=,F10.3,17H(LENGTH OF SHELL)/2H T,T6,2H =
     2,F10.3,20H(THICKNESS OF SHELL)/5H PHIK,T6,1H=,F10.5,33H(HALF INCLU
     3DED ANGLE IN RADIANS)/2H E,T6,1H=,F10.0,16H(YOUNGS MODULUS)/4H  P
     4R,T6,1H=,F10.5,16H(POISSONS RATIO))
      WRITE(6,101)SRN,R,G,T,PHIK,E,PR
      READ(5,102) NSECT,NP,NDO
      IF(NDO.GT.3)NDO=3
      IF(NP.GT.12)NP=12
      IF(NSECT.GT.9)NSECT=9
       NDNP=NSECT*NP
  102 FORMAT(8I10)
      WRITE(6,103) NSECT,NP,NDO
  103 FORMAT(6H NSECT,T6,1H=,I10,23H(NO. OF CROSS-SECTIONS)/3H NP,T6,
     11H=,I10,32H(NO. OF POINTS ON CROSS-SECTION)/4H NDO,T6,I10,25H(TYPE
     1 OF OUTPUT REQUIRED))
      READ(5,100) (C(I),I=1,NSECT)
      C(1)=0.0
      C(NSECT)=G/2.0
      WRITE(6,105) (C(I),I=1,NSECT)
  105 FORMAT(58H POSITIONS OF CROSS-SECTIONS MEASURED FROM CENTRE OF SHE
     1LL/1H ,9F12.4)
      READ(5,100) (P(I),I=1,NP)
       P(1)=R*PHIK
      WRITE(6,104) (P(I),I=1,NP)
  104 FORMAT(91H POSITIONS OF POINTS ON CROSS-SECTIONS , MEASURED FROM C
     1ENTRE-LINE OF SHELL AS ARC DISTANCE/1H ,5F12.4)
    8 READ(5,110) VAR
   11 DO 300I=1,12
      DO300J=1,9
      DO303K=1,6
  302 AU(K,J,I)=0.0
  303 AS(K,J,I)=0.0
      DO300K=1,7
  300 AN(K,J,I)=0.0
      IF(VAR.EQ.T1.OR.VAR.EQ.T2) GO TO 2
      IF(VAR.EQ.T3) GO TO 9
      IF(VAR.EQ.T4) GO TO 18
      IF(VAR.EQ.T5) GO TO 5
      IF(VAR.EQ.T6) GO TO 25
      IF(VAR.EQ.T7) GO TO 2
      IF(VAR.EQ.T8) GO TO 2
      WRITE(6,10)
   10 FORMAT('MISTAKE IN LOADING FORMAT')
      STOP
    2 CALL SURFLD (VAR)
      GO TO 8
    9 CALL PRESLD
      GO TO 8
   18 CALL SUMLD
      GO TO 8
   25 WRITE(6,109)
  109 FORMAT(14H JOB COMPLETED)
      END



C
      SUBROUTINE PRESLD
C
      COMMON/SHELL/R,G,T,PHIK,E,PR,NSECT,NP,SRN,NDNP,PI,NDO
      COMMON/XBY/XU1,BETA,YMAX ,PXU,WK
      COMMON/GENY/Y(5)
      COMMON/FOURT/H(5,12,4)
      COMMON/KO/KODE,P,FA,F,FR,NN,NB,NS,NC,NSH
      READ(5,102) KODE,P,FA,F,FR,NN,NB,NS,NC,NSH,PXU,WK
  102 FORMAT(I5,4F10.2,5I5,2F5.5)
      WRITE(6,103) KODE,P,FA,F,NN
  103 FORMAT('0KODE = ',I5/8X,' PRESTRESS FORCE = ',F10.2/8X,' ANCHORAGE
     1 ECCENTRICITY = ',F10.5,5X,'DRAPE = ',F10.5/8X,'NO OF FOURIER TERM
     2S = ',I5///)
      WRITE(6,104) FR,NB,NS,NC,NSH,WK,PXU
  104 FORMAT(8X,' FR = ',F10.1,2X,' NB = ',I5,2X,' NS = ',I5/8X,' NC = '
     1,I5,2X,' NSH = ',I5/'  WOBBLE FACTOR (WK)  = ',F6.5,'COEFF. OF FRI
     2CTION (PXU)= ',F6.5////)
      REWIND 3
      REWIND 8
      CALL CHAP1
      CALL CHAP2
      CALL CHAP3
      CALL CHAP4
      RETURN
      END
```

```
C
      SUBROUTINE PARTI(NFX,X,Y,Z,VAR)
C
C     PARTICULAR INTEGRAL SUBPROGRAM
C     LOADING IS TAKEN IN FORM
C     X=XSIN(X)COS(Y),Y=YCOS(X)SIN(Y),Z=ZCOS(X)COS(Y)
C
      COMMON/SHELL/R,G,T,PHIK,E,PR,NSECT,NP,SRN,NDNP,PI,NDO,EDGB
      COMMON/STRESS/AN(7,9,12),AU(6,9,12),AS(6,9,12)
      COMMON/SICOS/SIX(9),SIY(12), COX(9),COY(12)
      COMMON/CS/C(9),P(12),ANM(4),AUM(4)
      COMMON/UCN/CCN(7,12),CCU(4,12)
      COMMON/COEFS/AL,GAM
      COMMON/NPO/NPO(8)
      DATA T1/'D.L.'/,T2/'L.L.'/,T3/'P.L.'/,T4/'SUML'/,T5/'NEWC'/,T6/'EN
     1D.'/,T7/'RADL'/,T8/'GENL'/
  150 FORMAT(8F10.0)
C     INITIALIZE REQUIRED CONSTANTS
      NPOO=1
      XSI=-1.0
      PI=3.1415927
      GAM=1.0/R
      BE4=3*(1-PR*PR)/(R*R*T*T)
      D=(T**3)/(12.0*(1-PR*PR))
      DO 4 IJ=1,NP
        GAMY=P(IJ)/R
      SIY(IJ)=SIN(GAMY)
    4 COY(IJ)=COS(GAMY)
C     DO LOOP FOR CARRYING OUT FOURIER DISTRIBUTION IN X DIRECTION
      DO 1 J=1,NFX
C     ESTABLISH COEFFICIENTS DEPENDENT ON PARTICULAR FOURIER
C     TERM BEING CONSIDERED
      AM=2*J-1
      AL=(AM*PI)/G
      V4=(AL**4/BE4)/4.0
      DO 2 IJ=1,NSECT
      ALX=AL*C(IJ)
      COX(IJ)=COS(ALX)
      IF(C(IJ).EQ.(G/2.0)) COX(IJ)=0.0
    2 SIX(IJ)=SIN(ALX)
      GA=GAM/AL
      GA2=GA**2
      FAC=(1.0+GA*GA)**2
      DEN=1.0+V4*FAC**2
      XSI=-XSI
      FOCEX=(4.0*XSI)/(PI*AM)
      X1=X*FOCEX
      Y1=Y*FOCEX
      Z1=Z*FOCEX
      HX=((R*(PR-GA2))/(AL*T*DEN))*X1
      HY=(R*GA*(GA2+2.0+PR)*Y1)/(AL*T*DEN)
      HZ=(R*R*FAC*Z1)/(T*DEN)
      FX=(V4*FAC*(GA2-PR)*X1)/(AL**3*DEN)
      FY=((V4*FAC*(1.0-PR*GA2)+1.0)*Y1)/(AL*AL*GAM*DEN)
      FZ=(R*Z1)/(AL*AL*DEN)
      H=HX+HY+HZ
      F=FX+FY+FZ
      ANM(1)=-AL*GAM*F
      ANM(2)=(-AL*AL*F+Y1/GAM)
      ANM(3)=(-D*AL**3)*(GA*GA2+GA*(2.0-PR))*H
      ANM(4)=(PR*GA2)*D*AL*AL*H
      AUM(1)=AL*(PR-GA2)*F/T+X1/(T*AL*AL)-PR*Y1/(T*AL*GAM)
      AUM(2)=AL*AL*(PR*G-1.0)*F/(T*GAM)-PR*X1/(T*AL*GAM)+Y1/(T*GAM*GAM)+
     1HY/(GAM*R)
      AUM(3)=H
      AUM(4)=GAM*H
      IF(VAR.EQ.T7) GO TO 3
      DO 7 K=1,NP
      CCN(1,K)=ANM(1)*SIY(K)
      CCN(2,K)=ANM(2)*COY(K)
      CCN(3,K)=ANM(3)*SIY(K)
      CCN(4,K)=ANM(4)*COY(K)
      CCU(1,K)=AUM(1)*COY(K)
      CCU(2,K)=AUM(2)*SIY(K)
      CCU(3,K)=AUM(3)*COY(K)
      CCU(4,K)=AUM(4)*SIY(K)
    7 CONTINUE
      CALL SYCF(AL,BE4)
      DO 8 K=1,NP
      CCN(5,K)=AL*T*CCU(1,K)+PR*CCN(2,K)
      CCN(6,K)=PR*CCN(4,K)+AL*AL*T**3*CCU(3,K)/(12.0*(1.0-PR*PR))
      CCN(7,K)=-AL*T**3*CCU(4,K)/(12.0*(1.0+PR))
    8 CONTINUE
C     DO LOOP TO CALCULATE VECTORS N,U AND LOADING AT EACH POINT FOR PAR
C     TICULAR FOURIER TERM BEING CONSIDERED.
C     RESULTS ARE ADDED ONTO RESULTS FROM PREVIOUS TERMS.
      DO 5 L=1,NSECT
      DO 5 K=1,NP
      CC=COX(L)*COY(K)
      CS=COX(L)*SIY(K)
      SS=SIX(L)*SIY(K)
      SC=SIX(L)*COY(K)
      AN(1,L,K)=AN(1,L,K)+CCN(1,K)*SIX(L)
      AN(2,L,K)=AN(2,L,K)+CCN(2,K)*COX(L)
      AN(3,L,K)=AN(3,L,K)+CCN(3,K)*COX(L)
      AN(4,L,K)=AN(4,L,K)+CCN(4,K)*COX(L)
      AN(5,L,K)=AN(5,L,K)+CCN(5,K)*COX(L)
      AN(6,L,K)=AN(6,L,K)+CCN(6,K)*COX(L)
      AN(7,L,K)=AN(7,L,K)+CCN(7,K)*SIX(L)
      AU(1,L,K)=AU(1,L,K)+CCU(1,K)*SIX(L)
      AU(2,L,K)=AU(2,L,K)+CCU(2,K)*COX(L)
      AU(3,L,K)=AU(3,L,K)+CCU(3,K)*COX(L)
      AU(4,L,K)=AU(4,L,K)+CCU(4,K)*COX(L)
    5 CONTINUE
    1 CONTINUE
      RETURN
    3 DO 6 K=1,NP
      CCN(1,K)=0.0
      CCN(2,K)=ANM(2)
      CCN(3,K)=0.0
      CCN(4,K)=ANM(4)
      CCU(1,K)=AUM(1)
      CCU(2,K)=0.0
      CCU(3,K)=AUM(3)
    6 CCU(4,K)=0.0
      GO TO 7
      END
```

```
C
      SUBROUTINE SURFLD(VAR)
C
      COMMON/SHELL/R,G,T,PHIK,E,PR,NSECT,NP,SRN,NDNP,PI,NDO
      COMMON/STRESS/AN(7,9,12),AU(6,9,12),AS(6,9,12)
      COMMON/SICOS/SIX(9),SIY(12), COX(9),COY(12)
      COMMON/CS/C(9),P(12),ANM(4),AUM(4)
      COMMON/UCN/CCN(7,12),CCU(4,12)
      COMMON/COEFS/AL,GAM
      COMMON/NPO/NPO(8)
      DATA T1/'D.L.'/,T2/'L.L.'/,T3/'P.L.'/,T4/'SUML'/,T5/'NEWC'/,T6/'EN
     1D.'/,T7/'RADL'/,T8/'GENL'/
        IF (VAR.EQ.T8) GO TO 1
  100 FORMAT(I10,F10.2,I10)
      READ(5,100) KODE,FLOAD,NFX
    1 IF(VAR.EQ.T1) GO TO 7
      IF(VAR.EQ.T2) GO TO 8
      IF(VAR.EQ.T7) GO TO 9
      IF(VAR.EQ.T8) GO TO 13
C
C     GENERAL LOAD CASE
C
   13 READ(6,101) KODE,X,Y,Z,NFX
  101 FORMAT(I10,3F10.2,I10)
      WRITE(6,14) KODE,X,Y,Z,NFX
   14 FORMAT('0GENERAL LOAD CASE'/' KODE NO = ',I5/' X =',F10.5/' Y =',F
     110.5/' Z =',F10.5/' NFX =',I5)
      CALL PARTI(NFX,X,Y,Z,VAR)
      GO TO 11
C
C     DEAD LOAD ROUTINE
C
    7 WRITE(6,12) FLOAD,KODE,NFX
   12 FORMAT('0DEAD LOAD = ',F10.5/' KODE NO = ',I5/' NFX =',I5///)
      X=0.0
      Y=FLOAD
      Z=FLOAD
      CALL PARTI(NFX,X,Y,Z,VAR)
      GO TO 11
C
C     RADIAL LOAD ROUTINE
C
    9 WRITE(6,10)FLOAD,KODE,NFX
   10 FORMAT('0RADIAL LOAD = ',F10.5/' KODE NO = ',I5/' NFX =',I5///)
      X=0.0
      Y=0.0
      Z=FLOAD
      CALL PARTI(NFX,X,Y,Z,VAR)
      GO TO 11
C
C     LIVE LOAD ROUTINE
C
    8 WRITE(6,16) FLOAD,KODE
   16 FORMAT('0LIVE LOAD = ',F10.5,'KODE NO = ',I5)
C
C  TO WRITE RESULTS ON DISC
C
   11 WRITE(1)KODE
      WRITE(1)(((AN(J,I,K),J=1,7),K=1,NP),I=1,NSECT)
      WRITE(1)(((AU(J,I,K),J=1,4),K=1,NP),I=1,NSECT)
      RETURN
      END
```

```
C
      SUBROUTINE SYCF(AL,BE4)
C
      COMMON/SHELL/R,G,T,PHIK,E,PR,NSECT,NP,SRN,NDNP,PI,NDO,EDGB
      COMMON/STRESS/AN(7,9,12),AU(6,9,12),AS(6,9,12)
      COMMON/SICOS/SIX(9),SIY(12), COX(9),COY(12)
      COMMON/CS/C(9),P(12),ANM(4),AUM(4)
      COMMON/UCN/CCN(7,12),CCU(4,12)
      COMMON/NPO/NPO(8)
      DIMENSION AB(4,4),S(4,4)
      DIMENSION W(4,4),AC(4),A(4,4),B(4,4),FY(4,2),FZ(4,2)
      DIMENSION A1(4,4),A2(4,4),B1(4,4),B2(4,4), EN(4),EU(4)
      DIMENSION WI(4,4) ,EF(4)
C     ESTABLISH CONSTANTS NOT DEPENDENT ON Y AND Z
  101 FORMAT(6E12.4)
      BT=BE4**.25
      ALM=SQRT(AL*BT)
      V=AL/BT
      AJ1=SQRT((SQRT(1.0+(1.0-V)**2)-1.0+V)/2.0)
      AJ=SQRT((SQRT(1.0+(1.0+V)**2)+1.0+V)/2.0)
      AK=1.0/(2.0*AJ)
      AK1=1.0/(2.0*AJ1)
      KO=0.0
      P1=R*PHIK
C     ESTABLISH MATRICES A AND B
      CALL ABMAT      (T,AL,ALM,AK,AJ,AK1,AJ1,V,PR,R,A,B)
C     FIND ARBITARY CONSTANTS FOR SHELL FOR EACH CROSS-SECTION AND
C     COMPLEMENTARY STRESSES
      Z= 2.0*R*PHIK
      CALL COMFUN(Z,FZ,AJ,AK,AJ1,AK1,ALM)
      CALL FMULT(S,FZ,A)
      CALL JSUB(W,A,S)
      CALL INVER(W,WI,KO)
      EF(1)=CCN(1,1)
      EF(2)=-CCN(2,1)
      EF(3)=CCN(3,1)
      EF(4)=-CCN(4,1)
      CALL RMULT(AC,WI,EF)
      DO 1 I=1,NP
      Y=P1+P(I)
      Z=P1-P(I)
      CALL COMFUN(Z,FZ,AJ,AK,AJ1,AK1,ALM)
      CALL COMFUN(Y,FY,AJ,AK,AJ1,AK1,ALM)
      CALL FMULT(A1,FY,A)
      CALL FMULT(A2,FZ,A)
      CALL FMULT(B1,FY,B)
      CALL FMULT(B2,FZ,B)
      CALL JSUB(A1,A1,A2)
      CALL JADD (B1,B1,B2)
      CALL RMULT (EN,A1,AC)
      CALL RMULT (EU,B1,AC)
      DO 2K=1,4
      CCN(K,I)=CCN(K,I)+EN(K)
      CCU(K,I)=CCU(K,I)+EU(K)
    2 CONTINUE
    1 CONTINUE
      RETURN
      END
```

```
C
      SUBROUTINE CHAP1
C
      COMMON/X8Y/XU1,BETA,YMAX ,PXU,WK
      COMMON/FOURT/H
      COMMON/GENY/Y
      COMMON/KO/KODE,P,FA,F,FR,NN,NB,NS,NC,NSH
      COMMON/SHELL/R,XL,T,PHIK,E,XU,ND,NY,SRN,NONP,PI
      DIMENSION Q(5,20,4),H(5,12,4),Y(5),X(20,5)
      IF(NC.EQ.4)NS=2
      IF(NC.EQ.1)NS=1
      IF(NS.GT.5)NS=5
C
C     INITIALIZE
      XU1=1.-XU**2
      BETA=(3.*XU1/(R*T)**2)**.25
      YMAX=R*PHIK
      DO 5 I=1,5
      DO 5 K=1,20
      DO 5 J=1,4
      IF(K.GT.12)GOTO5
      H(I,K,J)=0.
    5 Q(I,K,J)=0.
      Y(1)=FA
      SNB=2*NB
      GOTO(1,2,2,11,2),NC
C     CURVATURE  AND  WOBBLE  LOADS
    2 IF(NC.EQ.5)NS=NS-1
      IF(NS.EQ.1)  DY=0.0
      IF(NS.EQ.1) GO TO 10
      SNS=NS-1
      DY=F/SNS
      DO3I=2,NS
    3 Y(I)=Y(I-1)+DY
   10 DX=XL/SNB
      X(1,1)=DX/2.
      DO 4 I=2,NB
    4 X(I,1)=X(I-1,1)+DX
      CALL LINE(F,XL,X,PA,P,R,NB,FR,PXU,WK)
      CALL EDGE(X,Q,DY,NB,NS,Y)
      CALL FOUR(PI,SNB,NB,NS,Q,H,X,XL,NN)
      GO TO (1,7,34,11,7),NC
C     ANCHORAGE LOADS
   11 Y(1)=FA-R/100.
      Y(2)=FA+R/100.
      NS=2.
      PA=P/2.
      GO TO 7
    1 PA=P
    7 SNB=2*NSH
      PIT=PI/(2.*SNB)
      PA=8.*SNB/(PI*XL)*PA
      DO 8 N=1,NN
      XN=2*N-1
    8 H(1,N,1)=PA/XN*SIN(XN*PIT)*SIN(XN*PI/2.)+H(1,N,1)
      WRITE(6,203) (H(1,N,1),N=1,NN)
  203 FORMAT (10E10.4)
C
C     OUTPUT
   34 DO 9 K=1,4
      DO 9 I=1,NS
      DO 9 J=1,NN
    9 H(I,J,K)=-H(I,J,K)
      GO TO (12,12,12,13,77),NC
   77 DO78J=1,NN
      DO78K=1,4
      DO79I=1,NS
   79 H(NS+2-I,J,K)=H(NS+1-I,J,K)
      H(2,J,K)=0.5*H(2,J,K)
   78 H(1,J,K)=H(2,J,K)
      DO 80I=1,NS
   80 Y(NS+2-I)=Y(NS+1-I)
      Y(1)=FA-R/100.
      Y(2)=FA+R/100.
      NS=NS+1
      GO TO 12
   13 DO 14 K=1,4
      DO 14 J=1,NN
   14 H(2,J,K)=H(1,J,K)
   12 FOOL =0.
      RETURN
      END
```

```
C
      SUBROUTINE FOUR (PI,SNB,NB,NS,Q,H,X,XL,NN)
C
C     TO OBTAIN FOURIER COEFFICIENTS FOR DISTRIBUTED LOADS
C
      DIMENSION X(20,5),H(5,12,4),Q(5,20,4)
      TQ=8./PI
      TS=PI/(2.*SNB)
      DO 3 N=1,NN
      XN=N*2-1
      SI=TQ/XN*SIN(XN*TS)
      AN=XN*PI/XL
      DO 3 M=1,NB
      C=X(M,1)*AN
      CU=COS(C)
      SU=SIN(C)
      DO3I=1,NS
      DO 3 L=1,3
      G=Q(I,M,L)
      IF(G)4,3,4
    4 GO TO (5,6,6),L
    5 CB=SU
      GO TO 7
    6 CB=CU
    7 H(I,N,L)=H(I,N,L)+CB*SI*G
    3 CONTINUE
      RETURN
      END
```

```
C
      SUBROUTINE CHAP2
C
      COMMON/FOURT/H(5,12,4)
      COMMON/GENY/V
      COMMON/XBY/XU1,BETA,YMAX
      COMMON/KO/KODE,P,FA,FB,FR,NN,NB,NS,NC,NSH
      COMMON/SHELL/R,XL,T,PHIK,E,XU,ND,NY,SRN,NDNP,PI
      DIMENSIONA(4,4),B(4,4),QF(4),F(4,2),EN(4),C1(4,4),C2(4,4),A1(4,4),
     1B1(4,4),B2(4,4),A2(4,4),E1(4,4),E2(4,4),AK1(4,4),AK2(4,4),V(5),AB1
     2(4),AB2(4),ABT(4),EB(4),G(4),VA(4),EU(4)
      REWIND 8
      D=T**3/(12.*XU1)
      Y2=2.*PI*R
      DO2I=1,4
    2 QF(I)=0.
C     COMPLIMENTARY FUNCTION SOLUTION
      DO1N=1,NN
      XN=2*N-1
      DO 14I=1,4
   14 EN(I)=0.
      AN=XN*PI/XL
      AN3=AN**3
      BM=SQRT(AN*BETA)
      CM=AN/BETA
      AJ=SQRT((SQRT(1.+(1.+CM)**2)+1.+CM)/2.)
      AK=.5/AJ
      BJ=SQRT((SQRT(1.+(1.-CM)**2)-1.+CM)/2.)
      BK=.5/BJ
      CALL ABMAT(T,AN,BM,AK,AJ,BK,BJ,CM,XU,R,A,B)
      WRITE(8) N,AJ,AK,BJ,BK,BM,AN
  101 FORMAT(8E10.3)
      WRITE(8) A,B
C     ARBITARY CONSTANTS FROM LOADED GENERATORS
      DO 15 I=1,NS
      DO22K=1,4
   22 QF(K)=H(I,N,K)
      Y=Y2-2.*V(I)
      CALL COMFUN(Y,F,AJ,AK,BJ,BK,BM)
      CALL FMULT(C1,F,B)
      CALL JADD(B1,B,C1)
      CALL FMULT(C2,F,A)
      CALL JSUB(A1,A,C2)
      CALL INVER(B1,E2,KO)
  100 FORMAT(8I10)
      GO TO (5,4),KO
    4 CALL MMULT(AK2,A1,E2)
      Y=2.*V(I)
      CALL COMFUN(Y,F,AJ,AK,BJ,BK,BM)
      CALL FMULT(C1,F,B)
      CALL JADD(B1,C1,B)
      CALL FMULT(C2,F,A)
      CALL JSUB(A1,C2,A)
      CALL INVER(B1,E1,KO)
      GO TO (5,6),KO
    6 CALL MMULT(AK1,A1,E1)
      DO 8 L=1,4
      DO 8 J=1,4
    8 AK1(L,J)=AK1(L,J)-AK2(L,J)
      CALL INVER(AK1,AK2,KO)
      GO TO (5,7),KO
    7 CALL RMULT(VA,AK2,QF)
C     CAL COM FUN
      CALL RMULT(AB1,E1,VA)
      CALL RMULT(AB2,E2,VA)
      Y=YMAX-V(I)
      Z=Y2-2.*V(I)-Y
      CALL COMFUN(Y,F,AJ,AK,BJ,BK,BM)
      CALL FMULT(C2,F,A)
      CALL COMFUN(Z,F,AJ,AK,BJ,BK,BM)
      CALL FMULT(C1,F,A)
      CALL JSUB(A1,C2,C1)
      CALL RMULT(EU,A1,AB2)
      DO 9 L=1,4
    9 EN(L)=EN(L)-EU(L)
   15 WRITE(8) AB1,AB2
C     ARBITARY CONSTANTS FOR EDGE OF SHELL
      ZXV=2.*YMAX
      CALL COMFUN(ZXV,F,AJ,AK,BJ,BK,BM)
      CALL FMULT(C2,F,A)
      CALL JSUB(A1,C2,A)
      CALL INVER(A1,A2,KO)
      GO TO (5,54),KO
   54 CALL RMULT(ABT,A2,EN)
      WRITE(8) ABT
   10 WRITE(6,106)N,EN
  106 FORMAT('0',I5,4(G15.8,5X))
    1 CONTINUE
   16 RETURN
    5 CALL EXIT
      END
C
      SUBROUTINE COMFUN(Y,F,AJ,AK,BJ,BK,BM)
C
C     COMPLEMENTARY FUNCTION PROGRAM TO CORRECT FOR SYMMETRICAL
C     STRESSES AT EDGE.
C     TO OBTAIN MATRIX F FOR Y=Y
C
      DIMENSION F(4,2)
      P=BM*Y
      Q1=EXP(-AJ*P)
      Q2=EXP(-BJ*P)
      P1=COS(AK*P)
      P2=SIN(AK*P)
      P3=COS(BK*P)
      P4=SIN(BK*P)
      F(1,1)=Q1*P1
      F(1,2)=Q1*P2
      F(2,1)=-Q1*P2
      F(2,2)=Q1*P1
      F(3,1)=Q2*P3
      F(3,2)=Q2*P4
      F(4,1)=-Q2*P4
      F(4,2)=Q2*P3
      RETURN
      END
```

```
C
      SUBROUTINE CHAP3
C
      COMMON/GENY/VA
      COMMON/CS/C(9),V
      COMMON/KO/KODE,P,FA,F,FR,NN,NB,NS,NC,NSH
      COMMON/SHELL/R,XL,T,PHIK,E,XU,ND,NY,SRN,NDNP,PI
      DIMENSIONV(12),VA(5),EU(4),EN(4),FY(4,2),FZ(4,2),A(4,4),B(4,4),AB1
     1(4),AB2(4),ABT(4),A1(4,4),A2(4,4),B1(4,4),B2(4,4),H(35,8)
      REWIND 3
      REWIND 8
C     READ AND PUNCH DIMENSIONS AND CONTROL
      NX=2*NN-1
      Y2=2.*PI*R
      YMAX=R*PHIK
C     OBTAIN VECTORS N AND U
   15 READ(8) N,AJ,AK,BJ,BK,BM,AN
      READ(8) A,B
      DO 2 I=1,NY
      DO 2 J=1,8
    2 H(I,J)=0.
      KA=2
      DO 6 K=1,NS
      READ(8) AB1,AB2
      Y1=VA(K)
      DO 6 I=1,NY
      IF(Y1-V(I))4,5,5
    5 KU=2
      Y=Y1+V(I)
      Z=Y1-V(I)
      GO TO 7
    4 KU=3
      Y=V(I)-Y1
      Z=Y2-2.*Y1-Y
      GO TO 7
    6 CONTINUE
      KU=1
      KA=1
      READ(8) ABT
      DO 13I=1,NY
      Y=V(I)+YMAX
      Z=YMAX-V(I)
      GO TO 7
   13 CONTINUE
      WRITE(3) N
      DO77I=1,NY
   77 WRITE(3)    (H(I,J),J=1,8)
      IF(NN-N)14,14,15
    7 CALL COMFUN(Y,FY,AJ,AK,BJ,BK,BM)
      CALL COMFUN(Z,FZ,AJ,AK,BJ,BK,BM)
      CALL FMULT(A1,FY,A)
      CALL FMULT(A2,FZ,A)
      CALL FMULT(B1,FY,B)
      CALL FMULT(B2,FZ,B)
      CALL JSUB(A1,A1,A2)
      CALL JADD(B1,B1,B2)
      GO TO (8,9,10),KU
    9 CALL RMULT(EN,A1,AB1)
      CALL RMULT(EU,B1,AB1)
      GO TO 11
   10 CALL RMULT(EN,A1,AB2)
      CALL RMULT(EU,B1,AB2)
      GO TO 11
    8 CALL RMULT(EN,A1,ABT)
      CALL RMULT(EU,B1,ABT)
   11 DO 12 J=1,4
      H(I,J)=EN(J)+H(I,J)
   12 H(I,J+4)=EU(J)+H(I,J+4)
      GO TO (13,6,6),KA
   14 RETURN
      END

C
      SUBROUTINE ABMAT(T,AL,ALM,AK,AJ,AK1,AJ1,V,PR,R,A,B)
C
      DIMENSIONA(4,4),B(4,4)
      AM1=T*AL**3/(2.0*R*ALM**3)
      A(1,1)=-AM1*AK
      A(1,2)=-AM1*AJ
      A(1,3)=+AM1*AK1
      A(1,4)=AM1*AJ1
      AM1=AM1*AL/ALM
      A(2,1)=0.0
      A(2,2)=-AM1
      A(2,3)=0.0
      A(2,4)=AM1
      AM1=AM1/(2.0*R*ALM)
      VPR=V*(1.0-PR)
      A(3,1)=AM1*(AJ*(1.0-VPR)-AK)
      A(3,2)=+AM1*(-AK*(1.0-VPR)-AJ)
      A(3,3)=AM1*(-AJ1*(1.0+VPR)-AK1)
      A(3,4)=AM1*(AK1*(1.0+VPR)-AJ1)
      AM1=AM1/ALM
      A(4,1)=AM1*(-1.0-VPR)
      A(4,2)=AM1
      A(4,3)=AM1*(1.0-VPR)
      A(4,4)=AM1
C     MATRIX B
      VPR=V*(1.0+PR)
      AM1=AL/(2.0*R*ALM*ALM)
      B(1,1)=AM1
      B(1,2)=AM1*(1.0+VPR)
      B(1,3)=-AM1
      B(1,4)=AM1*(1.0-VPR)
      AM1=1.0/(2.0*R*ALM)
      B(2,1)=AM1*(-AK*(1.0-VPR)-AJ)
      B(2,2)=AM1*(-AJ*(1.0-VPR)+AK)
      B(2,3)=AM1*(-AK1*(1.0+VPR)+AJ1)
      B(2,4)=AM1*(-AJ1*(1.0+VPR)-AK1)
      B(3,1)=1.0
      B(3,2)=0.0
      B(3,3)=1.0
      B(3,4)=0.0
      AM1=ALM
      B(4,1)=ALM*AJ
      B(4,2)=-ALM*AK
      B(4,3)=ALM*AJ1
      B(4,4)=-ALM*AK1
      RETURN
      END
```

```
C
      SUBROUTINE OUTPUT
C
C     PRINTS OUT MATRIX AN(7,9,5),AU(6,9,5),AS(6,9,5)
C
      COMMON/SHELL/R,G,T,PHIK,E,PR,NSECT,NP,SRN,NDNP,PI,NO
      COMMON/STRESS/AN(7,9,12),AU(6,9,12),AS(6,9,12)
      COMMON/SICOS/SIX(9),SIY(12), COX(9),COY(12)
      COMMON/CS/C(9),P(12),ANM(4),AUM(4)
      COMMON/UCN/CCN(7,12),CCU(4,12)
      COMMON/COEFS/AL,GAM
      COMMON/NPO/NPO(8)
      DIMENSION DD(6)
      WRITE(6,200) SRN
  200 FORMAT(' RESULTS FOR SHELL',F10.5)
      WRITE(6,208)
  208 FORMAT(40HOX IS MEASURED FROM CENTRE-LINE OF SHELL)
      WRITE(6,202)
  202 FORMAT(48H NP IS MEASURED AS ARC DISTANCE FROM CENTRE-LINE//T5,3H
     1NP,T15,3HN12,T29,2HN2,T41,2HR2,T53,2HM2,T65,2HN1,T77,2HM1,T89,3HM1
     22)
      DO 3 JK=1,NSECT
      WRITE(6,201) C(JK)
  201 FORMAT(31HOSTRESSES FOR CROSS-SECTION X =,F15.5)
      DO 3 L=1,NP
      WRITE(6,203)P(L),(AN(I,JK,L),I=1,7)
  203 FORMAT(F10.3,T10,10(F12.4))
    3 CONTINUE
      IF(NO.EQ.1) GO TO 10
      WRITE(6,204) SRN
  204 FORMAT(24H1DISPLACEMENTS FOR SHELL,F15.5)
      WRITE(6,207)
  207 FORMAT(T5,3H NP,T17,1HU,T29,1HV,T41,1HW,T53,6HTHETA2,T65,5HHORIZ,T
     177,4HVERT)
      DO 8 JK=1,NSECT
      WRITE(6,205) C(JK)
  205 FORMAT(36HODISPLACEMENTS FOR CROSS-SECTION X =,F15.5)
      DO 8 L=1,NP
      DO 4 I=1,6
    4 DD(I)=AU(I,JK,L)/E
      WRITE(6,206) P(L),(DD(I),I=1,6)
  206 FORMAT(F10.3,T12,6(2X,F10.4))
    8 CONTINUE
      IF(NO.EQ.2) GO TO 10
C
C        PRINT OUT SURFACE SRESSES
C
      WRITE(6,210)SRN
  210 FORMAT('OSURFACE STRESSES FOR SHELL',F10.1)
      WRITE(6,211)
  211 FORMAT(T20,'LONG STRESS',T39,'TRANS STRESS',T59,'SHEAR STRESS'/T5,
     1'NP',T15,3('INT',7X,'EXT',7X))
      DO12JK=1,NSECT
      WRITE(6,201)C(JK)
      DO 12 L=1,NP
   12 WRITE(6,212)P(L),(AS(I,JK,L),I=1,6)
  212 FORMAT(F10.3,T15,6(F8.2,2X))
   10 RETURN
      END
```

```
C
      SUBROUTINE CHAP4
C
      COMMON/SHELL/R,XL,T,PHIK,E,XU,NO,NY,SRN,NDNP,PI,NDO
      COMMON/KO/KODE,P,FA,FB,FR,NN,NB,NS,NC,NSH
      COMMON/GENY/VA
      COMMON/CS/X,V
      DIMENSIONX(9),CH(12),SH(12),EN(4),EU(4),Q(108,7),
     1V(12),C(10),S(10),HC(7),VA(5),HD(7),QA(108,7)
      REWIND 3
      REWIND 8
  100 FORMAT(4E14.8)
      KU=ND*NY
      CA=T**3/(12.*(1.-XU**2))
      KUP=0
      DO3I=1,KU
      DO3J=1,7
      QA(I,J)=0.
    3  Q(I,J)=0.
      DO1I=1,NY
      CH(I)=COS(V(I)/R)
    1 SH(I)=SIN(V(I)/R)
   16 READ(3) N
      XN=2*N-1
      AN=XN*PI/XL
      DO2I=1,ND
      C(I)=COS(AN*X(I))
    2 S(I)=SIN(AN*X(I))
      CAT=CA*AN**2*(1.-XU**2)
      CAS=CA*(1.-XU)*AN
      DO4I=1,NY
      READ(3) EN,EU
      HC(2)=EN(2)
      HC(4)=EN(4)
      HC(7)=EN(3)
      HC(1)=XU*HC(2)+AN*T*EU(1)
      HC(3)=XU*HC(4)+CAT*EU(3)
      HC(5)=EN(1)
      HC(6)=-CAS*EU(4)
      HD(1)=EU(1)
      HD(2)=EU(2)
      HD(3)=EU(3)
      HD(4)=EU(4)
      DO4K=1,ND
      L=K*NY+I-NY
      Q(L,1)=Q(L,1)+HC(1)*C(K)
      QA(L,1)=QA(L,1)+HD(1)*S(K)
      DO9J=2,4
      Q(L,J)=Q(L,J)+HC(J)*C(K)
    9 QA(L,J)=QA(L,J)+HD(J)*C(K)
      DO8J=5,6
    8 Q(L,J)=Q(L,J)+HC(J)*S(K)
    4 Q(L,7)=Q(L,7)+HC(7)*C(K)
      IF(NN-N)115,115,16
  115 WRITE(1)KODE
      WRITE(1)((Q(L,5),Q(L,2),Q(L,7),Q(L,4),Q(L,1),Q(L,3),Q(L,6)),L=1,ND
     1NP)
      WRITE(1)((QA(L,J),J=1,4),L=1,NDNP)
 5002 FORMAT('0',2X,I3,7(3X,G15.7))
   27 RETURN
      END
```

```
C
      SUBROUTINE SUMLD
C
C      TO ADD COMBINATIONS OF LOADING FROM DISC READY FOR OUTPUT
C
      COMMON/SHELL/R,G,T,PHIK,E,PR,NSECT,NP,SRN,NDNP,PI,NDO
      COMMON/STRESS/AN(7,9,12),AU(6,9,12),AS(6,9,12)
      COMMON/SICOS/SIX(9),SIY(12), COX(9),COY(12)/LOAD/XYZ(3,9,12)
      COMMON/CS/C(9),P(12),ANM(4),AUM(4)
      COMMON/UCN/CCN(7,12),CCU(4,12)
      COMMON/COEFS/AL,GAM
      COMMON/NPO/NPO(8)
      DIMENSION DAN(7,9,12),DAU(6,9,12),DAS(6,9,12)
      ZED=6./(T*T)
   11 DO 300I=1,12
      DO300J=1,9
      DO303K=1,6
  302 AU(K,J,I)=0.0
  303 AS(K,J,I)=0.0
      DO300K=1,7
  300 AN(K,J,I)=0.0
C     KODE NOS. OF RESULTS TO BE ADDED
      READ(5,100)(NPO(I),I=1,8)
  100 FORMAT(8I10)
      WRITE(6,101)(NPO(I),I=1,8)
  101 FORMAT('  ******************'//' ********************************
     1'//' KODE NOS OF RESULTS THAT HAVE BEEN ADDED'//8I10///' *********
     2$$$$$$$$$$$$$$$$$$$$$$$$$$$$$$$$$$$$'//)
      DO1L=1,8
      REWIND 1
      IF (NPO(L).EQ.0) GO TO 2
    4 READ (1) KODE
      IF(KODE.EQ.NPO(L)) GO TO 3
       IF(KODE.EQ.0) GO TO 5
      READ (1) (((DAN(J,I,K),J=1,7),K=1,NP),I=1,NSECT)
      READ (1) (((DAU(J,I,K),J=1,4),K=1,NP),I=1,NSECT)
      GO TO 4
    5 WRITE(6,102) KODE
  102 FORMAT(' RESULTS FOR KODE =',I10,'  CANNOT BE FOUND')
    1 CONTINUE
    2 CONTINUE
C      CALCULATE SURFACE STRESSES AND HOR AND VERT DEFLECTIONS
      DO 8 I=1,NP
      SIY(I)=SIN(P(I)/R)
    8 COY(I)=COS(P(I)/R)
      DO 9K=1,NP
      DO 9 J=1,NSECT
      AU(5,J,K)  = -(AU(3,J,K)*SIY(K) + AU(2,J,K)*COY(K))
      AU(6,J,K)=(AU(3,J,K)*COY(K)+AU(2,J,K)*SIY(K))
      AS(1,J,K)=AN(5,J,K)/T+AN(6,J,K)*ZED
      AS(2,J,K)=AN(5,J,K)/T-AN(6,J,K)*ZED
      AS(3,J,K)=AN(2,J,K)/T+AN(4,J,K)*ZED
      AS(4,J,K)=AN(2,J,K)/T-AN(4,J,K)*ZED
      AS(5,J,K)=AN(1,J,K)/T+AN(7,J,K)*ZED
    9 AS(6,J,K)=AN(1,J,K)/T-AN(7,J,K)*ZED
      CALL OUTPUT
      RETURN
    3 READ (1) (((DAN(J,I,K),J=1,7),K=1,NP),I=1,NSECT)
      READ (1) (((DAU(J,I,K),J=1,4),K=1,NP),I=1,NSECT)
C       ADD TO EXISTING RESULTS
      DO 6K=1,NP
      DO 6J=1,NSECT
      DO 7I=1,7
    7 AN(I,J,K) = AN(I,J,K)+ DAN(I,J,K)
      DO 6I=1,4
    6 AU(I,J,K) = AU(I,J,K)+ DAU(I,J,K)
      GO TO 1
      END
C
      SUBROUTINE INVER(A,B,KO)
C
      DIMENSIONA(4,4),B(4,4)
      N=4
      DO 3 I=1,N
      DO 3 J=1,N
      IF(I-J)1,2,1
    1 B(I,J)=0.
      GO TO 3
    2 B(I,J)=1.
    3 CONTINUE
      DO 12 I=1,N
      BIG= ABS(A(I,I))
      JJ=I
      IF(I-N)14,15,15
   14 MM=N-1
      DO6J=I,MM
      IF(BIG- ABS(A(J+1,I)))7,6,6
    7 BIG= ABS(A(J+1,I))
      JJ=J+1
    6 CONTINUE
   15 IF(BIG-1.E-07)8,8,9
    8 WRITE(6,36)
   36 FORMAT('0 1LL CONDITIONED MATRIX')
      KO=1
      RETURN
    9 IF(JJ-I)18,4,18
   18 DO 10 K=1,N
      C=A(I,K)
      D=B(I,K)
      A(I,K)=A(JJ,K)
      B(I,K)=B(JJ,K)
      A(JJ,K)=C
   10 B(JJ,K)=D
    4 P=1./A(I,I)
      DO 11 L=1,N
   11 B(I,L)=P*B(I,L)
      DO16L=I,N
   16 A(I,L)=P*A(I,L)
      DO 12 L=1,N
      IF(L-I)13,12,13
   13 P=A(L,I)
      DO17M=I,N
   17 A(L,M)=A(L,M)-P*A(I,M)
      DO24M=1,N
   24 B(L,M)=B(L,M)-P*B(I,M)
   12 CONTINUE
      KO=2
      RETURN
      END
```

```
C
      SUBROUTINE LINE(F,XL,X,PA,P,R,NB,FR,XU,WK)
C
C     TO CALCULATE LINE - LOADS ALONG CABLES
C
      DIMENSION X(20,5),E(20,8),PB(20),PC(20),PR(20)
      BN=2*NB
      A=4.*F/XL**2
      DX=XL/BN
      A2=2.*A
      DO 1 I=1,NB
      T=X(I,1)*A2
      T2=T**2
      IF(F.NE.0.) GOTO300
      D=0.0
      X(I,2)=0.
      GOTO303
  300 D=-T2/(A2*R)
      X(I,2)=F-T2/(4.*A)
  303  D2=D**2
      AB=SQRT(1.+D2+T2*D2)
      AC=SQRT(1.+T2)
      E(I,1)=A2*AB/AC**3
      AD=-1./(AB*AC)
      E(I,2)=T*AD
      E(I,3)=AD
      E(I,4)=D*(T2+1.)*AD
      E(I,5)=DX*AC
      E(I,6)=1./AC
      E(I,7)=-T/AC
    1 E(I,8)=0.
      IF(FR.EQ.0.0) GO TO 7
      IF(F.NE.0.)XU=FR*XL/(4.*P*F)
      PR(1)=P-FR*(BN-1.)/BN
      PB(1)=E(1,1)*PR(1)
    5 PC(1)=XU*PB(1)
      DO2I=2,NB
      PR(I)=PR(I-1)+PC(I-1)*E(I-1,5)
      PB(I)=E(I,1)*PR(I)
    2 PC(I)=XU*PB(I)
      WRITE(6,200) XU
  200 FORMAT('0  XU= ',F7.3)
      IF(XU) 8,3,8
    8 PUN=(PR(NB)+PC(NB)*E(NB,5)*0.5-P)/FR
      IF(ABS(PUN)-.02)3,3,4
    4 XU=(1.-PUN)*XU
      GO TO 5
    3 DO 6 I=1,NB
      DO 6 J=1,3
    6 X(I,J+2)=-(E(I,J+1)*PB(I)+E(I,J+5)*PC(I))*AC
      AL=ATAN(4.*F/XL)
      PA=P*COS(AL)
      RETURN
    7 PC(NB)= P*(WK + XU*E(NB,1))
      PR(NB) =P-0.5*PC(NB)*E(NB,5)
      PB(NB) = PR(NB)*E(NB,1)
      PC(NB)= PB(NB)*XU + PR(NB)*WK
      NBB=NB-1
      DO9I=1,NBB
      J=NB-I
      PR(J) = PR(J+1)-PC(J+1)*E(J+1,5)
      PB(J) = PR(J)*E(J,1)
    9 PC(J) = XU*PB(J)+PR(J)*WK
      FR=P-PR(1)-0.5*PC(1)*E(1,5)
      WRITE(6,201)FR
  201 FORMAT(' CABLE LOSS ALONG HALF CABLE = ',F8.2)
      GO TO 3
      END


C
      SUBROUTINE EDGE (X,Q,DY,NB,NS,Y)
C
C     TO DIVIDE LINE - LOADS BETWEEN GENERATORS
C
      DIMENSION X(20,5),Q(5,20,4),Y(5)
      DO 1 M=1,NB
      DO 2 I=1,NS
      CA=X(M,2)+Y(1)-Y(I)
      IF(CA) 3,3,2
    2 CONTINUE
    3 A=0.
      IF(DY.NE.0)A=-CA/DY
      B=1.-A
      DO 1 J=1,3
      Q(I-1,M,J)=Q(I-1,M,J)+A*X(M,J+2)
    1 Q(I,M,J)=Q(I,M,J)+B*X(M,J+2)
      RETURN
      END
```

```
C
      SUBROUTINE MMULT(C,A,B)
C
C     C=A*B
C
      DIMENSION A(4,4),B(4,4),C(4,4)
      DO 1 I=1,4
      DO 1 J=1,4
      S=0.
      DO 2 K=1,4
    2 S=S+A(I,K)*B(K,J)
    1 C(I,J)=S
      RETURN
      END
```

```
C
      SUBROUTINE JSUB(C,A,B)
C
C     C=A-J*B
C
      DIMENSIONA(4,4),B(4,4),C(4,4)
      DO 1 I=1,3,2
      DO 1 J=1,4
      C(I,J)=A(I,J)-B(I,J)
    1 C(I+1,J)=A(I+1,J)+B(I+1,J)
      RETURN
      END
```

```
C
      SUBROUTINE JADD(C,A,B)
C
C     C=A+J*B
C
      DIMENSION C(4,4),B(4,4),A(4,4)
      DO 1 I=1,3,2
      DO 1 J=1,4
      C(I,J)=A(I,J)+B(I,J)
    1 C(I+1,J)=A(I+1,J)-B(I+1,J)
      RETURN
      END
```

```
C
      SUBROUTINE RMULT(C,A,B)
C
C     C=B*A
C
      DIMENSION C(4),A(4,4),B(4)
      DO 1 I=1,4
      S=0.
      DO 2 J=1,4
    2 S=S+A(I,J)*B(J)
    1 C(I)=S
      RETURN
      END
```

```
C
      SUBROUTINE FMULT(B,F,A)
C
C     B=A*F
C
      DIMENSION B(4,4),F(4,2),A(4,4)
      DO 1 I=1,4
      DO 1 J=1,2
      B(I,J)=A(I,1)*F(1,J)+A(I,2)*F(2,J)
    1 B(I,J+2)=A(I,3)*F(3,J)+A(I,4)*F(4,J)
      RETURN
      END
```

APPENDIX B

B.1 STEEL TENSILE TESTS

Tensile tests were carried out on an Avery 25,000 lb testing machine using test specimens 8" - 10" long. The extension was measured over a 2" gauge length using a Baty (0.0001") extensometer.

Typical load strain curves for both the prestressing and cold drawn wires are given in Figures B.1 and B.2. Figure B.3 shows a typical load strain curve of a length of cold drawn wire which has had a wire spot welded across it within the 2" gauge length.

B.2 MORTAR PROPERTY TESTS

For each concrete mix, Table B.1 lists the mixes used, the position in the shell where each mix was used and the age of the mix when the shell was prestressed and tested.

Compression Tests. These tests were carried out on 4" x 2" cylinders, which had been capped with dental plaster, loaded at a rate of 2000 lb/in^2/min. Results obtained are given in Table B.2. The apparent decrease of some mortar strengths with age is due to the fact that good quality cylinders were tested first. In addition a number of cylinders were strain gauged circumferentially and longitudinally to obtain values of Young's modulus and Poission's ratio. It was attempted to load these cylinders also at 2000 lb/in^2/min, but this was not completely achieved due to the time taken to measure and record the strain readings. Table B.3 lists the results obtained.

Brazilian Tensile Tests. Tensile tests were performed on

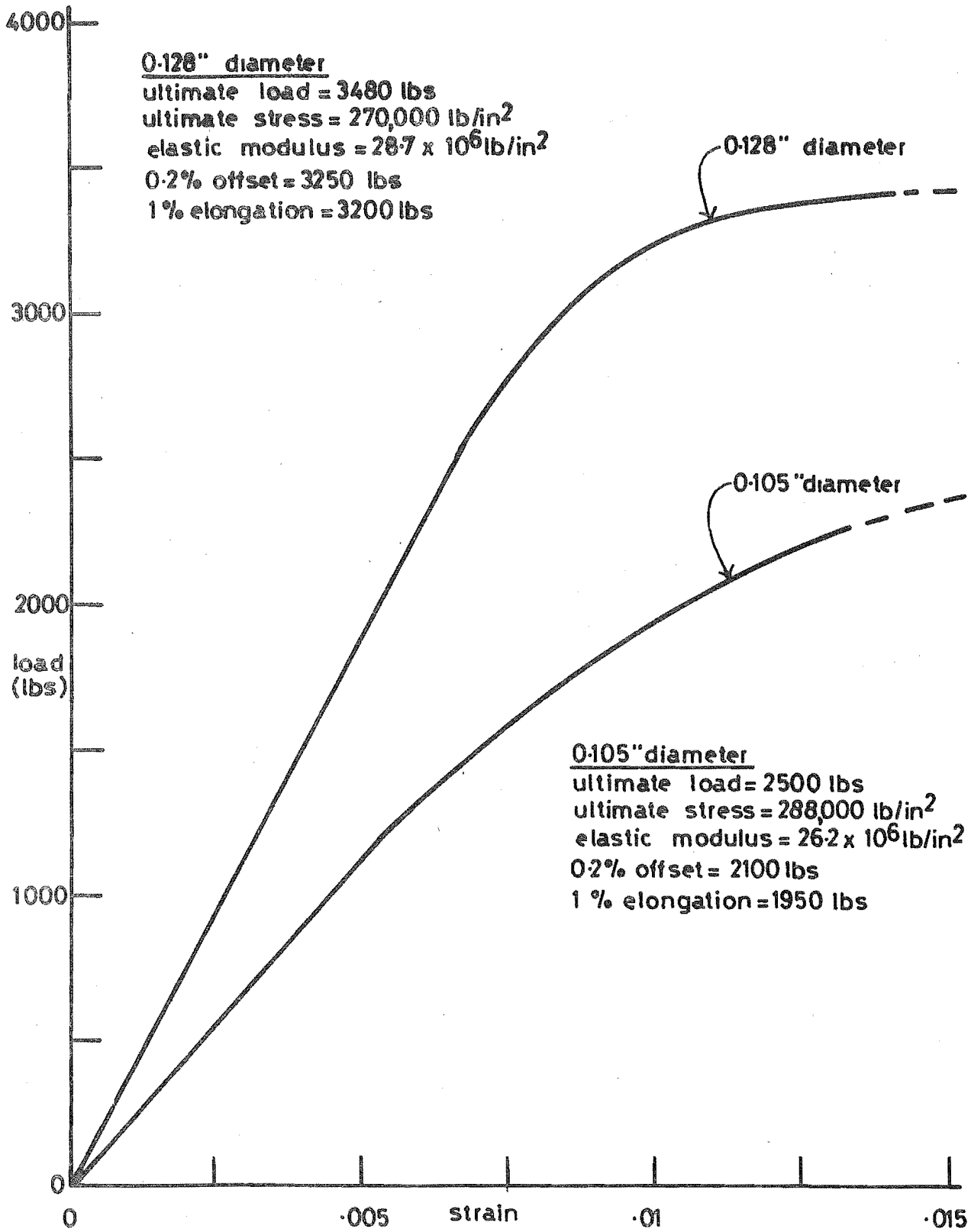

FIG. B.1 LOAD—STRAIN CURVE FOR PRESTRESSING STEEL

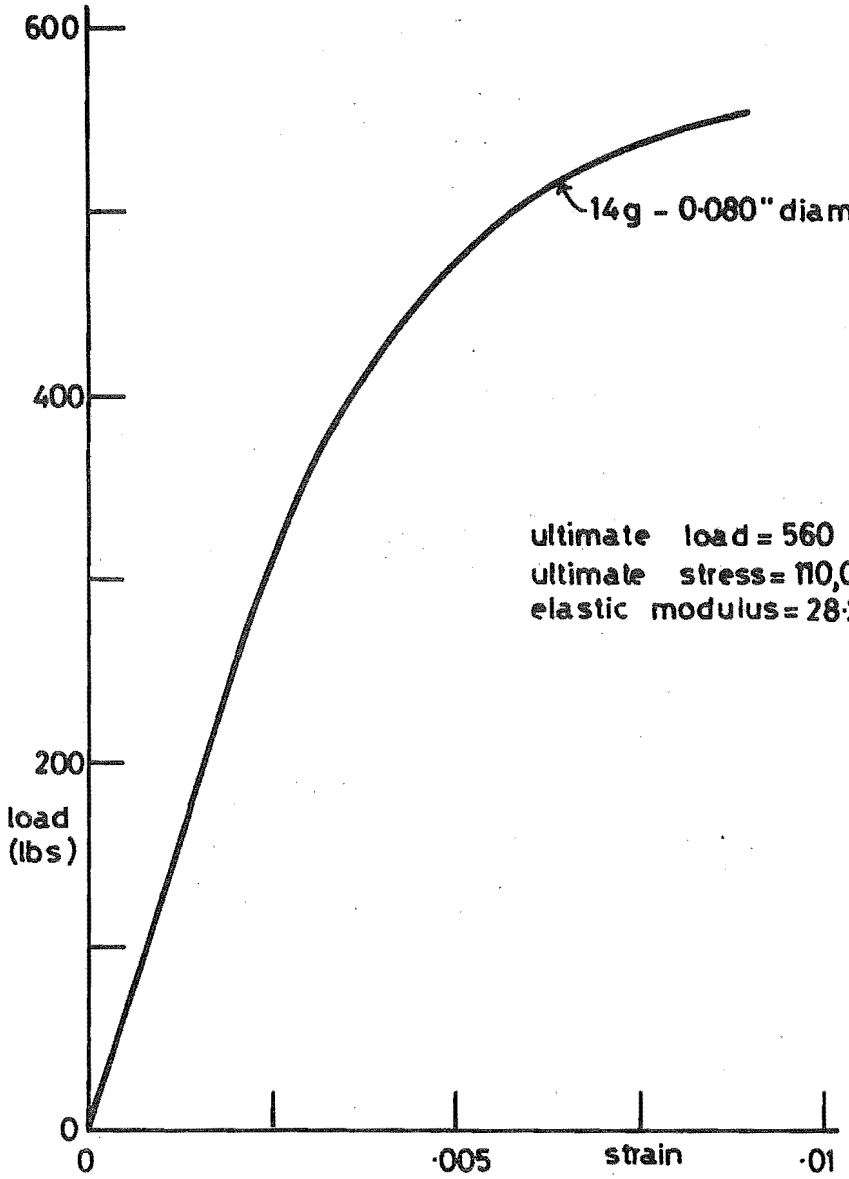

FIG. B.2 LOAD–STRAIN CURVE FOR COLD DRAWN WIRE

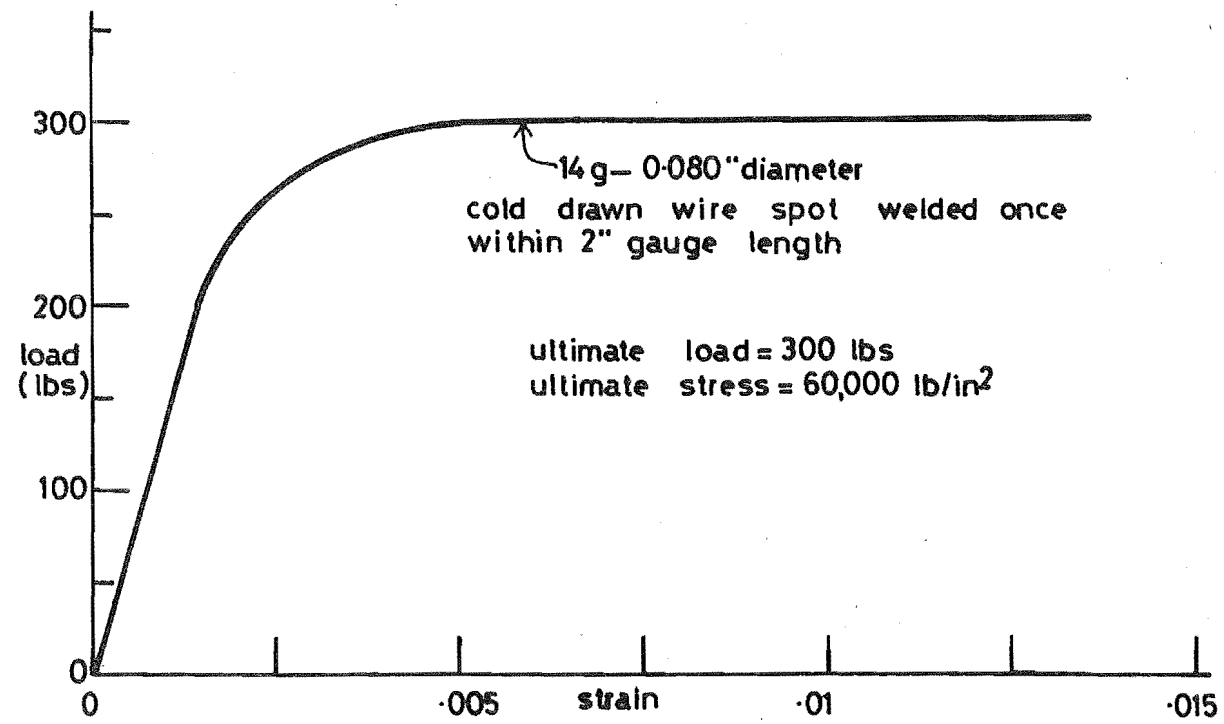

FIG. B.3 LOAD–STRAIN CURVE FOR SPOT WELDED WIRE

a number of 4" x 2" cylinders at a loading rate of 1200 lb/in^2/min, measured at the maximum cross-section. Load was distributed by $\frac{1}{8}$" x 1" x 5" ivory board strips.

The tensile splitting strength, f_t, was calculated by the formula:

$$f_t = \frac{P}{\pi RL}$$ where P = total splitting load
R = radius of cylinder
L = length of cylinder

Values of f_t obtained are given in Table B.4.

Bending Tests. Slabs, 24" x 6" x 0.6", were tested in bending to obtain values for Young's modulus and ultimate flexural tensile stress for the shell section. The slabs were simply supported over a distance of 1'-6" and line loaded equally at their third points. Thus there was constant moment across the midspan third of the slab. Loading platforms and supports were made from 1" diameter steel bar and extended the full width of the slab. Strain gauges were mounted longitudinally at midspan, on both the top and bottom surfaces of the slabs. Midspan deflections were measured with 0.0001" graduated deflection gauges. Testing was carried out by loading each slab in increments of 10 lbs to failure. At each load increment, strain and deflection measurements were taken. It was found that initially both strains and displacements were linear with load.

Values of Young's modulus were calculated using the initial linear slope of the load-strain and load-deflection curves, and by assuming linear elastic behaviour of the slabs.

Initially the tests were carried out using an Avery 25,000 lb test machine, but considerable difficulty was experienced in obtaining accurate deflection measurements.

Later a small test frame was constructed where deflection measurements could be accurately obtained, the slabs being loaded by hanging weights at the third points. Results from slabs tested on the frame indicated that a lower value of Young's modulus was being obtained by using deflection measurements than by using strain measurements. Thus in an effort to solve the dilemma a number of extra slabs were made and tested from mixes identical to those used for the shells. Two of these slabs were prestressed longitudinally. Results obtained from the original slabs and extra slabs are given in Table B.5.

Ultimate flexural tensile stress was obtained by calculating the stress at midspan when cracking first began, assuming linear elastic behaviour of the slab.

SHELL	MORTAR MIX CODE	POSITION IN SHELL	AGE AT PREST-RESSING (days)	AGE AT TEST (days)	AVERAGE AGE FOR SHELL	
					PRESTRESS-ING	TEST
1	1,1	(one piece	49	58	49	58
	1,2	(shell	49	58		
2	2,1	(traverse +	88	115	76	103
	2,2	(end (segments	88	115		
	2,3	centre segment	54	80		
3	3,1	centre segment	80	130	57	107
	3,2	(traverse +	46	96		
	3,3	(end (segments	46	96		
4	4,1	end segment	46	60	34	48
	4,2	traverse	28	42		
	4,3	end segment	39	53		
	4,4	traverse	24	38		
	4,5	centre segment	32	46		
5	5,1	traverse	41	48	32	39
	5,2	end segment	35	42		
	5,3	traverse	31	38		
	5,4	end segment	27	34		
	5,5	centre segment	23	30		

N.B. The centre segments of shells 2 and 3 were constructed together and thus mixes 2,3 and 3,1 are the same mix.

TABLE B.1 MORTAR MIX CODE

SHELL	MIX CODE	AGE (days)	AVERAGE f'_c (psi)	NUMBER TESTED	AVERAGE psi	COMMENTS
1	1,1P	11	6,350	2		
	1,2P	11	5,570	2	}5,950	stripping
	1,1	49	7,140	3		
	1,2	49	8,430	3	}7,700	prestressing
	1,1P	62	9,500	3		
	1,2P	62	9,100	3	}9,300	4 days after test
2	2,1P	91	8,500	3		
	2,2P	91	9,700	3	}9,200	prestressing
	2,1	125	10,500	2		
	2,2	125	8,400	2	}7,690	4 days after test
	2,1P	125	5,550	2		
	2,2P	125	6,300	2		
3	3,1P	182	7,550	3		
	3,3P	148	7,150	3	}7,350	42 days after test
4	4,4	23	7,260	3		
	4,5	31	7,400	3	}7,330	prestressing
	4,1	64	6,700	3		
	4,2	46	6,610	3		
	4,3	57	5,200	3	}6,204	4 days after test
	4,4	42	7,160	3		
	4,5	50	5,350	3		
5	5,1	56	7,680	3		
	5,2	50	7,850	3		
	5,3	46	8,500	3	}8,050	8 days after test
	5,4	42	7,490	3		
	5,5	38	8,710	3		

P after mix code indicates the test specimen was air-vibrated.

TABLE B.2 MORTAR COMPRESSION TESTS ON 4" x 2" CYLINDERS

SHELL	MIX CODE	AGE (days)	E x 10^{-6} (Secant Modulus)	POISSONS RATIO
2	2,1	131	5.53	
	2,2	131	5.74	
3	3,2	148	6.04	
	3,2	148		.130
	3,3	148		.124

TABLE B.3 YOUNG'S MODULUS AND POISSION'S RATIO VALUES FROM STRAIN GAUGED 4" x 2" CYLINDERS

SHELL	MIX CODE	AGE (days)	AVERAGE f_t (psi)	NUMBER TESTED	AVERAGE psi	COMMENTS
3	3,1	182	1,350	2	)	42 days after test
	3,1P	182	923	2	)	
	3,2	148	1,250	2	)1160	
	3,3	148	1,160	2	)	
	3,3P	148	1,100	1	)	
4	4,1	67	935	3	)	7 days after test
	4,2	49	904	1	) 931	
	4,3	60	926	3	)	
	4,5	53	950	3	)	
5	5,1	57	896	3	)	9 days after test
	5,2	51	796	3	)	
	5,3	47	855	3	) 780	
	5,4	43	750	3	)	
	5,5	39	760	3	)	

P after mix indicates the test specimen was air-vibrated

TABLE B.4 TENSILE TESTS ON 4" x 2" CYLINDERS

MIX CODE	AGE (days)	E x 10^{-6} STRAIN	CALCULATED FROM DEFLECTION	f_t 1st CRACK
1,1	90	5.75		1080
1,2	90	5.95		918
2,1P	91	5.85		
2,1P	91	5.7	5.4	1080
2,2P	91	5.05		
2,2P	91	5.33	5.2	1115
3,2	148	6.16		1160
A	46	5.6	4.9	1100
A	48	5.7	5.1	1150
A	46		5.3	
Average		5.7	5.1	
4,3	63	4.0		665
B	41	4.7	3.96	474
B	41	5.0	3.8	
B	41	4.38	4.36	
B	44		4.4	780
B	50		4.2	
B	50		4.1	
Average		4.5	4.1	
SLABS PRESTRESSED LONGITUDINALLY TO AN AVERAGE STRESS OF 500 PSI				
A	48	5.52	5.65	
B	41	4.32	4.4	

P after mix code indicates the test specimen was air-vibrated

Mix A - identical to that used in shells 1, 2 & 3

Mix B - identical to that used in shells 4 & 5

TABLE B.5 BEAM FLEXURE TEST RESULTS